U.S. DEPARTMENT OF COMMERCE
National Technical Information Service

PB-256 397

Mechanism of Photochemically Initiated Oxidations

Ohio State University

Prepared For
Environmental Sciences Research Lab.

June 1976

PB 256 397

REPRODUCED BY
NATIONAL TECHNICAL
INFORMATION SERVICE
U. S. DEPARTMENT OF COMMERCE
SPRINGFIELD, VA. 22161

TECHNICAL REPORT DATA
(Please read Instructions on the reverse before completing)

1. REPORT NO. EPA-600/3-76-070	2.	3. RECIPIENT'S ACCESSION NO.
4. TITLE AND SUBTITLE MECHANISM OF PHOTOCHEMICALLY INITIATED OXIDATIONS		5. REPORT DATE June 1976
		6. PERFORMING ORGANIZATION CODE
7. AUTHOR(S) Jack G. Calvert		8. PERFORMING ORGANIZATION REPORT NO.
9. PERFORMING ORGANIZATION NAME AND ADDRESS Chemistry Department The Ohio State University 140 West 18th Avenue Columbus, Ohio 43210		10. PROGRAM ELEMENT NO. 1A1008
		11. CONTRACT/GRANT NO. R800398
12. SPONSORING AGENCY NAME AND ADDRESS Environmental Sciences Research Laboratory Office of Research and Development U.S. Environmental Protection Agency Research Triangle Park, North Carolina 27711		13. TYPE OF REPORT AND PERIOD COVERED Final 1/73 - 12/75
		14. SPONSORING AGENCY CODE EPA-ORD

(triplet B 1)

15. SUPPLEMENTARY NOTES

Reproduced from best available copy.

16. ABSTRACT

Several significant new observations have been made relative to chemical reactions that occur in sunlight-irradiated NO_x/hydrocarbon/aldehyde/CO/SO_2 polluted atmospheres. Many of the primary reactions that are needed to quantitatively evaluate the photo-oxidation mechanisms of SO_2 in the atmosphere were measured. Rate constants for the reactions of the excited $SO_2(^3B_1)$ state of SO_2 with various atmospheric gases, alkanes, alkenes, NO, CO, etc., were determined. In view of these results, the rate of SO_2 photooxidation in the atmosphere is estimated, and the possible role of excited-SO_2/alkene interactions that generate aerosols is evaluated. Rate constants for the homogeneous reaction of SO_2 with O_3, NO_3, and N_2O_5 were also estimated. All of these reactions are relatively slow for conditions that usually exist in polluted atmospheres. The unusual reaction of SO_3 with NO_2 was observed, although its importance in the atmosphere cannot be evaluated accurately from the existing data. An evaluation was made of the photochemical smog mechanisms using a computer to simulate the rates of change in various polluted atmospheres. Several important features of special interest in developing control strategies were observed.

17. KEY WORDS AND DOCUMENT ANALYSIS

a. DESCRIPTORS		b. IDENTIFIERS/OPEN ENDED TERMS	c. COSATI Field/Group
*Air pollution Tests *Oxidation *Photochemical reactions *Reaction kinetics *Sulfur dioxide *Nitrogen oxides	*Alkanes *Alkene hydrocarbons Computerized simulation		13B 14B 07B 07C 07E 07D 09B

18. DISTRIBUTION STATEMENT RELEASE TO PUBLIC	19. SECURITY CLASS *(This Report)* UNCLASSIFIED	21. NO. OF PAGES 200
	20. SECURITY CLASS *(This page)* UNCLASSIFIED	22. PRICE 7.50

EPA Form 2220-1 (9-73)

PRICES SUBJECT TO CHANGE

EPA-600/3-76-070
June 1976

MECHANISM OF PHOTOCHEMICALLY INITIATED OXIDATIONS

by

Jack G. Calvert
Chemistry Department
The Ohio State University
Columbus, Ohio 43210

Grant No. R800398

Project Officer
Joseph J. Bufalini
Atmospheric Chemistry and Physics Division
Environmental Sciences Research Laboratory
Research Triangle Park, N.C. 27711

U. S. ENVIRONMENTAL PROTECTION AGENCY
OFFICE OF RESEARCH AND DEVELOPMENT
ENVIRONMENTAL SCIENCES RESEARCH LABORATORY
RESEARCH TRIANGLE PARK, N.C. 27711

DISCLAIMER

This report has been reviewed by the Environmental Sciences Research Laboratory, U.S. Environmental Protection Agency, and approved for publication. Approval does not signify that the contents necessarily reflect the views and policies of the U.S. Environmental Protection Agency, nor does mention of trade names or commercial products constitute endorsement or recommendation for use.

ABSTRACT

Several significant new observations have been made relative to chemical reactions that occur in sunlight-irradiated NO_x/hydrocarbon/aldehyde/CO/SO_2 polluted atmospheres. Many of the primary reactions that are needed to quantitatively evaluate the photooxidation mechanisms of SO_2 in the atmosphere were measured. Rate constants for the reactions of the excited $SO_2(^3B_1)$ state of SO_2 with various atmospheric gases, alkanes, alkenes, NO, CO, etc., were determined. In view of these results, the rate of SO_2 photooxidation in the atmosphere is estimated, and the possible role of excited-SO_2/alkene interactions that generate aerosols is evaluated. Rate constants for the homogeneous reaction of SO_2 with O_3, NO_3, and N_2O_5 were also estimated. All of these reactions are relatively slow for conditions that usually exist in polluted atmospheres. The unusual reaction of SO_3 with NO_2 was observed, although its importance in the atmosphere cannot be evaluated accurately from the existing data. An evaluation was made of the photochemical smog mechanisms using a computer to simulate the rates of change in various polluted atmospheres. Several important features of special interest in developing control strategies were observed.

Table of Contents

Introduction. 1

Part I. The Atmospheric Removal Paths of SO_2 2

I-A. The Efficiency of SO_2 Triplet Formation Induced in the Excited Singlet SO_2 by Collisions with O_2 and Other Atmospheric Gases. 3
- 1. Experimental Methods and Results 3
- 2. Discussion of Results 6
  - The mechanism of $^3SO_2$ formation in the 2400-3200 Å irradiation of SO_2 6
  - Estimation of the intersystem crossing ratio in $^1SO_2$-M collisions with various partners 7
  - Effect of the nature of the collision partner on the intersystem crossing rate in excited singlet sulfur dioxide 9
  - Efficiency of $^3SO_2$ formation in N_2- and CO-containing mixtures 9
  - "Excess" triplet in the 3130 Å-irradiated SO_2-CO mixtures at high pressures 11
  - The theoretical maximum rates of SO_2 photo-oxidation in sunlight-irradiated, SO_2-containing atmospheres 11

I-B. A Study of the Nature of the SO_2 Excited States Formed at High Added Gas Pressures 11
- 1. Experimental Methods and Results 12
- 2. Discussion 14
  - The "excess" biacetyl phosphorescence from 2875 Å-irradiated SO_2-biacetyl mixtures at high added-gas pressures 14
  - Treatment of the data in terms of the Wampler, Horowitz, Calvert mechanism 18
  - Treatment of the present data in terms of the Cehelnik, Spicer, Heicklen mechanism of SO_2 photochemistry 19
  - The nature of the intermediate species involved in SO_2 photochemistry at high added-gas pressures 21
  - The theoretical maximum rate of SO_2 photo-oxidation in the lower atmosphere 24

I-C. The Temperature Dependence and the Mechanism of the $SO_2(^3B_1)$ Quenching Reaction 25
- 1. Experimental Methods 26
- 2. Results and Discussion 27
  - The mechanism of $SO_2(^3B_1)$ quenching 27
  - Mechanism of $SO_2(^3B_1)$ quenching by the atmospheric gases 30
  - The $SO_2(^3B_1)$ quenching by the paraffinic hydrocarbons 39
  - The $SO_2(^3B_1)$ quenching by NO and by the olefinic and aromatic hydrocarbons 40

Table of Contents (continued)

I-D. A Kinetic Study of the Photoexcited $SO_2(^3B_1)$-Alkene Reactions. 42
  1. Experimental 43
  2. Discussion of Results 47
    Mechanism of $SO_2(^3B_1)$ Induced cis-trans isomerization of 2-butenes 47
    Mechanism of aerosol formation in 3500-4100 Å irradiated SO_2-2-butene mixtures 54

I-E. The Mechanism and Kinetics of the Alkene-SO_2 Reactions Excited Within the First Allowed Band of SO_2 (3130 Å). 56
  1. Experimental Procedures and Results 57
  2. Discussion 57
    The simple two-state reaction mechanism of cis-2-butene isomerization sensitized by electronically excited SO_2 57
    The isomerization mechanism in experiments at low $[SO_2]/[C_4H_8]$ ratios 62
    The isomerization mechanism in experiments with high pressures of added CO_2 67

I-F. The Mechanism and Kinetics of SO_3 Formation in the Photolysis of SO_2 Mixtures. 69
  1. Experimental 70
  2. Discussion of the Results 76
    Dependence of quantum yields of SO_3 formation on reactant flow rates 76
    Mechanism of SO_3 formation in 3600-4000 Å $SO_2(^3B_1)$ Excitation experiments 81
    Mechanism of SO_3 formation in SO_2 excited at 3130 Å 83
    Conclusions 86

I-G. The Nature of the Excited Singlet States in SO_2 Photolysis Within the First Allowed Absorption Band 87

Part II. Some Thermal Reactions of Possible Significance in the Sunlight-Irradiated, Polluted Troposphere. 92

II-A. A Kinetic Study of the SO_2-O_3, SO_2-NO_3, and SO_2-N_2O_5 Reactions. 92
  1. Experimental 93
  2. Discussion of the Results 95
    Estimates of the rate constants for the NO_3-SO_2 and N_2O_5-SO_2 reactions 95
    The predicted influence of N_2O_5 photodecomposition on the levels of N_2O_5 and NO_3 in the sunlight-irradiated polluted urban atmosphere 98
    The reaction between gaseous SO_3 and NO_2 98

Table of Contents (continued)

II-B. The Reaction of O_3 with Perfluorinated Polyolefins 99
  1. Experimental 99
  2. Results and Discussion 101

Part III: The Computer Simulation of the Rates of Chemical Reactions in Sunlight-Irradiated Polluted Atmospheres. 111

III-A. The Relative Importance of Various Active Intermediates in the Attack on Alkenes in the Polluted Atmosphere 112
  1. Discussion 112

III-B. The Effect of CO on the Chemistry of Photochemical Smog Systems. 123
  1. Results and Discussion 124

III-C. Computer Simulation of the Rates and Mechanisms of Photochemical Smog Formation. 135
  1. Results and Discussion 136
    Computer analysis of the chemistry of smog formation in a simulated NO_x-hydrocarbon polluted atmosphere 136
    The theoretical concentrations of HO and HO_2 in the simulated smoggy atmospheres and related data from real atmospheres 147
    Theoretical mass balance of the nitrogen-containing compounds formed in the simulated polluted atmosphere 154
    Effects of the variation of the concentrations of the impurities on product formation in simulated sunlight-irradiated polluted atmosphere 155
      The saturated "reactive" hydrocarbons 155
      Effects of variation of NO_x concentrations 156
      Effects of variation in initial CO concentrations 159
      Effects of SO_2 addition on the reactions in the simulated polluted atmospheres 162
    Summary 167

References. 169

Conclusions 183

List of Figures

Figure No.		Page
1	The extinction coefficients of sulfur dioxide gas	2
2	Plot of the equation B for $M = O_2$, Ar, and CO	8
3	Plot of equation B for $M = CO_2$ and N_2	8
4	Absorption spectra of SO_2 and excitation spectra of biacetyl phosphorescence emission measured at 5120 Å as excited in SO_2-Ac_2-CO_2 mixtures	15
5	Plot of $1/\Phi_{sens}$ vs. $1/[Ac_2]$ for data from SO_2-Ac_2-CO_2 mixture photolyses	20
6	Plot of $1/(\Phi_{sens} - \Phi_{sens(2)})$ vs. $1/[CO_2]$	22
7	Plot of $1/(\Phi_{sens} - \Phi_{sens(2)})$ vs. $1/[N_2]$ or $1/[CO]$	23
8	Temperature dependence of the $SO_2(^3B_1)$ lifetimes in pure SO_2	34
9	Arrhenius plots of the rate constants for the $SO_2(^3B_1)$ quenching reactions for several atmospheric gases: O_2, Ar	34
10	Arrhenius plots of the rate constant data for the $SO_2(^3B_1)$ quenching reactions for several atmospheric gases: NO, CO_2, N_2, CO	35
11	Arrhenius plots of the rate constant data for the $SO_2(^3B_1)$ quenching reactions for several paraffinic hydrocarbons: CH_4, C_2H_6, C_3H_8, n-C_4H_{10}	35
12	Arrhenius plots of the rate constants for the $SO_2(^3B_1)$ quenching reactions for some paraffinic hydrocarbons: iso-C_4H_{10}, neopentane, cyclohexane	36
13	Arrhenius plots of the rate constants for the $SO_2(^3B_1)$ quenching reactions for the olefinic and aromatic hydrocarbons	36
14	Arrhenius plots of the $SO_2(^3B_1)$ quenching constants per hydrogen atom for primary, secondary, and tertiary C-H bonds	40
15	Time dependence of $[t\text{-}2\text{-}C_4H_8]/[cis\text{-}2\text{-butene}]$ ratio in 3500-4100 Å irradiated mixtures of 2-butenes and SO_2	47
16	Plot of reciprocal of initial quantum yield of isomerization of 2-butenes versus $[SO_2]/[2\text{-butene}]$ ratio	49
17	Stern-Volmer plot of $SO_2(^3B_1)$ lifetime data in SO_2-2-butene mixtures	49

List of Figures (Continued)

Figure No.		Page
18	Plot of the reciprocal of the initial quantum yield of t-2-butene versus $[SO_2]/[C_4H_8]$ ratio	63
19	Plot of function C versus $[SO_2]/[C_4H_8]$ in 3130 Å photolysis of SO_2-cis-2-butene mixtures	63
20	Plot of function C versus $[SO_2]/[C_4H_8]$ from Cox data	64
21	Plot of function D versus $[SO_2]/[C_4H_8]$ ratio in 3130 Å photolysis of SO_2-cis-2-butene mixtures	66
22	Plot of function D versus $[SO_2]/[C_4H_8]$ ratio from Cox data	66
23	Plot of function G versus $1/[CO_2]$ from 3130 Å photolysis of SO_2-2-butene-CO_2 mixtures	69
24	Molar extinction coefficients for the first allowed band and the forbidden band of SO_2 at 25°C	71
25	Gas handling and flow reaction system used in this study	72
26	Effect of residence time of SO_2 on the quantum yield of SO_3 formation in 3600-4000 Å excited SO_2	78
27	Effect of residence time of SO_2 on the quantum yield of SO_3 formation in 3130 Å irradiated SO_2	78
28	Plot of the ratio of the quantum yield of SO_3 formation in pure SO_2 to that in SO_2-added gas mixtures: NO-SO_2, CO_2-SO_2, O_2-SO_2	82
29	Plot of function G versus $[CO_2]/[SO_2]$ in 3130 Å irradiated mixtures of SO_2-CO_2 in the flow system	85
30	Diagram of the apparatus used to prepare N_2O_5	95
31	The molar extinction coefficient for N_2O_5 vapor	96
32	Infrared spectral changes used to monitor the reaction of ozone and Teflon	102
33	Infrared spectrum of products resulting from the reaction of ozone with Teflon	103
34	Rate of formation of CF_2O plus CO_2 products of the O_3-Teflon reaction versus the O_3 concentration	107
35a	The major reaction paths for degradation of t-2-butene in a sunlight-irradiated, NO_x-polluted atmosphere: O_3, $O(^3P)$, $O_2(^1\Delta_g)$	113

List of Figures (Continued)

Figure No.		Page
35b	The HO radical reaction paths with trans-2-butene	114
36	The HO_2, CH_3O, and NO_3 reaction paths with trans-2-butene	115
37	Theoretical rates of product formation in a sunlight-irradiated simulated auto-exhaust polluted atmospheres	116
38	Comparison of experimental and computer simulated chemical changes in NO-NO_2-CO mixtures irradiated in moist air (100 ppm CO)	126
39	Comparison of experimental and computer simulated chemical changes in NO-NO_2-CO mixtures irradiated in moist air (400 ppm CO)	127
40	The expected effects of water vapor and carbon monoxide addition on the products of the NO photooxidation in air	128
41	The NO-NO_2-CO-polluted atmosphere; simulation of the effects of added CO	129
42	The photooxidation of NO in CO-containing mixtures; comparison of experimental and computer simulated chemical changes in NO-NO_2-CO mixtures irradiated in relatively dry and moist air	132
43	The photooxidation of NO in CO-containing mixtures; comparison of the experimental and computer simulated chemical changes in NO-NO_2-CO mixtures irradiated in moist air	133
44	Theoretical rates of product formation in a computer simulated sunlight-irradiated NO_x-hydrocarbon-aldehyde-polluted atmosphere	137
45	Theoretical rates of reaction of various free radical species with alkene in the simulated sunlight-irradiated, polluted atmosphere of Figure 44	143
46	Theoretical HO and HO_2 concentrations as a function of irradiation time in simulated sunlight-irradiated, polluted atmospheres of Figure 44	150
47	The theoretical effects of varied alkene concentration on the HO concentration in the simulated sunlight-irradiated, polluted atmospheres	151
48	The theoretical effect of varied $[NO]^{o}$ on the HO concentration in the simulated sunlight-irradiated polluted atmospheres	152
49	The theoretical effects of varied $[CO]^{o}$ on the HO and HO_2 concentration in simulated sunlight-irradiated, polluted atmospheres	153

List of Figures (Continued)

Figure No. Page

50 The time dependence of the theoretical composition of the nitrogen containing compounds formed in the simulated, sunlight-irradiated polluted atmosphere 155

51 Relation of eye irritation to hydrocarbon and oxides of nitrogen levels in smog chamber experiments from Faith, Renzetti and Rogers 157

52 Relationship between the maximum daily 1-h average oxidant levels and the 6-9 A.M. average concentration of nonmethane hydrocarbons (Schuck, Altshuller, Barth, and Morgan) 157

53 The theoretical effect of reactive hydrocarbon concentration on the integral of the $[O_3]$ and [PAN] versus time data derived from the simulated polluted atmosphere 158

54 Theoretical effects of variation of the concentrations of the nitrogen oxides on the 8-h integrals of the $[O_3]$ and [PAN] versus time curves obtained from the simulated polluted atmosphere 158

55 Theoretical effect of increased $[NO]^{\circ}$ on the $[O_3]$-time profile in simulated polluted atmospheres 160

56 The theoretical effect of dilution of a highly polluted atmosphere on the 8-h integrals of the $[O_3]$ and [PAN] versus time curves obtained in simulated polluted atmospheres 160

57 The theoretical effect of variation of the initial concentration of the carbon monoxide on the O_3 and PAN formation in a simulated polluted atmosphere 161

58 The theoretical rate of attack of various free radical species on SO_2 for a simulated sunlight-irradiated, polluted atmosphere 168

List of Tables

Number		Page
I	Relative intensities of phosphorescence determined at $t = 0$ after laser pulse and at 25° C	4
II	Relative $^1SO_2$ quenching efficiencies of various atmospheric gases	9
III	Summary of the relative $^3SO_2$ formation rate constants and intersystem crossing ratios for various atmospheric gases at 25° C	10
IV	The 2875 Å-excited SO_2-sensitized phosphorescence of biacetyl in Ac_2-SO_2-CO_2 mixtures at room temperature	13
V	2875 Å-excited SO_2-sensitized phosphorescence of biacetyl in Ac_2-SO_2-CO_2 mixtures at room temperature	13
VI	2875 Å-excited SO_2-sensitized phosphorescence of biacetyl in Ac_2-SO_2-CO and Ac_2-SO_2-N_2 mixtures	14
VII	The effect of excitation wavelength on the quantum yield of SO_2-sensitized phosphorescence excited in SO_2-Ac_2-CO_2 mictures	17
VIII	Summary of parameters derived from the plots of $1/\phi_{sens}$ versus $1/[Ac_2]$	19
IX	Kinetic parameters related to the reactions of the $^1SO_2$ and X species formed in the 2875 Å-irradiation of SO_2-Ac_2-mixtures with added CO_2, CO, or N_2	23
X	The $SO_2(^3B_1)$ lifetime at various SO_2 concentrations and temperatures	28
XI	Rate constants for $SO_2(^3B_1)$ quenching reactions with various atmospheric components at several temperature	29
XII	Rate constants for the $SO_2(^3B_1)$-quenching reactions with various saturated hydrocarbon gases at several temperatures	31
XIII	Rate constants for the $SO_2(^3B_1)$-quenching reactions with various olefinic and aromatic hydrocarbon gases at several temperatures	33
XIV	Summary of Arrhenius parameters for $SO_2(^3B_1)$-quenching rate constants with various collision partners	37
XV	Arrhenius parameters E_a and $\log_{10}A$ for the $SO_2(^3B_1)$-quenching rate constants per H atom for C-H bonds of different type	41
XVI	Quantum yields of $SO_2(^3B_1)$-sensitized isomerization of the 2-butenes	45
XVII	Aerosol formation in the $SO_2(^3B_1)$ reaction in SO_2-2-butene mixtures	46

List of Tables (Continued)

Number		Page
XVIII	Lifetimes of $SO_2(^3B_1)$ molecules excited in SO_2-2-butene mixtures	47
XIX	Initial quantum yields of the SO_2-photosensitized isomerization of cis-2-butene at 3130 Å	58
XX	Effect of flow rate on the quantum yields of SO_3 formation in pure SO_2 irradiated within the first forbidden band	73
XXI	Effect of foreign gases on SO_3 quantum yields in SO_2 mixtures irradiated within the first forbidden band in the flow system	74
XXII	Quantum yields of SO_3 formation in pure SO_2 irradiated at 3130 Å in the static system	75
XXIII	Effect of flow rate on the quantum yield of SO_3 formation in pure SO_2 irradiated at 3130 Å in the flow system	75
XXIV	Effect of foreign gases on the quantum yield of SO_3 formation in 3130 Å irradiated SO_2 mixtures in the flow system	76
XXV	Comparison of the rate constant ratios derived from the present product SO_3 quantum yield data and $SO_2(^3B_1)$ lifetime data	83
XXVI	Summary of new rate constant estimates derived in this work	86
XXVII	Comparison of quenching rate constants for excited singlet SO_2 (long-lived component)	88
XXVIII	Estimated ratio of intensities of the fluorescence from the short-lived SO_2 singlet species to that for the long-lived species	89
XXIX	Estimation of ϕ_f from lifetime data of Brus and McDonald and data of Calvert et al., and Mettee and co-workers	90
XXX	Rate data for the reaction of gaseous ozone with Teflon gasket material at room temperature	105
XXXI	Rate data for the reaction of gaseous ozone with different samples of perfluorinated polyolefins at room temperature	106
XXXII	The rate of attack of various reactive intermediate species on trans-2-butene in a sunlight-irradiated, simulated atmosphere	117
XXXIII	Comparison of the theoretical rates of the HO-radical forming reactions in a simulated sunlight-irradiated auto-exhaust polluted atmosphere	119
XXXIV	Comparison of the theoretical rates of the HO_2-forming reactions in a sunlight-irradiated, auto-exhaust polluted atmosphere	121
XXXV	The effect of carbon monoxide level on the concentrations of products formed in the sunlight-irradiated moist atmospheres	130

List of Tables (Continued)

Number		Page
XXXVI	Rates of the major NO_2 formation and decay reactions in a simulated smoggy atmosphere	144
XXXVII	The theoretical primary rates of the major radical generation reactions in the simulated polluted atmosphere	145
XXXVIII	Theoretical rates of the major HO formation and loss reactions in the simulated polluted atmosphere	146
XXXIX	Theoretical rates of the major HO_2 formation and loss reactions in the simulated polluted atmosphere	146
XL	Theoretical rates of RO_2 formation and NO oxidation to NO_2 by the major RO_2 radicals formed in the simulated polluted atmosphere	147
XLI	The theoretical chain lengths for the HO, HO_2, and RO_2 radical reactions in the simulated polluted atmosphere	148
XLII	The theoretical rates of the major chain termination reactions in the simulated polluted atmosphere	148
XLIII	The fractional NO → NO_2 conversion rate due to the various reactants in the simulated polluted atmosphere at 10 min into the reaction	149
XLIV	Estimated enthalpy changes, rate constants of possible homogeneous elementary reaction paths for SO_2 in a polluted urban atmosphere	163

INTRODUCTION

Interest in the sulfur dioxide removal mechanisms in the atmosphere remains high among atmospheric scientists. There is substantial evidence that health hazards are associated with urban atmospheres containing moderately low levels of sulfur dioxide (above 0.2 ppm), and that these harmful effects are apparently enhanced when there are significant levels of suspended particulates. The special problem of aerosols containing high sulfate levels has focused new concern on atmospheric SO_2 levels since the recent CHESS report.[1] However, there is now little evidence as to the chemical nature of the active species responsible for these effects. The detailed mechanism of sulfur dioxide oxidation remains unclear. For examples, see the reviews of Alshuller and Bufalini,[2] Cadle and Allen,[3] and Urone and Schroeder.[5] The majority of existing evidence suggests that a major fraction of the sulfur dioxide is ultimately converted to sulfuric acid and sulfate salts, but the intermediate species involved and the reaction paths which lead to these products are open to question. The relatively slow rates of photooxidation of sulfur dioxide in air exposed to sunlight[6-8] and the demonstrated catalytic influence of certain solids and moisture on the rate of SO_2 oxidation[9-15] have led to the common belief that heterogeneous paths for SO_2 oxidation probably far outweigh the homogeneous modes. Although this conclusion may prove to be true for certain atmospheric conditions, it is by no means established today. There is a real question as to the availability of sufficient reactive metallic oxide, catalyst particles, and acid-neutralizing compounds in many atmospheres to promote SO_2 removal at the observed rates. The most compelling argument which has favored the importance of the heterogeneous removal processes has been the apparent lack of alternative homogeneous reactions of sufficient rate which might be invoked. It now appears to us that there are several such possible processes which are open for sunlight-irradiated atmospheres, but these remain quantitatively unevaluated. Our approach to this problem is based on the hypothesis that it is more realistic to evaluate the contributions from these homogeneous processes and arrive indirectly at the contribution of the heterogeneous modes than to establish unambiguously and directly the importance of heterogeneous paths in the real atmospheres.

A major portion of the work completed under this grant bears directly on the evaluation of the possible removal mechanisms of SO_2 in the troposphere. These kinetic studies are described in Section I of this final report. In Section II we summarize the results of our kinetic studies of some chemical systems of major interest in the understanding of photochemical smog mechanisms and the development of scientifically sound control strategies. These relate to several important intermediates and their reactions. In Section III we discuss our computer simulation studies which allow an extrapolation of our current knowledge to conditions which simulate those of the polluted atmosphere. We derive in this section theoretical rates of development of ozone, peroxyacetyl nitrate, and other compounds of special interest in simulated polluted atmospheres of varied composition. Predictions are made of the effects of alteration of the concentrations of the reactive hydrocarbon, NO, NO_2, CO, aldehydes, and SO_2 on the levels and dosages of O_3, PAN, and other compounds of special interest in air pollution control. Finally conclusions can be formulated from these results which provide a reasonable guidance in the development of more refined control strategies. These simulations provide as well recognition of areas which are still ill-defined and in which further definitive work is needed to provide unambiguous conclusions concerning SO_2 removal paths and the mechanism of photochemical smog formation.

PART I

THE ATMOSPHERIC REMOVAL PATHS OF SO_2

The absorption of solar energy by sulfur dioxide in the troposphere occurs within the relatively strong, "allowed" band which extends from 2400-3300 Å and the "forbidden", weaker band which extends from 3400-4000 Å; see Figure 1.

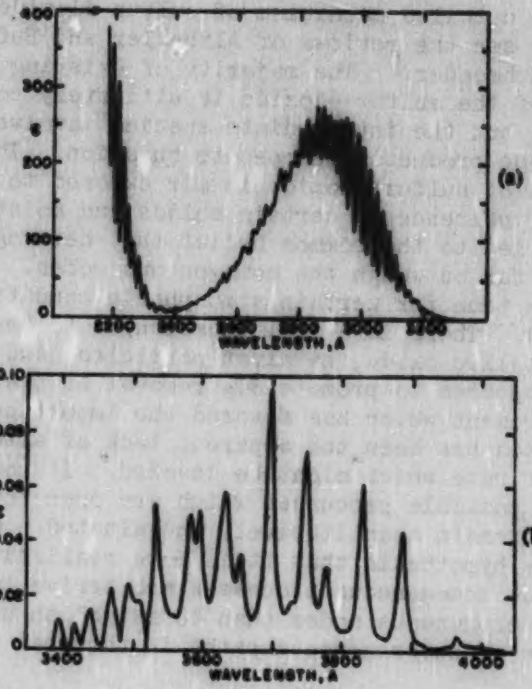

Figure 1. The extinction coefficients of sulfur dioxide gas in the first allowed band (a) and the "forbidden" band (b); $\epsilon = [\log_{10}(I_0/I)]/cl$ (liter mole^{-1}cm^{-1}).

Excitation of SO_2 within its first absorption band (2400-3300 Å) leads to the generation of three emitting species: (1) a very short-lived singlet state [perhaps $SO_2(^1A_2)$]; (2) a long-lived singlet state [probably $SO_2(^1B_1)$]; (3) a triplet state [$SO_2(^3B_1)$]. In addition to these optically detectable or emitting states, indirect chemical and physical evidence which we will review later suggests that at least one other non-emitting triplet [presumably $SO_2(^3A_2)$] and possibly a third triplet [conceivably $SO_2(^3B_2)$] may be important in the photochemistry of SO_2. An understanding of the kinetics and mechanisms which control the population of these SO_2 states and the rate constants for the various decay reactions of these states are essential ingredients to our evaluation of SO_2 removal mechanisms in the atmosphere. Significant progress toward this end was accomplished in this work and is described in the following sections.

I-A. The Efficiency of SO_2 Triplet Formation Induced in the Excited Singlet SO_2 by Collisions with O_2 and Other Atmospheric Gases.[16]

Molecules of sulfur dioxide in the first excited triplet state ($^3B_1$), designated here as $^3SO_2$, have been shown to be important reactants in several irradiated SO_2-containing systems[17-22]. Excited singlet sulfur dioxide molecules ($^1SO_2$), formed by absorption within the 2400-3200 Å band, generate the triplet species largely in a second-order, collisionally induced reaction [reaction (2)]. The $^1SO_2$ deactivation also occurs in a competitive second-order process [reaction (1)] of ill-defined mechanism involving the ground-state, nonoptical excited states or isomeric SO_2 states:

(1) $^1SO_2 + M \rightarrow (SO_2 - M) \rightarrow SO_2 + M$ (or products)

(2) $^1SO_2 + M \rightarrow {^3SO_2} + M$

The efficiency with which $^3SO_2$ molecules are formed in the spin-inverting reaction (2) is of primary importance in elucidating the kinetics of product formation in SO_2-reactant mixtures irradiated within the 2400-3200 Å absorption band of SO_2.

Rao et al.,[18,23] Wampler et al.,[22] and Horowitz and Calvert[24,25] have determined the quantum efficiency of the production of $^3SO_2$ (2400-3200 Å irradiation) by reaction (2) and the bimolecular intersystem crossing ratio, $k_2/(k_1 + k_2)$, for $M = SO_2$, N_2, CO, and cyclohexane. They employed an indirect method based on the $^3SO_2$-sensitized phosphorescence of biacetyl. This method suffers from the disadvantage that it cannot be used to determine the intersystem crossing ratio induced in $^1SO_2$ by collisions with oxygen or other compounds which are good quenchers of the triplet state of biacetyl. However, a knowledge of $k_2/(k_1 + k_2)$ for $M = O_2$ is of special importance in evaluating those processes which occur in SO_2-polluted atmospheres.

In this work we used a new method to determine intersystem crossing ratios for $^1SO_2$; the relative intensity of the phosphorescence from $^3SO_2$ molecules was determined as a function of time following the 2662 Å laser excitation of $^1SO_2$ molecules. Extrapolation of the phosphorescent intensity to zero time following the laser pulse allowed the estimation of intersystem crossing efficiency using O_2 as a collision partner for $^1SO_2$. Also, we have applied this method to estimate this important ratio with the other major atmospheric gases acting as collision partners.

I-A—1. Experimental Methods and Results

Laser excitation source

The first excited singlet state of SO_2 was populated by absorption of radiation from a 2662 Å laser pulse. This wavelength was produced by the application of nonlinear optical techniques to a Q-switched neodymium laser. The 10,650 Å neodymium fundamental was frequency doubled by the use of a precisely oriented, 2-in.-long potassium dihydrogen phosphate crystal. The 100-megawatt neodymium fundamental generated a 2-megawatt 5324 Å laser pulse which was further doubled by a precisely oriented ammonium dihydrogen phosphate crystal to give a 2662 ± 1 Å laser pulse of 30 kilowatts having a half-intensity duration of 20 nanoseconds. Because of the peculiar limitation of our equipment it was most convenient to have the laser and associated optical apparatus in one horizontal plane and the reaction cell and associated equipment in a different horizontal position. The laser beam could be readily aligned with the reaction cell using two adjustable aluminium-coated mirrors. Because of the reflectivity characteristics of the aluminium mirrors, the laser intensity entering the cell was reduced to about 15 kilowatts, but this was quite adequate for the experimental requirements.

Radiation detectors and treatment of the data for the decay of phosphorescence

Because the laser power does vary somewhat from pulse to pulse, it was necessary to monitor the power of each laser pulse so that the initial intensities of phosphorescence could be corrected for variations in laser pulse intensities. Power measurements of the 2662-Å radiation exiting the cell were made by connecting only the first stage of an RCA 1P28 photomultiplier tube. Phosphorescence was monitored at right angles to the cell using a RCA 7265 photomultiplier tube. A Jena WG-2 filter having a sharp wavelength cut-off at 3500 Å was placed in front of the photomultiplier unit to help discriminate against the fluorescent emission envelope of SO_2 and to protect the photomultiplier tube from the laser radiation. The fluorescence was reduced largely by the WG-2 filter. For the reactant pressures employed and the sweep speed of 20 µsec/cm, the intensity of fluorescence became negligible within a very short period, and the phosphorescent decay was clearly defined. The oscilloscopic traces of the phosphorescence and the 2662-Å laser pulse signals were photographed with high-speed 410 Polaroid film; the phosphorescent decay photographs were digitized and treated as described by Sidebottom et al.[26]

The sweep of the oscilloscope to record the response from the photomultiplier tube was triggered externally at the time of the laser pulse. The relative intensities of the phosphorescent traces at t = 0 following the laser pulse were determined from the antilogarithm of the intercept of the least-squares fit of the ln I_p-versus-time data. Data for the ratio of the phosphorescent intensity at t = 0 for SO_2, $[M] \neq 0$ (I_p^M) to that for SO_2, $[M] = 0$ (I_p) are given in Table I.

Table I. Relative intensities of phosphorescence determined at t = 0 after the laser pulse and at 25° C.[a]

P_M, torr	$[M]/[SO_2]$	$(I_p^M/I_p)_{t=0}$	$\left(1+\frac{(k_{1b}+k_{2b})[M]}{(k_{1a}+k_{2a})[SO_2]}\right)\left(\frac{I_p^M}{I_p}\right)_{t=0}$[b]
		$M = O_2$	
1.04	1.95	0.729	1.16
2.04	3.82	0.663	1.43
2.54	4.76	0.659	1.60
3.07	5.75	0.536	1.46
3.64	3.50	0.666	1.37
6.81	6.55	0.561	1.67
9.95	9.57	0.480	1.86
13.3	12.8	0.500	2.42
		$M = N_2$	
0.534	1.00	0.882	1.14
2.04	3.82	0.751	1.58
2.54	4.75	0.627	1.49
3.02	5.65	0.631	1.67
3.46	6.48	0.697	2.01
3.96	7.42	0.531	1.67
4.77	8.93	0.601	2.16

Table I. (Cont'd)

P_M, torr	$[M]/[SO_2]$	$(I_p^M/I_p)_{t=0}$	$\left(1+\frac{(k_{1b}+k_{2b})[M]}{(k_{1a}+k_{2a})[SO_2]}\right)\left(\frac{I_p^M}{I_p}\right)_{t=0}^{b}$
		M = Ar	
0.994	3.64	0.623	1.19
1.49	5.47	0.607	1.44
1.94	3.64	0.647	1.24
2.92	5.47	0.587	1.39
3.79	3.64	0.675	1.29
5.14	9.62	0.522	1.78
10.0	9.62	0.469	1.60
		M = CO	
0.534	1.00	0.880	1.21
1.04	1.95	0.774	1.35
2.04	3.82	0.792	1.94
2.04	4.13	0.833	2.14
2.55	4.78	0.713	2.01
3.02	5.66	0.624	1.97
3.42	6.40	0.747	2.56
3.53	7.15	0.633	2.35
4.00	7.49	0.691	2.66
		M = CO_2	
0.169	0.379	0.937	1.18
0.338	0.758	0.839	1.28
0.626	1.40	0.699	1.38
1.25	2.80	0.655	1.92
1.88	4.22	0.649	2.34
2.50	5.61	0.630	3.07
3.82	3.67	0.737	2.60
7.64	7.34	0.718	4.35
11.5	11.1	0.660	5.72

[a] I_p represents the relative phosphorescent intensity in a given experiment divided by the laser pulse power in that same run; I_p^M is the same quantity determined in a run at equal $[SO_2]$ but with added quencher gas M.

[b] This quantity is the ordinate employed in Figures 1 and 2 to obtain the rate constant ratio k_{2b}/k_{2a}; see relation [B] in text.

Reaction cell and associated apparatus

The reaction cell body was constructed of Pyrex and was 88 cm in length and 2.5 cm in diameter. Suprasil windows were cemented to the cell at the Brewster angle, using low-vapor-pressure epoxy cement. Reactants were mixed using a thermal gradient pump. The cell was connected to a grease-free vacuum line, and pressure measurements were made using a quartz spiral manometer.

Materials

Burdett high-purity nitrogen was used in experiments with added nitrogen. All other gases used in this work were obtained from Matheson and were of the quality indicated; argon (high purity), O_2 (research grade), CO (C.P. grade), and CO_2 (Coleman instrument grade); SO_2 (anhydrous grade) was purified further by bulb-to-bulb distillation in a high vacuum system, and the middle third was taken for the experiments.

I-A—2. Discussion of Results

The mechanism of $^3SO_2$ formation in the 2400-3200 Å irradiation of SO_2

In recent studies the 3130-Å of irradiation of the SO_2-CO system, Cehelnik et al.[21] have postulated that two nonradiative excited states of SO_2 as well as the optical states of SO_2 are involved as reactants leading to CO_2 formation. In a recent similar study of Wampler et al.[22], we concluded that $^3SO_2$ molecules were the major reactant in this system even at high gas pressures; we suggested that a bimolecular route of forming $^3SO_2$ in addition to reaction (2) became important at high gas pressures. We noted that our kinetics were consistent with the generation of $^3SO_2$ molecules by some unknown precursor, X, which was produced by $^1SO_2 + M \rightarrow X + M$, and it formed $^3SO_2$ at a significant rate only when reactant pressures were high enough for the reaction $X + M \rightarrow {}^3SO_2 + M$ to compete with the unimolecular disappearance of X. Investigations are presently under way to gain more definitive information regarding this proposed pathway to $^3SO_2$ and the alternative hypothesis of Cehelnik et al.[21]. Preliminary results from experiments utilizing the 2662-Å laser excitation of SO_2 indicate that in the presence of added gases, the observed phosphorescent lifetimes in experiments below about 30 torr total pressure are nearly identical to those observed for $SO_2(^3B_1)$ molecules produced by direct excitation utilizing a 3829-Å laser pulse. However, in experiments above 30 torr, the measured decay of the phosphorescence is slower than the low pressure rate data would have suggested. Possibly the apparent enhancement in the $^3SO_2$ lifetime may be due to the bimolecular participation of X to produce $^3SO_2$ during the monitored decay of $^3SO_2$. If this hypothesis is correct, a nonexponential decay of the phosphorescence is expected. Because of experimental limitations, our phosphorescent measurements cannot be extended now over a sufficiently large time scale to unequivocally verify or disprove the presence of a nonexponential decay. Further work is necessary before we can properly assess these findings in terms of alternative hypotheses.[21,22]. However, our observations are clear on one result: below about 30 torr total pressure, the major bimolecular route of producing $^3SO_2$ is from the $^1SO_2$ precursor. Accordingly, for the experimental conditions employed (total pressure less than 30 torr), the participation of X in the previously proposed reaction scheme may be neglected, and we now introduce only those reactions which are pertinent for our present conditions:

(I) $SO_2 + h\nu\ (2662\ \text{Å}) \rightarrow {}^1SO_2$

(1a) $^1SO_2 + SO_2 \rightarrow (2SO_2 \text{ or products})$

(2a) $^1SO_2 + SO_2 \rightarrow {}^3SO_2 + SO_2$

(1b) $^1SO_2 + M \rightarrow (SO_2, M \text{ or products})$

(2b) $^1SO_2 + M \rightarrow {}^3SO_2 + M$

(6) $^3SO_2 \rightarrow SO_2 + h\nu_p$

(7) $^3SO_2 \rightarrow SO_2$

(8a) $^3SO_2 + SO_2 \rightarrow SO_3 + SO$

(8b) $^3SO_2 + SO_2 \rightarrow (2SO_2$ or products not $SO_3)$

(9) $^3SO_2 + M \rightarrow (SO_2$, M, or products)

Estimation of the intersystem crossing ratio in $^1SO_2$-M collisions with various partners

Immediately following the laser excitation of SO_2 to $^1SO_2$, the relative intensity of phosphorescence, $(I_p)_{t=0}$, is directly proportional to the concentration of triplets formed by intersystem crossing. (The unimolecular decay of $^1SO_2$ to $^3SO_2$ is unimportant for our reactant pressures, and the fast bimolecular reactions steps (2a) and (2b) are responsible for the population of molecules in the $SO_2(^3B_1)$ state.) From a consideration of the above mechanism at t = 0, we have the following relationship for the ratio of initial phosphorescent intensity with SO_2 alone at a given pressure to that in which SO_2 is at the same pressure but an added gas M is present:

$$[A] \qquad \left(\frac{I_p^M}{I_p}\right)_{t=0} = \frac{1 + (k_{2b}/k_{2a})\,[M]/[SO_2]}{1 + [k_{1b} + k_{2b})/(k_{1a} + k_{2a})]\,[M]/[SO_2]}$$

Equation [A] may be arranged to give the useful relationship [B]:

$$[B] \qquad (I_p^M/I_p)_{t=0}\,\{1 + [(k_{1b} + k_{2b})/(k_{1a} + k_{2a})]\,[M]/[SO_2]\} = 1 + (k_{2b}/k_{2a})\,[M]/[SO_2]$$

Relationship [B] is tested graphically in Figure 2 using the data from Table I for M = O_2, Ar, and CO; a similar test for M = CO_2, and N_2 is shown in Figure 3. According to equation [B], the intercept value should be unity. The experimental intercept values from a least-squares treatment of the data for M = O_2, N_2, Ar, CO_2, and CO are: 0.98 ± 0.15, 1.04 ± 0.30, 0.98 ± 0.13, 0.86 ± 0.20, and 1.04 ± 0.28, respectively.* Within the error limits the graphical representations are in agreement with the functional form required by equation [B]. The slopes of the plots in Figures 2 and 3 are equal to k_{2b}/k_{2a} for the various added quenching gases. These results are summarized in Table III. We may take the value of $k_{2a}/(k_{1a} + k_{2a}) = 0.082 \pm 0.003$ as determined at 2650 Å[24] and the average value of the ratio $(k_{1b} + k_{2b})/(k_{1a} + k_{2a})$ from the published data summarized in Table II. With these and our present data we can estimate the intersystem crossing ratio; these results are shown in Table III also.†

---

*All error limits reported represent the 95% confidence limit (twice the standard deviation).

†In calculating the error limits for $k_{2b}/(k_{1b} + k_{2b})$, the error limits for $(k_{1b} + k_{2b})/(k_{1a} + k_{2a})$ were estimated by the difference between the average and the extreme values.

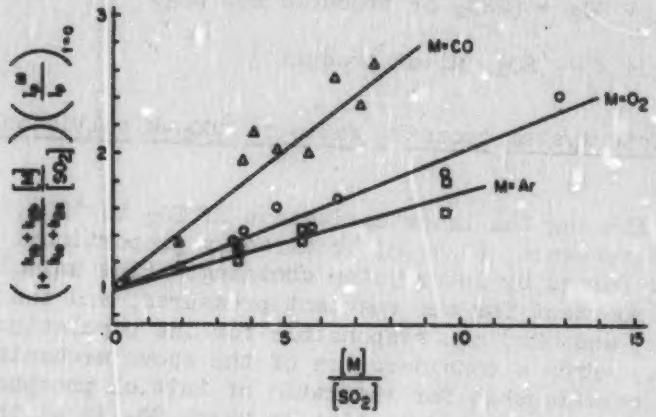

Figure 2. Plot of equation [B] for M = O_2, Ar, and CO. The slope of each plot is equal to k_{2b}/k_{2a} for the particular quenching gas. Data used are from Table I.

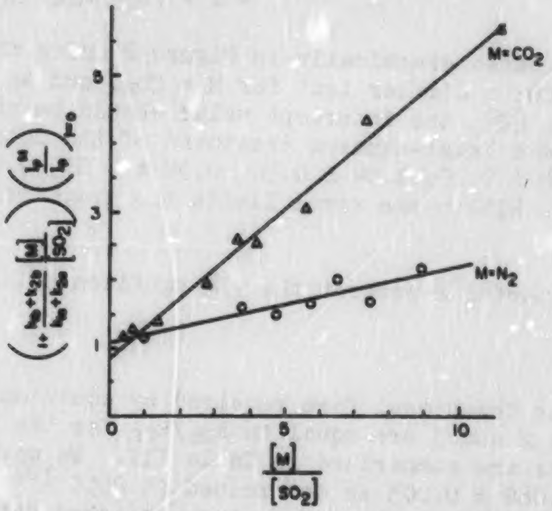

Figure 3. Plot of equation [B] for M = CO_2 and N_2. The slope of each plot is equal to k_{2b}/k_{2a} for the particular quenching gas. Data used are from Table I.

Table II. Relative $^1SO_2$ quenching efficiencies of various atmospheric gases: $(k_{1b} + k_{2b})/(k_{1a} + k_{2a})$.

Compound	Relative $^1SO_2$ quenching efficiency			
	Sidebottom et al.[a]	Mettee[b]	Rao et al.[c]	Horowitz et al.[d]
SO_2	1.0	1.0	1.0	1.0
Ar	0.28	0.21	—	—
N_2	0.30	0.28	—	0.29
O_2	0.31	0.27	0.31	—
CO	0.43	0.35	—	0.35
CO_2	0.71	0.63	0.74	—

[a] Reference 27

[b] Reference 28

[c] Reference 29

[d] Reference 24 and 22

The Effect of the nature of the collision partner on the intersystem crossing rate in excited singlet sulfur dioxide

Compare the estimates for k_{2b}/k_{2a} and $k_{2b}/(k_{1b} + k_{2b})$ for the various collision partners in Table III. These data support the earlier conclusions of Horowitz and Calvert which were based on much more limited data.[25] The individual rate constants for the collision-induced spin inversion of $^1SO_2$ increase significantly with the increase in the internal degrees of freedom of the collision partner; the values for k_{2b}/k_{2a} with M = Ar, O_2, N_2, CO, CO_2, SO_2, and cyclohexane are: 0.075, 0.11, 0.12, 0.21, 0.44, 1.0, and 1.1, respectively. However, the intersystem crossing ratio, $k_{2b}/(k_{1b} + k_{2b})$, is relatively less sensitive to the nature of the collision partner M; for M = Ar, O_2, N_2, CO, CO_2, SO_2, and cyclohexane, $k_{2b}/(k_{1b} + k_{2b})$ = 0.025, 0.030, 0.034, 0.045, 0.052, 0.082, and 0.073, respectively. The extent of the partitioning of the excited $^1SO_2$ between the alternative energy degradation paths of reactions (1) and (2) is probably controlled largely by the properties of the SO_2 molecule, that is, the relative density of states in the triplet and the singlet state manifolds near the vibronic level of the excited singlet and the extent of the mixing of the singlet and triplet states.

The efficiency of $^3SO_2$ formation in N_2- and CO-containing mixtures

The present estimates of k_{2b}/k_{2a} and $k_{2b}/(k_{1b} + k_{2b})$ for M = N_2, agree well with those of Horowitz and Calvert[25] who employed the triplet-sensitized biacetyl phosphorescent technique. However, the k_{2b}/k_{2a} ratio for M = CO reported here (excitation at 2662 Å) is significantly higher than that found previously using the biacetyl technique and excitation of SO_2 at 2875 Å. The reason for this difference is not clear. In view of the nitrogen data from the two studies and the apparent insensitivity of the $k_{2a}/(k_{1a} + k_{2a})$ to the wavelength of the exciting light for M = SO_2 (see Table III), it seems unlikely that the apparent discrepancy arises from the difference in wavelength employed in the two studies. The biacetyl method employed previously is very sensitive to the presence of oxygen

Table III. Summary of the relative $^3SO_2$ formation rate constants, k_{2b}/k_{2a}, and the intersystem crossing ratios, $k_{2b}/(k_{1b} + k_{2b})$, for various atmospheric gases at 25° C.

	k_{2b}/k_{2a}		$k_{2b}/(k_{1b} + k_{2b})$	
Gas	This work (2662 Å)	Previous work	This work (2662 Å)	Previous work
O_2	0.11 ± 0.02	—	0.030 ± 0.013	—
N_2	0.12 ± 0.05	0.10 ± 0.03 (2875 Å)^a	0.034 ± 0.029	0.033 ± 0.008 (2875 Å)^a
Ar	0.075 ± 0.021	—	0.025 ± 0.005	—
CO_2	0.44 ± 0.04	—	0.052 ± 0.014	—
CO	0.21 ± 0.06	0.063 ± 0.027 (2875 Å)^b	0.045 ± 0.028	0.017 ± 0.010 (2875 Å)^b
SO_2	1.0	1.0	0.082 ± 0.003 (assumed)	0.082 ± 0.003 (2650 Å)^c 0.095 ± 0.005 (2875 Å)^c 0.080 ± 0.014 (2875 Å)^d 0.09 (2963 Å)^e 0.10 (3020 Å)^e
$c\text{-}C_6H_{12}$	—	1.11 ± 0.37^a	—	0.073 ± 0.024^a

[a] From Horowitz and Calvert[25].

[b] From Wampler, Horowitz, and Calvert[21].

[c] From Horowitz and Calvert[24].

[d] From Rao, Collier, and Calvert[18].

[e] From Rao and Calvert[23].

impurity in the quenching gas employed. This is not a problem with quenching gases which can be condensed and degassed well. The removal of traces of O_2 from CO gas is not a simple matter, and as little as 1% of oxygen in the CO could cause the difference seen here. Although the stated analysis of the CO reagent used in the previous work did not suggest this extent of contamination, it may have been the source of the difference. In any case the present value of $k_{eb}/(k_{ib} + k_{eb})$ is relatively insensitive to oxygen impurity in the reactants, and for this reason it is considered to be more reliable data for the case of CO as the quenching gas.

The "excess" triplet in the 3130 Å-irradiated SO_2-CO mixtures at high pressures

In view of the present more reliable estimates of $k_{eb}/(k_{ib} + k_{eb})$ for M = CO, a reevaluation should be made of the relative importance of the previously reported "excess" triplet SO_2 reactant leading to CO_2 in the 3130 Å-irradiated SO_2-CO mixtures at high pressures[21,22]. We estimate that the quantum yield of CO_2 from the $^3SO_2$ species derived only from the $^1SO_2$ precursor may be as high as 4.3×10^{-3} in experiments at high $[CO]/[SO_2]$ ratios; our previous data suggested a maximum of 2.0×10^{-3}. Our previous work showed that the excited singlet SO_2 will contribute about 1.4×10^{-3} to the total ϕ_{CO_2} value at high $[CO]/[SO_2]$ ratios. The total measured quantum yields of CO_2 from the 3130 Å-irradiated SO_2-CO mixtures exceed the sum of these maximum triplet and singlet yields (5.7×10^{-3}) in experiments at high $[CO]/[SO_2]$ ratios and at pressures of CO above about 100 torr. Thus it remains necessary to invoke an additional source of triplet molecules in runs at pressures above 100 torr, but the importance of this source is somewhat less than we[22] and Cehelnik et al.[21] had suggested in the earlier studies.

The theoretical maximum rates of SO_2 photo-oxidation in sunlight-irradiated SO_2-containing atmospheres

The present data allow an improved estimate of the rate of $^3SO_2$ generation in the sunlight-irradiated atmosphere of the earth[30]. For a relatively dry atmosphere, the effective intersystem crossing ratio will be about 0.033. In making our previous estimate we used the only intersystem crossing data then available, which was for M = SO_2 in reaction (2b), $k_{eb}/(k_{ib} + k_{eb}) = 0.09$. Use of the more appropriate present rate constant data will result in values for the theoretically maximum rates of $^3SO_2$ formation from (2b) which are roughly one third lower than those estimated previously from the less complete information. However, the additional "high pressure" mechanism of triplet sulfur dioxide formation must be present at the pressure of the atmosphere and must now be included in any revised quantitative treatment of the problem. Our recent work suggests that the rate of triplet generation from this source is roughly two to three times that formed in reaction (2b) in air. A more sophisticated estimate of the theoretical maximum SO_2 photo-oxidation rates is possible utilizing our results outlined in our further work described in the following section.

I-B. A Study of the Nature of the SO_2 Excited States Formed at High Added Gas Pressures.[31]

Recently, some very interesting and unexpected observations concerning the nature of the excited states of SO_2 have been made using irradiated SO_2-CO mixtures. Jackson and Calvert[32] generated ${}^3SO_2$ by direct absorption within the forbidden ${}^3B_1 \leftarrow {}^1A_1$ band (3400-3970 Å) of SO_2; the ${}^3SO_2$ molecules were found to be rather efficient reactants with CO to form CO_2 for these conditions. However, Cehelnik, Spicer, and Heicklen[21] observed that the kinetics of the formation of CO_2 in SO_2-CO mixtures irradiated within the first allowed band of SO_2 at 3130 Å required the participation of reactive states of SO_2 in addition to the ${}^3SO_2$ species. At high CO pressures, there was an "excess" of CO_2 product formation which exceeded that anticipated from the measured rate constants for the ${}^1SO_2$ and ${}^3SO_2$ states. Cehelnik et al.[21] invoked as reactants both the emitting singlet and triplet states as well as two new nonemitting excited states of SO_2. Wampler et al[22] reinvestigated this system and confirmed most of the observations of Cehelnik et al[21]; however, some key differences in the results led these workers to interpret their results in terms of the involvement of the ${}^1SO_2$ and ${}^3SO_2$ states plus one additional nonemitting state of SO_2; this species was not a reactant to form CO_2, but was an additional source of ${}^3SO_2$ generated at high added-gas pressures.

In this phase of our work, we have attempted to gain further insight into the nature of the intermediate states involved in SO_2 photochemistry which might allow a more definitive test of the mechanistic alternatives in the photochemistry of SO_2-CO mixtures. We have employed biacetyl as a triplet energy acceptor in 2875 Å-irradiated mixtures of SO_2, biacetyl, and added gases (CO_2, CO, or N_2). In other experiments, the wavelength dependence of the intensity of the sensitized emission has been determined at varied added-gas pressures. The kinetic functions which define the quantum yields of the sensitized phosphorescence emission in biacetyl provide interesting new details of the mechanism of SO_2 photochemistry.

I-B—1. Experimental Methods and Results

Equipment

The absolute spectrofluorometer of Turner (Model 210) was used in all of these studies. The SO_2 was excited at 2875 Å using a band width of 150 Å; the triplet biacetyl emission was scanned using a 250 Å band width. The same band widths were employed in the determination of the excitation spectra. Biacetyl excited at 4350 Å was used as a standard for the quantum yield determinations as described previously[33].

The quantum yields of the 2875 Å-excited SO_2-sensitized phosphorescence of biacetyl (ϕ_{sens}) were measured at several SO_2 and Ac_2 reactant concentrations and added CO_2 pressures (25-750 torr). The results from several series of experiments carried out at constant SO_2 and CO_2 concentrations and room temperature (~ 25° C) are reported in Table IV. Several other series of experiments were made with SO_2-Ac_2-CO_2 mixtures in which the concentration ratio of the three components was kept constant in a given series; these are given in Table V. The results from similar series of experiments using SO_2-Ac_2-CO and SO_2-Ac_2-N_2 mixtures at constant concentration ratios are summarized in Table VI.

For our experimental conditions, no biacetyl emission could be detected in the direct 2875-Å excitation of Ac_2 in a mixture containing $[CO_2] = 3 \times 10^{-2}$ and $[Ac_2] = 1 \times 10^{-4}$ M; it is clear that the second excited singlet state of biacetyl was not stabilized measurably against dissociation, even at the highest pressures of added gas employed here.

Table IV. The 2875 Å-excited SO_2-sensitized phosphorescence of biacetyl in Ac_2-SO_2-CO_2 mixtures at room temperature; constant pressure experiments

$[Ac_2]$, $M \times 10^6$	$\Phi_{em} \times 10^3$ $4 \times 10^{-3} M$[a]	$10 \times 10^{-3} M$[a]	$25 \times 10^{-3} M$[a]	$40 \times 10^{-3} M$[a]
2	2.25	2.23	1.84	2.05
3	2.87	2.65	2.32	2.48
4	3.20	3.30	3.23	3.41
7	4.07	4.64	4.74	6.35
10	5.04	5.32	5.94	6.75 (6.56)[b]
50	7.75	8.54	10.35	13.84
100	9.08	9.19	11.54	14.1

[a] CO_2 concentration, $[CO_2]$.

[b] $[SO_2] = 1.0 \times 10^{-4}$ M in all cases except for this run, in which $[SO_2] = 1.0 \times 10^{-5}$ M.

Table V. 2875 Å-excited SO_2-sensitized phosphorescence of biacetyl in Ac_2-SO_2-CO_2 mixtures at room temperature; constant reactant ratio experiments

$[CO_2]$, $M \times 10^3$	$\Phi_{em} \times 10^3$ 0.75×10^{-3a}	1.00×10^{-3a}	1.75×10^{-3a}	2.50×10^{-3a}	12.5×10^{-3a}	25.0×10^{-3a}
1.36	1.88	1.90	3.02	3.28	5.43	6.88
1.63	1.98	2.13	3.22	3.47	5.83	7.03
2.14	2.12	2.36	3.21	3.86	6.30	7.48
2.56	2.29	2.60	3.40	4.14	6.63	7.87
3.34	2.60	2.88	3.77	4.62	7.21	8.43
4.00	2.87	3.20	4.07	5.04	7.75	9.08
	$\Phi_{em} \times 10^3$ 0.50×10^{-4b}	1.00×10^{-4b}	1.75×10^{-4b}	2.50×10^{-4b}	12.5×10^{-4b}	25.0×10^{-4b}
5.55	—	—	—	—	—	3.28
6.65	—	—	—	—	—	3.74
8.72	—	—	—	2.11	5.65	6.66
10.4	—	—	—	2.51	6.29	8.24
13.6	—	—	2.59	2.99	7.32	8.35
16.3	—	1.59	2.99	3.47	8.19	9.05
21.4	1.16	2.04	3.67	4.15	9.59	10.4
25.6	1.39	2.37	4.29	4.93	10.5	11.4
33.4	1.70	2.94	5.44	5.93	12.4	12.8
40.0	2.05	3.41	6.35	6.75	13.8	14.1

[a] $[Ac_2]/[CO_2]$ ratio; $[CO_2]$ in the low concentration region; $[SO_2]/[CO_2] = 2.52 \times 10^{-2}$ throughout the low concentration series.

[b] $[Ac_2]/[CO_2]$ ratio; $[CO_2]$ in the high concentration region; $[SO_2]/[CO_2] = 2.50 \times 10^{-3}$ throughout the high concentration series.

Table VI. The 2875 Å-excited SO_2-sensitized phosphorescence of biacetyl in Ac_2-SO_2-CO and Ac_2-SO_2-N_2 mixtures in experiments at constant concentration ratio[a]

[CO], $M \times 10^3$	$\Phi_{sens} \times 10^3$	[N_2], $M \times 10^3$	$\Phi_{sens} \times 10^3$
3.13	4.71	3.56	4.56
3.76	4.96	4.21	4.92
4.91	5.60	5.40	5.44
5.87	5.98	6.58	6.02
7.70	6.36	8.39	6.63
9.20	7.11	10.3	7.14
12.0	7.57	13.5	8.02
14.8	8.18	16.1	8.63
18.8	9.60	21.0	9.74
22.5	9.76	25.2	10.4

[a] The reactant concentration ratio was held constant in a given series of runs: [CO]: [SO_2]:[Ac_2], 225:1:1; [N_2]:[SO_2]:[Ac_2], 252:1:1.

The effect of excitation wavelength on Φ_{sens} was determined in various SO_2-Ac_2-CO_2 mixtures using a 150-Å band width. These data are summarized in Figure 4 together with the absorption spectrum of SO_2 determined at the same excitation band width (150 Å).

I-B-2. Discussion

The "excess" biacetyl phosphorescence from 2875 Å-irradiated SO_2-biacetyl mixtures at high added-gas pressures; deficiencies in the "low pressure" SO_2 photolysis mechanism

The previously proposed mechanism of SO_2 photochemistry[18] has been found to be quantitatively consistent with the results of the SO_2 emission studies reported to date[34-42]; however, because of the very large second-order quenching rate constants for the $^1SO_2$ species ($\sim 10^{10} - 10^{11}$ l./mole-sec), the previous studies were necessarily carried out at relatively low total gas pressure ($P <$ 10 torr) in order to allow detection of the weak singlet emission. This "low pressure" mechanism and the measured rate constants require that the only significant triplet-SO_2 formation for experiments above about 1 torr arise in the second order reaction (2):

(I) $$SO_2 + h\nu\ (2400\text{-}3200\ Å) \rightarrow {}^1SO_2$$

(1) $$^1SO_2 + M \rightarrow (SO_2\text{-}M)$$

(2) $$^1SO_2 + M \rightarrow {}^3SO_2 + M$$

When the concentration of added gas M is relatively high and biacetyl (Ac_2) is added to the SO_2-M mixture, as in this work, then the first-order decay reactions of the $^1SO_2$ and $^3SO_2$ are unimportant and only the following reactions of the $^3SO_2$ and Ac_2 are expected to occur following reaction (2):

(6) $^{3}SO_2 + M \rightarrow SO_2 + M$ (or products)

(7) $^{3}SO_2 + Ac_2 \rightarrow {}^{3}Ac_2 + SO_2$

(8) $^{3}Ac_2 \rightarrow Ac_2 + h\nu_p$

(9) $^{3}Ac_2 \rightarrow Ac_2$

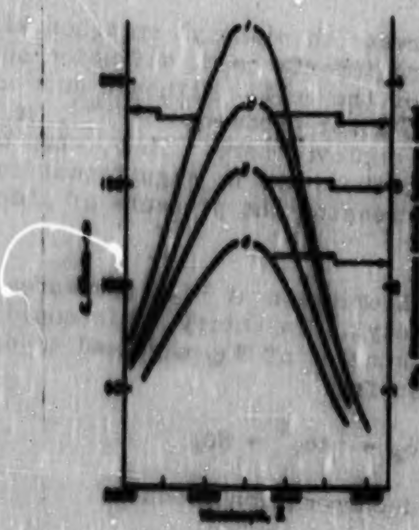

Figure 4. Absorption spectra of SO_2 (curve 1) and excitation spectra of biacetyl phosphorescence emission measured at 5120 Å as excited in irradiated SO_2-Ac_2-CO_2 mixtures; curve 2: $[SO_2] = 1.0 \times 10^{-4}$ M, $[Ac_2] = 2.0 \times 10^{-5}$ M, $[CO_2] = 2.0 \times 10^{-2}$ M; curve 3: $[SO_2] = 1.0 \times 10^{-4}$ M, $[Ac_2] = 2.0 \times 10^{-6}$ M, $[CO_2] = 0.0$ M; curve 4: $[SO_2] = 1.0 \times 10^{-4}$ M, $[Ac_2] = 5.0 \times 10^{-5}$ M, $[CO_2] = 2.0 \times 10^{-2}$ M. For all these measurements, the excitation and emission band widths were set at 150 and 250 Å, respectively; the ordinate for emission intensity is in arbitrary units which are different for each of the curves 2, 3, and 4.

In terms of this mechanism of the irradiated SO_2-Ac_2-M system and for our present conditions of essentially complete quenching of the $^{1}SO_2$ by added gas M, relation (A) should describe the quantum yield of the sensitized biacetyl emission (Φ_{sens}):

$$\frac{1}{\Phi_{sens}} = \left(\frac{k_1 + k_2}{k_2}\right)\left(1 + \frac{[M]k_6}{[Ac_2]k_7}\right)\left(\frac{k_8 + k_9}{k_8}\right) \qquad (A)$$

Thus, for experiments at constant $[M]/[Ac_2]$ ratio, we expect Φ_{sens} to be independent of the added gas pressure. Note in Table V that at the high gas concentrations employed here (up to 4×10^{-2} M), the expectations of the above "low pressure" mechanism are not borne out. Furthermore, for experiments at fixed $[SO_2]$ and $[Ac_2]$, one expects from relation (A) that the Φ_{sens} would decrease as the pressure of the added gas in increased. The data of Table IV do not support this prediction either; the Φ_{sens} continues to rise as the total pressure of the gas mixture is increased. Although the simple mechanism outlined in (I), (1), (2), and (6)-(9) is followed well at low gas pressures[39,40], obviously it is not a sufficiently complete mechanism to account for the results obtained here at high pressures (up to 1 atm).

There are two possible trivial sources of these unusual results which should be evaluated before considering other more sophisticated alternative mechanisms:

1. Conceivably, the increase in biacetyl emission with increasing pressure could result from the decreasing importance of diffusion and deactivation of biacetyl triplets at the wall of the cell. Although such an effect has been observed in experiments at much lower pressure[33,39,40], we have found that it is unimportant for the conditions employed here. Thus, when biacetyl was excited by direct absorption at 4350 Å, there was no significant increase in quantum yield of phosphorescence on increasing the pressure of added gas from 70 to 700 torr.

2. The "excess" biacetyl emission at high pressures might arise from a reaction between ${}^1SO_2$ and biacetyl. In theory, this could occur by either of two paths. First, an excited singlet of SO_2 may lead to excited singlet of biacetyl by singlet energy transfer:

(10) $${}^1SO_2 + Ac_2 \rightarrow {}^1Ac_2^{\ddagger} + SO_2$$

(11) $${}^1Ac_2^{\ddagger} \rightarrow \text{decomposition products}$$

(12) $${}^1Ac_2^{\ddagger} + M \rightarrow {}^1Ac_2 + M$$

(13) $${}^1Ac_2 \rightarrow {}^3Ac_2$$

There is good overlap between the 2400-3200 Å absorption band of SO_2 and the absorption band corresponding to the second excited singlet of Ac_2. If relaxation of the ${}^1SO_2$ is unimportant, we would expect energy transfer of this type to form biacetyl in the second excited singlet state (${}^1Ac_2^{\ddagger}$), reaction (10). Presumably the excess emission seen at high added-gas pressures could have arisen as a result of vibrational and electronic energy dissipation through collisions which would ultimately populate the lowest triplet of biacetyl, reactions (12) and (13). This hypothesis cannot be correct either, since we have found that the direct excitation of biacetyl within its second allowed absorption region (2200-3200 Å) produces no detectable emission even when 760 torr of added gas is present; obviously, $k_{11} \gg k_{12}[M]$ even at high $[M]$.

Alternatively, one may assume that at the very high inert gas pressures employed here, the ${}^1SO_2$ which survive the electronic quenching collisions with M and finally encounter biacetyl molecules are vibrationally relaxed to near the lowest vibrational level of the excited singlet (~ 3370 Å). Thus, singlet energy transfer for these circumstances will form singlet biacetyl equivalent to that generated by light absorption within the first excited singlet band of Ac_2; in this case, vibrational quenching of the initially dissociative state is significant, although for 3340 Å-excited Ac_2, stablization of ${}^1Ac_2^{\ddagger}$ is only ~ 80% at 1 atm of quenching gas. Taking the relative rate constants for ${}^1SO_2$

quenching by SO_2, CO_2, and biacetyl (1.00, 0.73[38], and 1.75[43], respectively) and $k_6/(k_5 + k_6) = 0.15$[44], we estimate that the maximum contribution of singlet energy transfer to the measured Φ_{sens} must be less than 7×10^{-4} when $[CO_2] = 4 \times 10^{-2}$ and $[Ac_2] = 1 \times 10^{-4}$ M; the observed Φ_{sens} is 1.4×10^{-2} for these conditions. Thus we must conclude that although as much as 5% of the observed Φ_{sens} may result from singlet energy transfer for these conditions, it cannot be the dominant source of "extra" biacetyl phosphorescence in these experiments.

Further support for this conclusion is had from the observed wavelength independence of the Φ_{sens} in SO_2-Ac_2 and SO_2-Ac_2-CO_2 mixtures (see the excitation spectra shown in Fig. 4). Note the wavelength dependence of the $^3Ac_2$ phosphorescence intensity is the same for a mixture of $[SO_2] = 1.0 \times 10^{-4}$, $[Ac_2] = 2.0 \times 10^{-6}$ M as that for the same mixture with $[CO_2] = 2 \times 10^{-2}$ M added; furthermore, each spectrum mirrors the dependence of SO_2 absorption on wavelength. This effect can be appreciated in a more quantitative fashion by inspection of the data of Table VII; although the absolute quantum yields of sensitized biacetyl phosphorescence increase significantly with increase in pressure at a given wavelength (see Table IV), there is no significant wavelength variation of the Φ_{sens} values for experiments at either a fixed high pressure or a fixed low pressure (see Table VII). If singlet energy transfer were important here, one would expect to see a significant increase in the ratio of Φ_{sens} at 2650 Å in the high-pressure runs compared to the same ratio from the low-pressure experiments. Obviously this is not the case.

A second possible alternative source of $^3Ac_2$ in these experiments is the intersystem crossing reaction (2) with Ac_2 acting as M. It is difficult to determine this ratio accurately since singlet energy transfer can be important if the $[Ac_2]$ represents an appreciable fraction of the quenching medium present, and the two reactions have identical kinetics with respect to $[^1SO_2]$ and $[Ac_2]$. It appears that at most 17% of the singlet SO_2 molecules quenched by collisions

---

Table VII. The effect of excitation wavelength on the quantum yield of SO_2-sensitized phosphorescence excited in SO_2-Ac_2-CO_2 mixtures

Excitation wavelength, Å	Φ_{sens} relative[a]		
	$[SO_2]$: 1.0×10^{-4} *M* $[Ac_2]$: 2.0×10^{-6} *M* $[CO_2]$: 0.0	1.0×10^{-4} *M* 2.0×10^{-6} *M* 2.0×10^{-2} *M*	1.0×10^{-4} *M* 5.0×10^{-6} *M* 2.0×10^{-2} *M*
2650	1.07	0.97	1.09
2700	1.03	0.95	1.00
2800	1.00	1.00	0.99
2900	1.00	1.00	1.00
3000	1.06	1.03	1.04
3100	1.07	1.14	1.06
3150	1.01	1.15	1.04

[a] The Φ_{sens} values are normalized for each series of runs at a given concentration of reactants by taking the value at 2900 Å as unity; all the values were determined by dividing the measured value of the sensitized biacetyl phosphorescence intensity by the apparent ϵ for these conditions (see Fig. 4).

with biacetyl are converted to $^3SO_2$ in reaction (2)[43,45]. Even with the most favorable conditions which we employed for SO_2 quenching by Ac_2, $[CO_2] = 4 \times 10^{-3}$ M and $[Ac_2] = 1 \times 10^{-4}$ M, the maximum quantum yield of sensitized emission from biacetyl would be about 1.4×10^{-3}. For the higher concentration conditions employed, $[CO_2] = 4 \times 10^{-2}$ M and $[Ac_2] = 1 \times 10^{-4}$ M, the maximum contribution to the measured Φ_{sens} from this effect will be 1.5×10^{-4}, about 100 times lower than the observed quantum yield for these conditions.

In summary, it appears to us that the observed "excess" biacetyl triplet emission, seen here in experiments at high added-gas pressures, cannot be rationalized by invoking singlet energy transfer, enhanced intersystem crossing in (2) with Ac_2 as M, or, for that matter, any other possible mechanistic feature which involves only the emitting $^1SO_2$ and $^3SO_2$ species. Recourse to the somewhat unusual mechanisms such as those invoked by Cehelnik et al.[21] and Wampler et al.[22] seems necessary.

Treatment of the data in terms of the Wampler, Horowitz, Calvert mechanism of "excess" triplet formation in SO₂ at high added-gas pressures

It is instructive to consider the present results in terms of the two alternative mechanisms for "excess" triplet SO_2 formation in these SO_2-added gas systems at high pressure. Consider first that suggested by Wampler, Horowitz, and Calvert[22]:

(I) $SO_2 + h\nu\ (2400\text{–}3200\ \text{Å}) \rightarrow {}^1SO_2$

(1) ${}^1SO_2 + M \rightarrow (SO_2\text{—}M)$

(2) ${}^1SO_2 + M \rightarrow {}^3SO_2 + M$

(3) ${}^1SO_2 + M \rightarrow X + M$

(4) $X + M \rightarrow {}^3SO_2 + M$

(5) $X \rightarrow SO_2$ (or nonemitting product)

(6) ${}^3SO_2 + M \rightarrow (SO_2\text{—}M)$ (or products)

(7) ${}^3SO_2 + Ac_2 \rightarrow SO_2 + {}^3Ac_2$

(8) ${}^3Ac_2 \rightarrow Ac_2 + h\nu_p$

(9) ${}^3Ac_2 \rightarrow Ac_2$

X in the sequence represents some unidentified species derived from $^1SO_2$. Presumably it could be an excited, nonemitting singlet state of SO_2 or one of its unstable geometrical isomers (S-O-O, 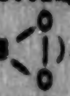). It cannot be a nonemitting triplet state of SO_2 which could transfer energy to Ac_2. For the conditions employed here, practically all of the $^1SO_2$ molecules are quenched by the added gas M (CO_2, CO, or N_2). The steady-state treatment of the above sequence for these conditions leads to relation (B):

$$(B)\qquad \frac{1}{\Phi_{sens}} = \left[\frac{(k_1 + k_2 + k_3)(k_4[M] + k_5)(k_8 + k_9)}{(k_2k_5 + k_2k_4[M] + k_3k_4[M])k_8}\right]\left[\frac{k_6[M]}{k_7[Ac_2]} + 1\right]$$

Thus, at constant [M], $1/\Phi_{sens}$ should be linear in $1/[Ac_2]$. A test of this dependence is shown in Figure 5 for the data of Table IV at $[CO_2] = 2.5 \times 10^{-2}$ M, $[SO_2] = 1.0 \times 10^{-4}$ M. The data appear to follow well the expected relation. In fact, each series of runs at other constant CO_2 concentrations also fit the the expected linear relation demanded by relation (B). The parameters which describe the least-squares lines of these plots are summarized in Table VIII. According to the functional dependence of (B), the ratio of slope to intercept

---

Table VIII. Summary of parameters derived from the plots of $1/\Phi_{sens}$ versus $1/[Ac_2]$ from experiments at various fixed pressures of CO_2[a].

$[CO_2]$, $M \times 10^3$	Slope, $M \times 10^4$	Intercept $\times 10^{-1}$	Slope/Intercept, $M \times 10^6$	$(k_8/k_7) \times 10^4$
4.0	6.7 ± 0.9	13 ± 2	5.2 ± 1.1	12 ± 3
10.0	7.2 ± 0.8	11 ± 2	6.5 ± 1.4	6.2 ± 1.3
25.0	9.4 ± 0.1	7.7 ± 0.4	12.2 ± 0.7	4.8 ± 0.3
40.0	9.1 ± 1.2	5.7 ± 3.0	16 ± 9	4.0 ± 2.2

[a] In each series of experiments, $[SO_2] = 1.0 \times 10^{-4}$ M; data were estimated by least-squares methods from Figure 4 and similar plots using the data of Table IV. Error limits shown represent the 95% confidence limits (twice the standard deviation), assuming only random errors are present in the data.

---

from plots of the data of Table IV should be given by relation (C):

$$(C) \qquad \left[\frac{\text{slope}}{\text{intercept}}\right]_{\text{Fig. 5}} = \frac{k_8[M]}{k_7}$$

Values of $(k_8/k_7) \times 10^4$ estimated from relation (C) and the slope/intercept ratios for each series of data for a given M are: 12 ± 3, 6.2 ± 1.3, 4.8 ± 0.3, and 4.0 ± 2.2; the average of these estimates gives $k_8/k_7 = (6.8 \pm 5) \times 10^{-4}$, where $M = CO_2$. This estimate checks reasonably well with the more accurate estimate of k_8/k_7 which can be calculated from the individual rate constants determined using the measured lifetime data for $^3SO_2$ directly excited by 3829-Å laser pulses; for $M = CO_2$, $k_8 = (1.14 \pm 0.07) \times 10^{8}$[21]; $k_7 = (1.4 \pm 0.1) \times 10^{11}$ l./mole-sec[22]; thus, $k_8/k_7 = (8.1 \pm 0.8) \times 10^{-4}$. It is not clear whether the apparent trend in the k_8/k_7 values with increasing pressure is real or a conquence of the necessarily high uncertainty which is inherent in the phosphorescence data and the slope/intercept method of treating these data to derive k_8/k_7. It seems to us that the latter explanation is most realistic. The data appear to add credence to the kinetic interpretation of "excess" triplet proposed by Wampler et al[22]. However, one should consider the present results in terms of the alternative mechanism of Cehelnik et al. before any reasonable conclusions between alternatives is made.

Treatment of the present data in terms of the Cehelnik, Spicer, Heicklen mechanism of SO_2 photochemistry at high added-gas pressures

The major differences between the SO_2 photolysis mechanism of Wampler et al[22] and that proposed by Cehelnik et al.[21] lies in the involvement of new excited

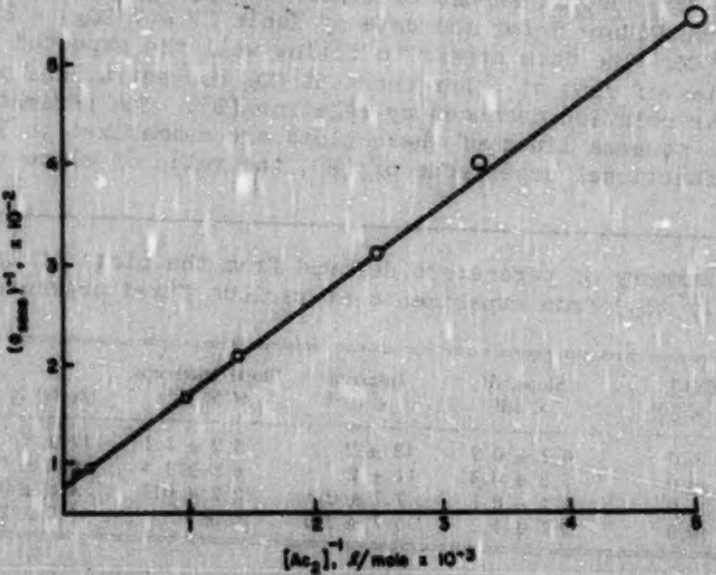

Figure 5. Plot of $1/\Phi_{sens}$ vs. $1/[Ac_2]$ for data from SO_2-Ac_2-CO_2 mixture photolyses at 2875 Å; $[SO_2] = 1.0 \times 10^{-4}$ M, $[CO_2] = 2.5 \times 10^{-2}$ M.

singlet ($SO_2{}^{*}$) and triplet ($SO_2{}^{**}$) species which are presumed to be some non-emitting excited states, possibly the $SO_2(^1A_2)$ and $SO_2(^3A_2)$ unidentified states of SO_2. Their mechanism for our experimental conditions of high [M] may be represented as follows:

(I) $SO_2 + h\nu\ (2400\text{-}3200\ Å) \rightarrow {}^1SO_2$

(1) ${}^1SO_2 + M \rightarrow (SO_2\text{-}M)$ (or products)

(2) ${}^1SO_2 + M \rightarrow {}^3SO_2 + M$

(10) ${}^1SO_2 + M \rightarrow SO_2{}^{*} + M$

(6) ${}^3SO_2 + M \rightarrow SO_2 + M$ (or products)

(11) $SO_2{}^{*} \rightarrow SO_2{}^{**}$

(12) $SO_2{}^{*} + M \rightarrow SO_2 + M$ (or products)

(13) $SO_2{}^{*} + M \rightarrow SO_2{}^{**} + M$

(14) $SO_2{}^{**} \rightarrow SO_2$

(15) $SO_2{}^{**} + M \rightarrow SO_2 + M$ (or products)

(7) ${}^3SO_2 + Ac_2 \rightarrow SO_2 + {}^3Ac_2$

(16) $SO_2{}^{**} + Ac_2 \rightarrow SO_2 + {}^3Ac_2$

(8) ${}^3Ac_2 \rightarrow Ac_2 + h\nu_p$

(9) ${}^3Ac_2 \rightarrow Ac_2$

There is not a complete correspondence between the SO_2^* of this mechanism and the X species of the Wampler mechanism although it might appear so at first sight. X does not generate triplet species unimolecularly as in (11), and it is not a reactant with CO as postulated by Cehelnik et al for the SO_2^* species. Presumably, the two triplet species, $^3SO_2$ and SO_2^{**}, can transfer triplet energy to Ac_2, and the expected relation of Φ_{sens} for this case is given by relation (F):

$$(F)\quad \Phi_{sens} = \left(\frac{k_8}{k_8 + k_9}\right)\left[\left(\frac{k_2}{k_1 + k_2 + k_{10}}\right)\left(\frac{[Ac_2]k_7}{[Ac_2]k_7 + [M]k_6}\right) + \left(\frac{k_{10}}{k_1 + k_2 + k_{10}}\right)\left(\frac{k_{11} + k_{12}[M]}{k_{11} + (k_{12} + k_{13})[M]}\right)\left(\frac{[Ac_2]k_{15}}{[Ac_2]k_{15} + [M]k_{16} + k_{14}}\right)\right]$$

The experimentally observed linear form of the $1/\Phi_{sens}$-versus-$1/[Ac_2]$ plot can be expected only if both the following equalities hold:

$$k_7 = \{k_{11} + (k_{12} + k_{13})[M]\}k_{15}$$

$$[M]k_6 = \{k_{11} + (k_{12} + k_{13})[M]\}\,([M]k_{16} + k_{14})$$

Although this fortuitous match of rate functions may occur at a given [M], a perfect match cannot occur at more than one [M] value unless certain peculiar inequalities exist: $k_{11} \gg (k_{12} + k_{13})\,[M]$ and $[M]\,k_{16} \gg k_{14}$. However, these conditions are not tenable. If reaction (11) were the dominant fate of SO_2^* at all [M] values, then one would not see the increase in SO_2^{**}, and the experimentally required increase in Φ_{sens} as [M] is increased. The experimental fact is that the $1/\Phi_{sens}$-versus-$1[Ac_2]$ plot is a straight line within the experimental error for values of [M] varied over a factor of 10 (4×10^{-3} to 40×10^{-3} M). Thus, it appears to us that the Cehelnik mechanism cannot explain the present results.

The nature of the intermediate X species involved in SO_2 photochemistry at high added-gas pressures

In terms of the Wampler et al. mechanism outlined above, we can treat the present data to derive kinetic constants for the reactions of the species X. From relation (D),

$$(D)\quad \Phi_{sens}^{(2)} = \left(\frac{k_2}{k_1 + k_2 + k_3}\right)\left(\frac{k_8}{k_8 + k_9}\right)\left(\frac{1}{(k_6[M]/[Ac_2]k_7) + 1}\right)$$

we may estimate that part of the quantum yield of biacetyl phosphorescence which is derived from $^3SO_2$ formed in reaction (2). We would expect from relation (D) that the value of $\Phi_{sens}^{(2)}$ will be a constant for a given series of experiments at constant $[M]/[Ac_2]$. Combining relations (B) and (D), equation (E) results:

$$(E)\quad \frac{1}{\Phi_{sens} - \Phi_{sens}^{(2)}} = \left(1 + \frac{k_5}{k_4[M]}\right)\left(\frac{k_1 + k_2 + k_3}{k_3}\right)\left(\frac{k_8 + k_9}{k_8}\right)\left(1 + \frac{k_6[M]}{k_7[Ac_2]}\right)$$

Thus, the Wampler et al. mechanism predicts a linear relation between $1/(\Phi_{sens} - \Phi_{sens}^{(2)})$ and $1/[M]$ for runs at constant $[M]/[Ac_2]$ ratio. The data of Table V may be used to estimate some of the kinetic parameters in (E). The most reliable data to test this function are those from the highest biacetyl concentration. For these conditions, any error in the value k_6/k_7 used has a minimum effect on the $\Phi_{sens}^{(2)}$, see relation (D). Results of this treatment are shown in Figure 6 for CO_2 as M in Figure 7 for M = CO or N_2. If $\Phi_{sens}^{(2)}$ is assumed to be zero, the curved function (defined by the squares in Figs. 6 and 7) is obtained. For a certain choice of $\Phi_{sens}^{(2)}$, the best least-squares straight line (defined by the circles in Figs. 6 and 7) was found. The values of $\Phi_{sens}^{(2)}$ obtained in this fashion are summarized in Table IX for M = CO_2, CO, and N_2. These estimates may be coupled with the values of $k_8/(k_8 + k_9) = 0.15$[44,33], and the most reliable estimate of $k_8/k_7 = (8.1 \pm 0.8) \times 10^{-4}$[41,42] to derive from relation (D) new estimates of the intersystem crossing ratio, $k_2/(k_1 + k_2 + k_3)$. These data and values of the intercepts and slopes of the linear plots in Figs. 6 and 7 provide the additional rate constant ratios $k_3/(k_1 + k_2 + k_3)$ and k_5/k_4. From these estimates, we can calculate as well the ratio $k_1/(k_1 + k_2 + k_3)$. All of these rate constant data are summarized in Table IX for the three different M species employed in this work.

The present estimates of $k_2/(k_1 + k_2 + k_3)$ may be compared to those derived previously from the low-pressure experiments of very different kinetic treatment. In the earlier work[40,46], a significant correction for $^3Ac_2$ destruction at the wall was necessary[39,40]. We find here for M = CO_2, CO, and N_2, respectively,

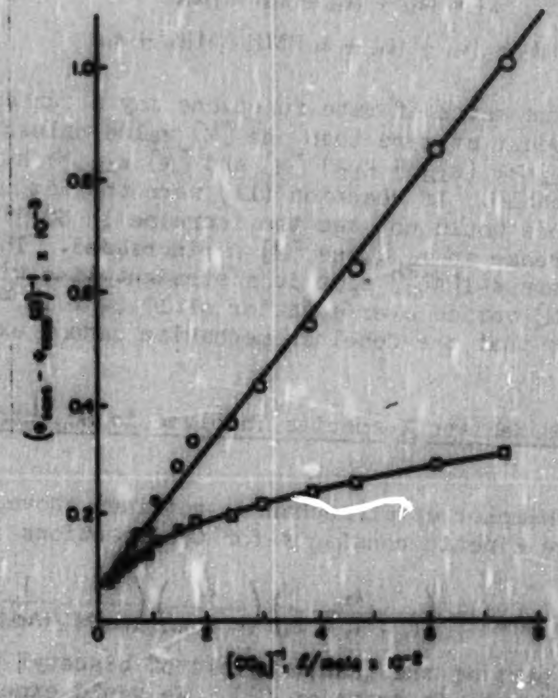

Figure 6. Plot of $1/(\Phi_{sens} - \Phi_{sens}^{(2)})$ vs. $1/[CO_2]$. Data are from the SO_2-Ac_2-CO_2 mixture photolyses at 2875 Å; $[CO_2]/[Ac_2]$ = 400; $[SO_2] = 1.0 \times 10^{-5}$ M; circles, $\Phi_{sens}^{(2)} = 2.3 \times 10^{-3}$; squares, $\Phi_{sens}^{(2)} = 0$.

Table IX. Kinetic parameters related to the reactions of the $^1SO_2$ and X species formed in the 2875 Å-irradiation of SO_2-Ac_2 mixtures with added CO_2, CO, or N_2 gases at high pressures.[a]

	M = CO_2		M = CO		M = N_2	
Slope, M (Figs. 6 or 7)	1.3	± 0.2	1.4	± 0.2	1.5	± 0.3
Intercept (Figs. 6 or 7)	65	± 10	50	± 12	72	± 10
$\Phi_{sens}^{(2)} \times 10^3$	2.3	± 0.3	2.8	± 0.4	2.5	± 0.3
$k_2/(k_1 + k_2 + k_3)$	0.020	± 0.010	0.021	± 0.010	0.019	± 0.010
$k_3/(k_1 + k_2 + k_3)$	0.14	± 0.02	0.085	± 0.012	0.11	± 0.02
$k_1/(k_1 + k_2 + k_3)$	0.84	± 0.03	0.89	± 0.02	0.86	± 0.03
k_5/k_4, mole/l.	0.020	± 0.004	0.016	± 0.005	0.021	± 0.005

[a] Error limits in most cases represent twice the standard deviation as determined by the method of least squares, assuming only random errors in the data. For the $k_2/(k_1 + k_2 + k_3)$ estimates, the errors are based on reasonable estimates of the sensitivity of the linear fit to the choice in $\Phi_{sens}^{(2)}$ and the other uncertainties in the method employed here.

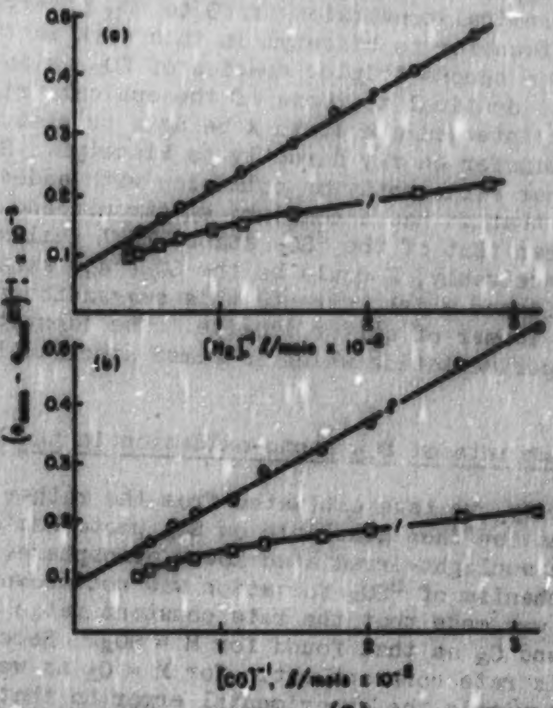

Figure 7. Plot of $1/(\Phi_{sens} - \Phi_{sens}^{(2)})$ vs. $1/[N_2]$ (a), or vs. $1/[CO]$ (b). Data are from the SO_2-Ac_2-N_2 and SO_2-Ac_2-CO mixture photolyses at 2875 Å. In (a), circles, $\Phi_{sens}^{(2)} = 2.5 \times 10^{-3}$; in (b), circles, $\Phi_{sens}^{(2)} = 2.8 \times 10^{-3}$; squares in each figure represent $\Phi_{sens}^{(2)} = 0$.

$k_3/(k_1 + k_2 + k_3) = 0.020 \pm 0.010$, 0.021 ± 0.010, and 0.019 ± 0.010. Within the error limits of the data for CO and N_2, these new estimates check well with those derived previously at low pressures; with M = CO, $k_3/(k_1 + k_2 + k_3) = 0.017 \pm 0.010$[46]; for M = N_2, this ratio is 0.033 ± 0.008[40]. There is no previous estimate of the ratio for M as CO_2.

Note that neither the fraction of $^1SO_2$ quenching collisions which form $^3SO_2$ in (2) nor the fraction of these collisions which form the undefined species X is very sensitive to the nature of M. For M = CO_2, CO, and N_2, respectively, $k_2/(k_1 + k_2 + k_3) = 0.14 \pm 0.02$, 0.085 ± 0.012, and 0.11 ± 0.02. The largest fraction of the $^1SO_2$-quenching collisions (84 - 89%) occurs by reaction (1), presumably proceeding by energy cascade through the ground-state SO_2 vibrational manifold.

The present data give few clues as to the identity of the intermediate species X. The efficiency of the bimolecular quenching of this species to form $^3SO_2$ on collision with M, reaction (4), is rather insensitive to the nature of M. Our data give the ratio of the first-order rate constant for the decay of X to SO_2 to that for the bimolecular reaction (4); for M = CO_2, CO, and N_2, respectively, $k_5/k_4 = 0.020 \pm 0.004$, 0.016 ± 0.003, and 0.021 ± 0.005 mole/ℓ. Since only a ratio of rate constants involving X can be derived here, the lifetime of X or other useful data which might allow characterization of X cannot be estimated. However the results reported here offer further support for the existence of the undefined species X in irradiated SO_2 systems at high pressure.

All of our data support the hypothesis that the only triplet state of SO_2 involved in both the chemical conversion of CO to CO_2 observed earlier[46,21], and in triplet energy transfer to biacetyl in this work is the optical triplet state of $SO_2(^3B_1)$. If a second triplet species of SO_2 is involved, then it must have properties almost identical to those of the optical triplet. The present evidence precludes the intermediate state X being a triplet species [e.g., $SO_2(^3A_2)$] which can transfer energy directly to biacetyl. Since we postulate that X forms $^3SO_2$ rather efficiently on collision with added gases in reaction (4), we must conclude that it has a combined electronic and internal energy near equal to or greater than that of the $^3SO_2$ state, 73.7 kcal/mole above the ground-state SO_2. Conceivably, X could be the $SO_2(^1A_2)$ state of SO_2, but there is no experimental evidence which warrents this suggestion now. It may equally well be a high-energy isomer of sulfur dioxide. The identity of X must await further definitive experimentation which is aimed specifically at its characterization.

The theoretical maximum rate of SO_2 photo-oxidation in the lower atmosphere

In a previous study, we have estimated from the rather limited rate constant and mechanism information then available on SO_2 photochemistry[41], the rate of $^3SO_2$ formation in the sunlight-irradiated lower atmosphere. The existence of the high-pressure mechanism of $^3SO_2$ formation was not known at that time. Furthermore, the assumption was made that the rate constant ratio $k_2/(k_1 + k_2 + k_3)$ was the same for M = N_2 and O_2 as that found for M = SO_2. Recently, we have been able to determine this rate constant ratio for M = O_2 as well as N_2 and SO_2; the ratio for O_2 is equal within the experimental error to that for N_2 as M; $k_2/(k_1 + k_2 + k_3) = 0.034 \pm 0.029$ for M = O_2 and 0.030 ± 0.013 for M = N_2[16]. However, these values are well below that for SO_2 as M, 0.095 ± 0.005[39]. We do not now have information on the rate ratios $k_3/(k_1 + k_2 + k_3)$ and k_5/k_4 for M = O_2; since $^3Ac_2$ molecules are quenched effectively by O_2, the present method cannot be used to determine these constants. However, in view of the apparent insensitivity of these rate ratios to the nature of M for the compounds CO_2, N_2, and CO, which is reported here, and the observed near equality of the ratio $k_2/(k_1 + k_2 + k_3)$ for M = N_2 and O_2[16], it is probably reasonable to assume that these other rate ratios for M = O_2 are near equal to those for N_2 as well. If we assume this, then the present data predict that the rate of ${}^3SO_2$ formation resulting from sunlight absorption by SO_2 in the lower atmosphere should be given by relation (G):

$$R^3_{SO_2} = I_a\left\{\frac{k_2}{k_1 + k_2 + k_3} + \left(\frac{k_3}{k_1 + k_2 + k_3}\right)\left(\frac{1}{1 + (k_5/k_4[M])}\right)\right\} + I_a' \qquad \text{(G)}$$

where I_a is the rate of solar energy absorption by SO_2 in the allowed band at 2400-3200 Å, and I_a' is the rate of absorption in the "forbidden" band at 3400-4000 Å. I_a and I_a' values have been estimated by us previously for various solar zenith angles[41]. Substituting in (G) the rate constant ratios derived here for N_2, and taking [M] = 0.041 M, we find

$$R^3_{SO_2} = 0.092\ I_a + I_a'$$

Fortuitiously, this is nearly identical to the final expression employed by us previously. Thus, the values derived previously for the maximum theoretical rates of photo-oxidation of SO_2 in the lower atmosphere (1.9% hr at z = 20°, etc.) are reliable as present rate information will allow[41].

I-C. The Temperature Dependence and the Mechanism of the $SO_2({}^3B_1)$ Quenching Reaction[47]

The detailed mechanism of the singlet quenching reactions (1a) and (1b) is incompletely understood at present. However, the data suggest that for experiments at pressures below about 30 Torr, the singlet quenching reaction (1a) leads to nonemitting products, including ground state SO_2, and little chemical change.

(I) $SO_2 + h\nu\ (3200\text{-}2400\ \text{Å}) \rightarrow {}^1SO_2$

(II) $SO_2 + h\nu\ (4000\text{-}3400\ \text{Å}) \rightarrow SO_2({}^3B_1)$

(1a) ${}^1SO_2 + SO_2 \rightarrow (2SO_2)$

(2a) ${}^1SO_2 + SO_2 \rightarrow SO_2({}^3B_1) + SO_2$

(1b) ${}^1SO_2 + M \rightarrow (M\text{-}SO_2)$

(2b) ${}^1SO_2 + M \rightarrow SO_2({}^3B_1) + M$

(3) ${}^1SO_2 \rightarrow SO_2 + h\nu_f$

(4) ${}^1SO_2 \rightarrow (SO_2)$

(5) ${}^1SO_2 \rightarrow SO_2({}^3B_1)$

(6) $SO_2({}^3B_1) \rightarrow SO_2 + h\nu_p$

(7) $SO_2({}^3B_1) \rightarrow (SO_2)$

(8a) $SO_2({}^3B_1) + SO_2 \rightarrow SO_3 + SO({}^3\Sigma_g^-)$

(8b) $SO_2({}^3B_1) + SO_2 \rightarrow (2SO_2)$

(9) $SO_2({}^3B_1) + M \rightarrow (SO_2\text{-}M)$

where M represents some quencher molecule other than SO_2. The product species designated in the above sequence by the general formulas, $(2SO_2)$, $(M - SO_2)$, and (SO_2), are either ground-state SO_2 and M molecules, ill defined nonemitting excited states, or other products formed in the quenching step.

The mechanism of $SO_2(^3B_1)$ quenching in reaction (9) also remains open to question for most collision partners M. It has been suggested that a large part of the quenching is directly associated with a chemical reaction when M is SO_2[17], C_2H_6, C_3H_8, and the higher paraffinic hydrocarbons[19], or C_2H_4, C_3H_6, and the higher olefinic hydrocarbons[20]. However, at room temperature, less than 10% of the $SO_2(^3B_1)$-quenching collisions with CO result in a chemical change (CO_2 formation)[32,22], while it appears that a much smaller fraction of the $SO_2(^3B_1)$-O_2 quenching encounters lead to final chemical change (SO_3 formation)[30,48]. With O_2 as M in (9), an energy transfer reaction, $SO_2(^3B_1) + O_2(^3\Sigma_g^-) \rightarrow SO_2(^1A_1) + O_2(^1\Sigma_g^+)$, has been observed to occur at an undetermined efficiency[49]. Although at 25° C the quenching rate constant for $SO_2(^3B_1)$ with N_2 is near equal to those for CO and O_2, it is apparent that no chemical quenching is possible for N_2 as the reactant, since formation of the possible products N_2O and SO is highly endothermic ($\Delta H = 47.6$ kcal mole^{-1}). Furthermore, such chemically unreactive species as CO_2, Ar, and He quench $SO_2(^3B_1)$ with fair efficiencies. Obviously, some unidentified form of physical quenching is operative for many of these systems.

Our work described in this section was initiated to help elucidate the $SO_2(^3B_1)$-quenching mechanisms through a determination of the Arrhenius parameters for the quenching rate constants for a variety of chemically reactive and unreactive molecules. The rate constants for $SO_2(^3B_1)$ decay were calculated from phosphorescence lifetime measurements. The triplet species were generated both by direct absorption of a 3829-Å laser pulse within the "forbidden" band and by intersystem crossing reactions (2a) and (2b), following excitation of singlet SO_2 using a broadband Xe-flash which overlapped the first allowed absorption band (2400-3200 Å).

The temperature dependences of the $SO_2(^3B_1)$-quenching rate constants reported here provide significant new insight into the mechanism of the quenching reactions involving a wide variety of quencher molecules.

I-C-1. Experimental Methods

The laser excitation equipment

The source of 3829-Å light pulse used in one phase of this work, a Raman-shifted, frequency-doubled ruby laser, has been described previously[50,26]. It generated a 50-kW pulse of 3829-Å radiation of 20-nanosec duration. In these experiments, the laser beam passed through the center of an all-Suprasil cylindrical reaction cell, 88 cm in length and 2.5 cm in diameter. The front and rear windows were fused to the cell body at the Brewster angle. The cell was surrounded by a specially constructed oven which maintained a selected temperature to within ± 1° C. Front and rear windows on the oven allowed passage of the excitation beam; phosphorescence emission was detected by an RCA 7265 photomultiplier tube which was mounted at right angles to the cell axis and received light through an additional side window in the oven. A Kodak Wratten gelatin 2B filter placed in front of the detector to remove scattered 3829-Å radiation. The phosphorescence intensity decay curves were photographed from the screen of an oscilloscope, and the data were reduced as described previously[26].

The Xe-flashlamp excitation equipment

The majority of the Xe-flashlamp equipment has been described previously[51], and it need not be outlined here in detail. However, there were some significant improvements which were made in the older system. A fast extinguishing flash lamp (Suntron 6, of the Xenon Corporation) was employed with a 0.5-μF, low-impedance capacitor (Xenon, Model No. C-10-0.5). The flash energy of 10-20 J created a burst of light (2400-3200 Å) of less than 2 μsec half-peak time. The cell, oven, and detection system were the same as those described previously[51].

Experimental procedures and treatment of the data

Gaseous mixtures were prepared in mercury-free systems using a calibrated transducer-digital voltmeter combination in the case of the flash excitation experiments. A quartz spiral manometer was employed in the laser excitation experiments. Homogeneity of the SO_2-added gas mixtures was effected using a thermal gradient pump which was in series with leads near the front and rear of the photolysis cell. The absorption properties of SO_2, the timing of the excitation light pulse, and the sensitivity of the detector system limited the range of SO_2 concentrations which could be employed from about 4×10^{-6} to 48×10^{-6} M in the flash experiments and from about 9×10^{-5} to 30×10^{-5} M in the laser experiments. In the flash excitation experiments, the concentration of the added quencher gas was varied only over the range of values which ensured a reasonable accuracy in the lifetime observations; that is, the concentration of added gas M was controlled so that the lifetime of $SO_2(^3B_1)$ in the mixture with added gas was no less than one half that observed in SO_2 alone at the concentration employed in the mixture. In all of the Xe-flash experiments and some of the laser experiments, about six to seven different [M] values were used at each temperature with a fixed [SO_2]. The rate constant k_9 was determined from the least-squares slope of the $1/\tau$-versus-[M] plots. These data for the pure SO_2 system are summarized in Table X. Because of space limitations all of the measured lifetimes, data obtained from SO_2-M mixtures are not presented here, but the rate constants derived from these estimates at several temperatures are tabulated in Tables XI, XII, and XIII, where M is an atmospheric gas, a saturated hydrocarbon, and an unsaturated hydrocarbon gas, respectively. In the third column of these tables, the symbols F and L refer to the experiments in which a Xe-flash and the laser, respectively, were used for excitation. The rate constants are shown with 95% confidence limits for those cases where the number of data points allowed a meaningful statistical treatment of the random error; this is the case for all of the Xe-flash experiments. In most of the laser excitation experiments, the k_9 value was determined from repeated measurements of τ in experiments at fixed [M] and [SO_2] values. In these cases, the reproducibility of the rate constant measurements was within about ± 10% of the mean value; this approximate error limit is shown in parentheses following the rate constant for these cases.

I-C—2. Results and Discussion

The mechanism of $SO_2(^3B_1)$ quenching

According to the mechanism of $SO_2(^3B_1)$ quenching outlined in the reaction sequence (1)-(9), the lifetime of the triplet molecules, following their generation in a pulse of short duration, should be given by relation (A):

$$(A) \qquad 1/\tau = (k_{3a} + k_{3b})[SO_2] + k_6 + k_7 + k_9[M]$$

Table X. The $SO_2(^3B_1)$ lifetime at various SO_2 concentrations and temperatures.[a]

Temp., °K	1/τ, sec⁻¹ × 10⁻⁴								k_s (l. mole⁻¹ sec⁻¹) × 10⁻⁸
	0.286[b]	0.637	0.875	1.57	2.24	2.81	3.71	4.26	
298	1.48	2.80	3.94	7.57	9.86	11.1	14.3	17.7	3.90 ± 0.59[c]
309	1.54	2.95	4.52	8.13	10.8	10.8	13.4	20.0	4.28 ± 0.56
318	1.74	3.34	5.02	9.80	12.3	14.3	16.0	21.9	4.68 ± 0.68
326	2.07	4.21	5.31	9.70	14:0	13.8	17.8	22.8	4.86 ± 0.62
333	2.11	3.98	5.78	11.8	14.2	16.0	19.5	24.4	5.31 ± 0.64
344	2.53	4.34	7.05	11.0	15.8	17.7	21.1	27.0	5.85 ± 0.58
361	2.96	5.52	7.00	11.5	17.1	19.8	24.7	31.1	6.79 ± 0.44
369	2.70	5.32	7.62	12.6	18.2	20.9	30.1	33.4	7.74 ± 0.36
378	3.12	5.64	8.43	16.2	21.0	21.2	27.9	38.5	7.77 ± 1.08
388	3.12	6.11	8.88	15.8	22.3	25.8	29.4	40.0	8.61 ± 1.02
399	3.87	7.46	10.6	19.4	25.0	29.1	30.1	38.5	8.38 ± 1.16

[a] Excitation of $SO_2(^3B_1)$ by 3829-Å laser pulse.

[b] $[SO_2]$, $M \times 10^4$.

[c] Error limits shown here and elsewhere in this paper refer to the 95% confidence limits (2σ) as determined by standard least-squares methods.

Indeed, this has been found to be the case in previous studies[26,30], and this is confirmed in the present work over a wide range of temperatures and reactant concentrations. Thus, in the pure SO_2 system excited by the 3829-Å laser pulse, the plot of $1/\tau$ versus $[SO_2]$ gives linear Stern-Volmer plots with slopes (equal to $k_{8a} + k_{8b}$) which increase with increase in temperature (see Fig. 8). In Figure 9 is given in Arrhenius plot of these new laser data (darkened circles) together with the previously published Xe-flash data of Otsuka and Calvert[51]. With the laser excitation of $SO_2(^3B_1)$ molecules at 3829 Å, the triplet is formed in a near vibrationally relaxed state; it has only one quantum of vibrational excitation and this is in the weak bending vibration. On the other hand, in the Xe-flash study, the average $^1SO_2$ molecule is formed with about 26 kcal mole^{-1} of internal energy above that of the vibrationally relaxed SO_2 $(^3B_1)$ level. However, we expect that the vibrational relaxation of the emitting triplet will be ensured even in this case by both the mechanics of the collisionally perturbed intersystem crossing reactions (2a) and (2b) and the reasonably large number of collisions which the $SO_2(^3B_1)$ molecules must undergo before emitting under our experimental conditions. Thus, it is not surprising that the $SO_2(^3B_1)$ molecules formed by either of the two very different methods have essentially identical quenching rate constants as is observed in Figure 9.

The $SO_2(^3B_1)$-quenching rate constants k_9 observed here for a great variety of quenching partners also appear to be independent of the method of triplet generation (see the Arrhenius plots for the data from the atmospheric gases in Figures 9 and 10, for the saturated paraffins in Figures 11 and 12, and the olefins and the aromatic hydrocarbons in Figure 13). The Arrhenius parameters derived from a statistical treatment of the data for the $SO_2(^3B_1)$-quenching rate constants for the 21 different quenching partners studied in this work are summarized in Table XIV.

Table XI. Rate constants for $SO_2(^3B_1)$ quenching reactions, $SO_2(^3B_1) + M \rightarrow (SO_2\text{-}M)$(9), with various atmospheric components at several temperatures.^{a}

$1/T \times 10^3$	k_q, (l. mole^{-1} sec^{-1}) $\times 10^{-8}$	Excitation method^b
	(a) $O_2 = M$	
3.36	0.92 ±0.13	F
3.36	1.27 (±0.13)	L
3.24	1.4[illegible] (±0.13)	L
[illegible]	1.[illegible] ±0.19	F
3.14	1.49 (±0.14)	L
3.12	1.21 ±0.25	F
3.07	1.23 (±0.12)	L
3.00	1.41 ±0.2[illegible]	F
3.00	1.97 (±0.2[illegible])	L
2.91	2.10 (±0.21)	L
2.77	2.38 (±0.24)	L
2.71	3.31 (±0.33)	L
2.64	2.52 (±0.25)	L
2.58	3.89 (±0.39)	L
2.51	4.15 (±0.42)	L
	(b) $N_2 = M$	
3.42	0.669 ±0.072	F
3.36	0.916 ±0.136	F
3.36	0.880 (±0.09)	L
3.35	0.848 ±0.072	F
3.29	0.816 ±0.066	F
3.25	0.701 ±0.081	F
3.24	0.697 ±0.105	F
3.24	1.09 (±0.11)	L
3.19	0.760 ±0.144	F
3.14	1.17 (±0.12)	L
3.08	1.06 ±0.17	F
3.07	1.19 (±0.12)	L
3.00	1.16 ±0.20	F
3.00	1.17 (±0.12)	L
2.91	1.42 (±0.14)	L
2.79	1.49 ±0.10	F
2.77	2.08 (±0.21)	L
2.71	2.66 (±0.27)	L
2.64	1.74 ±0.25	F
2.64	2.41 (±0.24)	L
2.58	2.30 (±0.23)	L
2.51	2.30 (±0.23)	L
2.44	3.09 (±0.31)	L
	(c) Ar = M	
3.37	0.975 ±[illegible]	F
[illegible]	[illegible]	L
3.24	0.721 (±0.07[illegible])	L
[illegible]	0.4[illegible] ±[illegible]	[illegible]
3.14	0.675 ([illegible])	L
3.07	0.617 ([illegible])	L
3.0[illegible]	0.[illegible] ±[illegible]	F
[illegible]	[illegible]	L
2.9[illegible]	0.700 ±[illegible]	F
2.91	1.15 (±0.12)	L
2.77	1.46 (±0.15)	L
2.71	1.71 (±0.17)	L
2.64	1.40 (±0.14)	L
2.58	1.42 (±0.14)	L
2.51	1.73 (±0.17)	L
2.44	1.47 (±0.15)	L
	(d) CO = M	
3.38	1.01 ±0.11	F
3.36	1.22 (±0.12)	L
3.35	0.900 ±0.12	F
3.30	0.900 ±0.11	F
3.29	1.13 ±0.17	F
3.26	0.984 ±0.19	F
3.24	1.22 (±0.12)	L
3.19	1.13 ±0.16	F
3.14	1.26 (±0.13)	L
3.09	1.26 ±0.20	F
3.07	1.55 (±0.16)	L
3.00	1.38 ±0.23	F
3.00	1.37 ±0.16	F
3.00	1.45 (±0.15)	L
2.91	1.68 (±0.17)	L
2.77	1.64 (±0.16)	L
2.71	2.30 (±0.23)	L
2.64	2.55 (±0.26)	L
2.58	3.01 (±0.30)	L
2.51	3.36 (±0.34)	L

(continued)

Table XI. (continued)

$1/T \times 10^3$	k_q (l. mole^{-1} sec^{-1}) $\times 10^{-8}$	Excitation method[b]	$1/T \times 10^3$	k_q (l. mole^{-1} sec^{-1}) $\times 10^{-11}$	Excitation method[b]
	(e) $CO_2 - M$			(f) $NO - M$	
3.36	1.73 (±0.17)	L	3.36	0.94 (±0.09)	L
3.24	2.10 (±0.21)	L	3.24	0.91 (±0.09)	L
3.14	2.06 (±0.21)	L	3.14	0.86 (±0.09)	L
3.07	2.01 (±0.20)	L	3.07	1.10 (±0.11)	L
3.00	2.63 (±0.26)	L	3.00	1.13 (±0.11)	L
2.91	2.92 (±0.29)	L	2.91	0.99 (±0.10)	L
2.77	4.39 (±0.44)	L	2.77	1.31 (±0.13)	L
2.71	[illegible]	L	2.71	1.62 (±0.16)	L
[illegible]	[illegible]	L	2.64	1.58 (±0.16)	L
[illegible]	[illegible]	L	2.58	[illegible] (±0.17)	L
2.51	3.08 (±0.31)	L	2.51	1.15 (±0.12)	L

[a] In Xe-flash experiments, $[SO_2] = 4.3 \times 10^{-4} M$, and [M] was varied from 0 to concentration shown ($M \times 10^3$): O_2, 2.8; N_2, 4.0; Ar, 3.6; CO, 3.4. In the 3829-Å laser experiments, $[SO_2] = 9.17 \times 10^{-4} M$, and [M] was fixed at the following concentrations ($M \times 10^3$): O_2 2.48; N_2, 2.74; Ar, 4.62; CO, 2.74; CO_2, 1.71; NO, 2.76×10^{-3}.

[b] In runs labeled *F*, triplets were generated by intersystem crossing from the excited $SO_2(^1B_1)$ following Xe-flash excitation; in runs labeled *L*, 3829-Å laser excitation was employed to form the $SO_2(^3B_1)$ species directly.

The values for $\log_{10}[A(\ell.\ \text{mole}^{-1}\ \text{sec}^{-1})]$ and E_a (kcal mole^{-1}) derived for a given compound from the flash data alone and the laser data alone agree within the error limits shown. In view of this. it is probable that the best estimates of these parameters are those derived utilizing both the flash and the laser data in the treatment. These results are also shown in Table XIV.

Some very interesting comparisons can be seen in the Arrhenius parameters of Table XIV for the variety of quencher molecules studied. One group of molecules, O_2, Ar, CO_2, N_2, CO, and CH_4, have nearly identical activation energies. The group of paraffinic hydrocarbons, C_3H_8, n-C_4H_{10}, iso-C_4H_{10}, and cyclohexane, tend to have somewhat decreased activation energies. On the other hand, the olefins and the aromatic hydrocarbons have very high preexponential factors and activation energies which are near zero. We will consider the possible mechanisms of these three groups of molecules in turn.

Mechanism of $SO_2(^3B_1)$ quenching by the atmospheric gases and the chemically unreactive molecules

There is a striking near equality in the magnitude of the activation energies for the atmospheric gases. The E_a values (kcal mole^{-1}) derived from the combined laser and flash data for the various quenchers are: O_2, 3.2 ± 0.5; N_2, 2.9 ± 0.4; Ar, 2.8 ± 0.6; CO_2, 2.8 ± 0.4; CO, 2.7 ± 0.4; CH_4, 2.5 ± 0.6. This near-equality in E_a values and the chemical diversity of the quencher molecules involved in this group suggest that in these cases some common physical process dominates the quenching act. The activation energy corresponds closely to that required for the promotion of the $SO_2(^3B_1)$ molecules to the $^3B_1$ (1,0,0)

Table XII. Rate constants for the $SO_2(^3B_1)$-quenching reactions, $SO_2(^3B_1) + M \rightarrow (SO_2\text{-}M)(9)$, with various saturated hydrocarbon gases at several temperatures.[a]

$1/T \times 10^3$	k_9, (l. mole^{-1} sec^{-1}) $\times 10^{-8}$		Excitation method[b]
	(a) CH_4 – M		
3.36	1.15	(±0.12)	L
3.35	1.26	±0.[illegible](1)[b]	F
3.35	1.34	±0.14(2)[b]	F
3.35	1.2[illegible]	±0.1[illegible](3)[b]	F
3.33	[illegible]	[illegible]	F
3.31	[illegible]	[illegible]	F
3.24	1.30	(±0.13)	L
3.23	1.46	±0.20	F
3.14	1.57	±0.25	F
3.14	1.42	(±0.14)	L
3.08	1.67	±0.21	F
3.07	1.40	(±0.14)	L
3.04	1.69	±0.15	F
3.00	1.59	(±0.16)	L
2.98	2.07	±0.34	F
2.91	1.95	(±0.20)	L
2.81	2.23	±0.13	F
2.77	2.69	(±0.27)	L
2.71	2.74	(±0.27)	L
2.67	2.69	±0.12	F
2.58	3.82	(±0.38)	L
2.54	3.16	±0.33	F
2.51	3.31	(±0.33)	L
2.42	3.87	±0.45	F
2.23	5.49	±1.10	F
	(b) C_2H_6 – M		
3.36	1.69	(±0.17)	L
3.35	1.43	±0.16	F
3.33	1.62	±0.09	F
3.18	1.71	±0.25	F
3.14	2.27	(±0.23)	L
3.07	2.58	(±0.24)	L
3.00	2.67	(±0.27)	L
2.98	2.46	±0.13	F
2.91	2.88	(±0.29)	L
2.77	3.46	(±0.35)	L
2.74	3.44	±0.28	F
2.71	4.35	(±0.44)	L
2.64	5.34	(±0.53)	L
2.58	5.18	(±0.52)	L
2.53	4.57	±0.40	F
2.51	6.86	(±0.69)	L
2.32	7.13	±0.64	F
2.15	9.59	±2.3	F
	(c) C_3H_8 – M		
3.40	3.45	±0.24	F
3.36	3.23	(±0.32)	L
3.35	4.22	±0.37(1)[c]	L
3.35	3.98	±0.41(2)[c]	L
3.35	3.68	±0.26(1)[d]	F
3.35	4.14	±0.56(2)[d]	F
3.25	3.86	±0.47	F
3.24	3.87	(±0.39)	L
3.14	3.66	(±0.37)	L
3.09	4.51	±0.43	F
3.07	4.64	(±0.46)	L
3.00	3.93	(±0.39)	L
2.99	6.11	±0.98	F
2.98	5.45	±0.18	F
2.91	5.12	(±0.51)	L
2.77	6.46	(±0.65)	L
2.74	6.91	±0.35	F
2.71	7.98	(±0.80)	L
2.64	7.60	(±0.76)	L
2.58	9.00	(±0.90)	L
2.54	10.0	±0.53	F
2.51	10.0	(±1.0)	L
2.30	14.7	±1.8	F
2.21	14.9	±1.8	F
	(d) n-C_4H_{10} – M		
3.38	8.40	±0.50	F
3.36	9.14	(±0.91)	L
3.35	10.0	±1.2[e]	L
3.35	8.57	±0.48(1)[f]	F
3.35	8.65	±0.51(2)[f]	F
3.35	8.49	±0.87(3)[f]	F
3.35	10.13	±0.83(4)[f]	F
3.34	8.57	±0.48	F
3.32	8.66	±0.89	F

(continued)

Table XII. (continued)

$1/T \times 10^3$	k_q (l. mole^{-1} sec^{-1}) $\times 10^{-6}$	Excitation method[a]
3.24	9.87 (±0.99)	L
3.14	11.5 (±1.2)	L
3.07	13.0 (±1.3)	L
3.00	14.2 (±1.4)	L
2.91	17.1 (±1.7)	L
2.77	16.3 (±1.6)	L
2.71	21.1 (±2.1)	L
2.64	19.8 (±2.0)	L
2.58	25.1 (±2.5)	L
2.51	23.5 (±2.4)	L
	(e) iso-C_4H_{10}	
3.38	7.88 ±0.52	F
3.35	11.2 ±1.5[e]	L
3.35	7.85 ±0.33(1)[f]	F
3.35	8.04 ±0.33(2)[f]	F
3.35	10.3 ±0.8(3)[g]	F
3.35	11.0 ±1.3(4)[g]	F
3.24	10.4 (±1.0)	L
3.20	8.75 ±0.50	F
3.14	9.15 (±0.92)	L
3.08	9.51 ±1.07	F
3.00	11.9 (±1.2)	L
2.99	10.3 ±1.1	F
2.91	12.8 (±1.3)	L
2.79	12.3 ±0.6	F
2.77	16.8 (±1.7)	L
2.64	18.4 (±1.8)	L
2.60	14.7 ±1.0	F
2.58	22.2 (±2.2)	L
2.51	24.4 (±2.4)	L
2.42	17.2 ±1.0	F
2.34	17.9 ±2.0	F
2.30	20.6 ±3.3	F
2.26	24.4 ±3.5	F
2.21	21.8 ±1.0	F
	(f) Neopentane	
3.31	3.63 ±0.17	F
3.28	3.60 ±0.21	F
3.12	4.56 ±0.45	F
3.00	5.66 ±0.48	F
2.91	6.20 ±0.42	F
2.58	9.64 ±0.82	F
2.44	11.1 ±0.6	F
2.36	12.9 ±0.6	F
2.21	15.7 ±1.3	F
	(g) cyclo-C_6H_{12}	
3.36	24.2 (±2.4)	L
3.24	27.0 (±2.7)	L
3.14	32.3 (±3.2)	L
3.07	35.4 (±3.5)	L
3.00	30.1 (±3.0)	L
2.91	36.3 (±3.6)	L
2.71	42.9 (±4.3)	L
2.64	45.7 (±4.6)	L
2.58	45.7 (±4.6)	L
2.51	48.8 (±4.9)	L

[a] In most of the Xe-flash experiments, labeled *F* under excitation method, the $[SO_2] = 4.3 \times 10^{-6}$ *M* and [M] was varied from 0 to the concentration shown ($M \times 10^5$): CH_4, 2.6; C_2H_6, 2.9; C_3H_8, 1.0; *n*-C_4H_{10}, 0.50; iso-C_4H_{10}, 0.45; neo-C_5H_{12}, 1.1. In most of the 3829-Å laser experiments, labeled *L* under excitation method, $[SO_2] = 9.17 \times 10^{-6}$ *M*, and [RH] was at the following concentrations ($M \times 10^4$): CH_4, 1.75; C_2H_6, 1.91; C_3H_8, 0.789; *n*-C_4H_{10}, 0.374; iso-C_4H_{10}, 0.316; cyclo-C_6H_{12}, 0.322.

[b] $[SO_2]$ ($M \times 10^5$) was fixed at :0.38, 0.39, and 3.09, respectively.

[c] $[SO_2]$ ($M \times 10^4$) was fixed at 1.38 and 2.85, respectively.

[d] $[SO_2]$ ($M \times 10^5$) was at: 0.41 and 4.4, respectively.

[e] $[SO_2]$ was fixed at 2.85×10^{-4} *M*.

[f] $[SO_2]$ ($M \times 10^5$) was fixed at: 0.39, 0.40, 0.40, and 4.79, respectively.

[g] $[SO_2]$ ($M \times 10^5$), was fixed at: 0.38, 0.40, 3.10, and 6.56, respectively.

Table XIII. Rate constants for the $SO_2(^3B_1)$-quenching reactions, $SO_2(^3B_1) + M \rightarrow (SO_2\text{-}M)(9)$, with various olefinic and aromatic hydrocarbon gases at several temperatures.[a]

$1/T \times 10^3$	k_q (l. mole^{-1} sec^{-1}) $\times 10^{-10}$
(a) C_2H_4 — M	
3.36	3.56(±0.36)
3.24	3.85(±0.38)
3.14	4.67(±0.46)
3.07	3.24(±0.32)
3.00	4.70(±0.47)
2.91	3.71(±0.37)
2.77	4.85(±0.48)
2.71	6.29(±0.63)
2.64	4.88(±0.49)
2.58	5.08(±0.51)
2.51	5.83(±0.58)
(b) CF_2CHF — M	
3.36	1.05(±0.11)
3.24	0.95(±0.10)
3.14	0.98(±0.10)
3.07	1.21(±0.12)
3.00	1.19(±0.12)
2.91	1.28(±0.13)
2.71	1.71(±0.17)
2.64	1.79(±0.18)
2.58	1.77(±0.18)
2.51	1.88(±0.19)
(c) C_6H_6 — M	
3.36	10.0 (±1.0)
3.24	8.70(±0.87)
3.14	10.0 (±1.0)
3.07	10.3 (±1.0)
3.00	10.2 (±1.0)
2.91	10.3 (±1.0)
2.77	11.5 (±1.2)
2.71	11.6 (±1.2)
2.64	10.4 (±1.1)
2.58	15.0 (±1.5)
2.51	16.6 (±1.7)
(d) *cis*-2-C_4H_8 — M	
3.36	13.9 (±1.4)
3.24	13.5 (±1.4)
3.14	13.9 (±1.4)
3.07	14.9 (±1.5)
3.00	14.9 (±1.5)
2.91	16.8 (±1.6)
2.77	16.0 (±1.6)
2.71	20.5 (±2.1)
2.64	18.4 (±1.8)
2.58	16.0 (±1.6)
2.51	17.4 (±1.7)
(e) Cyclopentene — M	
3.36	15.7 (±1.6)
3.24	14.6 (±1.5)
3.14	16.7 (±1.7)
3.07	16.2 (±1.6)
3.00	13.5 (±1.4)
2.91	16.9 (±1.7)
2.77	20.0 (±2.0)
2.71	18.6 (±1.9)
2.64	14.2 (±1.4)
2.58	16.3 (±1.6)
2.51	19.0 (±1.9)
(f) C_6H_6 — M	
3.36	11.2 (±1.1)
3.24	9.6 (±1.0)
3.14	11.4 (±1.2)
3.07	10.8 (±1.1)
3.00	11.6 (±1.2)
2.91	9.5 (±1.0)
2.77	10.6 (±1.1)
2.71	15.6 (±1.6)
2.64	15.6 (±1.6)
2.58	12.3 (±1.2)
2.51	10.6 (±1.1)
(g) C_6F_6 — M	
3.36	0.706(±0.071)
3.24	0.936(±0.094)
3.14	0.887(±0.089)
3.07	0.795(±0.080)
3.00	0.658(±0.066)
2.91	0.875(±0.088)
2.77	0.760(±0.076)
2.71	0.780(±0.078)
2.64	0.883(±0.088)
2.58	1.23 (±0.12)
2.51	1.09 (±0.11)

[a] $SO_2(^3B_1)$ excitation was by 3829-Å laser; $[SO_2] = 9.17 \times 10^{-4}$ *M*; [RH] was at the following concentrations (*M* × 10^4): C_2H_4, 1.32; CF_2CHF, 3.68; C_6H_6, 0.301; *cis*-2-C_4H_8, 0.268; cyclopentene, 0.295; C_6H_6, 0.301; C_6F_6, 4.87.

or $^3B_1$ (0,0,1) levels at 905.7 cm^{-1} (2.6 kcal mole^{-1}) and near 964-1071 cm^{-1} (2.8-3.1 kcal mole^{-1}),* involving one quantum of vibration in the symmetric and antisymmetric stretching modes, respectively. Note that Brand and coworkers[52] have observed that the line structure in the 3730-3750 Å bands within the $SO_2(^3B_1) \leftarrow SO_2(^1A_1)$ absorption region shows the transitions in this region to be perturbed through the mixing of the $SO_2(^3B_1)$ levels with those of an electronic state other than the ground state. They concluded that in the $^3B_1(1,1,0) \leftarrow$

---

*The range of values has been estimated approximately assuming that the ratios of the frequencies for the antisymmetric and symmetric stretching modes of SO_2 in the $SO_2(^3B_1)$ state are the same as those in the $SO_2(^1A_1)$, 1.18 and $SO_2(^1B_1)$ states, 1.06[55].

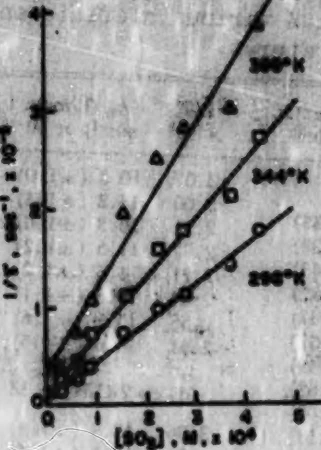

[illegible]. Temperature dependence of the $SO_2(^3B_1)$ lifetimes in pure SO_2. Stern-Volmer plots of the reciprocal lifetimes of the $SO_2(^3B_1)$ molecules vs. $[SO_2]$ for experiments at several temperatures; excitation of the triplet was made using a 3829-Å laser pulse.

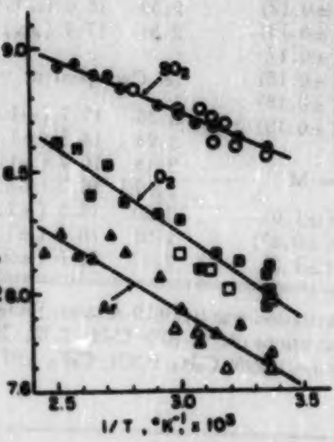

[illegible]. Arrhenius plots of the rate constant for the $SO_2(^3B_1)$ quenching reaction (9), $SO_2(^3B_1) + M \rightarrow (SO_2 - M)$, for several atmospheric gases: M = SO_2 (circles), O_2 (squares), and Ar (triangles); open symbols are data from experiments with the Xe-flash excitation, and closed symbols are data from runs using the 3829-Å-laser excitation of the triplet.

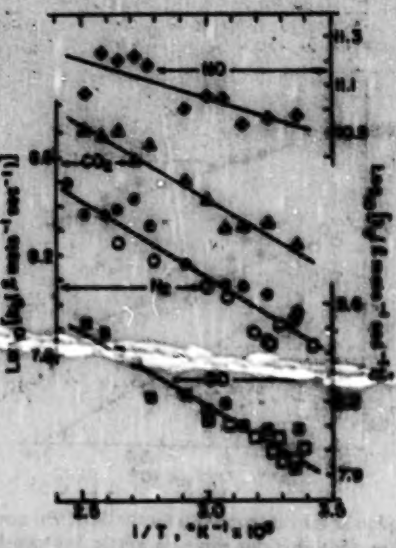

Figure 10. Arrhenius plots of the rate constant data for the $SO_2(^3B_1)$ quenching reaction (9), $SO_2(^3B_1) + M \rightarrow (SO_2\text{–}M)$, for several atmospheric gases: M = NO (diamonds), CO_2 (triangles), N_2 (circles), and CO (squares); open symbols are data from experiments using the Xe-flash excitation, and closed symbols are data from runs using the 3829-Å laser excitation of the triplets; arrows shown with each compound formula indicate the ordinate scales which apply.

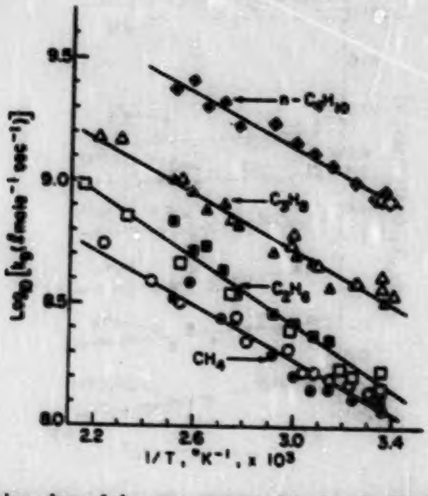

Figure 11. Arrhenius plots of the rate constant data for the $SO_2(^3B_1)$ quenching reaction (9), $SO_2(^3B_1) + M \rightarrow (SO_2\text{–}M)$, for several paraffinic hydrocarbons: M = CH_4 (circles), C_2H_6 (squares), C_3H_8 (triangles), and $n\text{-}C_4H_{10}$ (diamonds); open symbols are data from experiments with the Xe-flash excitation, and the closed symbols are data from runs using the 3829-Å laser excitation of the triplets.

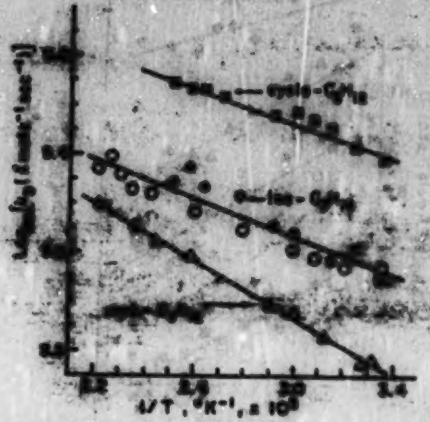

Figure 1.2 Arrhenius plots of the rate constants for the $SO_2(^3B_1)$ quenching reaction (9), $SO_2(^3B_1) + M \rightarrow (SO_2\text{-}M)$, for some paraffinic hydrocarbons: M = iso-C_4H_{10} (circles), neopentane (triangles), and cyclohexane (squares); open symbols are data from experiments with the Xe-flash excitation, and the closed symbols are data from runs using the 3829-Å laser excitation of the triplets.

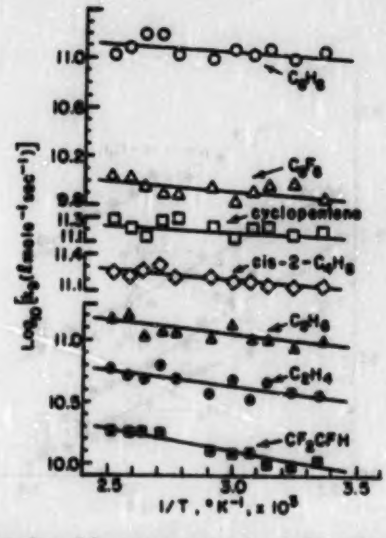

Figure 1.3 Arrhenius plots of the rate constants for the $SO_2(^3B_1)$ quenching reaction (9), $SO_2(^3B_1) + M \rightarrow (SO_2\text{-}M)$, for the olefinic and aromatic hydrocarbons which are indicated on the figure. All these data are derived from experiments employing the 3829-Å laser excitation of the triplets.

Table XIV. Summary of Arrhenius parameters for $SO_2(^3B_1)$-quenching rate constants with various collision partners: $SO_2(^3B_1) + M \rightarrow (SO_2\text{-}M)(9)$.

M	$\log_{10}[A(\text{l. mole}^{-1}\text{ sec}^{-1})]$	E_a, kcal mole^{-1}	Source
SO_2	10.04 ± 0.11	3.0 ± 0.2	laser data
	10.80 ± 0.47	2.8 ± 0.7	flash data[a]
	10.05 ± 0.15	2.0 ± 0.2	all data[b]
O_2	10.16 ± 0.71	2.9 ± 0.6	laser data
	9.69 ± 0.60	2.4 ± 0.8	flash data
	10.35 ± 0.35	3.2 ± 0.5	all data[c]
Ar	9.61 ± 0.64	2.6 ± 0.7	laser data
	9.30 ± 1.00	2.2 ± 1.5	flash data
	9.78 ± 0.37	2.8 ± 0.6	all data[c]
CO_2	10.26 ± 0.44	2.8 ± 0.4	laser data
N_2	9.90 ± 0.66	2.7 ± 0.8	laser data
	9.57 ± 0.48	2.3 ± 0.7	flash data
	9.98 ± 0.28	2.9 ± 0.4	all data[c]
CO	9.80 ± 0.35	2.4 ± 0.6	laser data
	9.50 ± 0.54	2.1 ± 0.7	flash data
	9.98 ± 0.26	2.7 ± 0.4	all data[d]
CH_4	10.29 ± 0.57	3.1 ± 0.6	laser data
	9.85 ± 0.11	2.4 ± 0.2	flash data
	9.93 ± 0.14	2.5 ± 0.6	all data
C_2H_6	10.53 ± 0.43	3.2 ± 0.4	laser data
	10.39 ± 0.15	3.1 ± 0.2	flash data
	10.43 ± 0.18	3.1 ± 0.3	all data
C_3H_8	10.21 ± 0.34	2.3 ± 0.5	laser data
	10.37 ± 0.16	2.6 ± 0.2	flash data
	10.31 ± 0.19	2.4 ± 0.3	all data
$n\text{-}C_4H_{10}$	10.64 ± 0.20	2.3 ± 0.3	laser data
	10.73 ± 0.15	2.4 ± 0.2	all data
$iso\text{-}C_4H_{10}$	10.51 ± 0.41	2.1 ± 0.6	laser data
	10.10 ± 0.18	1.6 ± 0.3	flash data
	10.18 ± 0.20	1.7 ± 0.3	all data
Neopentane	10.48 ± 0.06	2.7 ± 0.1	flash data[a]
$cyclo\text{-}C_6H_{12}$	10.56 ± 0.18	1.6 ± 0.3	laser data
NO	11.96 ± 1.02	1.4 ± 0.7	laser data
C_2H_4	11.36 ± 0.83	1.1 ± 0.6	laser data
CF_2CHF	11.22 ± 0.42	1.7 ± 0.4	laser data
C_3H_6	11.65 ± 0.85	0.9 ± 0.6	laser data
$cis\text{-}2\text{-}C_4H_8$	11.66 ± 0.50	0.7 ± 0.4	laser data
Cyclopentene	11.44 ± 0.79	0.4 ± 0.5	laser data
C_6H_6	11.38 ± 1.03	0.5 ± 0.7	laser data
C_6F_6	10.37 ± 0.94	0.7 ± 0.7	laser data

[a] Data of Otsuka and Calvert[51].

[b] All data from present laser and flash experiments of Otsuka and Calvert excluding the high-temperature point at 373.2° K.

[c] All data from the present study plus data of Sidebottom, et al., for 298.2° K[30].

[d] All data from present study plus data of Jackson and Calvert for 298.2° K[32].

$^1A_1(0,0,0)$ band there is a vibronic perturbation by b_2 vibrational levels of a neighboring $^3A_2$ state; also in this band and in the $^3B_1(1,0,0) \leftarrow {}^1A_1(0,0,0)$ band, rotational-type perturbations occur which may possibly arise from a neighboring $^3B_2$ state. It is probably not fortuitous that the energy region above the $^3B_1(0,0,0)$ level at which marked perturbations are observed in the SO_2 spectrum, 900-1000 cm^{-1} or 2.6-2.9 kcal $mole^{-1}$, is exactly coincident with the region to which the $SO_2(^3B_1)$ molecule must be excited by collision in order to effect physical quenching as measured in this work: $E_a = 2.8 \pm 0.3$ kcal $mole^{-1}$. One might hypothesize that in this energy region, the potential energy surface for the $SO_2(^3B_1)$ state intersects that for another lower-lying state, conceivably the $SO_2(^3A_2)$ or the $SO_2(^3B_2)$ states. SCFMO calculations suggest that the $SO_2(^3A_2)$ state lies somewhat above the $SO_2(^3B_1)$ and that the $SO_2(^3B_2)$ may lie somewhat below the $SO_2(^3B_1)$ level[53,54]. Such approximate calculations are unreliable in predicting small energy differences between states, but it seems likely that the $^3B_2$, $^3B_1$, and $^3A_2$ states may all have very similar energies. The theoretically predicted large singlet-triplet energy separation between the B_2 states ($> 16,800$ cm^{-1}) is in contrast with the much smaller separation (3856 cm^{-1}) observed experimentally between the B_1 states. However, this difference is consistent with the $\pi \rightarrow \pi^*$ character of the $SO_2(^{1,3}B_2) \leftarrow SO_2(^1A_1)$ transitions and the $n \rightarrow \pi^*$ character of the $SO_2(^{1,3}B_1) \leftarrow SO_2(^1A_1)$ transitions.

Then conceivably the physical quenching act may occur as the $SO_2(^3B_1)$ molecules are promoted to the energy region ($\sim$ 900-1000 cm^{-1}) where intersystem crossing to another potential energy surface may occur; this may be the $SO_2(^3A_2)$ or the $SO_2(^3B_2)$ state. If the potential surface crossing is to lead to an efficient energy sink for the $SO_2(^3B_1)$ molecules and result in quenching of the emission, then we require that the new state must have either one of the two following special properties: (1) the new state is very short-lived because it couples much better with the ground state and allows internal conversion of the electronic energy through relaxation within the vibrational manifold of the ground state; (2) the new state is very long-lived, and when vibrational relaxation within the new lower state has occurred so that the efficient return to the $SO_2(^3B_1)$ state is impossible, it cannot emit readily; its radiative lifetime must be very much longer than that of the $SO_2(^3B_1)$ state. In the latter case, the failure to detect such a low-lying state experimentally may be rationalized in terms of the very low intensity of the emission and the probable heterogeneous destruction of a large fraction of the molecules at the walls of the cell in the previous emission studies carried out at low pressures. A proper choice between alternative states and mechanisms of quenching of $SO_2(^3B_1)$ molecules cannot be made from the information at hand. It should be noted here that some of these considerations among others have been offered earlier by Sidebottom et al.[26] in their attempt to rationalize the low quantum yields of emission from the isolated $SO_2(^3B_1)$ molecules. Heicklen and coworkers have postulated that the $SO_2(^1A_2)$ and $SO_2(^3A_2)$ states, as well as the optical states, $SO_2(^1B_2)$ and $SO_2(^3B_1)$, are involved in the chemistry of SO_2-CO[56], SO_2-C_2F_4[56], and SO_2-thiophene[57] mixtures irradiated within the first allowed absorption band of SO_2. However, their interpretation and other alternatives suggested in subsequent work by Calvert and coworkers remain open to question. Calvert's group found that the optical states alone could account for the chemical reactions in their studies of the SO_2-CO system[22,31]; their kinetic results required that some ill-defined, nonreactive, nonemissive state formed from the excited singlet constituted a source of $SO_2(^3B_1)$ reactant in addition to (2a) and (2b) at high pressures. Obviously, further spectroscopic studies are needed to characterize better the nature of the unidentified state(s) involved in the physical quenching of the $SO_2(^3B_1)$ molecule.

The $SO_2(^3B_1)$ quenching by the paraffinic hydrocarbons

The quantum yields of sulfinic acid formation in irradiated SO_2-hydrocarbon mixtures have been studied by Dainton and Ivin[58] using the full mercury arc and Timmons[59] employing 3130-Å irradiation. Badcock et al[19] have rationalized these quantum yields well in terms of their $SO_2(^3B_1)$ quenching data. It appeared that the quenching for methane was largely physical in nature. This conclusion is supported here as well; the k_9, A, and E_a values for CH_4 as M are near-identical to those for O_2, N_2, Ar, CO, and CO_2, where this mechanism most certainly prevails. However, in the higher paraffins the rates of product formation paralleled closely the anticipated rate of $SO_2(^3B_1)$ quenching by the paraffinic hydrocarbon. The present information on the temperature dependence of these rate constants is also consistent with this interpretation. The observed activation energies (kcal mole^{-1}) for $SO_2(^3B_1)$ quenching decrease as M changes in the series: ethane, 3.1 ± 0.3; neopentane, 2.7 ± 0.1; propane, 2.4 ± 0.2; n-butane, 2.4 ± 0.2; cyclohexane, 1.6 ± 0.3; and isobutane, 1.7 ± 0.3. If H atom abstraction is the primary chemical event in the quenching reaction in these cases, then the observed trend is consistent with the lowered C-H bond strengths of the hydrocarbons in the order shown above. In testing this hypothesis it is instructive to attempt to separate the quenching constant into components which reflect the different reactivities for primary, secondary, and tertiary H atoms.

We may estimate the reactivity in reaction (9) per methyl group from the relations (B) and (C):

$$k_{CH_3} = \frac{k_{C_2H_6}}{2} \qquad (B)$$

$$k_{CH_3} = \frac{k_{neopentane}}{4} \qquad (C)$$

Relations (B) and (C), respectively, applied to the present combined laser and flash data, give the following rather consistent k_{CH_3} values (ℓ. mole^{-1} sec^{-1}) for the temperatures indicated: 298° K: 7.16×10^7, 7.90×10^7; 350° K: 1.56×10^8, 1.56×10^8; 400° K: 2.72×10^8, 2.53×10^8. Using these estimates, we can treat the data for C_3H_8, n-C_4H_{10}, and cyclohexane to attempt to separate the reactivity of a CH_2 group toward $SO_2(^3B_1)$ quenching. According to this simple picture, the following relations may apply:

$$k_{CH_2} = k_{C_3H_8} - 2k_{CH_3} \qquad (D)$$

$$k_{CH_2} = (k_{n-C_4H_{10}} - 2k_{CH_3})/2 \qquad (E)$$

$$k_{CH_2} = k_{cyclohexane}/6 \qquad (F)$$

Relations (E) and (F) yield near-equal estimates of k_{CH_2} while those derived from (D) are somewhat lower. Values calculated from our present data for k_{CH_2} (ℓ. mole^{-1} sec^{-1}) from (D), (E), and (F), respectively, are as follows: 298° K: 2.04×10^8, 3.91×10^8, 4.06×10^8; 350° K: 3.36×10^8, 6.96×10^8, 6.06×10^8; 400° K: 4.72×10^8, 10.5×10^8, 8.08×10^8. If we couple the k_{CH_3} estimates with the present data for isobutane, the reactivity for the tertiary C-H group can be estimated from (G):

$$k_{CH} = k_{iso-C_4H_{10}} - 3k_{CH_3} \qquad (G)$$

Values of k_{CH} (ℓ. mole^{-1}sec^{-1}) are: 298° K: 6.31×10^8; 350° K: 8.45×10^8, 400° K: 9.94×10^8.

Values for the $SO_2(^3B_1)$ quenching per hydrogen atom type estimated from these data are shown in the Arrhenius plot of Figure 14, where k_p, k_s, and k_t are the rate constants per primary, secondary, and tertiary H atom, respectively. The activation energies and preexponential factors which result from these plots are summarised in Table XV. The preexponential factor for the $SO_2(^3B_1)$-quenching rate constants per H atom is the same for the three types of C-H bonds within the experimental error. However, it can be seen that the activation energies (kcal mole^{-1}) decrease regularly from about 2.9 for primary C-H bonds, to 2.0 for secondary C-H bonds, and to 1.1 for tertiary C-H bonds. The Evans-Polanyi-type relation, E_a (kcal mole^{-1}) = 0.26 [D_{R-H}(kcal mole^{-1}) - 86.7] fits this variation in E reasonably well.

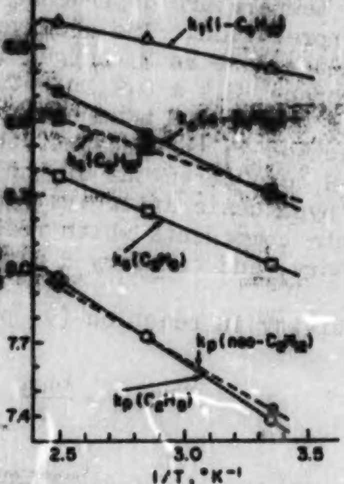

Figure 14. Arrhenius plots of the $SO_2(^3B_1)$ quenching constants per hydrogen atom for primary (k_p), secondary (k_s), and tertiary (k_t) C–H bonds in the paraffinic hydrocarbons. Data were derived from quenching data of the compounds shown in parentheses.

Thus it appears that the present data for the temperature dependence of the $SO_2(^3B_1)$-quenching rate constants are in accord with the dominance of chemical quenching in the case of ethane and higher paraffinic hydrocarbons. The H atom abstraction mechanism favored by Badcock et al[19] would be consistent with the data reported here; the insertion reaction suggested by some previous workers[58,59] cannot be excluded, but it seems less probable for reasons cited previously[19].

The $SO_2(^3B_1)$ quenching by NO and by the olefinic and aromatic hydrocarbons

The very large rate constants for $SO_2(^3B_1)$ quenching by NO and the olefinic and the aromatic hydrocarbons observed at room temperature by Sidebottom et al[20] are confirmed in this work. In Table XIV we note that most of these compounds exhibit very large preexponential factors; $\log_{10}$ [A (ℓ. mole^{-1} sec^{-1})]: NO, 11.96; C_2H_4, 11.36; CF_2CFH, 11.22; C_3H_6, 11.65; cis-2-C_4H_8, 11.66; cyclopentene, 11.44; C_6H_6, 11.38; the value of A for C_6F_6 is about a factor of 10 lower than that for C_6H_6. The activation energies for these reaction are very low; in some cases E_a is equal to zero within the experimental error. E_a values (kcal mole^{-1}) are: NO, 1.4 ± 0.7; C_2H_4, 1.1 ± 0.6; CF_2CHF, 1.7 ± 0.4; C_3H_6, 0.9 ± 0.6; cis-2-C_4H_8, 0.7 ± 0.4; cyclopentene, 0.4 ± 0.5; C_6H_6, 0.5 ± 0.7; and C_6F_6, 0.7 ± 0.7.

Table XV. Arrhenius parameters E_a and $\log_{10} A$ for the $SO_2(^3B_1)$-quenching rate constants (k_a) per H atom for C-H bonds of different type.

C-H Bond type	Relation used in estimate	E_a, kcal mole^{-1}	$\log_{10}[A$(l. mol^{-1} sec^{-1})]
Primary	(*B*)	3.1	9.65
	(C)	2.7	9.40
		Average 2.9	9.53
Secondary	(*D*)	2.0	9.44
	(*E*)	2.3	9.97
	(*F*)	1.6	9.48
		Average 2.0	9.66
Tertiary	(*G*)	1.1	9.38

Recent chemical studies of the $SO_2(^3B_1)$-cis-2-butene, $SO_2(^3B_1)$-trans-2-butene[60], $SO_2(^3B_1)$-cis-CHDCHD, and $SO_2(^3B_1)$-trans-CDHCDH[61] show that the quenching act in these cases results primarily in an isomerization reaction which occurs with near-perfect quantum efficiency. The triplet levels of these hydrocarbons are probably too high to allow triplet energy transfer to the olefin with the observed very high efficiency. Triplet energy transfer has been suggested by Cundall and Palmer[62] as the mechanism of isomerization in SO_2-cis-2-butene mixtures irradiated within the $SO_2(^1B_1) \leftarrow SO_2(^1A_1)$ band. The primary addition of triplet SO_2 to the olefinic double bond appears to rationalize all of the results best in our view. In accord with the previous suggestion of Sidebottom et al.[20], the quenching reaction may proceed through a highly polarized, charge transfer-like intermediate formed between $SO_2(^3B_1)$ and the π-system of the olefin. The collapse of this complex into an addition product which allows bond rotation probably occurs as observed in the $O(^3P)$-olefin reactions[63]. However, in the case of $SO_2(^3B_1)$ addition to a double bond in the gas phase, the addition complex seems to be unstable toward decomposition and regenerates isomerized olefin and SO_2 largely[60,61]. The present data are in accord with this view of the primary quenching act. The preexponential factors for reaction (9) are about the same for all of the olefins studied and are presumably characteristic of the $SO_2(^3B_1)$-π-bond interaction which is common to all these compounds. There is an apparent decrease in E_a (kcal mole^{-1}) as one progresses in the series of olefins in the order CF_2CFH, 1.7; C_2H_4, 1.1; C_3H_6, 0.9; cis-2-C_4H_8, 0.7; cyclopentene, 0.4. This is just the trend expected if the activation energy barrier in these reactions is inversely related to the polarizability of the π-bond in the formation of the charge transfer-like complex between $SO_2(^3B_1)$ and the π-system of the olefins. The accuracy of the present data is not sufficient to establish the origin of the comparative slowness of the $SO_2(^3B_1)$ quenching rate for C_6F_6 compared to C_6H_6. It appears that in this case a lower preexponential factor as well as a higher activation energy may exist.

The rate constant for the $SO_2(^3B_1)$-NO reaction has a low E_a (1.4 ± 0.7 kcal mole^{-1}) and a very high preexponential factor which appears to be peculiar of a chemical quenching mechanism. Conceivably the O atom transfer reaction, NO +

$SO_2(^3B_1) \rightarrow NO_2 + SO(^3\Sigma_g^-)$, may occur in this case, as it is somewhat exothermic: $\Delta H = -16$ kcal mole^{-1}. However, no spectroscopic or chemical information has been obtained from this system to test this or other alternative hypotheses.

I-D. A Kinetic Study of the Photoexcited $SO_2(^3B_1)$-Alkene Reactions[64]

The rate constants for the $SO_2(^3B_1)$ quenching reactions have been determined for a great variety of reactant molecules using phosphorescence lifetime studies in SO_2 quencher molecule mixtures[30,19,20]. The most rapid reactions observed in the previous work were those involving the olefinic hydrocarbons as the quencher molecule; the rate constants in this case were very near the collision number[20,47]. This result focuses new interest on the $SO_2(^3B_1)$-alkene reaction, since it may occur at a significant rate even in very dilute mixtures of alkene in the polluted atmosphere; the rate constant for $SO_2(^3B_1)$ quenching with O_2 and N_2 is only about 1/1400 of that for the butenes[30].

Little unambiguous information is now available concerning the chemistry of the $SO_2(^3B_1)$-alkene interactions, although some significant insight into the physical parameters of the reaction have been derived in recent years[20,47]. Sidebottom and coworkers[20] have suggested that the reaction may proceed through a highly polarized, charge-transfer-like intermediate formed between $SO_2(^3B_1)$ and the π-system of the olefin. The collapse of this complex into an intermediate addition product may occur as observed in the analogous $O(^3P)$-olefin reactions[63].

There are no published chemical studies which can be attributed unambiguously to the $SO_2(^3B_1)$-alkene reactions. There is considerable information related to the reactions in SO_2-alkene mixtures irradiated in the $SO_2(^1B_1) \leftarrow SO_2(\tilde{X}, {}^1A_1)$ band, but the fraction of the observed products which is derived from the $SO_2(^3B_1)$ state is unclear. Thus the previous studies of SO_2-alkene mixture photolysis of Bristow and Dainton[65], Cundall and Palmer[62], Penzhorn and Güsten[66], and Cox[67] suggest that SO_2 initially excited to the $^1B_1$ state may lead to the isomerization of the olefin. It is probable that the $^3B_1$ state is one of the reactants which leads to this overall change. Penzhorn and Güsten[66] have interpreted their results in terms of $SO_2(^3B_1)$ as the sole reactant with the olefin. Cox[67] gave this interpretation as well but concluded that some participation of other excited states may lead to olefin isomerization as well. The initial driving force for the change was thought to be the result of a triplet energy transfer from SO_2 to olefin[62], although this interpretation has been questioned by Sidebottom and coworkers[20]. Dainton and Ivin[58] photolyzed SO_2 in gaseous mixtures with 1-butene and found a product which had characteristics of an unsaturated sulfinic acid. Polysulfones are formed in irradiated SO_2-olefin solutions[65]. Cehelnik and coworkers[21] found that an O-atom transfer occurred from photoexcited SO_2 in gaseous CF_2CF_2 mixtures, and CF_2O was an observed product. Jones and Adelman[68] identified cyclic sulfites as products of irradiated SO_2-alkene-O_2 solutions. The very great variety of products which have been observed in the 2500-3200-Å irradiated SO_2-alkene mixtures have been rationalized by a number of different reaction schemes.

In this portion of our work we have attempted to characterize quantitatively the chemical pathways in which one of the excited states of sulfur dioxide, the phosphorescent $SO_2(^3B_1)$ state, reacts with the olefins cis-2-butene and trans-2-butene. We have excited this state directly by irradiating SO_2 within its "forbidden" $SO_2(^3B_1) \leftarrow SO_2(\tilde{X}, {}^1A_1)$ band at 3500-4100 Å. Quantum yields of olefin loss and isomerization were determined in a variety of experiments. In addition aerosol growth was monitored using light scattering measurements. In other experiments we have excited $SO_2(^3B_1)$ molecules using a 3630-Å laser beam and have determined directly the quenching rate constants for the 2-butenes. These results give a substantially new insight into the nature of the chemical mechanism of the $SO_2(^3B_1)$-alkene interactions.

I-D-1. Experimental

Equipment for Photochemical Studies

Photolyses were carried out in a cylindrical Pyrex reaction cell (diameter 4.5 cm; length 50 cm). The cell was connected in series with a thermal gradient pump for reactant mixing. The grease-free vacuum line and gas-handling system employed only Teflon stopcocks. Pressures of 20 torr or less were measured directly using a calibrated transducer-digital voltmeter combination. Pressures greater than 20 torr were measured on a mercury manometer using the transducer as a null device. The light source was an Osram XBO 450 high-pressure xenon arc held in an air-cooled housing equipped with a quartz condensing lens assembly. The light was filtered by passing it through several solutions and glass filters in combination[69]: (a) $CuSO_4$ (5.0 g/100 ml H_2O), 10-cm path; (b) 2,7-dimethyl-3,6-diazocyclohepta-1,6-diene perchlorate (0.01 g/100 ml of H_2O), 1-cm path; (c) Jena WG-1, 1-mm glass plate; (d) Corning 7-51 (5970), 5-mm glass plate; (e) the Pyrex front window of the photolysis cell. The light incident on the reactant mixture extended in a band from 3500 to 4100 Å and matched well the long wavelength region of the $^3B_1 \leftarrow X, {}^1A_1$ transition in SO_2[70]. The intensity versus wavelength spectrum of the arc and filter combination was determined using a Turner spectrofluorometer (model 210) in the luminescence-energy mode. A nearly uniform parallel beam of light was formed using light stops and condensing lens. The intensity of the beam was determined at regular intervals employing a 3.3-cm path of a 0.012 M potassium ferrioxalate solution and the procedures described by Hatchard and Parker[71]. The relative intensity of the incident light was also monitored continuously during photolyses by reflecting a small fraction of the beam with a quartz plate, angled with respect to the optical axis of the cell, onto a 935 phototube. These reflectance measurements and actinometry performed both after lamp warmup of one hour and at the finish of the eight-hour runs, showed less than ±3% variation in incident intensity during the run. However, because aerosol is formed in this system of alkene-SO_2 as the run progresses, the uncertainty in the absorbed intensities is somewhat greater, especially in runs at high pressures of SO_2. The average extinction coefficient of SO_2 for the band of incident light employed was estimated by two procedures. The small fraction of light absorbed by SO_2 was measured directly using a thermopile potentiometer-galvanometer system. This method gave the average decadic extinction coefficient $\bar{\epsilon} = 0.0266 \pm 0.0064$ ℓ./mole·cm. We also calculated $\bar{\epsilon}$ from the experimentally measured relative incident intensity versus wavelength data obtained from our lamp-filter system and experimental ϵ versus wavelength data for SO_2 in the forbidden $^3B_1 \leftarrow$, $X\ {}^1A_1$ band[70] determined on a spectrophotometer;

$$\epsilon = \int_{\lambda_1}^{\lambda_2} \epsilon I_0 d(\lambda) \Big/ \int_{\lambda_1}^{\lambda_2} I_0 d(\lambda) = 0.0206 \pm 0.002 \text{ l./mole·cm}, \quad \lambda_1 = 3400 \text{ Å and } \lambda_2 = 4300 \text{ Å}.$$

In one series of experiments the intensity of light scattering from aerosol was determined throughout the photolyses using a system designed by Dr. Charles Badcock. A horizontal He-Ne laser beam transversed the photolysis cell at right angles to the cell axis. An 1P28 phototube detector system was mounted in a light shield which surrounded the cell and received scattered radiation at 90° from the laser beam and at right angles to the cell axis.

Equipment for $SO_2(^3B_1)$ Phosphorescence quenching studies

A tunable dye laser, using 3,3'-dimethyl-2,2'-oxatricarbocyanine iodide (Candella Co.) in acetone solution as the active medium and a 75-MW ruby laser as the pumping source, was employed to excite SO_2 directly from the ground state to the $^3B_1$ state. The 20-nanosecond 5-10 kW dye laser pulse had a half-width of about 2 Å and was centered at 3630 Å. The cell used for excitation was a 21-liter Pyrex flask to the sides of which were attached cylindrical sections with Supracil windows sealed at the Brewster angle. The relative intensity of the emission from the $SO_2(^3B_1)$ as a function of the time was observed at right angles to the incident laser beam using a phototube receiver and photographing the oscilloscopic trace of the signal.

A Perkin-Elmer (model F11) flame ionization gas chromatograph was used in the analyses of the cis- and trans-2-butene. A 3-ft by 1/8-in stainless-steel column packed with 10% by weight NaCl on 90% by weight activated alumina (90-100 mesh) gave excellent separations of the butene isomers. The column was prepared as described by Brookman and Sawyer[72]. It was found that optimum isomer separation of the butenes was attained at a column temperature of 130° C rather than 200° C for our conditions. We found that large concentrations of SO_2 introduced error in the analyses, first by increasing the noise level in the FID signal and second (in cases of very large SO_2 concentrations, i.e., $P_{SO_2} >$ 300 torr) by sensitizing the column to catalytically convert one butene isomer to the other. This problem was solved by use of a 1-ft by 1/4-in stainless steel precolumn packed with NaOH-coated glass beads, which stripped away the SO_2. Calibration curves from the butenes were made with and without the stripping precolumn, and the results were identical within the experimental error. The major limitation to the use of the alumina-salt column was that of sample size. With butene samples of 0.07 torr in 10 cm^3 (3.8×10^{-8} moles) or greater, tailing was observed; therefore, samples of this size were reduced by expansion before analysis. The column gave linear response to the butenes from 0.07 torr in 10 cm^3 down to the limit of the FID response (0.0001 torr). Peak areas were automatically calculated by an Infotronics (model CRS-11 HDB) electronic digital integrator with paper tape print out.

Quantum Yield Measurements of $SO_2(^3B_1)$-sensitized Isomerization of the 2-Butenes

The photolysis of SO_2-2-butene (cis- or trans-) mixtures within the triplet absorption band of SO_2 results largely in isomerization. Aerosol formation was observed in experiments with high concentrations of SO_2, but 2-butene loss was very small. Photolysis studies in which the photostationary concentrations of isomers were determined, showed $< 6.0 \pm 1.0\%$ butene loss in 1000 min of irradiation time. From the known rate of light absorption in these experiments we estimate the quantum yield of butene loss to be less than or equal to 0.016 ± 0.003. A summary of the quantum yields of isomerization from photolysis experiments of SO_2-cis-2-butene and SO_2-trans-2-butene mixtures is given in Table XVI. Quantum yields of isomerization were calculated using initial rates determined from the least squares fit of the percent isomerization versus time curves. In most cases data with conversions $\leq 15\%$ and irradiation times less than 100 min were used in the treatment of the data. This reduced the possible error introduced by the occurrence of the back reaction, butene loss, and uncertainties in the absorbed intensity of light which resulted at long exposure times from light

Table XVI. Quantum yields of $SO_2(^3B_1)$-sensitized isomerization of the 2-butenes.[a]

Run No.	P_{SO_2}, Torr	$P_{C_4H_8}$, Torr	$P_{SO_2}/P_{C_4H_8}$	Incident Light Intensity, quanta cell^{-1}sec^{-1} × 10^{-14}	Initial Quantum Yield of Isomerization of 2-Butene
1	17.4	0.803	21.7	3.37	0.48
2	97.8	2.04	47.9	2.59	0.41
3	80.8	0.908	89.0	3.82	0.50
4	97.9	1.00	97.9	2.68	0.48
5	80.1	0.513	156	3.27	0.37
6	123	0.815	151	4.14	0.40
7	98.7	[illegible]	[illegible]	2.45	0.33
8	173	[illegible]	[illegible]	3.88	0.45
9	99.9	[illegible]	328	2.91	0.40
10	79.9	[illegible]	[illegible]	[illegible]	[illegible]
11	95.2	[illegible]	[illegible]	[illegible]	[illegible]
12	[illegible]	[illegible]	[illegible]	[illegible]	[illegible]
13	[illegible]	[illegible]	[illegible]	[illegible]	[illegible]
14	373	[illegible]	[illegible]	[illegible]	[illegible]
15	[illegible]	[illegible]	[illegible]	[illegible]	[illegible]
16	[illegible]	[illegible]	[illegible]	[illegible]	[illegible]
17	[illegible]	[illegible]	[illegible]	3.73	[illegible]
18[b]	[illegible]	[illegible]	1017	[illegible]	[illegible]
19[b]	109	0.981	111	[illegible]	[illegible]
20[b]	137	0.714	192	[illegible]	[illegible]
21[c]	198	0.612	324	3.24	[illegible]
22[c]	376	0.385	976	2.60	[illegible]
23[c]	297	0.523	568	2.76	[illegible]
24[c]	302	0.523	577	2.65	0.28
25	569	0.585	971	2.75	0.25
26	23.6	0.383	61.6	2.95	0.28
27	270	0.697	387	3.32	0.31
28	385	0.483	797	3.35	0.14
29	737	0.885	833	3.36	0.15

[a] Excitation of $SO_2(^3B_1)$ was effected by irradiation using 3500–4100-Å light; in runs 1–25 the initial olefin was the *cis*-2-butene isomer, and in runs 26–29 the initial olefin was the *trans*-2-butene isomer; all runs were carried out at room temperature.

[b] Helium gas was added in these runs; 19, 20, and 21 had 519, 487, and 632 torr, respectively.

[c] Oxygen gas was added in these runs; 22, 23, 24, and 25 had 0.46, 0.97, 2.47, and 47.6 torr, respectively.

scatter due to aerosol formation in the mixtures at high SO_2 pressures.

The effects of added helium and oxygen gases on the quantum yields is isomerization in SO_2-cis-butene mixtures were determined in runs 19-21 and 22-25, respectively.

Light Scattering Measurements

Some information regarding aerosol formation in the $SO_2(^3B_1)$-butene system was obtained in one series of runs summarized in Table XVII. There are several measures of the relative importance of aerosol formation provided in the table: (a) the time of first detection of the 6328-Å light scattering; (b) the initial rate of increase of the intensity of this scattered light; and (c) the initial rate of decrease of the 4100-3500-Å "transmitted" light as observed at the rear of the photolysis cell.

$SO_2(^3B_1)$ Quenching by 2-Butenes

The lifetimes of the $SO_2(^3B_1)$ molecules excited within the forbidden band at 3630 Å were determined in SO_2-2-butene mixtures at a constant $[SO_2]$ but varied butene concentration. These data are given in Table XVIII. Each lifetime point was derived from the average of several (usually five) determinations. The error limits shown for each data point represent the rms deviation of the individual determinations of $1/\tau$ from the average.

Table XVII. Aerosol formation in the $SO_2(^3B_1)$ reaction in SO_2-2-butene mixtures.[a]

Run No.	Reactant Pressure, Torr SO_2	Reactant Pressure, Torr 2-C_4H_8[b]	(1) Rate of Increase of 6328 Å Scattered Light Intensity, Relative Units	(2) Time of First Detection of 6328 Å Light Scatter, min.	(3) Rate of Decrease of 4100-3500 Å Transmitted Light Intensity, % min^{-1}	(4) Relative Rate of $SO_2(^3B_1)$ Quenching: SO_2	(5) Relative Rate of $SO_2(^3B_1)$ Quenching: 2-C_4H_8	(6) $\frac{(3)}{(5)}$	(7) $\frac{(3)}{(4)}$	(8) $\frac{(1)}{(5)}$	(9) $\frac{(1)}{(4)}$
1	650	0.000	3.1	1	0.81	1.00	0.00	∞	0.8	∞	3.1
2	635	0.683	5.3	6	1.08	0.71	0.27	4.0	1.5	20	7.5
3	626	0.674	5.5	3	1.25	0.69	0.27	4.6	1.8	20	8.0
4	617	0.664	4.3	1	1.15	0.69	0.27	4.3	1.7	16	6.2
5	609	0.655	3.9	3	1.22	0.68	0.26	4.7	1.8	15	5.7
6	519	0.604	3.7	12	0.76	0.56	0.24	3.2	1.4	15	6.6
7	509	0.596	5.4	8	0.86	0.55	0.23	3.7	1.6	23	9.8
8	502	0.587	4.6	6	0.83	0.54	0.23	3.6	1.5	20	8.5
9	374	0.627	3.9	18	0.58	0.36	0.22	2.6	1.6	18	10.8
10	368	0.618	2.6	16	0.62	0.35	0.22	2.8	1.8	12	7.4
11	364	0.610	2.5	16	0.67	0.35	0.21	3.2	1.9	12	7.1
12	359	0.601	1.3	18	0.50	0.34	0.21	2.4	1.5	6	3.8
13	287	0.635	0.0	42	c	0.25	0.20	---	---	0	0.0
14	283	0.626	1.3	28	c	0.25	0.19	---	---	7	5.2
15	279	0.617	0.0	36	c	0.24	0.19	---	---	0	0.0
16	215	0.612	0.0	55	0.22	0.17	0.17	1.3	1.3	0	0.0
17	212	0.605	0.71	39	c	0.16	0.16	---	---	4.4	4.4
18	209	0.595	0.76	39	c	0.16	0.16	---	---	4.8	4.8
19	737	0.886	3.0	2	1.30	0.80	0.34	3.8	1.6	8.8	3.8
20	727	0.874	3.7	5	1.17	0.78	0.34	3.4	1.5	11	4.7
21	716	0.861	4.4	9	0.83	0.77	0.33	2.5	1.1	13	5.7
22	707	0.850	3.4	5	0.96	0.76	0.33	2.9	1.3	10	4.4
23	384	0.483	0.0	30	0.3	0.41	0.18	1.7	0.7	0	0.0
24	379	0.476	1.94	19	0.6	0.40	0.18	3.3	1.5	11	4.9
25	373	0.470	0.97	24	0.5	0.40	0.18	2.8	1.3	5.4	2.4
26	368	0.463	0.63	22	0.6	0.39	0.17	3.5	1.5	3.7	1.6

[a] All runs were carried out at room temperature. No detectable aerosol was present at the start of each photolysis period. Excitation was effected using 3500–4100-Å light.

[b] The initial reactant, 2-butene, was the *cis*-isomer in runs 1–18 and the *trans*-isomer in runs 19–26.

[c] Data not obtained in this experiment.

Table XVIII. Lifetimes of $SO_2(^3B_1)$ molecules excited in SO_2-2-butene mixtures.[a]

Pressure, cis-2-C_4H_8 $\times 10^3$ torr	$1/\tau \times 10^{-4}$, sec^{-1}	Pressure, trans-2-C_4H_8 $\times 10^3$ torr	$1/\tau \times 10^{-4}$ sec^{-1}
0.0	4.66 ± 0.32[b]	0.0	5.32 ± 1.13
1.84	5.79 ± 0.38	2.84	6.12 ± 1.15
4.21	6.77 ± 0.50	3.06	6.85 ± 0.90
6.50	9.27 ± 0.43	4.48	7.49 ± 0.70
8.74	11.47 ± 0.77	4.52	7.86 ± 0.43
10.58	13.85 ± 1.42	6.54	9.69 ± 0.89
11.72	13.60 ± 0.58	6.98	10.59 ± 1.45
15.05	14.95 ± 0.68	9.25	12.18 ± 1.59
17.25	15.97 ± 0.96	11.40	14.23 ± 2.02
		16.46	16.38 ± 3.29
		19.55	16.87 ± 0.68

[a] The $SO_2(^3B_1)$ molecules were excited at 21°C using a 3830-Å laser pulse in mixtures containing 1.55 torr of SO_2 and pressures of the 2-butene isomer indicated.

[b] Error limits shown represent the rms deviation of the measured values from the reported average $1/\tau$ value.

I-D-2. Discussion of Results

Mechanism of $SO_2(^3B_1)$ Induced cis-trans Isomerization of 2-Butenes

The major chemical result of the excitation of $SO_2(^3B_1)$ molecules in cis-2-butene or trans-2-butene containing mixtures is an isomerization of the alkene. Note in Figure 15 that the composition of a mixture containing initially either pure trans- or pure cis-isomer with SO_2 reaches the same photostationary state after extended irradiation with light absorbed within the $SO_2(^3B_1) \leftarrow SO_2(\tilde{X}, {}^1A_1)$

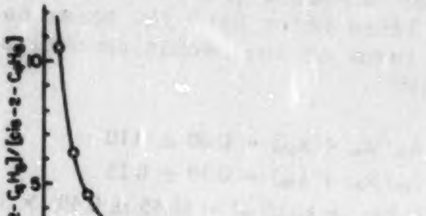

Figure 15. Time dependence of [*trans*-2-butene]/[*cis*-2-butene] ratio in 3500–4100-Å irradiated mixtures of 2-butenes and SO_2. Upper curve—initial pressures (torr): SO_2 737, *trans*-2-butene 0.852; lower curve— initial pressures (torr): SO_2 211, *cis*-2-butene 0.642; temperature 25°C.

band; [trans-2-butene]/[cis-2-butene] = 1.9 ± 0.1. Some interesting mechanistic details concerning this chemical change can be had from a consideration of the initial quantum yields of $SO_2(^3B_1)$-sensitized isomerization of the 2-butenes reported in Table XVI. First consider the simplest possible reaction mechanism (1)-(5) which can rationalize the data. Other alternatives and possible complications will be considered subsequently.

$$\text{(I)} \quad SO_2 + h\nu\ (3600\text{–}4100\ \text{Å}) \rightarrow SO_2(^3B_1)$$

$$\text{(1a)} \quad SO_2(^3B_1) \rightarrow SO_2 + h\nu_p$$

$$\text{(1b)} \quad SO_2(^3B_1) \rightarrow (SO_2)$$

$$\text{(2a)} \quad SO_2(^3B_1) + SO_2 \rightarrow SO_3 + SO(^3\Sigma^-)$$

$$\text{(2b)} \quad SO_2(^3B_1) + SO_2 \rightarrow (2SO_2)$$

$$\text{(3a)} \quad SO_2(^3B_1) + cis\text{-2-}C_4H_8 \rightarrow (cis\text{-2-}C_4H_8SO_2)^3$$

$$\text{(3b)} \quad SO_2(^3B_1) + trans\text{-2-}C_4H_8 \rightarrow (trans\text{-2-}C_4H_8SO_2)^3$$

$$\text{(4)} \quad (cis\text{-2-}C_4H_8SO_2)^3 \rightarrow (2\text{-}C_4H_8SO_2)^3 \leftarrow (trans\text{-2-}C_4H_8SO_2)^3$$

$$\text{(5a)} \quad (2\text{-}C_4H_8SO_2)^3 \rightarrow cis\text{-2-}C_4H_8 + SO_2$$

$$\text{(5b)} \quad (2\text{-}C_4H_8SO_2)^3 \rightarrow trans\text{-2-}C_4H_8 + SO_2$$

Here we have assumed that the $SO_2(^3B_1)$-alkene interaction leads to transient triplet addition complexes which, within the time scale of events measured in this work, are structurally indistinguishable and decay rapidly to ground state cis- or trans-2-butene and SO_2. If these reactions occur, then the quantum yield results should be described by relations (A) and (B):

$$\text{(A)} \quad \frac{1}{\Phi_{c\rightarrow t}} = \left(\frac{k_{5a} + k_{5b}}{k_{5b}}\right)\left(\frac{k_{2a} + k_{2b}}{k_{3a}}\right)\frac{[SO_2]}{[cis\text{-2-}C_4H_8]} + \frac{k_{5a} + k_{5b}}{k_{5b}}$$

$$\text{(B)} \quad \frac{1}{\Phi_{t\rightarrow c}} = \left(\frac{k_{5a} + k_{5b}}{k_{5a}}\right)\left(\frac{k_{2a} + k_{2b}}{k_{3b}}\right)\frac{[SO_2]}{[trans\text{-2-}C_4H_8]} + \frac{k_{5a} + k_{5b}}{k_{5a}}$$

The data of Table XVI have been plotted in Figure 16 to test the theoretically expected linear relationship between the reciprocal of the initial quantum yield of isomerization and the $[SO_2]/[2\text{-}C_4H_8]$ ratio. Within the experimental error of the data a reasonable fit to relations (A) and (B) is seen. The slopes and intercepts of the least squares lines which best fit these data provide the following rate constant estimates in terms of the mechanism outlined; error limits represent the 95% confidence limits (2σ).

$$k_{5b}/(k_{5a} + k_{5b}) = 0.60 \pm 0.10$$

$$k_{5a}/(k_{5a} + k_{5b}) = 0.39 \pm 0.15$$

$$[(k_{2a} + k_{2b})/k_{3a}][(k_{5a} + k_{5b})/k_{5b}] = (3.45 \pm 0.48) \times 10^{-3}$$

$$[(k_{2a} + k_{2b})/k_{3b}][(k_{5a} + k_{5b})/k_{5a}] = (5.18 \pm 1.60) \times 10^{-3}$$

Within the large experimental error the sum of the ratios $k_{5a}/(k_{5a} + k_{5b}) + k_{5b}/(k_{5a} + k_{5b})$ is unity as one would expect if a common precursor to the cis- and trans-2-butenes is involved. Combining the slope to intercept ratios obtained here with the experimental values for $k_{2a} + k_{2b} = (3.9 \pm 0.1) \times 10^8$ ℓ./mole·sec at 25° C[50,26,47], the data give the following rough estimates for

k_{3a} and k_{3b}:

$$k_{3a} = (1.9 \pm 0.4) \times 10^{11}\ \text{l./mole·sec}$$
$$k_{3b} = (1.9 \pm 0.9) \times 10^{11}\ \text{l./mole·sec}$$

According to the suggested mechanism the ratio of [*trans*-2-butene]/[*cis*-2-butene] at the photostationary state should be equal to $(k_{3a}/k_{3b})(k_{5b}/k_{5a})$; using the above rate constant estimates the expected *trans*/*cis* ratio is 1.5 ± 1.0. Within the very large error limits this is in accord with the directly measured ratio of 1.9 ± 0.1.

The quantum yield data presented suggest the near equality of the $SO_2(^3B_1)$ quenching rate constants for *cis*-2-butene and *trans*-2-butene as quenchers. To test this point more directly we determined these constants independently in $SO_2(^3B_1)$ lifetime studies in this work using a 3630-Å laser pulse excitation. A Stern-Volmer plot of these data (Table XVIII) is shown in Figure 17. The slopes of these lines give direct estimates of k_{3a} and k_{3b} at the temperature of the experiments, 21° C:

$$k_{3a} = (1.29 \pm 0.16) \times 10^{11}\ \text{l./mole·sec}$$
$$k_{3b} = (1.22 \pm 0.15) \times 10^{11}\ \text{l./mole·sec}$$

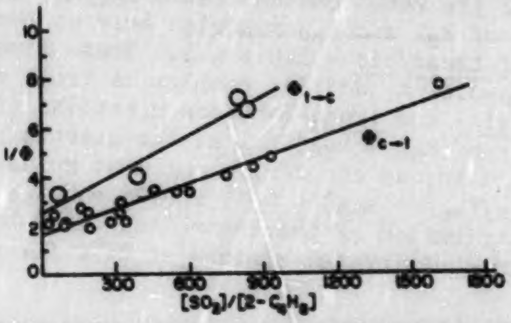

Figure 16. Plot of reciprocal of initial quantum yield of isomerization of 2-butenes versus [SO$_2$]/[2-butene] ratio from 3500–4100-Å irradiated mixtures. Upper curve—*trans*-2-butene and SO$_2$; lower curve—*cis*-2-butene and SO$_2$; temperature 25°C.

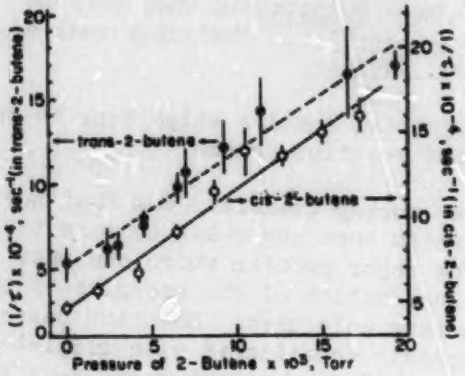

Figure 17. Stern–Volmer plot of SO$_2$($^3B_1$) lifetime data. Upper curve—in *trans*-2-butene-SO$_2$ mixtures; lower curve—in *cis*-2-butene-SO$_2$ mixtures; excitation of SO$_2$ by 3630-Å laser pulse; pressure of SO$_2$ constant at 1.55 torr; temperature 21°C.

These estimates agree well within the experimental error with the less accurate indirect estimates derived from the slope/intercept ratios obtained from the $1/\Phi$ versus $[SO_2]/[2\text{-}C_4H_8]$ plots in Figure 16. The lifetime data confirm the conclusion that the $SO_2(^3B_1)$ quenching rate constants for cis- and trans-2-butenes are the same within the experimental error. These estimates are in fair agreement with those derived indirectly by Cox[67] from photochemical studies of SO_2-2-butene mixtures excited within the first allowed band of SO_2 which he attributed to these reactions: $k_{3a} = (1.62 \pm 0.08) \times 10^{11}$ and $k_{3b} = (1.42 \pm 0.09) \times 10^{11}$ ℓ./mole·sec. However, this agreement may be somewhat fortuitious, since we have observed some previously unrecognized complicating factors related to the Cox interpretation of the reactions of singlet excited SO_2 in 2-butene mixtures; see the section I-E following.

The present data for k_{3a} show that the magnitude of this rate constant is insensitive to the degree of the initial vibrational excitation of the $SO_2(^3B_1)$ molecule formed, at least over the range of the triplet energies excited in the broadband quantum yield experiments reported here. In our previous work $SO_2(^3B_1)$ excitation was effected near the (0,1,0) level at 3829 ± 1 Å (74.6 kcal/mole), and we found $k_{3a} = (1.34 \pm 0.10) \times 10^{11}$ ℓ./mole·sec at 25° C[42] and $(1.38 \pm 0.15) \times 10^{11}$ ℓ./mole·sec at 21° C, calculated from the measured Arrhenius parameters derived from studies at several temperatures[47]. Thus our present neglect of the $SO_2(^3B_1)$ vibrational relaxation steps and alternate reactions (2) and (3) from various vibronic levels is justified.

The best estimate of the rate constant ratio k_{5b}/k_{5a} is obtained using our directly measured values of k_{3a} and k_{3b} reported here at the observed photostationary-state ratio of trans/cis = 1.9 ± 0.1. These give $k_{5b}/k_{5a} = 1.80 \pm 0.35$. If the triplet SO_2-olefin addition complex is truly structurally indistinguishable for the cis- and trans-2-butene reactions (5a) and (5b), and hence $k_{5a}/(k_{5a} + k_{5b}) + k_{5b}/(k_{5a} + k_{5b}) = 1$ as the quantum yield data suggest within the large error limits, we can derive our most reliable estimate of the rate constant ratios: $k_{5a}/(k_{5a} + k_{5b}) = 0.35 \pm 0.05$ and $k_{5b}/(k_{5a} + k_{5b}) = 0.65 \pm 0.05$. Note that the distribution of the trans- and cis-2-butenes is very different from the thermally equilibrated mixture at 25° C for which trans/cis = 3.85*, and the observed ratio of 0.92-0.94 obtained when benzene triplet was the sensitizer of the butene isomerization[74-77]. Obviously real mechanism differences exist between these different systems.

Consider now the experimental results which bear on several mechanistic alternatives to the suggested reaction scheme.

Conceivably the triplet energy transfer from $SO_2(^3B_1)$ may occur directly to excite the triplet alkene which then may relax to form the cis- and trans-isomers in their ground states. The major problem which one must face in the evaluation of this alternative is the estimation of the energies of the different configurations of the triplet 2-butene molecules. Solution phase studies of Fukano and Sato[78] suggest that many organic sensitizers with triplet energies greater than 70 kcal/mole (pyrazine, $E_T = 84.8$, to acetophenone, $E_T = 73.6, 76.3$) efficiently isomerize cis- or trans-2-butene. Even some sensitizers with triplet energies less than 70 kcal/mole cause isomerization (benzophenone, $E_T = 68.5, 69.3$, to naphthalene, $E_T = 60.9$), although the reaction is very slow in these cases. Also Shekk and Alfimov[79] found that *cis*- and *trans*-2-butene quenched the phosphorescence of various organic triplet excited species in polycrystalline glasses of the alkenes at liquid nitrogen temperature, when the triplet donors had energies which lay above 73.6-71.8 kcal/mole. Penzhorn and Güsten[66] estimated from the oxygen perturbed singlet-triplet spectra of 2-butene solutions that for the *trans*-2-butene $E_T > 76$ kcal/mole and for *cis*-2-butene $E_T = 70 \pm 2$ kcal/mole. Indeed triplet energy transfer was suggested by Cundall and Palmer[62] as the mechanism of the *cis*-2-butene $\rightleftarrows$ *trans*-2-butene isomerization observed in gaseous SO_2-butene mixtures irradiated within the first allowed band of SO_2; this alternative has also been considered among others in more recent studies of this system[66,67]. However, the possibility that the *cis-trans* isomerization and the phosphorescence quenching observed in the previous solution phase studies resulted from the addition of the triplet donor to the alkene double bond cannot be discounted from the evidence at hand. Furthermore, as Wagner and Hammond have pointed out previously[80], the fact that the triplet energy transfer may occur in solution even at the diffusion-controlled rate merely means that its inefficiency is not so great that reaction cannot occur during the characteristic prolonged encounter time between reactants in solution.

---

* Obtained from the least squares extrapolation to room temperature of the equilibrium data of ref. 73.

The results of gas phase studies appear to give more definitive data on the nature and efficiency of the triplet energy transfer to the alkenes. The transfer of triplet energy from excited acetone ($E_T = 77 \pm 2$ kcal/mole)* to the olefinic hydrocarbons is relatively inefficient in the gas phase; in fact the probability that energy transfer will occur on collision between triplet acetone and 2-pentene is only 2.1×10^{-5}. Rebbert and Ausloos[81] attribute this inefficiency to the endothermicity of the energy transfer reaction. As Sidebottom and coworkers have argued[20], if in the acetone triplet-olefin reaction, energy transfer is already inefficient because of its endothermicity, the energy transfer from $SO_2(^3B_1)$, $E_T = 73.6$ kcal/mole, to olefins must be much less efficient.

Ion energy-loss spectroscopy with the olefins has been carried out by Moore[84] who estimated that the energy for the maximum transition intensity (related to the ground state to first excited triplet transition) both in *cis*- and trans-2-butenes occurs at 4.2 eV (97 ± 2 kcal/mole); recent results from sililar studies of Flicker, Mosher, and Kupperman[85] gave preliminary values for the vertical transition energy for *cis*-2-butene of 4.22 ± 0.07 eV (97 ± 2 kcal) and for *trans*-2-butene of 4.25 ± 0.06 eV (98 ± 1 kcal). Moore's data suggest that the low-intensity onset of the transition with *cis*-2-butene appears to be near the $SO_2(^3B_1)$ energy of 73.6 kcal/mole.

---

* An upper limit of 79 kcal/mole can be set for acetone triplet energy by the position of the 0-0 band of the $S_0 \rightarrow S_1$ transition at 3600 Å[82]. A lower limit has been suggested by Sidebottom and coworkers[20], who found that quenching SO_2 $(^3B_1)$ by acetone is rather inefficient ($k_q = 1.2 \times 10^9$ l./mole·sec), yet SO_2 quenches acetone triplet at a rate near the collision number[83]. Thus it is highly probable that the acetone triplet lies above 73.6 kcal/mole. If the rate of quenching of $SO_2(^3B_1)$ by acetone is from the energy transfer reaction exclusively and the relative slowness is a consequence of the endothermicity of the reaction alone, then E_T for acetone $\cong 77$ kcal/mole.

On the basis of all available information it appears to us that the $SO_2(^3B_1)$ energy may be insufficient to excite the alkene triplets with a rate constant which is near the collision number as was observed experimentally, since most $SO_2(^3B_1)$-alkene encounters must involve molecules of the olefin in the near-planar configurations expected at 25° C in the gas phase; direct triplet energy transfer is probably considerably endothermic for most of these encounters. We also note from the data of Sidebottom and coworkers[20] that the measured $SO_2(^3B_1)$ quenching rate constant for trichlorethylene, $(2.3 \pm 0.2) \times 10^{10}$ ℓ./mole·sec, is less than that for ethylene, $(4.2 \pm 0.5) \times 10^{10}$ ℓ./mole·sec, although the triplet energy for the chloroethylenes lies below that of ethylene[84,86,87]. This again does not support a hypothesis of quenching by a direct triplet energy transfer mechanism.

The rate constants (ℓ./mole·sec) for the $^3B_1$ quenching by the simple olefins correlate well with the polarizability of the olefinic hydrocarbon double bonds[20]: C_2H_4, 4.2×10^{10}; C_3H_6, 8.5×10^{10}; cis-2-C_4H_8, 13×10^{10}; CF_2CFH, 1.1×10^{10}; CCl_2CClH, 2.3×10^{10}; cyclopentene, 11×10^{10}. This correlation is similar to that observed for the $O(^3P)$ reactions with the alkenes[63] where a charge transfer intermediate has been suggested and the ultimate addition of the O atom to the double bond of the alkene does occur. The preexponential factors for the quenching rate constants for the simple olefins are all about the same and very near the collision number; $\log_{10}A$ (ℓ./mole·sec): C_2H_4, 11.36; CF_2CFH, 11.22: C_3H_6, 11.65; cis-2-butene, 11.66; cyclopentene, 11.44[47]. Presumably this reflects a relatively unhindered $SO_2(^3B_1)$-π-bond interaction which is common to all of these alkenes. The rate constant differences observed with structural changes of the olefins originate largely in differences in the activation energy (kcal/mole) for the quenching rate constants: C_2H_4, 1:1; CF_2CHF, 1.7; C_3H_6, 0.9; cis-2-C_4H_8, 0.7; cyclopentene, 0.4. This is just the trend expected if the activation energy barrier in these reactions is inversely related to the polarizability of the π bond. The observed differences in activation energies do not seem to be in line with those expected for the occurrence of direct triplet energy transfer and reasonable triplet energy differences between the structurally different species.

In our opinion the chemical mechanism outlined by Sidebottom and coworkers[20] seems most consistent with all the results observed here and previously for this system. That is, the quenching may proceed through a highly polarized charge transfer-like intermediate formed between $SO_2(^3B_1)$ and the π system of the alkene. Presumably this complex may collapse into a transitory addition product which allows rotation of the groups about the central C - C bond with the ultimate dissociation of the complex into the alkene isomers and SO_2. This is very similar to the mechanism favored by Caldwell and James[86] for the benzophenone triplet sensitized isomerization of cis- and trans-2-butene in benzene solution where the observed deuterium isotope effect on the quenching rate constants is very small, and addition to the butene double bond is evident from the formation of some oxetane product. It is also analogous to the mechanism of Kochevar and Wagner who studied the olefin quenching of the Norrish type II photoelimination in butyrophenone triplet in benzene solution[87]. Both groups of workers conclude that triplet energy transfer is not the major quenching reaction in the simple olefin-$RCOC_6H_5$-triplet systems, but suggest that some type of charge transfer complex is involved in the rate-determining step of the quenching process.

The effect of added gases on the quantum yield of isomerization gives some insight into the timing of the isomerization reactions. Large quantities of He gas were added in runs 19-21 and small quantities of a commonly employed triplet quencher gas O_2 were added in runs 22-25 of Table XVI. Presumably added gases could affect the quantum yield in at least three critical points in the reaction mechanism: (a) The $SO_2(^3B_1)$ can be quenched by the added gas in reaction (6):

$$\text{(6)} \qquad SO_2(^3B_1) + He\ (\text{or } O_2) \rightarrow (SO_2) + He\ (\text{or } O_2)$$

(b) The internal energy of the SO_2-2-butene triplet complex may be altered by the collisional relaxation, and some product other than the olefin isomers might be stabilized. (c) Oxygen may trap the SO_2-2-butene triplet complex and form some stable oxygenated SO_2-olefin containing species such as

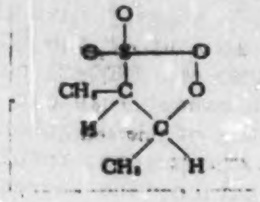

The quantum yield data show that the main influence of the added gases is in reaction (6). Assuming that the only effect on the rate of isomerization will be that due to the deactivation of the triplets in reaction (6) and taking the experimental estimates of $k_6 = 6.8 \times 10^7$ (He) and 9.6×10^7 (O_2) ℓ./mole·sec[16], the average of our best estimates of $k_{3a} = 1.34 \times 10^{11}$ ℓ./mole·sec and $k_{5b}/(k_{5a} + k_{5b}) = 0.65$, we may calculate the theoretically expected values of $\Phi_{c\rightarrow t}$ from the relation (C) where M is He or O_2:

$$\text{(C)} \qquad \frac{1}{\Phi_{c\rightarrow t}} = \left(\frac{[SO_2](k_{3a} + k_{3b}) + [M]k_6}{[cis\text{-}2\text{-}C_4H_8]k_{3a}}\right)\left(\frac{k_{5a} + k_{5b}}{k_{5b}}\right) + \frac{k_{5a} + k_{5b}}{k_{5b}}$$

The experimental quantum yields for runs 19-21 with added He (0.35, 0.33, and 0.33, respectively) check reasonably well with the theoretical values (0.41, 0.34, and 0.27, respectively). Again in runs 22-25 with added O_2 the experimental values (0.24, 0.28, 0.23, and 0.22 respectively) are in accord with the theoretical values (0.24, 0.24, 0.24, and 0.24, respectively). The lifetime of the precursor SO_2-2-butene triplet adduct must be very short lived in that there is no evidence of its interaction with these added gases.

It is possible that the reactions (3a) and (3b) are rate determining, yet (5a) and (5b) proceed through the intermediacy of the stable twisted 2-butene triplet state. Conceivably as rotation about the central C — C bond occurs in the addition complex, and the original planar configuration of the carbon skeleton approaches more nearly that of the stable twisted triplet of 2-butene, the potential energy surface of the complex will cross that leading to the triplet olefin and ground state SO_2 as well as the surface leading to two ground state molecules in reaction (5a) and (5b). Such a reaction path avoids the endothermic route of vertical triplet energy transfer. One might designate this potential reaction as a "chemically induced triplet energy transfer". The ultimate involvement of the triplet alkene here seems unlikely in that it would appear to favor a near equal distribution of the isomers as is seen in the benzene-triplet sensitized cis-trans isomerization of the 2-butenes, both in solution[74,75] and in the gaseous state[76,77]. In these experiments with the benzene triplet, probably a true triplet energy transfer to the olefin does occur.

The indefinite product designation (SO_2) and ($2SO_2$) in reactions (1b) and (2b) specifies some undetermined state or states of SO_2 such as SO_2 ($\tilde{X}$, $^1A_1$),

$SO_2(^3A_2)$, and $SO_2(^3B_2)$. The latter two excited states could be involved in the isomerization of the 2-butenes as well as the initially excited species $SO_2(^3B_1)$. This possible complication must be considered seriously in view of the mechanistic suggestions of Heicklen and coworkers[56,57,88-90]. In addition to these possible reactive products of reaction (1b) and (2b), $SO(^3\Sigma^-)$ and SO_3 formed in reaction (2a) could conceivably react with olefin to induce isomerization. Our recent results show that 10% of the quenching collisions of $SO_2(^3B_1)$ with SO_2 lead to the chemical path (2a) at 25° C[91]. Perturbations in the $SO_2(^3B_1) \leftarrow SO_2\ (X,{}^1A_1)$ spectrum seen by Brand and coworkers[92] suggest that the potential energy surfaces for the $^3B_2$ and $^3A_2$ states cross that of the $^3B_1$ state somewhere near the (1,1,0) level of the $^3B_1$ state. SCFMO and INDO-CI calculations on SO_2 also are consistent with this view[53,54]. One cannot rule out entirely some contribution to the isomerization from the reaction of these intermediates and products with the olefin, but it can be seen from the present results that such reactions can provide no more than a minor contribution; the increase of the values of $1/\Phi$ with the increase in the $[SO_2]/[2\text{-butene}]$ ratio seen in Figure 2 is only consistent with the formation of those products of reactions (2a) and (2b) which are relatively inactive chemically in producing 2-butene isomerization. A further piece of experimental evidence supporting this view comes from our experiments with added gases. He and O_2 are thought to quench a large fraction of the $SO_2(^3B_1)$ molecules to the $^3A_2$ or $^3B_2$ states because of the exact match of the experimental activation energy of reaction (6) with the difference between the (0,0,0) energy of the $SO_2(^3B_1)$ molecule and that of the (1,1,0) region of this molecule where a potential curve crossing appears to occur[47]. However, in this work we have seen that the effect of added gas is to quench the isomerization of the 2-butene by a fraction which is, within the error limits, just that fraction of the $^3B_1$ molecules which have been quenched in (6). If the $^3B_2$ or $^3A_2$ molecules are formed in reaction (6) as seems likely to us[47], then these species are not as chemically reactive toward the olefinic hydrocarbons as is the $SO_2(^3B_1)$ species, and they play little or no part in the isomerization reaction.

The evidence considered above also excludes $SO(^3\Sigma^-)$ and SO_3 as important reactants in the isomerization of the 2-butenes. However, it is possible that some of the scatter in the quantum yield data comes from a small irreproducible heterogeneous alkene isomerization reaction that is catalyzed by H_2SO_4 formed from the SO_3 product of reaction (2a). Aerosol formation is observed in this system, and its nature and possible mechanistic significance are considered in the following section.

Mechanism of Aerosol Formation in 3500-4100 Å Irradiated SO_2-2-Butene Mixtures

From a study of the data presented in Table XVII some further clues can be had as to the chemistry, reaction mechanisms, and origin of the light scattering observed in the SO_2-2-butene mixtures irradiated within the forbidden band. There are three independent qualitative measures of the initial rate of aerosol formation in these experiments: (a) the rate of increase of 6328-Å scattered light observed early in the experiment, column 1 of Table XVII; (b) the time of first detection of 6328-Å light scatter, column 2; and (c) the rate of decrease of the transmitted 4100-3500-Å light as monitored at the rear of the cell early in the experiment. In general it can be seen that the two direct measures of light scatter (a) and (c) increase with increase in SO_2 pressure, and the time at which aerosol light scattering is first detectable is shortest in runs with the highest SO_2 pressures. Furthermore, note that pure SO_2 with no added olefin, run 1 of Table XVII, shows significant light scatter, although runs with both olefin and SO_2 show a somewhat enhanced scattering. In columns 4 and 5 of

Table XVII are listed the calculated relative rates of quenching of $SO_2(^3B_1)$ molecules by SO_2 and 2-butene, respectively. We have made the reasonable assumption in this calculation that the incident light intensity was essentially constant over the 26 runs listed. The ratios of the rates in column 1 or column 3 to the quenching rates in columns 4 and 5 are shown in columns 6 through 9 of Table XVII. The degrees of constancy of the ratios with varied $[SO_2]$ and [2-butene] can be compared. The best correlation with the observed rate of aerosol formation is with the rate of $SO_2(^3B_1)$ quenching by SO_2. This quenching reaction results in SO_3 formation by reaction (2a) about 10% of the time[91]. Presumably SO_3 will lead to H_2SO_4 aerosol by reaction with traces of water in the cell. Once H_2SO_4 aerosol is present in the cell, olefin molecules may in theory participate in the growth mechanism by polymerizing in the aerosol droplet. The fraction of the total olefin removed by this path is very small however, since the maximum quantum yield of olefin removal is equal to or less than 0.016 ± 0.003, as estimated in the runs with the longest exposure time (see Fig. 1). This is in reasonable accord with the results of Cox[67] which were obtained in SO_2-2-butene mixtures irradiated within the first allowed band of SO_2 (near 3115 Å); he reported a quantum yield of 2-butene loss = 0.007, somewhat lower than the reported yields of "sulfinic acid" of 0.033 observed by Dainton and Ivin[58]. Cox observed a small quantum yield of 1-butene formation as well (0.00014) in his $SO_2(^1B_1)$ studies. No detectable isomerization to 1-butene was observed in this work, although such a product would not be unexpected in runs at long times since the heterogeneous, H_2SO_4 catalyzed isomerization of the butene-2 could become important for these conditions.

Since the formation of SO_3 is insured in all of these irradiated SO_2-olefin mixtures, the ultimate formation of sulfuric acid aerosol is expected; the complete elimination of water from the glass wall of the photolysis cell is impossible with the techniques which we and the previous investigators have employed. Thus one suspects that the aerosol formation in irradiated SO_2-olefin mixtures may be initiated largely from excited SO_2 reactions with SO_2. A reasonable extrapolation of these results shows that aerosol formation observed in dilute NO_xSO_2-olefinic hydrocarbon mixtures in irradiated air probably does not originate either from $SO_2(^3B_1)$-SO_2 or $SO_2(^3B_1)$-olefin interactions. It is likely that in this case aerosol forms following very different reactions which involve free radical attack on the SO_2 molecule; reactions such as the following have been suggested as the primary steps in SO_2 removal[83,93]. These and other alternative reactions are now under extensive study in many laboratories including our own:

$$HO_2 + SO_2 \rightarrow SO_3 + HO$$
$$HO_2 + SO_2 + M \rightarrow HO_2SO_2 + M$$
$$HO + SO_2 + M \rightarrow HOSO_2 + M$$
$$RO_2 + SO_2 \rightarrow RO + SO_3$$
$$RO_2 + SO_2 \rightarrow RO_2SO_2$$

Aerosol formation in the irradiated SO_2-olefin systems at high SO_2 pressures is a serious source of error, particularly in runs at long exposure time. In the present work the scatter of the incident 3500-4100-Å exciting light lowered the apparent transmitted light at the end of the cell by as much as 20% after 60 min of irradiation in runs with 600 torr of SO_2. Some of the appreciable scatter in the quantum yield data must reflect this source of error which could not be entirely eliminated, even by extrapolation of the rate data to zero time. To our knowledge other researchers apparently have either not recognized or not reported this problem. Those who study irradiated SO_2 systems at high SO_2 pressures should be warned of this unexpected source of error in any optical absorption or emission measurements which are made with these systems.

I-E. The Mechanism and Kinetics of the Alkene-SO_2 Reactions Excited Within the First Allowed Band of SO_2 (3130 Å)[94]

The mechanism and rate constants for the interactions of photoexcited SO_2 with the alkenes are of special interest because of the potential of these reactions to form condensation nuclei and sulfate containing aerosols. Previous photochemical studies of the SO_2-alkene mixtures irradiated within the first allowed band of sulfur dioxide, $SO_2(^1B_1) \leftarrow SO_2(\tilde{X}, {}^1A_1)$, have shown that a major chemical reaction in this system is the isomerization of the alkene[65,62,66,67]. It is a reasonable extrapolation of existing data to conclude that the $SO_2(^3B_1)$ species is one of the reactants which leads to this change. Directly excited $SO_2(^3B_1)$ molecules are quenched at a rate which is equal to that of formation of an addition compound which leads rapidly to isomerized alkene and SO_2[64]. Furthermore $SO_2(^3B_1)$ molecules are formed from excited singlet SO_2 through collisional perturbation in a significant fraction of the excited singlet quenching collisions with a variety of quenching partners[22-33].

Penzhorn and Güsten[66] have interpreted the results of their study of singlet-SO_2 excited in 2-butene-SO_2 mixtures in terms of $SO_2(^3B_1)$ as the sole reactant leading to isomerization of the alkene. Cox[67] also employed this rationale in his treatment of results from a similar study. He concluded, however, that possibly some other excited states may be reactants as well. Indirect evidence has been presented that the $SO_2(^1B_1)$ and several other electronic states of SO_2, possibly $^3B_2$, $^1A_2$, and $^3A_2$, which may be generated from the $SO_2(^1B_1)$ species, may be involved in the chemistry of the SO_2 molecules excited within the first allowed absorption band, 3200-2500 Å[22,31,21,57,88-90]. Certainly the possible participation of these additional species in the alkene isomerization reaction must be considered among the other alternatives. The data at hand do not allow an unambiguous designation of the state of the SO_2 reactant in this system.

Existing product studies offer somewhat divergent views as to the nature and extent of the chemistry in irradiated SO_2-alkene mixtures. Dainton and Ivin[58] suggested that an unsaturated sulfinic acid formed with a quantum yield of about 0.044 in a mercury-arc irradiated mixture of SO_2 and 1-butene. Cox[67] found the quantum yield of olefin loss, attributed to sulfinic acid formation, to be 0.007 for SO_2-cis-2-butene mixtures excited with a band of 3000-3200-Å light. He also reported a small quantum yield of 1-butene formation in this mixture; $\Phi_{1\text{-}C_4H_8} = 1.4 \times 10^{-4}$. Cehelnik and coworkers[56] found evidence of an O-atom transfer from SO_2 photoexcited at 3130 Å in CF_2CF_2 mixtures where CF_2O was an observed product; $\Phi_{CF_2O} = 0.05$ at high pressures of C_2F_4. Irradiated solutions of SO_2 and alkenes gave polysulfones[65], while cyclic sulfites apparently form in irradiated SO_2-alkene-O_2-containing solutions[68].

In this study the quantum yields of the products of the 3130-Å excited SO_2-cis-2-butene gaseous mixtures were determined in an attempt to further define the nature of the reactive states of SO_2 involved in this system. At the time that this work was completed[60] the reports of the somewhat similar studies of Penzhorn and Güsten[66] and Cox[67] appeared. In general the work reported here supports the conclusions of the previous workers, but some interesting differences both in the results and the interpretation of these results exist. The kinetic treatment of the data presented here and a reevaluation of the data of the previous studies provide new and more definitive information about the detailed mechanism of the excited SO_2-alkene reaction system.

I-E—1. Experimental Procedures and Results

Reactions were carried out at 25 ± 3°C in a cylindrical quartz reaction cell (diameter 3.5 cm, length 39.3 cm). The cell was attached in series with a thermal gradient pump which was used to ensure uniform mixing of the reactants. The vacuum system and pressure measuring components were the same as those described previously[64]. Light from a medium pressure (PEK 200 W) mercury arc was collimated by a lens and light stops and filtered through a series of solutions and glass filters to isolate the 3130-Å band[69]. The incident light intensity was measured at regular intervals using potassium ferrioxalate actinometry[71]. The relative intensity was monitored continuously during photolyses by reflectance of a small fraction of the incident beam into a 935 phototube by means of an angled quartz plate placed in the light beam. The lamp was allowed to warm up for one hour before starting irradiations. The variation in incident intensity during a run was found to be less than ±2%, as indicated by both actinometry and reflectance monitoring. The fraction of the incident light which was absorbed was measured with a 935 phototube mounted at the rear of the cell. Within the range of SO_2 pressures of 2-11 torr employed in this study, the absorption followed Beer's law well with the decadic extinction coefficient for SO_2, $\epsilon = 29.7$ ℓ./mole·cm.

Reactant purification and chromatographic product analyses were made as described in the earlier $SO_2(^3B_1)$-alkene study[64]. Initial quantum yields of the SO_2-sensitized isomerization of *cis*-2-butene were determined by extrapolation to rates at zero time using the least squares fit of the *cis*- and *trans*-2-butene composition versus time curves. These data from experiments at 3130 Å and 25 ± 3°C with varied initial SO_2 and *cis*-2-butene pressures, are summarized in Table XIX. CO_2 gas was added to the SO_2-alkene mixtures in experiments 16-18.

No detectable aerosol was observed by light scattering in these studies at the relatively low pressures of SO_2 employed here. The quantum yield of 2-butene disappearance was below the detection limits in these runs of short duration, and the only chemical change which occurred measurably was the *cis* → *trans* isomerization of the 2-butene.

I-E—2. Discussion

The Simple Two-State Reaction Mechanism of cis-2-butene Isomerization Sensitized by Electronically Excited SO_2

The present kinetic data provide some new insight into the detailed mechanism of the electronically excited SO_2-sensitized isomerization of *cis*-2-butene. In the consideration of our findings we will draw also on the results of Penzhorn and Güsten[66] and Cox[67] which appeared soon after this work was completed[60]. Both previously published studies support the view that $SO_2(^3B_1)$ is the major reactive SO_2 state in this system. Penzhorn and Güsten derived rate constant estimates for the $SO_2(^3B_1)$-quenching reactions with NO and O_2 through kinetic studies of the inhibition of the rate of the excited SO_2-sensitized *cis*- to *trans*-2-butene isomerization by added NO and O_2. Quenching rate constants for $SO_2(^3B_1)$ with

Table XIX. Initial quantum yields of the SO_2-photosensitized isomerization of cis-2-butene at 3130 Å.

Run No.	Pressure reactant, torr: SO_2	Pressure reactant, torr: cis-2-C_4H_8	$[SO_2]/[C_4H_8]$	I_0, quanta/sec-cell face, x 10^{-14}	Initial quantum yield of trans-2-butene formation: Experimental	Calculated: Method 1[a]	Calculated: Method 2[b]
1	2.58	0.173	14.9	7.15	0.22	0.062	0.17
2	2.61	0.084	30.9	7.15	0.18	0.060	0.15
3	2.62	0.042	62.0	7.48	0.14	0.055	0.13
4	2.63	0.026	100.6	7.30	0.11	0.050	0.11
5	5.14	1.094	4.7	7.05	0.34	0.064	0.25
6	5.03	0.335	14.9	7.34	0.23	0.062	0.17
7	5.06	0.164	30.9	7.15	0.19	0.060	0.15
8	5.09	0.082	62.0	7.48	0.14	0.055	0.13
9	5.09	0.051	100.6	7.30	0.11	0.050	0.11
10	5.16	0.033	154.3	7.30	0.096	0.044	0.096
11	9.87	2.100	4.7	7.05	0.31	0.064	0.25
12	9.80	0.317	30.9	7.15	0.20	0.060	0.15
13	9.86	0.159	62.0	7.48	0.15	0.055	0.13
14	9.85	0.098	100.6	7.30	0.11	0.050	0.11
15	9.99	0.065	154.3	7.30	0.100	0.044	0.096
16[c]	2.67	0.259	10.3	7.06	0.24	0.025	0.14
17[c]	5.17	0.503	10.3	7.06	0.20	0.022	0.20
18[c]	10.02	0.973	10.3	7.06	0.26	0.022	0.27

[a] Calculated from relation (A) assuming $k_{3a}/((k_{3a} + k_{3b}) = k_{2a} + k_{2b}) = 0.10$, $k_{4a} + k_{4b}) = 0.052$ as derived from biacetyl-SO_2 studies at shorter wavelengths together with other rate constant estimates specified in the text.

[b] Calculated from relation (A) for runs 1-15 and relation (G) for runs 16-18, using present estimates of $k_{3a}/(k_{3a} + k_{3b}) = 0.85$, $k_{4a}/(k_{4a} + k_{4b}) = 0.14$, $k_{2a}/(k_{2a} + k_{2b}) = 0.116$, $k_{11}/(k_{10a} + k_{10b}) = 0.026$ mole/*l.* together with the other rate constants specified in text.

[c] CO_2 added in runs 16, 17, and 18 was 105.4, 308.0, and 609.7 torr, respectively.

NO and O_2 relative to that for SO_2 were derived. Coupled with our previous direct rate constant estimates of $SO_2(^3B_1)$ quenching with SO_2, they estimate the NO and O_2 quenching constants as (7.8 ± 1.9) x 10^{10} and (2.4 ± 0.5) x 10^8 ℓ./mole·sec, respectively. These values are in reasonable accord with the direct measured rate constant estimates from our $SO_2(^3B_1)$ lifetime studies[30], (7.4 ± 0.3) x 10^{10} and (0.96 ± 0.05) x 10^8 ℓ./mole·sec for NO and O_2, respectively as quencher*.

---

*In the case of O_2 as the $SO_2(^3B_1)$ quencher, the agreement would be improved significantly if proper account were taken of the difference in triplet SO_2 forming facility on collision of singlet-excited SO_2 with SO_2 and O_2. It was assumed by Penzhorn and Güsten that the intersystem crossing ratio for excited singlet quenching collisions with O_2 was equal to that for collisions with SO_2. Our recent work suggests that the fraction of the excited SO_2 singlet quenching collisions with O_2, which result in $SO_2(^3B_1)$ formation, is only about one third of that with SO_2 as quencher[16].

Cox[67] assumed also that $SO_2(^3B_1)$ is the major reactant leading to alkene isomerization in 3000-3200-Å irradiated SO_2-cis-2-butene mixtures, and he derived estimates of the $SO_2(^3B_1)$-quenching rate constants with the 2-butenes relative to that for SO_2. Using our published rate constant for $SO_2(^3B_1)$ quenching with SO_2, he obtained (1.62 ± 0.08) x 10^{11} and (1.42 ± 0.09) x 10^{11} ℓ./mole·sec for the $SO_2(^3B_1)$ quenching constant with cis-2-butene and trans-2-butene, respectively. Again these indirect estimates check well with those found from our direct $SO_2(^3B_1)$ lifetime studies within the experimental error of the determinations, (1.29 ± 0.18) x 10^{11} and (1.22 ± 0.15) x 10^{11} ℓ./mole·sec for the cis- and trans-2-butene, respectively[64]. Thus the results of these previous studies and our recent direct study of the $SO_2(^3B_1)$-sensitized isomerization of the cis- and trans-2-butenes[64] suggest that the phosphorescent $SO_2(^3B_1)$ state of SO_2 may be an important, or perhaps the exclusive, reactive SO_2 state in the 3130-Å excited SO_2-sensitized 2-butene isomerization. Then it is reasonable to attempt first a fit of the present data to this simplest possible mechanism choice.†

(I) $SO_2 + h\nu(3130\ \text{Å} \rightarrow SO_2(^1B_1)$

(1) $SO_2(^1B_1) \rightarrow SO_2 + h\nu_f$

(2a) $SO_2(^1B_1) + SO_2 \rightarrow SO_2(^3B_1) + SO_2$

(2b) $SO_2(^1B_1) + SO_2 \rightarrow (2SO_2)$

(3a) $SO_2(^1B_1) + cis\text{-}2\text{-}C_4H_8 \rightarrow SO_2(^3B_1) + cis\text{-}2\text{-}C_4H_8$

(3b) $SO_2(^1B_1) + cis\text{-}2\text{-}C_4H_8 \rightarrow (SO_2) + cis\text{-}2\text{-}C_4H_8$

(4a) $SO_2(^1B_1) + CO_2 \rightarrow SO_2(^3B_1) + CO_2$

(4b) $SO_2(^1B_1) + CO_2 \rightarrow (SO_2) + CO_2$

(5a) $SO_2(^3B_1) \rightarrow SO_2 + h\nu_p$

(5b) $SO_2(^3B_1) \rightarrow (SO_2)$

(6a) $SO_2(^3B_1) + SO_2 \rightarrow SO_3 + SO(^3\Sigma^-)$

(6b) $SO_2(^3B_1) + SO_2 \rightarrow (2SO_2)$

(7) $SO_2(^3B_1) + cis\text{-}2\text{-}C_4H_8 \rightarrow (SO_2\text{—}C_4H_8)^3$

(8a) $(SO_2\text{—}C_4H_8)^3 \rightarrow cis\text{-}2\text{-}C_4H_8 + SO_2$

(8b) $(SO_2\text{—}C_4H_8)^3 \rightarrow trans\text{-}2\text{-}C_4H_8 + SO_2$

(9) $SO_2(^3B_1) + CO_2 \rightarrow (SO_2) + CO_2$

The indefinite product designation (SO_2) and $(2SO_2)$ shown in the above sequence signifies a ground state or some excited nonemissive state of SO_2. $(SO_2\text{-}C_4H_8)^3$ represents the transient triplet adduct suggested in our previous work[64]. The concentration conditions employed in the present work ensure that the fraction of the excited SO_2 molecules which react in the first-order decay paths is negligibly small, 3.5×10^{-4} in reaction (1) and 2.0×10^{-2} in reactions (5a) and (5b). Thus if this simple mechanism is operative then relation (A) should describe the present results from the cis-2-butene-SO_2-CO_2 mixture photolyses:

---

†Recent spectroscopic analyses of the first allowed absorption band in SO_2[95] and SO_2 fluorescence lifetime determinations[96] suggest that structural features in the 3340-3400-Å region belong to the $^1A_2 \leftarrow \tilde{X}, {}^1A_1$ transition which derives intensity from the allowed $^1B_1 \leftarrow \tilde{X}, {}^1A_1$ transition by way of b_2 vibronic coupling. Presumably the $^1B_1 \leftarrow \tilde{X}, {}^1A_1$ transition origin lies near 3200 Å. We have assumed that the long-lived component of the SO_2 fluorescence for which we have determined rate constants previously, is the $^1B_1$ species. A more definitive, and detailed description of these processes is not possible at this time.

$$\text{(A)}\quad \Phi_{c\to t} = \frac{\left(\dfrac{k_{8b}}{k_{8a}+k_{8b}}\right)\left\{\dfrac{k_{3a}[SO_2]}{(k_{3a}+k_{3b})[C_4H_8]} + \dfrac{k_{2a}}{k_{2a}+k_{2b}} + \dfrac{k_{4a}[CO_2]}{(k_{3a}+k_{3b})[C_4H_8]}\right\}}{\left\{1 + \dfrac{(k_{2a}+k_{2b})[SO_2]}{(k_{3a}+k_{3b})[C_4H_8]} + \dfrac{(k_{4a}+k_{4b})[CO_2]}{(k_{3a}+k_{3b})[C_4H_8]}\right\} \times \left\{1 + \dfrac{(k_{8a}+k_{8b})[SO_2]}{k_7[C_4H_8]} + \dfrac{k_9[CO_2]}{k_7[C_4H_8]}\right\}}$$

In Table XIX it can be seen that the experimental quantum yield data from SO_2-cis-2-butene binary mixtures are in accord with one of the expectations of relations (A). For a given $[SO_2]/[C_4H_8]$ ratio the quantum yield should be independent of the total SO_2 pressure within the experimental error. This is seen to be the case; for $[SO_2]/[C_4H_8] = 154$, $\Phi_{c\to t} = 0.096$ and 0.102 at 5.16 and 9.99 torr of SO_2, respectively; for $[SO_2]/[C_4H_8] = 100.6$, $\Phi_{c\to t} = 0.11$, 0.11, and 0.11 at 2.63, 5.09, and 9.85 torr of SO_2, respectively; for $[SO_2]/[C_4H_8] = 62.0$, $\Phi_{c\to t} =$ 0.14, 0.14, 0.15 for 2.62, 5.09, and 9.86 torr, respectively; for $[SO_2]/[C_4H_8] =$ 62.0, $\Phi_{c\to t} = 0.14$, 0.14, 0.15 for 2.62, 5.09, and 9.86 torr, respectively; for $[SO_2]/[C_4H_8] = 30.9$, $\Phi_{c\to t} = 0.18$, 0.19, and 0.20 for 2.62, 5.09, and 9.81 torr, respectively; for $[SO_2]/[C_4H_8] = 14.9$, $\Phi_{c\to t} = 0.22$ and 0.23 for 2.58 and 5.01 torr, respectively.

It is instructive to test the quantitative magnitude and variation of the experimental values of $\Phi_{c\to t}$ with the $[SO_2]/[C_4H_8]$ ratio in terms of relation (A). We have estimates of most rate constants which appear in this relation from previous work at other wavelengths. Although one must exercise caution in extrapolating these data to rationalize the present study at 3130 Å, a first attempt at fitting the present data can be made using them: $(k_{2a} + k_{2b})/(k_{3a} + k_{3b}) = 0.55$[97]* $k_{4a} + k_{4b} = 0.052$[16]; $(k_{4a} + k_{4b})/(k_{3a} + k_{3b}) = 0.39$[97-99]; $k_{2a}/(k_{3a} + k_{3b}) = [k_{2a} + k_{2b}][(k_{2a} + k_{2b})/(k_{3a} + k_{3b})] = (0.10)(0.55) = 0.055$[24];† $k_{8b}/(k_{8a} + k_{8b}) = 0.65$[64]; $(k_{8a} + k_{8b})/k_7 = 2.91 \times 10^{3}$[64,101,102]; $k_9/k_7 = 8.5 \times 10^{-4}$[30]. Only the value of the ratio $k_{3a}/(k_{3a} + k_{3b})$ has not yet been determined. The simplest possible interpretation of the data can be had assuming that $k_{2a}/(k_{2a} + k_{2b}) = k_{3a}/(k_{3a} + k_{3b}) = 0.10$ as have the previous workers[66,67]. With this assumption and the other rate constant estimates given, we may calculate from relation (A) the theoretically expected initial values of $\Phi_{c\to t}$ for various reactant concentrations employed in the experiments summarized in Table XIX.

---

* The estimates for $(k_{2a} + k_{2b})/(k_{3a} + k_{3b})$ and $(k_{4a} + k_{4b})/(k_{3a} + k_{3b})$ come from direct singlet lifetime studies for SO_2 excited at 2662 Å[27]. They appear to be reasonable values to choose also for the present experiments at 3130 Å, since Mettee[35] and Horowitz and Calvert[39] have observed that the relative quenching efficiencing of excited singlet SO_2 by SO_2 and one of a variety of other added gases is independent of the wavelength of light used to excite the SO_2.

† The choice of $k_{2a}/(k_{2a} + k_{2b}) = 0.10$ here for experiments at 3130 Å is consistent with Cox's data[67], but it must be considered suspect in terms of the intercept value of our data in the plot of Figure 18. See the treatment in the discussion which follows.

These estimates are given in the column headed "Calculated, Method 1." If you compare these values with those found experimentally, it can be seen that the calculated values are much less than the experimental values. In experiments with binary mixtures of SO_2 and butene they are roughly a factor of 2 or 3 less. The disagreement is even greater in runs with added CO_2 where the calculated quantum yields are lower than the measured values by a factor of about ten (runs 17, 18, of Table XIX. If the simple mechanism were operative and $k_{2a}/(k_{2a} + k_{2b}) = k_{3a}/(k_{3a} + k_{3b})$, then in runs with mixtures containing only SO_2 and butene relation (A) simplifies to

$$\text{(B)} \qquad \frac{1}{\Phi_{c\to t}} = \left(\frac{k_{3a} + k_{3b}}{k_{3a}}\right)\left(\frac{k_{8a} + k_{8b}}{k_{8b}}\right)\left(1 + \frac{[SO_2](k_{8a} + k_{8b})}{[C_4H_8]k_7}\right)$$

Thus, for these assumed conditions we expect $1/\Phi_{c\to t}$ to be a linear function of the $[SO_2]/[C_4H_8]$ ratio. The dashed line labeled "simple theory" in Figure 18 shows the theoretical dependence expected from Relation (B). Compare this in Figure 18 with the results obtained by Cox[67] and those observed in this work. The Cox data for $[SO_2]/[C_4H_8]$ ratios above 50 fit reasonably well with the expectations of simple theory and relation (B), but the $1/\Phi_{c\to t}$ values from this work are consistently lower than those of Cox and simple theory by a factor of about 2 within the range of $[SO_2]/[C_4H_8]$ values which is common to the two experimental studies. The reasons for the difference is not clear, but obviously the absolute values for $\Phi_{c\to t}$ from both sets of data cannot be correct. It appears to us that the absolute values of $\Phi_{c\to t}$ which we report in this work may be more accurate than those of Cox. His estimation of the fractions of the broad wavelength band (half intensity width of 3000-3200 Å) of the incident light which were absorbed by the SO_2 and the actinometer solution was seemingly much more involved and presumably subject to greater error than the same estimates in our experiments. We employed a nearly monochromatic beam of light, and a Beer's law dependence of absorption on pressure of SO_2 was observed. However, Cox kept the SO_2 pressure essentially constant at about 30 torr in all of his experiments. So if there were an error in measurement of the intensity of the absorbed light, his results would give experimental $\Phi_{c\to t}$ values which would only differ from the true $\Phi_{c\to t}$ values by a constant multiplying factor. Furthermore the values of the slope-to-intercept ratio of the linear portion of the $1/\Phi_{c\to t}$ versus $[SO_2]/[C_4H_8]$ ratios should be independent of any constant factor of error, and should provide reliable values for $(k_{8a} + k_{8b})/k_7$. Indeed the Cox data give $(2.40 \pm 0.09) \times 10^{-3}$ which does agree reasonably well with that measured directly from our lifetime studies, $(2.91 \pm 0.23) \times 10^{-3}$ [26,51,42,64]. The application of the potential absolute error hypothesis to our data suggests that the slope-to-intercept ratio from our data should also give a reliable estimate of $(k_{8a} + k_{8b})/k_7$. We may use the data for the highest $[SO_2]/[C_4H_8]$ ratio to test this hypothesis, since for ratios equal to or greater than 100, the quenching of singlet SO_2 by SO_2 is ensured, and relation (B) should apply reasonably well regardless of the magnitude of the unknown rate ratio $k_{3a}/(k_{3a} + k_{3b})$. Our present data give $(k_{8a} + k_{8b})/k_7 = (2.7 \pm 1.2) \times 10^{-3}$, a reasonable check with the indirect value from the Cox data and our previously determined direct estimate of this ratio.

The magnitude of the intercept observed from the extrapolation of the $1/\Phi_{c\to t}$ versus $[SO_2]/[C_4H_8]$ plot in Figure 18 for the linear high ratio range gives in theory an estimate of the rate ratio, $[(k_{2a} + k_{2b})/k_{2a}][(k_{8a} + k_{8b})/k_{8b}]$. Using our estimate of $k_{8b}/(k_{8a} + k_{8b}) = 0.65 \pm 0.05$ and the intercept of the Cox data, we find $k_{2a}/(k_{2a} + k_{2b}) = 0.10 \pm 0.01$, in almost exact agreement with our estimates of this quantity from the SO_2-triplet sensitized biacetyl phosphorescence data for 2875 Å (0.095 ± 0.005). The intercept of our present data, however, gives $k_{2a}/(k_{2a} + k_{2b}) = 0.21 \pm 0.04$. The factor of 2 difference in the absolute quantum yields of our work and that of Cox is reflected in this observed difference. There has been no direct measurement of $k_{2a}/(k_{2a} + k_{2b})$ by the biacetyl method for experiments at 3130 Å. Previous estimates of $k_{2a}/(k_{2a} + k_{2b})$ are 0.082 ± 0.003 at 2650 Å[38]; 0.095 ± 0.005 at 2875 Å[24]; ~ 0.10 at 3020 Å[38]. It is not clear whether the high value for this constant estimated here represents a real wavelength effect or whether it is an artifact related to the uncertainties in the present data and the detailed mechanisms involved in the sensitized cis-2-butene isomerization and the sensitized biacetyl phosphorescence methods of estimation of triplet quantum yields. Certainly a new SO_2-biacetyl mixture study at 3130 Å is highly desirable. From the present work we conclude tentatively that the intersystem crossing ratio $k_{2a}/(k_{2a} + k_{2b}) = 0.21 \pm 0.04$ for SO_2 excited at 3130 Å. All of the published data from the high $[SO_2]/[C_4H_8]$ ratios, which guarantee singlet quenching by SO_2, appear to be consistent with the simple mechanism and relation (B).

The Isomerization Mechanism in Experiments at Low $[SO_2]/[C_4H_8]$ Ratios

The curvature in the $1/\Phi_{c\rightarrow t}$ versus $[SO_2]/[C_4H_8]$ ratios seen in Figure 18 for both the Cox data and those determined here, points to an increasing efficiency in the cis → trans isomerization as the extent of SO_2-singlet quenching by the alkene increases. This could arise from an enhanced singlet-to-triplet intersystem crossing ratio for excited singlet SO_2-butene collisions, that is, $k_{3a}/(k_{3a} + k_{3b})$ may be greater than $k_{2a}/(k_{2a} + k_{2b})$. Indeed Cox has shown that his data for the low $[SO_2]/[cis\text{-}2\text{-}C_4H_8]$ ratios may be interpreted in this fashion. We may treat our present data using this more realistic mechanism alternative which allows $k_{3a}/(k_{3a} + k_{3b})$ to be an adjustable variable which we may evaluate. Relation (A) may be rearranged, substitution of the known rate constant ratios made, and the consideration restricted to the CO_2-free systems. Relation (C) is then generated:

$$\text{(C)} \quad \Phi_{c\rightarrow t}\left(1 + 2.91 \times 10^{-3}\,\frac{[SO_2]}{[C_4H_8]}\right)\left(0.55\,\frac{[SO_2]}{[C_4H_8]} + 1\right)$$
$$= \left(\frac{k_{8b}}{k_{8a} + k_{8b}}\right)\left(\frac{k_{2a}}{k_{3a} + k_{3b}}\,\frac{[SO_2]}{[C_4H_8]} + \frac{k_{3a}}{k_{3a} + k_{3b}}\right)$$

The left-hand side of relation (C) has been calculated from our present data and this function is plotted versus $[SO_2]/[C_4H_8]$ in Figure 19. A reasonably good linear relation is observed between the variables. Accepting the modified simple mechanism, the slope and intercept of this plot may be used to derive rate constant estimates. The most accurate estimate of the slope, derived from all the data, gives $[k_{8b}/(k_{8a} + k_{8b})][k_{2a}/(k_{3a} + k_{3b})] = 0.0728 \pm 0.0042$. The best estimate of the intercept, derived from the data from low $[SO_2]/[C_4H_8]$ ratios (≤ 30.9), gives $[k_{8b}/(k_{8a} + k_{8b})][k_{3a}/(k_{3a} + k_{3b})] = 0.55 \pm 0.24$. The slope-to-intercept ratio gives $k_{2a}/k_{3a} = 0.13 \pm 0.06$. Taking $k_{2a} = 8.3 \times 10^{9}$ ℓ./mole·sec[97,99,28,38,24], we estimate $k_{3a} = (6.3 \pm 2.9) \times 10^{10}$ ℓ./mole·sec. From the intercept and our previous estimate of $k_{8b}/(k_{8a} + k_{8b}) = 0.65 \pm 0.05$, we find $k_{3a}/(k_{3a} + k_{3b}) = 0.85 \pm 0.38$. Combining this with our present estimate of k_{3a}, we get $k_{3a} + k_{3b} = (7.4 \pm 4.7) \times 10^{10}$ ℓ./mole·sec. This should be compared with our directly measured value from singlet lifetime studies at 2662 Å, $k_{3a} + k_{3b} = (6.9 \pm 0.4) \times 10^{10}$ ℓ./mole·sec[97].

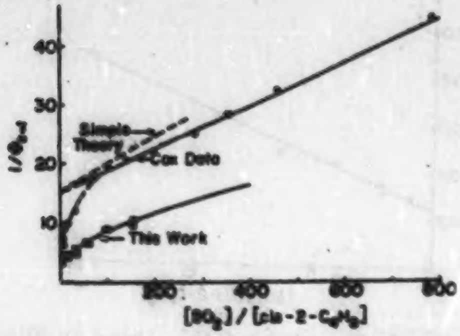

Figure 18. Plot of the reciprocal of the initial quantum yield of *trans*-2-butene vs. $[SO_2]/[C_4H_8]$ ratio. Photolysis of SO_2-*cis*-2-butene mixtures from data of Cox[67] with broadband excitation of SO_2 (3200-3000 Å) and from this work at 3130 Å; upper dashed curve labeled "simple theory" is calculated from relation (B) using our published rate data from very different experiments.

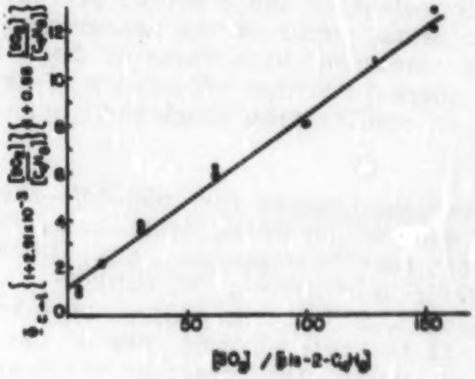

Figure 19. Plot of function (C) vs. $[SO_2]/[C_4H_8]$. Data from 3130-Å photolysis of SO_2-*cis*-2-butene mixtures derived in this work.

The Cox data[67] from low $[SO_2]/[C_4H_8]$ ratios may be retreated to obtain an independent estimate of these rate constants. In his original treatment Cox did not have access to our experimental values for $(k_{2a} + k_{2b})/(k_{3a} + k_{3b}) = 0.55$, and he assumed that this ratio was unity. If we employ only his data for $[SO_2]/[C_4H_8]$ ratios in the range 0.96 to 14.5, the fraction of triplet SO_2 quenched by the alkene is near unity (0.997 to 0.958), and the first term multiplying $\Phi_{c\to t}$ in relation (C) is essentially unity for these conditions. The retreated Cox data are shown in Figure 20. In this case the slope is 0.044 ± 0.005 and the intercept is 0.24 ± 0.03. In terms of the mechanism given, the slope-to-intercept ratio gives $k_{2a}/k_{3a} = 0.18 \pm 0.03$. Within the large error inherent with such slope-to-intercept methods, this value is in fair accord with the present estimate of this ratio derived from our data (0.13 ± 0.06). The intercept and our previous estimate of $k_{8b}/(k_{8a} + k_{8b})$ give $k_{3a}/(k_{3a} + k_{3b}) = 0.37 \pm 0.05$. The difference between this value and that estimated from our data reflects again the

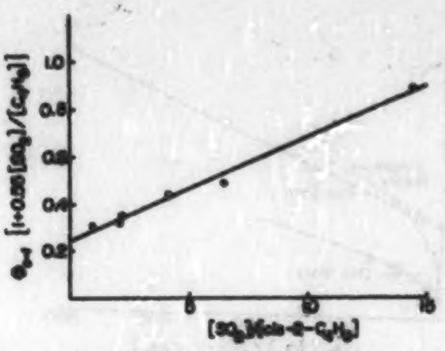

Figure 20. Plot of function (C) vs. $[SO_2]/[C_4H_8]$. Data from 3000-3200-Å photolysis of SO_2-*cis*-2-butene mixtures by Cox[67]

same factor of 2 difference between our absolute quantum yields and those of Cox. However, in every case, the rate constant ratios derived from slope-to-intercept ratios, which should be independent of any constant percentage error in the data, check well within the experimental error of the measurements, and the present results are in most details consistent with those of Cox. Both these sets of date suggest strongly that there is a high efficiency of triplet formation, or at least isomerization, which results from singlet-SO_2 quenching collision with cis-2-butene.

The results of many previous studies for 2660-2875-Å excitation of SO_2 have shown that the fraction of singlet quenching collisions, which form the $SO_2(^3B_1)$ species, varies somewhat with quenching partner, SO_2, 0.082-0.095[24]; N_2, 0.033[25], 0.034[16], 0.019[31]; O_2, 0.030[16]; Ar, 0.025[16]; CO, 0.017[22], 0.019[31], 0.045[16]; CO_2, 0.052[16], 0.020[31]; cyclohexane, 0.073[25]. No studies have been made with excitation at 3130 Å. However, from all the data at hand none of the singlet quenchers studied has an efficiency of SO_2 triplet formation which approaches that suggested here for cis-2-butene. The reason for the unusual behavior of the alkene may lie in the unique nature of the singlet → triplet conversion process in this case. The spin inversion which is perturbed by collision of excited singlets with a chemically unreactive collision partner presumably results in a certain fraction of the quenching collisions and is followed by triplet separation from the perturbing molecule. Interaction of this triplet then occurs with one of a variety of competing molecules in a subsequent collision. Our previous work has shown that the interaction between $SO_2(^3B_1)$ and alkene molecules is strong with a rate constant for triplet quenching and subsequent alkene isomerization which is near the collision number[64]. If a perturbation occurred creating a triplet SO_2 during an SO_2-excited singlet-alkene collision, then it seems to us that it is unlikely that the two molecules could separate before reaction of the triplet and alkene would occur, and efficient isomerization of the olefin would result. The abnormally high efficiency of isomerization then might result since there will be no competing reactions which can remove the triplets in this case.

If this mechanism is operative, then we expect a somewhat modified form of the rate law to hold for mixtures at low $[SO_2]/[C_4H_8]$ ratios. Excited singlet SO_2 quenching by cis-2-butene which involves entrapment of the triplet generated on collision requires that reaction (3a) be reformulated as follows:

$$(3a') \qquad SO_2(^1B_1) + cis\text{-}2\text{-}C_4H_8 \rightarrow [SO_2(^3B_1)\text{-}C_4H_8] \rightarrow (SO_2\text{-}C_4H_8)^3$$

$$(3b) \qquad \rightarrow (SO_2) + cis\text{-}2\text{-}C_4H_8$$

This mechanism choice leads to the theoretical rate law (D) for the initial quantum yield of trans-2-butene formation:

$$(D) \quad \frac{1}{\Phi_{c\rightarrow t} - E} = \left(\frac{k_{8a} + k_{8b}}{k_{8b}}\right)\left(\frac{k_{3a'} + k_{3b}}{k_{3a'}}\right)\left(1 + \frac{(k_{2a} + k_{2b})}{(k_{3a'} + k_{3b})}\frac{[SO_2]}{[C_4H_8]}\right)$$

where

$$E = \frac{\left(\frac{k_{8b}}{k_{8a} + k_{8b}}\right)\left(\frac{k_{2a}}{k_{3a'} + k_{3b}}\right)\frac{[SO_2]}{[C_4H_8]}}{\left(\frac{(k_{2a} + k_{2b})}{(k_{3a'} + k_{3b})}\frac{[SO_2]}{[C_4H_8]} + 1\right)\left(1 + \frac{(k_{8a} + k_{8b})}{k_7}\frac{[SO_2]}{[C_4H_8]}\right)}$$

From our present data one may calculate $(1/\Phi_{c\rightarrow t} - E)$* and test its dependence on $[SO_2]/[C_4H_8]$; these data are plotted in Figure 21. The functional form of relation (D) is followed quite well over the range of data for which the $\Phi_{c\rightarrow t} - E$ difference is of meaningful accuracy. However, the intercept determination is highly inaccurate since few data at low $[SO_2]/[C_4H_8]$ ratios were determined here. The ratio of slope to intercept, equal in theory to $(k_{2a} + k_{2b})/(k_{3a}' + k_{3b})$ gives 0.18 ± 0.25. We may treat our present data in an alternative fashion to test this singlet quenching mechanism if we accept the previously measured value of $(k_{2a} + k_{2b})/(k_{3a}' + k_{3b}) = 0.55$ together with the other rate constant ratios derived in the present work. Then we may calculate the values of $k_{3a}'/(k_{3a}' + k_{3b})$ from relation (D). This procedure gives $k_{3a}'/(k_{3a}' + k_{3b})$ values in the range of 0.81 to 2.4. Although our present results are not inconsistent with the mechanism (3a′) of singlet quenching by cis-2-butene, they provide no real definitive test of it.

The data from Cox cover a wider range of $[SO_2]/[C_4H_8]$ ratios and are better suited to test this relation (D). We may evaluate E using for consistency the estimate $k_{2a}/(k_{3a}' + k_{3b}) = 0.055$ which we derived from his data, and our previous estimate of $k_{8b}/(k_{8a} + k_{8b}) = 0.65$, $(k_{2a} + k_{2b})/(k_{3a}' + k_{3b}) = 0.55$, and $(k_{8a} + k_{8b})/k_7 = 2.91 \times 10^{-3}$. A plot of $1/(\Phi_{c\rightarrow t} - E)$ versus $[SO_2]/[C_4H_8]$ is shown in Figure 22, determined with data up to $6.45 = [SO_2]/[C_4H_8]$, where reasonable accuracy in the difference $\Phi_{c\rightarrow t} - E$ is maintained. The ratio of slope (2.10 ± 0.38) to intercept (3.7 ± 1.4) gives 0.57 ± 0.14; this estimate should be independent of any constant fractional error in quantum yield values. The value is in good accord with the ratio of the direct estimates of $(k_{2a} + k_{2b})/(k_{3a}' + k_{3b})$ made from SO_2 singlet lifetime studies, 0.55 ± 0.04[97-99]. Thus the limited

---

*We have arbitrarily chosen our previous estimate of $k_{8b}/(k_{8a} + k_{8b}) = 0.65$[64] derived from $SO_2(^3B_1)$-cis-2-butene and $SO_2(^3B_1)$-trans-2-butene rate data; the value applicable to the species $(SO_2\text{-}C_4H_8)^3$ formed in reaction (3a) may be nearer to 0.50 as observed in the triplet benzene interaction with cis-2-butene[74-77], since the total energy of the excited singlet SO_2 (91 kcal/mole) is available to the $SO_2\text{-}C_4H_8$ triplet complex formed in reaction (3a′) rather than 73.6 kcal/mole which is characteristic of the $SO_2(^3B_1)$ vibrationally relaxed molecule.

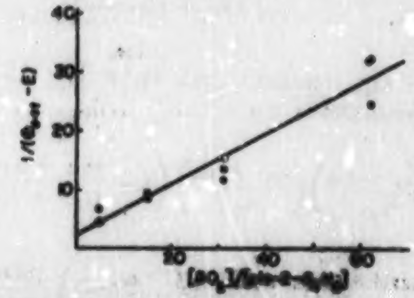

Figure 21. Plot of function (D) vs. $[SO_2]/[C_4H_8]$ ratio. Data from 3130-Å photolysis of SO_2-*cis*-2-butene mixtures derived in this work.

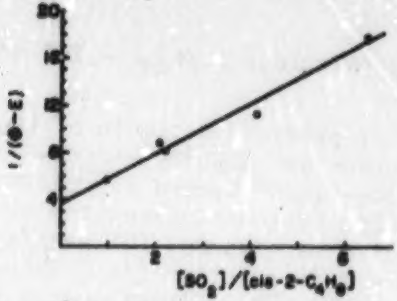

Figure 22. Plot of function (D) vs. $[SO_2]/[C_4H_8]$ ratio. Data from 3000-3200-Å photolysis of SO_2-*cis*-2-butene mixtures by Cox[67]

---

data now in hand do favor the modified interpretation of the singlet SO_2-alkene interaction given by reaction (3a′), although no definitive choice of alternative reaction mechanisms (3a) and (3a′) can be made at present. In any case we can conclude that excited singlet SO_2-cis-2-butene collisions do result in the generation of $SO_2(^3B_1)$ and/or $\overline{(SO_2\text{-}C_4H_8)}^3$ complex a very large fraction of the time. According to the mechanism outlined, this fraction varies from 0.85 ± 0.38 to 0.37 ± 0.05. With the alternative mechanism (3a′) replacing (3a), Cox's data suggest $k_{3a}'/(k_{3a}' + k_{3b}) = 0.42 \pm 0.16$. It should be noted, however, that the latter estimate may be low by a factor of 2.

In preliminary reports from Horowitz and Calvert[31] and Fatta and coworkers[90], a high efficiency of triplet formation has been observed also with excited singlet SO_2-biacetyl collisions. About 17% of the quenching collisions for SO_2 excited at 2875 Å create triplet SO_2. In this case the very rapid triplet energy transfer from triplet SO_2 to biacetyl ($k = 1.4 \times 10^{11}$ ℓ./mole·sec[26] could occur following triplet formation in perturbing collisions between excited singlet SO_2 and biacetyl.

Another interesting mechanistic variation is possible to rationalize the high efficiency of triplet generation from $SO_2(^1B_1)$ quenching reactions with both cis-2-butene and biacetyl. Conceivably $SO_2(^3A_2)$ and/or $SO_2(^3B_2)$ molecules, as well as $SO_2(^3B_1)$ molecules, may be created whenever quenching of the $SO_2(^1B_1)$ occurs by collision with any quencher molecule. If the lifetime of the $SO_2(^3A_2)$ and/or $SO_2(^3B_2)$ states were very short as a result of efficient collisional quenching or internal conversion processes, then in the usual dilute mixture of the triplet quencher and reactant gases only the $^3B_1$ species would be counted by the techniques which we have employed in the previous SO_2-biacetyl mixture studies. However, when the quenching collisions and subsequent intersystem crossing of the singlet to triplet is induced by the triplet trapping agent itself, then the total of the $SO_2(^3B_1)$, $SO_2(^3A_2)$, and $SO_2(^3B_2)$ may be counted. Since nothing is now known about the lifetimes of the $SO_2(^3A_2)$ and $SO_2(^3B_2)$ species, it is impossible to test this alternative mechanism at this time.

The Isomerization Mechanism in Experiments with High Pressures of Added CO_2

It appears to us that all of the available photochemical data for the binary SO_2-cis-2-butene system are rationalized well in terms of the well-known phosphorescent $SO_2(^3B_1)$ and fluorescent $SO_2(^1B_1)$ states, and there is no compelling reason to invoke the participation of the $^3B_2$, $^3A_2$, or $^1A_2$ states of SO_2 in the kinetic scheme. However, in our study of the ternary mixtures of SO_2-cis-2-butene-CO_2 reported here, this simple mechanism is not adequate. It predicts isomerization quantum yields which are about a factor of ten too low for experiments at very high pressures of added CO_2 gas. Compare the experimental values for runs 16, 17, and 18 of Table XIX with those calculated from relation (A). This result is entirely analogous to that observed by Cehelnik and coworkers[21] and Wampler, Horowitz, and Calvert[22] in photolyses of CO - SO_2 mixtures at high CO pressures. We must invoke some new state or states of SO_2 to describe these results quantitatively.

The excess quantum yield of isomerization observed at high CO_2 pressures may be considered in terms of several alternative mechanisms. Heicklen and coworkers[56,57,88-90] have speculated on the role of SO_2 singlet and triplets other than the optical states in the photochemistry of SO_2 mixtures with high pressures of CO, C_2F_4[26], and thiophene[57]. Wampler, Horowitz, and Calvert[22,31] have proposed an alternative reaction scheme to rationalize their study of CO_2 product quantum yields in 3130-Å photolyses of SO_2 - CO mixtures at high CO mixtures at high CO pressures. They suggested that some undefined intermediate state (X) was formed in the quenching $SO_2(^1B_1)$ in reactions (2b), (4b), and (4b). This state was unreactive toward CO to form CO_2 directly, but it could generated $SO_2(^3B_1)$ on collision with other species in experiments at the higher pressures. According to the mechanism of Wampler and coworkers, the following additional reactions should be important in our present experiments with high pressures of added CO_2 gas:

(4b′) $SO_2(^1B_1) + CO_2 \rightarrow X + CO_2$

(10a) $X + CO_2 \rightarrow SO_2(^3B_1) + CO_2$

(10b) $X + CO_2 \rightarrow SO_2 + CO_2$

(11) $X \rightarrow SO_2$

The excited singlet SO_2 will be quenched largely by CO_2 in runs 16-18 of Table XIX so the above reactions coupled with reactions (4a), (4b), (6a), (6b), (7), (8a), (8b), and (9) should describe the major happendings related to alkene isomerization in these experiments. The steady-state treatment of these reactions leads to relation (F) for the initial quantum yield of trans-2-butene formation:

$$\text{(F)} \qquad \Phi_{c-t} = \frac{\left(\frac{k_{8b}}{k_{8a} + k_{8b}}\right)\left[\frac{k_{4a}}{k_{4a} + k_{4b} + k_{4b'}} + \frac{k_{4b'}}{k_{4a} + k_{4b} + k_{4b'}} \times \left(\frac{[CO_2]k_{10a}}{[CO_2](k_{10a} + k_{10b}) + k_{11}}\right)\right]}{1 + \frac{k_9[CO_2]}{k_7[C_4H_8]} + \frac{(k_{8a} + k_{8b})}{k_7}\frac{[SO_2]}{[C_4H_8]}}$$

We may rearrange the terms of relation (F) to obtain the more useful form of reaction (G):

$$\text{(G)} \qquad \frac{1}{H - \left(\frac{k_{4a}}{k_{4a} + k_{4b} + k_{4b'}}\right)} = \left(\frac{k_{4a} + k_{4b} + k_{4b'}}{k_{4b'}}\right)\left(\frac{k_{10a} + k_{10b}}{k_{10a}} + \frac{k_{11}}{k_{10a}[CO_2]}\right)$$

where

$$H = \left(\frac{k_{8a} + k_{8b}}{k_{8b}}\right)\Phi_{c-t}\left(1 + \frac{k_9[CO_2]}{k_7[C_4H_8]} + \frac{(k_{8a} + k_{8b})}{k_7}\frac{[SO_2]}{[C_4H_8]}\right)$$

All the rate constant ratios required to evaluate the left-hand side of relation (G) are available from previous studies, $k_{4a}/(k_{4a} + k_{4b} + k_{4b}') = 0.052$[47]; $k_9/k_7 = 8.5 \times 10^{-4}$[41]; $(k_{8a} + k_{8b})/k_7 = 2.91 \times 10^{-3}$[64,26,51]; $k_{8b}/(k_{8a} + k_{8b}) = 0.65$[64]. This function is plotted versus $1/[CO_2]$ in Figure 23. From the ratio of the slope (0.0159 ± 0.0017) to the intercept (1.32 ± 0.19) of this plot we obtain $k_{11}/(k_{10a} + k_{10b}) = 0.012 \pm 0.002$ mole/ℓ. This may be compared with the estimate of the same rate constant ratio derived from the very different measurements of the quantum yields of SO_2-sensitized biacetyl phosphorescence with excitation of SO_2 at 2875 Å in SO_2-biacetyl-CO_2 mixtures, 0.020 ± 0.004[31]. The intercept of the plot given in Figure 23 gives $k_{4b}'/(k_{4a} + k_{4b} + k_{4b}') = 0.76 \pm 0.11$, a number considerably larger than the previous estimate of this ratio from experiments at 2875 Å, 0.14 ± 0.02[31]. The data from the experiments with added CO_2 can be treated in an alternative fashion to find a fit to the mechanism outlined. We may allow $k_{4a}/(k_{4a} + k_{4b} + k_{4b}')$ to be a variable as well as the slope and intercept values of relation (G) and solve directly for these three unknowns. This treatment gives $k_{4a}/(k_{4a} + k_{4b} + k_{4b}') = 0.14$ and $k_{11}/(k_{10a} + k_{10b}) = 0.026$ mole/ℓ. The latter value is in reasonable accord with the previous estimate, 0.020 ± 0.004 mole/ℓ.[31]. The ratio $k_{4a}/(k_{4a} + k_{4b} + k_{4b}')$ is somewhat higher than the previous estimate of this ratio at 2875 Å (0.052[16]). There have been no other measurements of this value for 3130-Å excitation of SO_2 of which we are aware. Considering the magnitude of the complications involved in the two very different experiments used to determine the $k_{11}/(k_{10a} + k_{10b})$, the degree of agreement observed is considered to be satisfactory. It can be seen by extrapolation of the high-pressure rate constant data to the conditions employed in runs 1-15 of Table XIX that the excess triplet mechanism will be of no significance at the pressures of reactants employed in these runs.

There are, of course, other mechanism alternatives which one may choose to treat the present data. Thus we may designate the species X as $SO_2(^1A_2)$ and invoke $SO_2(^3A_2)$, or conceivably $SO_2(^3B_2)$, as the product of reaction (10a) in a fashion analogous to that of Cehelnik and coworkers. However, if this is done there are several significant changes which must be made in the original mechanism

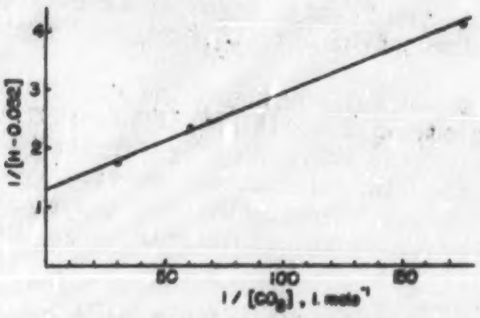

Figure 23. Plot of function (G) vs. 1/[CO_2] from 3130-Å photolysis of SO_2-*cis*-2-butene-CO_2 mixtures derived in this work.

choice of Cehelnik and coworkers. Thus we must require that the $SO_2(^1A_2)$ state be unreactive toward isomerization of the alkene and the $SO_2(^3A_2)$, and/or the $SO_2(^3B_2)$ states must be near identical in their reactivity to that observed for $SO_2(^3B_1)$ in its quenching reactions with SO_2, cis-2-butene, trans-2-butene, NO, O_2, and CO_2. At this stage in the development of our knowledge of these systems, no completely unambiguous choice of mechanism can be made. However, all of the available data from the butene-SO_2 mixture photolyses in both the first allowed band (2400-3200 Å) and the forbidden band (3400-4300 Å) seem to be rationalized well in terms of the participation of the known phosphorescent triplet state ($^3B_1$), the long-lived excited singlet state ($^1B_1$), and at least one other chemically unreactive state of SO_2 which either regenerates $SO_2(^3B_1)$ in part by a collisionally induced reaction at high added gas pressures, or which gives other triplets ($^3B_2$, $^3A_2$) of almost identical reactivity to that observed for $SO_2(^3B_1)$. However, the introduction of the $SO_2(^3B_2)$ and $SO_2(^3A_2)$ species as potential reactants which promote isomerization of the alkene in irradiated SO_2-cis-2-butene systems seems to us to be both unnecessary and speculative at this stage of our knowledge of these systems.

I-F. The Mechanism and Kinetics of SO_3 Formation in the Photolysis of SO_2 Mixtures[101]

In principle the photochemistry of the pure SO_2 gas offers the simplest chemical system from which we may gain information on the chemical reactivity of the different excited states of SO_2. However, the two most recent studies of SO_3 formation in pure SO_2 irradiated within the first absorption band gave widely divergent results. Thus Cox[102] estimated that the quantum yield of SO_3 formation in irradiated SO_2 was $(3.8 \pm 1.0) \times 10^{-3}$, only about one-twentieth of the value observed by Okuda and coworkers[17]: $\Phi_{SO_3} = (8 \pm 2) \times 10^{-2}$. In both studies a broad band of light which overlapped the first allowed singlet band was employed. In rationalizing the difference between these results, Cox has suggested that the very nonuniform light absorption which must have occurred in the studies of Okuda and coworkers, carried out at 1 atm pressure of SO_2 gas, may have favored a possible heterogeneous wall reaction forming SO_3. However Cox's explanation of the difference between the results of the two studies is difficult to accept, since in the study of Okuda and coworkers a fast flow system was employed with a very short residence time for the products in the reaction cell; while Cox used rather extended irradiations period (2-17 hr) in a static system over a range of pressures (25 - 730 torr). It appeared to be more likely that some difference between the two results might enter as a result of the contrasting flow and static experimental conditions employed in the two studies.

In the previous study of Okuda and coworkers the extent of inhibition of SO_3 formation which resulted from small additions of biacetyl to the SO_2 gas was rationalized well in terms of the known $SO_2(^3B_1)$ quenching rate constants, and it was concluded that $SO_2(^3B_1)$ is the dominant chemically active species which leads to SO_3 in SO_2 photolyses. Presumably the important chemical reaction leading to SO_3 in the system is the exothermic, spin conserving reaction (1a):

$$\text{(1a)} \qquad SO_2(^3B_1) + SO_2 \rightarrow SO_3 + SO(^3\Sigma^-)$$

The experimental data from both recent studies are very limited, and no rigorous test of mechanism or unambiguous proof of reactant states now exists. It is obvious that further work is necessary to resolve the observed differences in the quantum yields of SO_3 from the photolysis of pure SO_2 and to establish the mechanism of product formation.

In this work we have determined the quantum yield of SO_3 formation in both static and flow systems using pure SO_2 and SO_2-NO, SO_2-CO_2 and SO_2-O_2 gaseous mixtures. In one series of experiments SO_2 was excited directly to the $SO_2(^3B_1)$ state by light absorption within the "forbidden" $SO_2(^3B_1) \leftarrow SO_2(\tilde{X}, {}^1A_1)$ band at 3700-4000 Å. In another series SO_2 was excited to the first excited singlet state ($^1B_1$) by light absorption within the first allowed band at 3130 Å. The results of these varied experiments provide new information on the detailed mechanism of SO_3 formation in irradiated SO_2 and allow a meaningful rationalization of the seemingly divergent results of Okuda and coworkers[17], Allen and coworkers[48,103], and Cox[102].

I-F—1. Experimental

Photolysis Systems

Two different photochemical systems were employed in this work. Excitation of SO_2 within the singlet band was effected using a narrow band of light near 3126-3132 Å. This was generated from a medium-pressure mercury arc (PEK 200 W), filter solutions, and glasses[69]. Dashed curve A in Figure 24 shows the excitation was made with emission from a high-pressure xenon arc (Osram XBO 450 W) which was filtered through a series of solution and glass plates to provide a band of light in the range of 3600-4100 Å[64]. Dashed curve B in Figure 24 defines the excitation region employed here and the overlap of this with the triplet bands. In each set of experiments a nearly uniform parallel beam of light was obtained using lenses and light stops. In triplet and singlet excitation experiments a cylindrical Pyrex cell (diameter 4.5 cm, length 50 cm) and a quartz cell (diameter 3 cm, length 15 cm), respectively, were used. The absolute incident light intensity was measured at frequent intervals between photolysis runs using potassium ferrioxalate actinometry[71]. The relative intensity was monitored during photolyses by reflecting a small fraction of the incident light into a 935 phototube by means of an angled quartz plate placed in the incident beam. The lamps were allowed to warm up for a 1-hour period before photolysis was started. The light intensity was constant to within ±5% during a given photolysis period. In

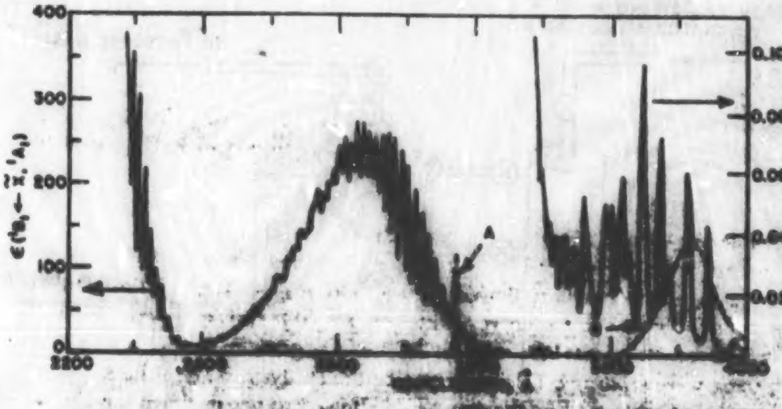

Figure 24. Molar extinction coefficients (ε = [illegible], l./mole/cm) for the first allowed band and the "forbidden" band of $SO_2(g)$ at 25°C. Curves A and B represent the relative intensity versus wavelength distribution of the incident light used in the singlet and triplet excitation experiments.

the singlet and triplet experiments the incident light intensity was varied in the ranges of 3.0×10^{14} to 13.0×10^{14} and 5.0×10^{17} to 8.5×10^{17} quanta (cell face•sec)$^{-1}$, respectively. The fraction of the incident light absorbed by SO_2 in the singlet experiments was measured using a phototube at the rear of the cell. Over the pressure range employed in these experiments (3-27 torr) the absorption followed Beer's law with ε = 28.4 ℓ./mole•cm. The very small fractions of the incident light absorbed by the SO_2 in the triplet excitation experiments were estimated using the average extinction coefficient (ε = 0.0276 ± 0.0051 ℓ./mole•cm) measured with a thermopile (Epply Laboratories) and potentiometer-galvanometer system. This estimate is consistent with that calculated from the incident light distribution and the SO_2 extinction data from the triplet band (ε ≅ 0.0206), and it is considered more reliable than the latter value.

Experimental Procedures

A grease-free high-vacuum line (pressure in the region of 10^{-5} torr) was used in all experiments. The gas-handling system with high vacuum is shown in Figure 25. Pressures of 20 torr or more were measured with a calibrated pressure gauge (Wallace and Tiernan) using a transducer (Dynascience, model P7D) with a digital voltmeter combination as a null device. Pressures less than 20 torr were measured directly with a calibrated transduced T. Flow rates for gases in the system were changed as desired by choosing suitable size capillaries C_1 and C_2 which were jointed to the outlet side of the photolysis cell R. Fine control of the flow rate was obtained using a needle valve F (Nupro SS-2SGD) connected to the inlet side of the reaction cell. Flow rates were varied from 0.13×10^{-6} to 13.6×10^{-6} mole/sec for the singlet band experiments and 0.8×10^{-6} to 73×10^{-6} mole/sec for the triplet band experiments.

The major fraction of the SO_3 produced remained gaseous; this together with the large excess of reactant flowed into a cold trap C kept at liquid nitrogen temperature. Following each run nitrogen gas (0.3 cm^3/sec) was used to flush the system for 30 min. When NO, CO_2, or O_2 gases in addition to SO_2 were used,

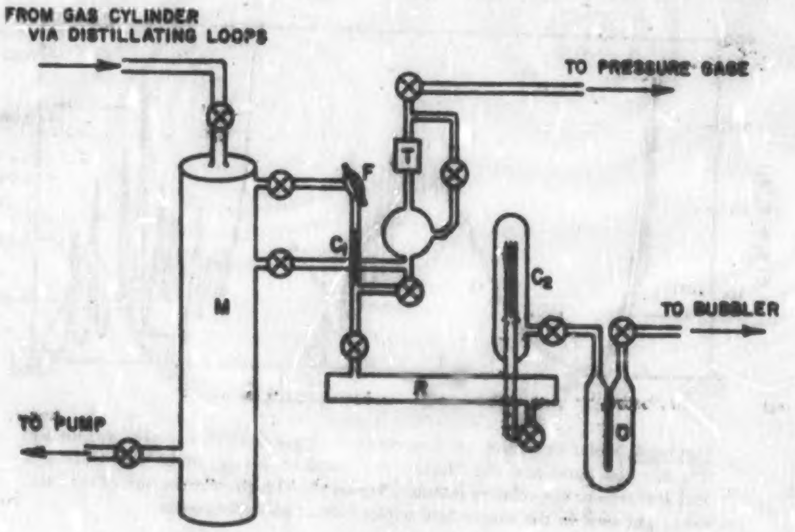

Figure [illegible]. Gas handling and flow reaction system used in this study.

these were separated by distillation before analysis. Then the product SO_3 and excess SO_2 collected in the trap were allowed to warm slowly and flow into two bubblers and an ice-temperature trap placed in series with trap C. Each bubbler contained 10 cm^3 of 80% isopropyl alcohol. The purpose of the last trap in the ice bath was to test for possible loss of product by vaporization. Excess SO_2 collected in the bubblers was flushed out by flowing nitrogen gas through the bubblers for 3 to 4 hours.

The cell and associated glass tubing leading to the traps were disassembled after each run and the walls washed with a small portion is isopropyl alcohol (80%). The SO_3 recovered from the bubblers in flow experiments amounted to at least 90% of the total SO_3 collected from all the system including the cell walls, connecting tubing, and traps. The quantum yields of SO_3 reported here include SO_3 from all sources. Since no measurable amount of SO_3 was found in the cold trap, no loss of SO_3 in the transferring process is assured.

The SO_3 collected was titrated in the form of sulfate with barium chloroanilate using a spectrophotometric method[104,105]. Measurements for the standard curve and photochemical runs were obtained with a 5-cm path length cell with absorption measured at 5300 Å using a spectrophotometer (Beckman model B). The analytical method was very reproducible and gave accurate results for standard samples of sulfate.

Following the analysis of a given run and before each new run, the cell and connecting tubing were washed thoroughly with double distilled water and isopropyl alcohol (100%), dried in the oven for several hours, reassembled, and evacuated until the pressure in the system reached 10^{-5} torr. Dark runs were made which were identical in other respects with the photochemical runs. The small amount of sulfate derived from these dark experiments was almost exactly the same for all reaction conditions, about 0.07 μmole. This suggests that the blank sulfate was formed in the analytical procedure itself, rather than in a chemical reaction occurring in the flow system.

The reactant gases employed were the highest purity products of the Matheson Chemical Company. All reagents which were condensable at liquid nitrogen temperature were purified further and degassed by bulb-to-bulb distillation in the vacuum lines to ensure the dryness and purity of all the reagents. The gases were premixed in the large storage bulb (M of Figure 25), diameter 15 cm, length 100 cm, and then allowed to flow into the reaction cell through the capillaries.

Other possible products collected in the trap besides SO_2 and SO_3 are SO and possibly its subsequent reaction products. In theory we expect equal amounts of SO and SO_3 to be formed from each bimolecular reaction of SO_2 and the excited SO_2 molecules. Therefore if there is no secondary reaction involving SO molecules, the amount of SO trapped must be equivalent to the amount of SO_3 collected. SO probably reacts with water to form H_2SO_3 and H_2S in the aqueous solution. Previous results suggested that H_2SO_2 (H_2O + SO) and $SO_4^=$ are not final products from SO in water[106-108]; the overall reaction may be, $3SO + 3H_2O \rightarrow 2H_2SO_3 + H_2S$. Thus the possible loss or increase of $SO_4^=$ due to the aqueous reaction products of SO is not expected. It seems unlikely to us that SO reacted with SO_3 during the transfer of products or the analysis. Our evidence suggests that these molecules do react extensively in the gas phase in the slow flow and static systems. However, the high solubility and reactivity of SO_3 to form H_2SO_4 in water solutions suggest the unimportance of SO_3-SO reactions in the fast-flow system. The kinetic behavior of the SO_3 quantum yields at high flow rates bears out this conclusion.

Table XX. Effect of flow rate on the quantum yields of SO_3 formation in pure SO_2 irradiated within the first forbidden absorption band.[a]

Run No.	Flow rate, mole sec^{-1}, $\times 10^6$	Residence time, sec	Light absorbed, quanta sec^{-1} $\times 10^{-14}$	Photolysis period, min	Sulfate formed, µmole	Φ_{SO_3} Experiment	Theory[b]
1	0.813	1400	3.16	120	0.13	0.036	0.034
2	2.73	435	3.18	120	0.22	0.057	0.058
3	5.16	232	3.39	120	0.31	0.077	0.075
4	7.35	159	3.12	120	0.34	0.093	0.086
5	9.63	123	2.88	120	0.29	0.085	0.093
6	13.95	91	3.20	120	0.36	0.094	0.098
7	73.38	16	3.16	60	0.20	0.108	0.108

[a] Pressure of SO_2, 25 ± 1 torr; radiation in band at 3700–4100 Å.

[b] Calculated from relations (A)–(D) using $\alpha = 0.108$ and rate constants $k_2 = 6.0 \times 10^6$ and $k_3 = 5.0 \times 10^8$ l./mole·sec and integrating by computer.

Experimental Results

Several series of experiments were made in an attempt to find the origin of the conflicting results of the previous published studies of the irradiated pure SO_2 system[17,102] and to establish the mechanism and the nature of the excited states involved in SO_3 formation. In the first series of runs direct triplet excitation was employed using radiation in a band near 3700-4000 Å (see Fig. 24. The data in Table XX summarize the effect of the reactant flow rate on the SO_3 product quantum yields. In Table XXI the effects of added NO, CO_2, and O_2 on the quantum yield of SO_3 formation in SO_2 mixtures are shown. In the second series of experiments excited singlet sulfur dioxide was generated by irradiation with a narrow band of light near 3130 Å (see Fig. 24). Quantum yields of SO_3 formation were determined for experiments using both a static system (Table XXII) and a dynamic system with varied reactant flow rates (Table XXIII). In Table XXIV are given the quantum yields of SO_3 from experiments using singlet excited SO_2 mixtures with added nitric oxide, carbon dioxide, and oxygen gases and with varied flow rates.

Table XXI. Effect of foreign gases on SO_3 quantum yields in SO_2 mixtures irradiated within the first forbidden band in the flow system.[a]

Run No.	P_M, Torr	P_M/P_{SO_2}	Φ_{SO_3}	$\Phi_{SO_3}^0/\Phi_{SO_3}^P$
a) M = NO				
8	4.75	0.190	0.000 ± 0.005	----
9	2.50	0.100	0.000 ± 0.003	----
10	0.20	0.0080	0.046	2.35
11	0.15	0.0060	0.053	2.04
12	0.10	0.0040	0.064	1.69
13	0.050	0.0020	0.081	1.33
	0.000	0.0000	0.108[b]	1.00
b) M = CO_2				
14	90.0	3.60	0.052	2.08
15	61.3	2.45	0.060	1.80
16	40.8	1.63	0.071	1.52
17	25.0	1.00	0.082	1.31
18	20.2	0.81	0.094	1.15
	0.0	0.00	0.108[b]	1.00
c) M = O_2				
19	11.54	0.46	0.077	1.40
20	7.04	0.28	0.085	1.27
21	1.91	0.076	0.092	1.17
22	0.87	0.035	0.083	1.30
	0.00	0.000	0.108[b]	1.00

[a] Pressure of SO_2, 25 ± 1 torr; radiation in band at 3700–4100 Å; flow rate 9.63×10^{-6} mole/sec.

[b] Limiting quantum yield derived from computer fit of Φ_{SO_3} versus flow rate data at high flow rates for the pure SO_2 system.

Table XXII. Quantum yields of SO_3 formation in pure SO_2 irradiated at 3130 Å in the static system.[a]

Run No.	Light absorbed, quanta $sec^{-1} cell^{-1} \times 10^{-14}$	Photolysis period, hr	Sulfate formed, μmole	Quantum yield SO_3 formation Experiment	Calculated Method I[b]	Method II[c]
23	13.84	3.00	0.22	0.0090	0.0019	0.0040
24	18.05	6.25	0.23	0.0032	0.0010	0.0033
25	8.30	8.33	0.18	0.0043	0.0011	0.0043
26	15.80	16.30	0.38	0.0030	0.00058	0.0033
27	12.80	21.75	0.21	0.0012	[illegible]	0.0036
28	[illegible]	36.84	[illegible]	0.0020	0.00031	[illegible]

[a] Pressure of SO_2, 25 ± 1 torr.

[b] Calculated from relations (A)–(D) using $\alpha = 0.090$ and rate constants $k_9 = 1.2 \times 10^6$, $k_8 = 5.0 \times 10^8$ l./mole·sec, $k_w = 0.0$, and integrated by computer.

[c] Calculated from relation (A)–(D) with one alteration: the heterogeneous wall removal of SO_3 gas was assumed to occur with a rate constant $k_w = 4 \times 10^{-4}$ sec^{-1}. The other rate constants were as employed in method I.

Table XXIII. Effect of flow rate on the quantum yield of SO_3 formation in pure SO_2 irradiated at 3130 Å in the flow system.[a]

Run No.	Flow rate, mole sec^{-1}, $\times 10^6$	Residence time, sec	Light absorbed, quanta sec^{-1} $cell^{-1} \times 10^{-14}$	Photolysis period, min	Sulfate formed, μmole	Quantum Yield of SO_3
29	0.13	1000	3.73	240	0.17	0.010
30	0.81	200	3.64	60	0.04	0.015
31	0.81	200	3.56	60	0.07	0.031
32	0.81	200	3.73	240	0.36	0.041
33	1.59	130	3.64	60	0.09	0.041
34	1.59	130	3.64	60	0.10	0.046
35	3.50	45	3.59	60	0.15	0.072
36	3.50	45	3.30	240	0.45	0.057
37	5.16	31	3.56	240	0.62	0.073
38	5.16	31	3.73	240	0.63	0.071
39	7.35	21	3.30	240	0.58	0.074
40	7.35	21	3.70	305	0.75	0.084
41	9.63	16	4.12	60	0.23	0.093
42	9.63	16	4.12	30	0.13	0.111
43	12.95	12	2.73	205	0.59	0.086
44	12.95	12	3.64	60	0.20	0.095
45	0.81	200	5.64	120	0.03	0.005
46	1.59	125	5.64	120	0.14	0.020
47	5.16	31	5.64	120	0.56	0.084
48	12.95	12	5.64	120	0.60	0.090
49	13.60	10	8.50	60	0.45	0.090
50	4.22	37	12.92	240	0.95	0.031
51	7.35	21	12.54	240	1.13	0.038
52	15.05	10	13.35	60	0.66	0.083

[a] Pressure of SO_2, 25 ± 1 torr.

Table XXIV. Effect of foreign gases on the quantum yield of SO_3 formation in 3130-Å irradiated SO_2 mixtures in the flow system.[a]

Run No.	P_M, Torr	Residence time, sec	P_M/P_{SO_2}	Quantum yield of SO_3 formation
a) M = NO				
53	2.10	125	0.084	0.008
54	2.10	31	0.084	0.023
55	2.10	31	0.084	0.027
56	2.10	21	0.084	0.029
57	2.10	12	0.084	0.024
58	0.21	21	0.0082	0.053
59	0.14	21	0.0055	0.058
60	0.10	21	0.0045	0.060
61	0.070	21	0.0032	0.067
	0.00	0	0.00	0.090[b]
b) M = CO_2				
62	90.0	21	3.60	0.049
63	67.0	21	2.70	0.057
64	40.0	21	1.60	0.066
65	20.0	21	0.80	0.070
66	30.0	21	0.75[a]	0.072
	0.0	0	0.00	0.090[b]
c) M = O_2				
67	2.76	21	0.11	0.080
68	1.50	21	0.060	0.083
69	0.44	21	0.018	0.079
	0.00	0	0.00	0.090[b]

[a] Pressure of SO_2, 25 ± 1 torr in all but run 66 in which 40 torr was employed; $I_a = 5 \times 10^{14}$ quanta/cell·sec.

[b] Limiting quantum yield derived from computer fit of Φ_{SO_3} versus flow rate data at high flow rates for the pure SO_2 system.

I-F—2. Discussion of the Results

Dependence of Quantum Yields of SO_3 Formation on Reactant Flow Rates

The absorption of light quanta of wavelengths greater than 2160 Å provides insufficient energy to dissociate a sulfur dioxide molecule [$SO_2 \rightarrow O(^3P) + SO(^3\Sigma^-)$]. Thus it is reasonable to speculate that SO_3 formation from the photolysis of SO_2 within the first allowed or the "forbidden" band is derived from an electronically excited SO_2 molecule reaction with ground state SO_2 molecules. Reaction (1a)

$$(1a) \qquad SO_2(^3B_1) + SO_2 \rightarrow SO_3 + SO(^3\Sigma^-)$$

involving the $SO_2(^3B_1)$ molecule has been suggested as an important source of SO_3 in SO_2 gas irradiated within the 2400-3200-Å band[17,51,26] and the "forbidden" triplet band of SO_2 (4000-3600 Å). $SO(^3\Sigma^-)$ was observed in the flash photolysis of SO_2 by Norrish and Oldershaw[109], but in these experiments the authors attributed its formation to the direct photodissociation of SO_2 at wavelengths shorter than 2200 Å present in the flash. Only recently both products of reaction (1a) have been identified spectroscopically in irradiated SO_2 at the longer wavelengths.

Thus Basco and Morse[110] and James, Kerr, and Simons[111] have observed $SO(^3\Sigma^-)$ in the flash excitation of SO_2 with wavelengths greater than 2500 Å. Until recently SO_3 formation in irradiated SO_2 has been inferred either from the observed SO_2 loss[48,112,103] or the identified sulfate ion product formed by the reaction of the primary products with water[6,113,114,17,102]. Through the study of SO_2 photolysis at 3130 Å in very dry photolysis cells, Daubendiek and Calvert have been able to characterize and follow the kinetics of gaseous SO_3 formation and decay directly through infrared absorption spectroscopy[115]. In view of the present data it seems highly probable that SO_3 and SO are primary products of the electronically excited SO_2 interaction with SO_2 molecules.

Reaction (1b)

$$\text{(1b)} \qquad SO_2(^1B_1) + SO_2 \rightarrow SO_3 + SO(^1\Delta)$$

involving the excited singlet state should also be considered as a possible source of SO_3 in 3130-Å irradiated SO_2. Both reactions (1a) and (1b) conserve spin and are significantly exothermic: $\Delta H_{1a} = -27.7$ (for $SO_2(^3B_1)$ in the 0,0,0 level), and $\Delta H_{1b} = -24.3$ kcal/mole (for internal excitation of $SO_2(^1B_1)$ as formed on light absorption at 3130 Å). Conceivably other reactions involving the other nonradiative excited states of SO_2 may also occur when SO_2 is irradiated within the first allowed band[21,57,88-90].

However, whatever the nature of the state of SO_2 forming SO_3, it is apparent that the molecule SO is formed in amounts equivalent to those of the SO_3 generated. We and others have tended to ignore the fate of the SO species in the photolysis of SO_2 and its mixtures. In particular it has been assumed that it does not interact with the primary product SO_3. From our present results it seems clear that this assumption is not valid. Note that the quantum yield of SO_3 formation is a function of the flow rate or the residence time of the irradiated SO_2; this is the case whether the irradiation is effected within the triplet band (Fig. 26) or the singlet band (Fig. 27). In each case the observed quantum yield increased dramatically as the residence time of the irradiated SO_2 was decreased from 1000 sec to 10 sec. In both systems the quantum yield approached limiting values at high flow rates. Also note in Table XXII that the quantum yields of SO_3 observed in the static system are only about one one-hundreth of those observed at high flow rates. This observation confirms the apparently conflicting results of Okuda and coworkers[17] and those of Cox[102] and Allen and coworkers[48,114,103]. There is an obvious mechanism choice which appears to explain the effect of flow rate on Φ_{SO_3}. At low flow rates the SO_3 and SO primary products of the excited SO_2 reactions (1a), (1b), and/or (1c) react significantly before these primary products can be trapped at low temperature and subsequently allowed to react with water. Reactions (2) and (3) should be considered in this regard:

$$\text{(1c)} \qquad SO_2(^1A_2, ^3A_2, ^3B_2) + SO_2 \rightarrow SO_3 + SO(^1\Delta \text{ or } ^3\Sigma^-)$$

Basco and Morse[110] have suggested that these reactions might explain qualitatively the ultimate decrease in SO concentration which they observed following its formation in reaction (1) in the flash photolysis of SO_2. To the best of our knowledge the present data provide the first experimental evidence to substantiate this mechanism. Schofield[116] has reviewed the rate data pertaining to reaction (3)[117-120], and he sets an upp[illegible] r $k_3 = 1.8 \times 10^6$ ℓ./mole·sec. Halstead and Thrush[117] quote an upper li[illegible] both k_2 and k_3 of 5×10^6

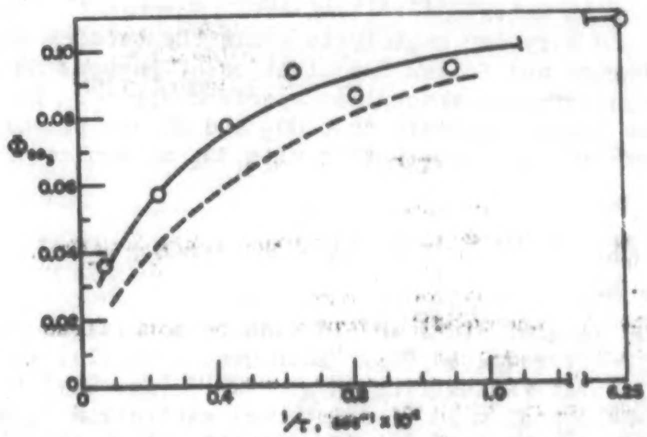

Figure 26. Effect of residence time τ of SO$_2$ on the quantum yield of SO$_3$ formation in 3600–4000-Å excited SO$_2$. P_{SO_2} = 25 torr; I_a = (6.6 ± 0.5) × 10^{-10} einstein/l./sec; the solid curve was derived by computer integration of relations (B)–(D) using $k_2 = 6.0 \times 10^4$ and $k_3 = 5.0 \times 10^8$ l./mole/sec; the dashed curve is the theoretical dependence estimated in the same fashion but using $k_2 = 1.2 \times 10^6$ and $k_3 = 5.0 \times 10^8$ l./mole/sec as derived from the excited singlet studies shown in Figure 27.

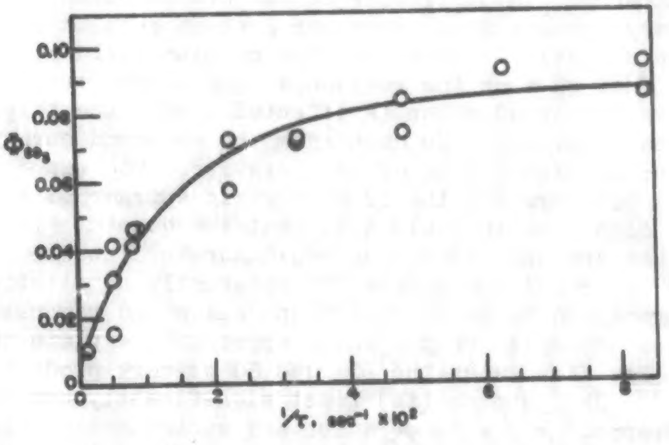

Figure 27. Effect of residence time τ of SO$_2$ on the quantum yield of SO$_3$ formation in 3130-Å irradiated SO$_2$. P_{SO_2} = 25 torr; I_a = (5.6 ± 0.8) × 10^{-9} einstein/l./sec; the solid curve was derived by computer integration of relations (B)–(D) using $k_2 = 1.2 \times 10^6$ and $k_3 = 5.0 \times 10^8$ l./mole/sec.

ℓ./mole·sec. It is significant to note that if the k_2 and k_3 values are this small, then the time required for SO to reach a steady-state concentration in an irradiated SO_2 system such as we employed falls in the range of hundreds of seconds, and only an insignificant fraction of the primary SO and SO_3 products formed should react at the shortest residence times for the fast flow system employed here (10 sec). Thus in theory the primary products can be carried to the trap and frozen out in our experiments at the fast flow rates before any significant reaction by (2) and (3) can occur.

Indeed a reasonably good quantitative fit of the Φ_{SO_3} versus flow rate data is possible using the simple reaction scheme outlined. In theory the dependence of the experimental overall quantum yield of SO_3 formation on residence time should be given by relations (A)-(D).

$$\text{(A)} \qquad \Phi_{SO_3} = [SO_3]_\tau / I_a\tau$$

$$\text{(B)} \qquad \int_{[SO_3]_0}^{[SO_3]_\tau} d[SO_3] = \int_0^\tau (I_a\alpha - [SO_3][SO]k_3)\, d\tau$$

$$\text{(C)} \qquad \int_{[SO]_0}^{[SO]_\tau} d[SO] = \int_0^\tau (I_a\alpha - [SO_3][SO]k_3 - [SO]^2 2k_2)\, d\tau$$

$$\text{(D)} \qquad \int_{[SO_2]_0}^{[SO_2]_\tau} -d[SO_2] = \int_0^\tau (2I_a\alpha - [SO_3][SO]2k_3 - [SO]^2 k_2)\, d\tau$$

I_a is the absorbed light intensity in einstein/ℓ.·sec, $[SO_3]_\tau$ is the molar concentration of SO_3 at the end of the time period of the irradiation τ, and α represents the fraction of the excited SO_2 molecules which react to form SO and SO_3 in reactions (1a), (1b), and (1c). The smallness of the rate constants k_2 and k_3 prevents the application of steady-state approximations for the time intervals employed in our flow systems, and the integration of relations (B), (C), and (D) must be carried out to establish the theoretical values of Φ_{SO_3} anticipated. This was accomplished in the present work using both digital and analog computer techniques. The value of α is obtained readily from the limiting quantum yield values obtained at high flow rates; thus $\alpha = 0.108 \pm 0.01$ for the triplet system and $\alpha = 0.090 \pm 0.005$ for the singlet excited system. The values of k_2 and k_3 were adjusted to obtain the best visual fit of the theoretical Φ_{SO_3} versus residence time curve to the experimental data points in Figures 26 and 27; the solid curves represent the computer-calculated relations. The "best" fit in Figure 26 with triplet SO_2 generation was obtained using $k_2 = 6.0 \times 10^5$ and $k_3 = 5.0 \times 10^5$ ℓ./mole·sec^{-1}, while that of Figure 27 with singlet SO_2 excitation was calculated using $k_2 = 1.2 \times 10^6$ and $k_3 = 5.0 \times 10^5$ ℓ./mole·sec. These estimates, the first of which we are aware, are in accord with the upper limits of k_2 and k_3 which were derived from the previous studies[117,120]. Some measure of the sensitivity of the theoretical fit to the choice of the rate constant k_2 can be seen in Figure 26, where the "best" fit k_2 derived from the singlet data (a factor of 2 higher than that from the triplet data) is used together with $k_3 = 5.0 \times 10^5$ ℓ./mole·sec. The fit of the data is much less sensitive to the magnitude of k_3 chosen, and the present estimate of this constant is subject to considerable uncertainty; we estimate that a value of $k_3 = (0.5 \pm 0.4) \times 10^6$ ℓ./mole·sec is reasonably consistent with our results.

It is interesting that the rate constant k_2 estimated from the singlet excitation of SO_2 is a factor of two higher than that for the triplet system. It is possible that this is due to the occurrence of a spin allowed reaction (2′) in the singlet system where $SO(^1\Delta)$ may be the product of reactions (1b) or (1c):

$$(2') \qquad SO(^1\Delta) + SO_3 \rightarrow 2SO_2$$

However there are several key points which would seem to discount this hypothesis. 1) As we shall see in later discussion most of the SO_3 product formed in the singlet experiments is derived from a quenchable triplet state which would not form $SO(^1\Delta)$ in its reaction with SO_2. 2) The rate of the wall quenching of the $SO(^1\Delta)$ species to $SO(^3\Sigma^-)$, observed by Breckenridge and Miller at low pressures[120], is large when extrapolated to our conditions, and this reaction is probably a major fate of $SO(^1\Delta)$ in our system. 3) The radiative decay rate of $SO(^1\Delta)$ is probably also fast on the time scale of the SO-SO_3 reaction (2)[120], and it probably accounts for the loss of another major fraction of the $SO(^1\Delta)$ generated in our system. 4) The actual rate constant for (2′) would have to be several orders of magnitude larger than that for reaction (2) in order for this reaction to be the origin of this result. It seems more likely to us that the minor mismatch of the k_2 values derived from the two systems has its origin in the necessarily large uncertainty in the measurement of the very small extinction coefficient of the SO_2 in the triplet band system, the values of I_a, and hence the Φ_{SO_3} estimates. Certainly within the experimental error the rate constant data from both systems are compatible.

It is clear that the occurrence of reactions (2) and (3) can account quantitatively for the observed variation of the quantum yield of SO_3 formation with flow rate in both the singlet and the triplet excitation experiments. It is instructive to use this mechanism to attempt to rationalize the quantum yield data obtained from the static photolysis experiments performed here and by other researchers. We must recognize that this procedure should underestimate SO_3 quantum yields in the very long static runs, since the transport of SO_3 from the gas phase to the wall will occur during these extended experiments, and its reaction there with adsorbed water may form the relatively nonvolatile H_2SO_4, as evident from the much larger fraction of the $SO_4^=$ derived from the wall of the cell in these experiments. Water will diffuse to the surface of the "dry" cell from the interior structure of the cell wall during the long experiments, and it will be a much more significant reactant than in the fast flow experiments. When SO_3 is removed from the gas phase, reaction (2) becomes less inhibiting, and the Φ_{SO_3}, as derived from the analysis of the combined H_2SO_4 condensed on the wall and the gaseous SO_3 in all of the studies, will rise. Table XXII summarizes the static experiments carried out in this work. Compare the experimental quantum yields with those calculated from relations (A)-(D). We have used the rate constant estimates derived from the singlet excitation of SO_2 in the flow system together with the measured values of I_a and integrated the differential equations (B)-(D) for the very long photolysis periods shown in Table XXII for runs 23-28. Although the irradiation times range from 3 to 34 hours in these cases, and the rate constants were derived from experiments of 10-2000-sec irradiation time, clearly the approximate magnitude of the quantum yield is predicted reasonably well through the application of the simple reaction scheme (1)-(3). In the best case (run 27) the theoretical value differs from the experimental one by only a factor of 2.3, while in the poorest case (run 23) the experimental and theoretical values differ by a factor of 4.7. In every case the predicted SO_3 is somewhat lower than that observed experimentally; we would expect this since SO_3 removal at the wall increases in importance in these long runs.

One can match more closely the present Φ_{SO_3} data from the extended exposures in the static system by adding an apparent first-order wall removal step for SO_3:

$$SO_3 + H_2O(\text{adsorbed on wall}) \xrightarrow{k_w} H_2SO_4(\text{adsorbed on wall})$$

Of course the apparent rate constant for any such heterogeneous reaction must be a complex function of the pressure of the reactant gas, the size of the cell, and the nature of the cell wall and its conditioning prior to the run, and it is expected to be of limited value in treating other systems. However, in our runs made at constant pressure of SO_2(25 torr) and with a set pattern of cell treatment, perhaps there is some justification for an attempt to include this wall reaction in a somewhat quantitative fashion. Assuming the values of k_2 and k_3 derived previously and taking $k_w = 4 \times 10^{-4}$ sec^{-1}, one can match quite well most of the Φ_{SO_3} data shown in Table XXII; see the last column, labeled "Calculated, Method II". It can be shown that the loss of SO_3 at the wall is only a minor reaction in the fast flow system; the choice of the homogeneous rate constants k_2 and k_3 derived from the flow data is not altered significantly by including this heterogeneous reaction.

It is interesting to estimate the theoretical quantum yield of SO_3 formation expected from the runs of Cox[102]. Using his 17-hr exposure time in experiments with $P_{SO_2} = 29$ torr and $I_a = 7.63 \times 10^{-8}$ einstein/ℓ.•sec, we estimate from the present homogeneous mechanism (reactions (1), (2), and (3), only) that $\Phi_{SO_3} = 0.48 \times 10^{-3}$; Cox reported an experimental value of $(3.4 \pm 1.0) \times 10^{-3}$. When one considers the potential significance of SO_3 removal from the gas phase by heterogeneous reaction, for which we have not attempted a correction here, the agreement between theory and the Cox experiment is considered satisfactory. The earlier study of Allen and Bonelli[103] which employed a static system with long exposure times using 3130-Å radiation, gave quantum yields of SO_3 formation similar to those reported here and to those of Cox. These results can be rationalized in terms of reactions (2) and (3) with about the same precision noted for the other results described above. Inclusion of the wall removal reaction using the value $k_w = 4 \times 10^{-4}$ picked for our system gives a surprisingly close fit for most of the Cox data and the Allen and Bonelli results. Obviously the potential importance of the unpredictable heterogeneous transport and capture of SO_3 at the wall makes such calculation of limited confirmatory value. However, it appears to us that all of the quantum yield data from the photolyses of pure SO_2 seem consistent with the simple mechanism involving reaction (1)-(3), and deviations from the values predicted from this mechanism for runs of extended time periods are qualitatively consistent with the expected wall removal of SO_3 as H_2SO_4. The "best" estimates from the flow experiments give the rate constants $k_2 = (1.2 \pm 0.7) \times 10^6$ and $k_3 = (0.5 \pm 0.4) \times 10^6$ ℓ./mole•sec.

Mechanism of SO_3 Formation in 3600-4000 Å $SO_2(^3B_1)$ Excitation Experiments

The rate data summarized in Table XXI offer a significant test of the mechanism of SO_3 formation. These were determined in mixtures of SO_2 with added NO, CO_2, and O_2 gases. In each case the pressure of SO_2 was constant at 25 torr, and a fast flow rate of reactants was employed. Thus the experimental quantum yields of SO_3 represent initial quantum yields since the SO_3 destruction in reaction (2) is unimportant for these conditions. The data can be rationalized well in terms of the following simple mechanism:

(1) $SO_2(\tilde{X}, {}^1A_1) + h\nu(3600\text{–}4000\ \text{Å}) \rightarrow SO_2({}^3B_1)$

(1a) $SO_2({}^3B_1) + SO_2 \rightarrow SO_3 + SO({}^3\Sigma^-)$

(4) $SO_2({}^3B_1) + SO_2 \rightarrow (2SO_2)$

(5) $SO_2({}^3B_1) + M \rightarrow (SO_2\text{—}M)$

M is an NO, CO_2, or O_2 molecule and (SO_2-M) represents ground state SO_2 and M molecules or any nonradiative products of the quenching reactions.

The limiting quantum yield of SO_3 formation from the triplet excitation experiments gives the first reliable experimental estimate of the rate constant ratio $k_{1a}/(k_{1a} + k_4) = 0.108 \pm 0.01$. Using the measured value of $k_{1a} + k_4 = (3.9 \pm 0.1) \times 10^8$ ℓ./mole·sec^{-1}[51,26], we estimate $k_1 = (4.2 \pm 0.4) \times 10^7$ ℓ./mole·sec.

Applying the steady-state assumption to the $SO_2(^3B_1)$ species in reactions (I), (1a), (4), and (5), we anticipate the ratio of the quantum yield of SO_3 in pure SO_2 ($\Phi_{SO_3}{}^0$) to that in SO_2 mixtures with added gas M ($\Phi_{SO_3}{}^M$) should be given by relation (E):

$$\frac{\Phi_{SO_3}{}^0}{\Phi_{SO_3}{}^M} = 1 + \frac{k_5}{(k_{1a} + k_4)} \frac{[M]}{[SO_2]} \tag{E}$$

In Figure 28 the quantum yield data for runs with M = NO, CO_2, and O_2 are plotted in the functional form of relation (E). The solid lines are determined by the least squares fit of the results without forcing the data through the intercept of unity expected theoretically from relation (E). Within the error limits both the NO and CO_2 data do conform to this expectation; the least squares intercepts for the NO and CO_2 data are 1.00 ± 0.04 and 0.91 ± 0.12, respectively. The slopes of these plots give estimates of $k_5/(k_{1a} + k_4)$ which may be compared in Table XXV with the same ratios derived from directly measured rate constants for reactions (4) and (5) in $SO_2(^3B_1)$ lifetime studies[30]. The rate data from the very different experiments for NO and CO_2 as M agree well within the experimental error, and they add credence to the mechanistic interpretation given here. The data for O_2 are not in accord with this simple mechanism outlined; an increase in SO_3 formation occurs with small O_2 additions, and then a decrease is observed as high pressures of O_2 are added. This is analogous to the findings of Cox[102] who proposed that the SO_3 increase at low O_2 concentrations resulted from the reaction (6):

$$SO + O_2 \rightarrow (SO{-}O_2) \rightarrow SO_3 \tag{6}$$

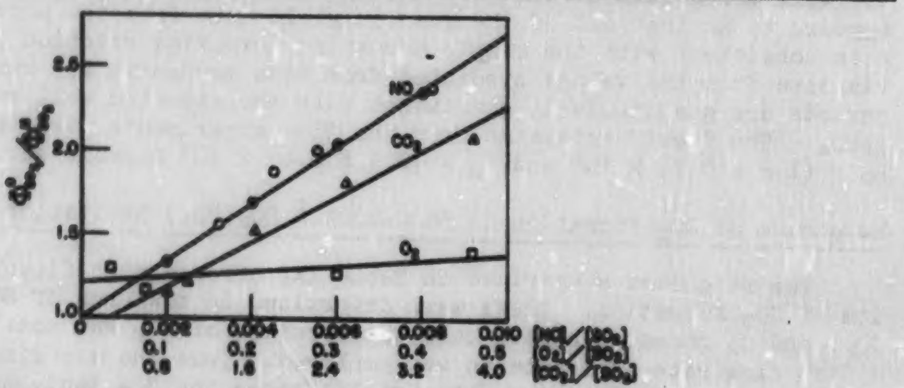

Figure 28 Plot of the ratio of the quantum yield of SO_3 formation in pure SO_2($\Phi_{SO_3}{}^0$) to that in SO_2-added gas mixtures ($\Phi_{SO_3}{}^M$); most of the data are from experiments with SO_2 excitation within the forbidden $SO_2(^3B_1) \leftarrow SO_2(\tilde{X}, {}^1A_1)$ band (3600–4000 Å) using fast flow rates of gases. The open circles are from singlet excitation experiments at 3130 Å calculated from relation (F) which corrects for SO_3 formed from singlet excited SO_2.

Table XXV. Comparison of the rate constant ratios $k_5/(k_1 + k_4)$ derived from the present product SO_3 quantum yield data and $SO_2(^3B_1)$ lifetime data[30]:

$$(1a) \quad SO_2(^3B_1) + SO_2 \rightarrow SO_3 + SO(^3\Sigma^-)$$
$$(4) \quad SO_2(^3B_1) + SO_2 \rightarrow (2SO_2)$$
$$(5) \quad SO_2(^3B_1) + M \rightarrow (SO_2 - M)$$

M	$k_5/(k_{1a} + k_4)$ Present data	 Lifetime studies (36)
NO	170 ± 8	190 ± 9
CO_2	0.34 ± 0.08	0.29 ± 0.03
O_2	0.34 ± 0.46	0.25 ± 0.01

In this mixture SO_3 may arise from reaction (7) as well[30]:

$$(7) \quad SO_2(^3B_1) + O_2 \rightarrow (SO_4) \rightarrow SO_3 + O(^3P)$$

Little is now known about the absolute magnitude of k_6 and k_7, although the available evidence suggests that both rate constants are rather small[116,102,30]. The limited data for the SO_2-O_2 system obtained here are consistent with this view but add little new to quantify this thesis.

It is important to recognize that all the present triplet excitation data are consistent with the $SO_2(^3B_1)$, phosphorescent state of SO_2, being the sole reactant to form SO_3. Not only are the ratios of the quenching rate constants obtained here nearly identical to those observed from lifetime measurements for $SO_2(^3B_1)$, but essentially complete quenching of SO_3 formation occurs at high added NO pressures; see runs 8 and 9 of Table XXI. It has been reasoned that the collisional quenching of $SO_2(^3B_1)$ by chemically "inert" gases such as CO_2 promotes crossover to other near lying nonradiative triplet states ($^3A_2$, $^3B_2$). This proposal seems attractive since the activation energy for this quenching reaction, $CO_2 + SO_2(^3B_1) \rightarrow CO_2 + (SO_2)$, 2.7 ± 0.3 kcal/mole, corresponds closely to the energy for the promotion of $SO_2(^3B_1)$ molecules to the lowest energy region of the triplet manifold in which distinctive perturbations give spectroscopic evidence of neighboring triplet states[92]. If this mechanism for quenching is correct, then one must conclude that $SO_2(^3A_2)$ and/or $SO_2(^3B_2)$ molecules do not form SO_3 in reactions analogous to (1). This conclusion is inconsistent with the suggestion of James, Kerr, and Simons who feel that the $SO_2(^3A_2)$ state would be ideally constituted to form SO_3 by reaction with SO_2[111]. Perhaps nonradiative coupling of the $^3A_2$ with the upper vibrational levels of the SO_2 ground state is sufficiently strong to lower its lifetime and lessen its chance to react with SO_2.

Mechanism of SO_3 Formation in SO_2 Excited at 3130 Å

The data from the fast flow experiments with pure SO_2 and SO_2-NO, SO_2-CO_2, and SO_2-O_2 mixtures (Tables XXIII and XXIV) may be used to illucidate the nature of the reactive states in singlet excited SO_2 mixtures. First it should be noted that unlike the triplet excitation experiments outlined previously, the addition of a relatively large quantity of NO gas to the SO_2 does not suppress SO_3 formation completely. See the fast flow experiments 54-57 of Table XXIII.

Thus we conclude that some excited singlet state reaction does occur in this system; possible contenders are reactions (1b) and (1c):

$$SO_2(^1B_1) + SO_2 \rightarrow SO_3 + SO(^1\Delta \text{ or } ^3\Sigma^-) \tag{1b}$$

$$SO_2(^1B_1) + SO_2 \rightarrow (2SO_2) \tag{8}$$

$$SO_2(^1B_1) + SO_2 \rightarrow SO_2^T + SO_2 \tag{9}$$

$$SO_2(^1A_2) + SO_2 \rightarrow SO_3 + SO(^1\Delta \text{ or } ^3\Sigma^-) \tag{1c}$$

$$SO_2(^1A_2) + SO_2 \rightarrow (2SO_2) \tag{10}$$

$$SO_2(^1A_2) + SO_2 \rightarrow SO_2^T + SO_2 \tag{11}$$

It is impossible to infer from these data alone which of these reactions is important in SO_3 formation here. However, if the $SO_2(^1B_1)$ molecule is this source, then we can estimate from the quantum yields for the NO inhibited runs, the rate constant ratio $k_{1b}/(k_{1b} + k_8 + k_9) = 0.026 \pm 0.003$. From the measured rate constant sum $k_{1b} + k_8 + k_9$ for SO_2 excited at $\lambda \geq 3000$ Å $(8.6 \pm 1.8) \times 10^{10}$ ℓ./mole·sec^{-1}[98,121,122] we estimate $k_{1b} = (2.2 \pm 0.5) \times 10^8$ ℓ./mole·sec.

Using the data of runs 58-61 on Table XXIV we may investigate the reactivity of the nitric oxide-quenchable species which leads to SO_3 formation in the singlet experiments. For the very small amounts of NO added in these runs, it is clear that the excited singlet is quenched largely by SO_2 in these runs. If only the $^1B_1$ and one other state of unknown designation (SO_2^T) is involved in SO_3 formation in the excited singlet experiments, then the rate function F should apply:

$$\frac{\Phi_{SO_3}^{0} - 0.026}{\Phi_{SO_3}^{NO} - 0.026} = 1 + \frac{k_{14}}{(k_{12} + k_{13})}\frac{[NO]}{[SO_2]} \tag{F}$$

Here k_{12}, k_{13}, and k_{14} refer to the quenching reactions for the undesignated reactive state SO_2^T which is quenchable with added NO.

$$SO_2^T + SO_2 \rightarrow SO_3 + SO(^3\Sigma^-) \tag{12}$$

$$SO_2^T + SO_2 \rightarrow (2SO_2) \tag{13}$$

$$SO_2^T + NO \rightarrow (SO_2\text{—}NO) \tag{14}$$

Function (F) is plotted in Figure 28 (open circles) along with the data from the $SO_2(^3B_1)$ quenching experiments from the direct triplet excitation with SO_2-NO mixtures (filled circles). Obviously the nitric oxide-quenchable, ill-defined state formed in the singlet excited experiments has the same rate constant ratio for quenching with NO and SO_2 as that for $SO_2(^3B_1)$ within the experimental error. We conclude that either $SO_2(^3B_1)$ is the most important reactive state which leads to SO_3 in singlet excited SO_2 mixtures or another NO-quenchable state such as $^3A_2$ or $^3B_2$ is generated here and it reacts to form SO_3 or is quenched by NO with the same relative rates as found for $SO_2(^3B_1)$. If the first alternative is correct, as was originally suggested by Okuda and coworkers[17], then we must speculate that the intersystem crossing ratio for 3130-Å excited SO_2 to form $SO_2(^3B_1)$ is much higher (0.59) than that estimated by us for the photolysis at the shorter wavelengths (~ 0.10). The high pressure mechanism of $SO_2(^3B_1)$ formation suggested by Wampler, Horowitz, and Calvert[22,31] cannot be an important source of $^3B_1$ molecules at the relative low pressures of SO_2 employed in this work.

The singlet excited SO_2 experiments with added CO_2 (runs 62-66, Table XXIV) should be considered also in light of the mechanism suggested here. In this case the quenching effect of CO_2 is small, and relative large quantities of CO_2 must be added to observe one at all. This leads to considerable complication in attempting to sort out the states involved, since singlet quenching by CO_2 as well as SO_2 must occur in these cases. We may simplify our considerations somewhat by assuming that only two reactive states of SO_2 are present in this system, $SO_2(^1B_1)$ and the undesignated reactive state SO_2^T. Reactions (15)-(17) must now be considered in addition to reactions (1b), (8), (9), (12), and (13):

$$(15) \qquad SO_2(^1B_1) + CO_2 \rightarrow SO_2^T + CO_2$$

$$(16) \qquad SO_2(^1B_1) + CO_2 \rightarrow SO_2 + CO_2$$

$$(17) \qquad SO_2^T + CO_2 \rightarrow SO_2 + CO_2$$

We may attempt to treat the data utilizing the measured rate constant ratios $(k_{15} + k_{16})/(k_{1b} + k_8 + k_9) = 0.71$[123], and assuming $k_{17}/(k_{12} + k_{13}) = 0.29$ as measured for the $SO_2(^3B_1)$ state[30]. Then the quantum yield of SO_3 formation in singlet excited SO_2-CO_2 mixtures should be given by relation (G).

$$(G) \qquad \frac{\left(\Phi_{SO_3} - \dfrac{0.026}{1 + 0.71\dfrac{[CO_2]}{[SO_2]}}\right)\left(1 + 0.71\dfrac{[CO_2]}{[SO_2]}\right)}{\left(\dfrac{0.108}{1 + 0.29\dfrac{[CO_2]}{[SO_2]}}\right)} = \frac{k_9}{k_{1b} + k_8 + k_9} + \frac{[CO_2]k_{15}}{[SO_2](k_{1b} + k_8 + k_9)}$$

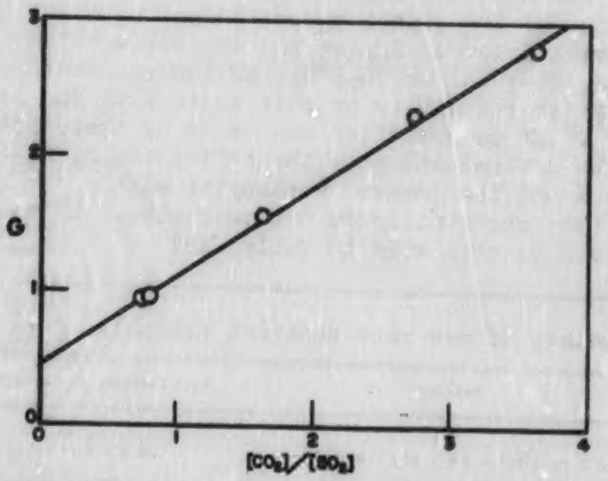

Figure 29. Plot of function (G) versus $[CO_2]/[SO_2]$; data are from the 3130-Å irradiated mixtures of SO_2 and CO_2.

The excess triplet mechanism will be relatively unimportant for these conditions[22,31]. A test of relation (G) is shown in Figure 29. The data are not accurate enough to define a reliable intercept, but they suggest (0.46 ± 0.09). In theory the intercept is equal to the rate constant ratio $k_9/(k_{1b} + k_8 + k_9)$ and should be compared with the ratio 0.59 derived elsewhere in this work. The slope in theory equals $k_{15}/(k_{1b} + k_8 + k_9) = 0.67 \pm 0.04$. The only other estimate of this rate constant ratio of which we are aware, was derived by Demerjian and Calvert[94] from the 3130-Å irradiated SO_2-CO_2-cis-2-butene mixtures at high CO_2 pressures. This gave the approximate value of 0.14. Within the large error inherent in this method of data treatment which involves differences in quantum yields which are near equal, the CO_2-SO_2 results are qualitatively consistent with the generalized two-state reaction scheme outlined above, but they do not provide any meaningful test of it.

The O_2-SO_2 singlet data (runs 67-69 of Table XXIV) are, as observed in the triplet study, complicated by the reaction of SO with O_2, and no quantitative rate information can be gleamed from them at this time.

Conclusions

The Φ_{SO_3} data obtained in this work using both flow and steady-state static systems confirm the apparently divergent results of both Okuda and coworkers[17], and Cox[102]. The clue to the quantitative rationalization of all of the results is the relative importance of reaction (2), $SO_3 + SO \rightarrow 2SO_2$, in static and slow flow-rate experiments. The SO_3 product rate data from irradiated SO_2 mixtures at high flow rates within the forbidden $SO_2(^3B_1) \leftarrow SO_2(\tilde{X}, {}^1A_1)$ band point to the involvement of $SO_2(^3B_1)$ as the sole reactant with SO_2 in forming the SO_3 product. Similar rate data from 3130-Å irradiated SO_2 mixtures show that both singlet (probably $^1B_1$) and some triplet state are reactants forming SO_3 in these systems. The ratio of the quenching rate constants of the reactive triplet state toward NO and SO_2 molecules is near identical to that observed for the $SO_2(^3B_1)$ molecule in lifetime studies. However, if $SO_2(^3B_1)$ is the reactant here, then the data require that the 3130-Å excited singlet SO_2 molecule form $SO_2(^3B_1)$ molecules in a much larger fraction of the quenching collisions with SO_2 than previous kinetic data allow for the excitation of SO_2 at the shorter wavelengths. If another triplet state such as $SO_2(^3A_2)$ or $SO_2(^3B_2)$ is the reactant here, then the results demand that the relative reactivity of this state with SO_2 and NO be near identical to that for $SO_2(^3B_1)$. It is not clear now which of these alternatives is correct. We are engaged in the determination of the efficiency of $SO_2(^3B_1)$ generation in SO_2 excited at 3130 Å and the longer wavelengths within the singlet band in an attempt to resolve this uncertainty in the mechanism. We have summarized the new rate constants derived in this work in Table XXVI.

Table XXVI. Summary of new rate constant estimates derived in this work.

	Reaction	Rate Constant (l. mole^{-1}sec^{-1})
(1a)	$SO_2(^3B_1) + SO_2 \rightarrow SO_3 + SO(^3\Sigma^-)$	$(4.2 \pm 0.4) \times 10^7$
(1b)	$SO_2(^1B_1) + SO_2 \rightarrow SO_3 + SO(^1\Delta$ or $^3\Sigma^-)$	$(2.2 \pm 0.5) \times 10^9$
(2)	$SO + SO_3 \rightarrow 2SO_2$	$(1.2 \pm 0.7) \times 10^6$
(3)	$2SO \rightarrow SO_2 + S$ [or $(SO)_2$]	$(5 \pm 4) \times 10^5$

I-G. The Nature of the Excited Singlet States in SO_2 Photolysis Within the First Allowed Absorption Band[124].

Until the recent detailed study of Brus and McDonald[122] the kinetics of fluorescence emission from SO_2 excited within the first allowed absorption band (2500-3200 Å) had been rationalized in terms of a simple mechanism involving only one emitting excited singlet state ($^1SO_2$):

$$SO_2 + h\nu \rightarrow {}^1SO_2 \qquad (I)$$

$${}^1SO_2 + SO_2 \rightarrow (2SO_2) \qquad (1)$$

$$\rightarrow {}^3SO_2 + SO_2 \qquad (2)$$

$${}^1SO_2 \rightarrow SO_2 + h\nu_f \qquad (3)$$

$$\rightarrow (SO_2) \qquad (4)$$

$$\rightarrow {}^3SO_2 \qquad (5)$$

$^3SO_2$ represents a triplet state, presumably $SO_2(^3B_1)$, and $(2SO_2)$ and (SO_2) designate ill-defined, non-emitting (or very long-lived) excited states, products other than SO_2, or ground state SO_2. The best current information from our group suggests $k_5 << k_3 + k_4$ for all wavelengths of excitation of SO_2[123]. However, a divergence of opinion has remained on the possible importance of the first order non-radiative process (4). Mettee and co-workers[34,35] have concluded from limiting quantum yield measurements at zero pressure that $k_3/(k_3 + k_4 + k_5) \approx 1$ at all wavelengths. Calvert and co-workers[18,23,98] have suggested that $k_3 \approx k_4$ at 2650 Å and $k_4 > k_3$ at the long wavelengths. The recently published note of Brus and McDonald[122] presented clear evidence for the existence of two emitting singlet states of SO_2 which are presumably both populated by direct absorption within the first allowed band of SO_2. As these authors suggest, their findings bear directly on the interpretation of previous steady-state studies of SO_2 emission. They conclude that the unexpectedly long lifetime and double exponential decay which they observe invalidates the conclusion of previous workers that SO_2 undergoes a unimolecular internal conversion. We now concur with this conclusion as also formulated by Mettee[34] several years ago, and we offer here support for it.

First, one should question why Sidebottom et al[98] did not see two emitting singlet states in their recent lifetime studies using SO_2 excited by a 2662 Å laser pulse. From the recent rate parameters obtained for the two emitting species by Brus and McDonald[122], one can estimate that the mean lifetime of the two states at $P_{SO_2} = 10\ \mu$ are 1.6 and 37 μsec, respectively, and at $P_{SO_2} = 100\ \mu$, 0.17 and 6.3 μsec, respectively. Since most of our experiments designed to detect a second component were carried out in this pressure range, it is somewhat surprising that the sensitivity of our method was not suitable to find the short-lived component. A clue to the reason for this failure may be had from the observation of Brus and McDonald who report that the ratio of the fluorescence intensities from the short-lived to that of the long-lived species was so small for the 2617 Å wavelength excitation that it was not possible to form an accurate Stern-Volmer plot for the lifetime data of the short-lived species for these conditions.

Note that the quenching rate constants observed by us previously[123,98] are near equal to those reported by Brus and McDonald for the long-lived species; see the data of Table XXVII. It is clear that our data refer to the dominant

Table XXVII. Comparison of quenching rate constants ($k_1 + k_2$) for excited singlet SO_2 (long-lived component)

Wavelength (A)	$k_1 + k_2$ (ℓ mole^{-1} sec^{-1} [a])	Reference and method of measurement
2617.4	$(2.7 \pm 0.2) \times 10^{10}$	ref. 122 laser excitation
2662	$(3.8 \pm 0.1) \times 10^{10}$	ref. 23 laser excitation
2662	$(3.2 \pm 0.2) \times 10^{10}$	extrapolated from near linear plot of $k_1 + k_2$ versus λ data of ref. 122
2715.2	$(3.9 \pm 0.2) \times 10^{10}$	filtered Xe-flash data of ref. 23
2860	$(5.1 \pm 0.8) \times 10^{10}$	filtered Xe-flash data of ref. 23
2856.7	$(4.9 \pm 0.4) \times 10^{10}$	ref. 122 laser excitation
2980.9	$(7.0 \pm 0.2) \times 10^{10}$	ref. 122 laser excitation
2980	$(8.6 \pm 1.8) \times 10^{10}$	filtered Xe-flash data of ref. 23
3000	$(7.8 \pm 0.7) \times 10^{10}$	excitation at 2662 but observation at long times from ref 23
3004	$(8.3 \pm 0.8) \times 10^{10}$	ref 122 laser excitation

a) Error limits shown here and elsewhere in this paper are ± 2σ.

long-lived state delineated by these workers. Our lifetime estimate from the 2662 Å laser experiments, $\tau_0 = 36 \pm 4$ μsec, is in fair accord with that of Greenough and Duncan[125] obtained using broadband flash lamp excitation, $\tau_0 = 42$ μsec, although it is somewhat less than that found by Brus and McDonald at 2617 Å, $\tau_0 = 79 \pm 30$ μsec. The only significant difference between the previously estimated properties of this emitting state and those for the long-lived species delineated by Brus and McDonald, lies in the lifetimes at the long wavelengths. Sidebottom et al[98] did not measure this quantity directly since a short lifetime excitation beam in the range of 3100 Å was not available to them at that time. Instead they attempted to observe the intensity of the fluorescence after a long delay time when presumably the 2662 Å excited species would be near vibrationally equilibrated and its reactivity similar to that for a long wavelength excited SO_2 species. Since the pressure of SO_2 had to be such that vibrational equilibration was ensured, the method is inherently inaccurate in establishing a zero pressure lifetime for the excited state. However, the quenching rate constant so determined was in excellent accord with that which we found by direct long wavelength excitation using a filtered Xe-flash lamp system, and we were thus led to accept the lifetime so determined as a preliminary estimate of some merit. It is interesting to note that the quenching rate constant so obtained is also in excellent agreement with the recent estimate of Brus and McDonald for near vibrationally equilibrated species; see Table XXVII. The unexpectedly long lifetime observed directly by Brus and McDonald, about 500 μsec, makes the Sidebottom et al lifetime estimate meaningless in retrospect. One can be sure that an extensive loss of excited singlet species through diffusion controlled processes must have occurred at the lower pressures. In fact, it is this unusual lifetime observation which requires a re-evaluation of the role of diffusional loss of singlets in the steady-state experiments from which much of the evidence for the non-radiative decay was obtained.

First, one must consider to what extent the presence of the two emitting singlets is expected to complicate the Stern-Volmer plots of $1/\Phi_f$ versus $[SO_2]$ found in stead-state experiments. From the rate parameters estimated by Brus and McDonald and their estimate that the concentration ratio of the short-lived to long-lived singlet is ≈ 0.28 immediately following the laser excitation, we may estimate the relative intensities of the fluorescence from the two states shown in Table XXVIII. Obviously no more than a few percent of the fluorescence

---

Table XXVIII. Estimated ratio of intensity of the fluorescence from the short-lived SO_2 singlet species (I_f^s) to that for the long-lived species (I_f^l) in steady-state experiments[a])

Wavelength (A)	P_{SO_2} (μ)	$(I_f^s)/(I_f^l)$
2617	150	0.011
	50	0.013
	5	0.029
	1	0.081
	0	0.28
2856.7	150	0.036
	50	0.037
	5	0.051
	1	0.098
	0	0.28
3043.9	150	0.17
	50	0.17
	5	0.17
	1	0.20
	0	0.28

a) Rate data of Brus and McDonald used for these estimates[122].

---

light which we observed in our steady-state experiments down to pressures of 1 μ would be that from the short-lived species for experiments in the 2650-2900 range. Clearly the steady-state experiments should apply well to the long-lived state for these conditions. Arguments which we have enunciated elsewhere[123] show that diffusional loss of the singlet of lifetime 40 μsec would not be very significant for our small cell in experiments down to about 10 μ pressure. However, at lifetimes of 500 μsec, there can be no question that diffusional loss of singlets must be important in a small cell at the lower pressures which we employed. Thus, the limiting quantum yield of emission which we measured may be greatly underestimated in experiments at 3050 Å, while they should be reasonably good for experiments at 2650 Å. For 2650 Å excitation the zero pressure limit gives ϕ_f^o = 0.55 ± 0.43 from the data of Rao et al[23] extrapolated from data at pressures of 50 μ and above, and 0.41 ± 0.24 from Sidebottom et al[123], extrapolated to zero pressure from data in the range 41-141 μ. If the Brus and McDonald estimate of the initial population of the two states is correct and there is little generation of one state from the other as they suggest, then we would expect a directly measured limiting quantum yield of 0.78 from these runs in which no significant number of quanta of the short-lived state would have been detected. In view of the very large extrapolation necessary to derive ϕ_f^o from the relatively high pressure data, the observed estimates agree reasonably well with this expectation. In other experiments which we will describe in detail elsewhere[123], we have measured the zero pressure quantum yield of the long-lived emission from SO_2 excited in a laser pulse at 2662 Å using benzene as a fluorescence actinometer. We estimate for conditions for which diffusional loss of singlets would be unimportant that $\phi_f^o = 0.46 \pm 0.14$. Certainly there is no evidence of a large unexplained inefficiency in light emission from any of the studies in the 2650 Å region.

Table XXIX. Estimation of ϕ_f^0 from lifetime data of Brus and McDonald[122] and $(k_1 + k_2)/k_3$ data of Calvert et al[123,126,23] and Mettee et al[34].

Wavelength (Å)	$k_1 + k_2$ a) (ℓ mole^{-1} sec^{-1}) × 10^{-10}	$(k_1+k_2)/k_3$ (ℓ mole^{-1}) × 10^{-4}	k_3 (sec^{-1}) × 10^{-4}	$k_3+k_4+k_5$ a) (sec^{-1}) × 10^{-4}	$\phi_f^0 = k_3/(k_3+k_4+k_5)$	Reference source of $(k_1+k_2)/k_3$
2650	3.1 ± 0.2	1.9 ± 0.4	1.63 ± 0.36	1.15 ± 0.44	1.41 ± 0.60	34
		1.9 ± 0.8	1.63 ± 0.69		1.41 ± 0.90	35
		5.3 ± 0.1	0.58 ± 0.04		0.50 ± 0.19	23
		2.9 ± 0.3	1.07 ± 0.13		0.93 ± 0.37	123
2750	4.1 ± 0.2	3.4 ± 0.3	1.21 ± 0.12	0.95 ± 0.06	1.27 ± 0.14	34
		3.4 ± 0.3	1.21 ± 0.12		1.27 ± 0.14	35
		6.0 ± 1.1	0.68 ± 0.13		0.72 ± 0.14	123
2875	5.6 ± 0.4	5.6 ± 0.6	1.00 ± 0.13	0.71 ± 0.06	1.41 ± 0.22	34
		3.9 ± 0.9	1.44 ± 0.35		2.03 ± 0.52	35
		6.6 ± 0.3	0.85 ± 0.07		1.20 ± 0.14	18
		10.9 ± 3.2	0.51 ± 0.15		0.72 ± 0.22	123
2963	6.6 ± 0.1	10.2 ± 1.0	0.65 ± 0.06	0.53 ± 0.02	1.23 ± 0.12	34
		8.1 ± 1.6	0.81 ± 0.16		1.53 ± 0.31	35
		13.8 ± 0.4	0.48 ± 0.02		0.91 ± 0.05	23
		20.1 ± 1.0	0.33 ± 0.02		0.62 ± 0.04	123
3020	7.2 ± 0.2	10.7 ± 0.8 b)	0.57 ± 0.04	0.41 ± 0.07	1.39 ± 0.26	34
		12.0 ± 3.3 b)	0.51 ± 0.15		1.24 ± 0.41	35
		15.9 ± 0.9 b)	0.38 ± 0.03		0.93 ± 0.17	23
		23.4 ± 3.0 b)	0.26 ± 0.04		0.65 ± 0.14	123

a) $k_1 + k_2$ and $k_3 + k_4 + k_5$ values were obtained by interpolation of the rate constant–wavelength data of Brus and McDonald[122]

b) These experimentally measured slopes were corrected to the "true" $(k_1 + k_2)/k_3$ values for the long-lived singlet species by multiplying by 1.17, since the measured quantum yields for this wavelength are expected to be 1.17-times the fluorescence quantum yield for the long-lived singlet species at the pressures employed here; see table XXVIII.

On the other hand, steady-state quantum yield studies carried out at 3020 Å gave ϕ_f^0 = 0.061 ± 0.12 and 0.069 ± 0.081, in the studies of Rao et al[23], and Sidebottom et al[123], respectively. We are now of the opinion that most or all of the apparent lowering of the ϕ_f^0 with wavelength increase may be an artifact of the diffusional loss of the excited singlet as a direct result of the then unrecognized very long lifetime of the state formed at long wavelengths. We may use our own and Mettee's steady-state data to test this hypothesis in a rather quantitative fashion which is independdent of diffusional problems.

The Stern-Volmer plots derived from the high pressure, stead-state data should have no appreciable influence from diffusional loss of singlets. However, in view of the well established result that a vibrational cascade mechanism operates for the quenching of the long-lived singlet formed at the short wavelengths[122,123,98], it is somewhat surprising at first consideration that no significant curvature has been seen in Stern-Volmer plots of $1/\phi_f$ versus $[SO_2]$ in any of the previous studies. This probably results from two main factors. In steady-state experiments most of the light quanta which are detected are emitted during the first few lifetimes of the emitting species, and during this time there is a very little vibrational relaxation of the excited SO_2 species; this is evident in the near linear character if the $1/\tau$ versus $[SO_2]$ plot during the first lifetime periods for SO_2 excited at 2662 Å[98]. Secondly, the failure of a plot of $[SO_2]/(I_f)_{\Delta\lambda}$ versus $[SO_2]$ to maintain linearity (where $(I_f)_{\Delta\lambda}$ is the intensity of a small band of wavelengths near the exciting light) is much more readily detected experimentally[98] than curvature in a Stern-Volmer plot of $1/\phi_f$ versus $[SO_2]$, since vibrational relaxation does not preclude the ultimate emission of a quantum at the longer wavelength. In any case, all previous studies give good Stern-Volmer plots whose slopes from the high pressure data should have no appreciable influence from diffusional loss of singlets. These slopes should give reasonable estimates of $(k_1 + k_2)/k_3$ for the long-lived species. These are shown in Table XXIX for several wavelength ranges along with estimates for $k_1 + k_2$ and $k_3 + k_4 + k_5 = 1/\tau_0$ for the long-lived SO_2 state which we have interpolated from the results of Brus and McDonald[122]. We can estimate k_3 from our $(k_1 + k_2)/k_3$ data and directly measured values of $k_1 + k_2$. Now the ratio of this value to the reciprocal of the limiting zero pressure lifetime of the long-lived SO_2 state $(1/\tau_0 = k_3 + k_4 + k_5)$ should give the limiting quantum yield of fluorescence of the long-lived state at zero pressure: $k_3/(k_3 + k_4 + k_5) = \phi_f^0$. Note in Table XXIX that the data from both the Mettee group and our own group show no significant trend of the data with λ, and a value near unity is certainly not inconsistent with these results.

All of the present data support the contention made by Mettee several years ago and reinforced recently by Brus and McDonald, that radiationless decay in excited SO_2 singlets is unimportant. It now appears that any small inefficiency in the emission of light quanta for SO_2 excited at short wavelengths is largely due to the population of a second very short-lived state which for all of our conditions is quenched effectively even at the lowest pressures we employed. The very low efficiency of quanta production which we observed at long wavelengths appears to have its origin not only in the second easily quenched state, but more importantly, in the diffusional loss of the singlet which has a 20-fold greater lifetime than was expected previously for these conditions.

PART II.

SOME THERMAL REACTIONS OF POSSIBLE SIGNIFICANCE ON THE SUNLIGHT-IRRADIATED, POLLUTED TROPOSPHERE.

The interaction of the free radicals HO, HO_2, RO (alkoxy), RO_2 (alkylperoxy), NO_3, and other reactive species such as $O(^3P)$, $O(^1D)$, N_2O_5, O_3, etc., with important pollutant molecules such as SO_2, NO, NO_2, RH, etc., may be of significant rates in the sunlight-irradiated, polluted troposphere. The recent computer simulation studies of the chemistry of the polluted atmosphere carried out by our group[127], have pointed toward the possible importance of several thermal reaction systems. In this section we discuss these results; some of these studies have been completed and published during the period, while studies on others remain incomplete at this report writing. We will consider these systems in this section.

II-A. A Kinetic Study of the SO_2-O_3, SO_2-NO_3, and the SO_2-N_2O_5 Reactions[128].

In addition to the heterogeneous pathways which are often invoked to rationalize SO_2 conversion to H_2SO_4 and sulfate salts in the atmosphere, there are a number of homogeneous elementary reaction paths which may control SO_2 removal in the sunlight irradiated NO_x-SO_2-hydrocarbon-polluted atmospheres[93]. The present study provides the first direct kinetic data related to two of these potentially important reactions 1 and 2:

$$SO_2 + NO_3 \rightarrow SO_3 + NO_2 \qquad (1)$$

$$SO_2 + N_2O_5 \rightarrow SO_3 + N_2O_4 \qquad (2)$$

In this work NO_3 symbolizes the symmetrical nitrogen trioxide species. A reaction analogous to 1 has been considered to be an important step in the NO_x-catalyzed thermal oxidation of SO_2 at high temperatures[129,130]; presumably the unsymmetrical, peroxy-bonded nitrogen trioxide species, O-N-O-O, was considered the reactant in these systems, since this is the primary species which is expected to form from the bimolecular interaction of molecular oxygen and nitric oxide for the conditions employed in the previous work.

The enthalpy changes associated with reactions 1 and 2 ($\Delta H_1^\circ = -33$; $\Delta H_2^\circ = -24$ kcal $mole^{-1}$ at 25° C) favor the consideration of these reactions as potentially important among the atmospheric SO_2 removal processes. Indeed reaction 1 has been suggested as an important source of SO_2 oxidation in irradiated NO_x-SO_2-hydrocarbon mixtures in smog chamber studies[131]. We report in this work the first direct experimental evidence concerning the magnitude of the rate constants for reactions 1 and 2.

We have studied mixtures of SO_2 and N_2O_5 with and without added O_3, and have employed direct infrared spectroscopic detection of SO_3[132]. The mechanisms and kinetics of the N_2O_5 decomposition (reactions 3, 4, and 6) and of the N_2O_5-catalyzed decomposition of O_3 (reactions 3-6) are well understood today, and reasonably accurate estimates of the rate constants for these reactions are available[133].

$$N_2O_5 \rightarrow NO_3 + NO_2 \tag{3}$$

$$NO_2 + NO_3 \rightarrow N_2O_5 \tag{4}$$

$$NO_2 + O_3 \rightarrow NO_3 + O_2 \tag{5}$$

$$NO_3 + NO_3 \rightarrow 2NO_2 + O_2 \tag{6}$$

Our recent results confirm the conclusions of previous workers that the rate of the homogeneous gas phase oxidation of SO_2 by O_3, $O_3 + SO_2 \rightarrow O_2 + SO_3$, is very slow at room temperature ($k \leq 5 \times 10^{-3}$ ℓ. $mole^{-1} sec^{-1}$)[132]. Therefore it is possible, at least in theory, to estimate the rate constants for the reactions 1 and 2 from a kinetic study of the N_2O_5-SO_2 and N_2O_5-SO_2-O_3 mixtures. The success of our method depends upon the feasibility of the direct, quantitative, infrared spectroscopic measurement of gaseous SO_3 concentrations. We have been able to follow SO_3 quantitatively in a CaF_2-windowed cell and a Pyrex vacuum system, free of mercury, stopcock lubricants, and other materials reactive to SO_3, and which were made essentially water-free through prolonged bakeout at 100° C and evacuation[132].

II-A—1. Experimental

Synthesis of N_2O_5

N_2O_5 was prepared by the dehydration of HNO_3 in an O_3-containing atmosphere by a procedure modified from that of Grunhut, et al[134] to insure the complete removal of water. The method appears to be one which would be of general use to atmospheric scientists so it will be described here in some detail. The method of dehydration of HNO_3 for N_2O_5 preparation was preferred to that of O_3 oxidation of N_2O_4 since it seemed to offer less danger of explosion[135]. The apparatus is shown in Figure 30. Fisher-Porter Teflon valves (4 or 6 mm) were used throughout. Silicone grease was used on standard tapers in the 3-neck flasks F_1 and F_2. Other demountable joints were Fisher-Porter Solve-Seal connectors. Prior to use the apparatus was dried. The trap T_1 which contained P_2O_5 on glass wool, and the Dewar trap T_2, were both outgassed for a 24 hr period at 100° C in a vacuum ($p < 10^{-5}$ Torr); the vacuum was maintained until the system was purged with an O_3-O_2 mixture following HNO_3 preparation. The U-tubes, U_1 and U_2, filled with 6-16 mesh silica gel, were dried in a vacuum at 150-180° for 2 hrs., then stored in a drying oven with the remainder of the apparatus until assemblage just before the start of the synthesis. During HNO_3 preparation, traps U_1 and U_2 were kept at -78° C to remove any traces of H_2O in the O_2 and N_2 gases.

HNO_3 was formed at 70-100° C from H_2SO_4 (25 cc, DuPont Reagent) placed in flask F_1 and $NaNO_3$ (7.9 g. Mallinkrodt Analytical Reagent) added by way of the bulb B_1. The HNO_3 vapors were transferred from F_1 to F_2 with a stream of N_2 gas (Burdette extra dry) while flask F_2 was cooled to -78° C. During this step, exposure of the other parts of the apparatus to HNO_3 was avoided by closing the appropriate valves. About 10 cc of pure HNO_3 liquid was formed. The system was then purged with an O_3-O_2 mixture which was generated from O_2 (Burdette extra dry) by passing it through a high voltage discharge D. In this and the two succeeding steps the valve V_1 to vessel F_1 and the nitrogen vent V_2 were closed, and the U-tube U_3 was kept at -78° C to avoid back diffusion of water vapor into the system. The O_3-O_2 mixture for our conditions contained 2.3% O_3 as shown by chemical analysis[136].

With HNO_3 at -78° C in vessel F_2 and the O_3-O_2 flow continued, the dehydration of the HNO_3 was accomplished using P_2O_5 (21 g, Mallinkrodt Analytical Reagent). This was added by upending the 125 ml bulb B_2 attached to F_2 and loosening the pinch clamp on the Tygon tubing connector. The reaction mixture was warmed gradually to 100° C over a period of 1 hr; as the viscosity of the mixture decreased sufficiently, the mixture was stirred magnetically. Dehydration was further assured by transporting the gaseous N_2O_5 product by means of the O_2-O_3 stream through the trap T_1 filled with P_2O_5 powder suspended on glass wool. The condensables were trapped on a 48 mm coldfinger maintained at -78° C in the Dewar trap T_2. P_2O_5 was also placed in the bottom of this trap. The condensed product N_2O_5 at -78° C was a white, fibrous solid. The O_2-O_3 gas flow was continued for an additional 4 hours after F_2 had cooled to room temperature. Then the Dewar trap T_2 was connected to a bakeable vacuum line[132], and the line and connecting tubing were outgassed at 100° C for several hours before degassing the sample. When the line had returned to room temperature, trap T_2 was evacuated while maintaining the coldfinger at -78° C, and then it was closed off. Next, the bottom of the Dewar was cooled with liquid nitrogen and the Dry ice-acetone mixture was removed from the central coldfinger chamber of T_2. The product condensed onto the P_2O_5 at the bottom of the Dewar, it was again outgassed, then recondensed onto the coldfinger. The sample of N_2O_5 was then allowed to warm to -55° C and any volatile fraction was pumped away. The fraction of the product which vaporized in the range -30 to -20° C was transferred over a 1 hour period to a carefully baked and dried storage Dewar, the coldfinger of which was kept at -78° C. This Dewar was similar to T_2 shown in Figure 30 except it had only one side arm (demountable) near the top, in order to allow cooling of a much larger portion of the exterior with a Dry ice-acetone bath. P_2O_5 was also placed at the bottom of this trap. The product which remained in trap T_2 at -20° C was discarded. The N_2O_5 product was stored at -78° C. The preparer of N_2O_5 should be cautioned to store it either on a coldfinger or in a very thin film of low mechanical strength on the inner walls of a bulb, since N_2O_5 solid has a larger coefficient of thermal expansion than glass and fracture of glass vessels may occur on warming[135].

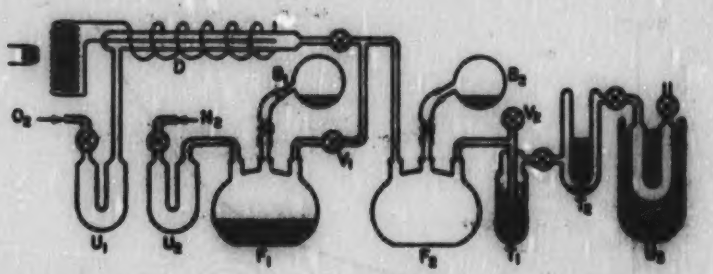

Fig. 30. Diagram of the apparatus used to prepare N_2O_5; see the text for the explanation of its use.

The Absorption Spectra of N_2O_5.

The gas phase infrared spectrum of the N_2O_5 product matched closely that given by Pierson, et al[137]. The visible-ultraviolet spectrum of N_2O_5 vapor was published twenty-seven years ago by Jones and Wulf[138]. Their sample of "N_2O_5" intentionally contained either O_3 or NO_2, presumably to suppress the decomposition of the N_2O_5 molecules. It is not clear how correction for these impurities was accomplished. We have redetermined the absorption spectrum of N_2O_5 and this is shown in Figure 31. During the time required for introduction and spectral measurements of the N_2O_5, some decomposition into NO_2 and O_2 occurred. The low resolution spectrum of N_2O_5 given in Figure 31 was calculated from the measured scans of $N_2O_5(g)$ at 27 Torr in a 10 cm cell by subtracting absorption due to the small NO_2 impurity product. The molar extinction coefficient ϵ versus wavelength is shown where $\epsilon = [\log_{10}(I_0/I)]/[N_2O_5]\ell$, $\ell.\text{mole}^{-1}\ \text{cm}^{-1}$.

Procedures in Kinetic Experiments with N_2O_5, SO_2, and O_3.

The reactions were carried out in a CaF_2-windowed cell which, prior to each experiment, was preconditioned with pure samples of SO_3 to insure the stability and the detectability of small quantities of the potential SO_3 product[132]. Low pressures ($p \geq 0.05$ Torr) of SO_3 could be measured easily through infrared analysis, so the appearance or the nonappearance of SO_3 absorption was a fairly sensitive test for the occurrence of reactions 1 or 2. Pressures of the individual components were measured in calibrated volumes on a vacuum line and mixed using an all glass, electromagnetically operated stirring pump. There was an interval of about 20-30 min between the start of the mixing and the start of the ir scan. The total cell pressure was measured again prior to removing the cell from the vacuum line and placing it into the spectrophotometer.

II-A—2. Discussion of the Results

Estimates of the Rate Constants for the NO_3-SO_2 and N_2O_5-SO_2 Reactions.

Several mixtures were prepared and the ir spectra followed as a function of time; in experiments at room temperature (~ 30° C) the initial reactant pressures (Torr) were as follows: 1) SO_2, 1.96; N_2O_5, 11.9; 2) SO_2, 8.5; N_2O_5, 2.5; O_3, 10.6; O_2, 450; 3) SO_2, 16.7; N_2O_5, 7.62; O_3, 35.6. No absorption by SO_3 and no

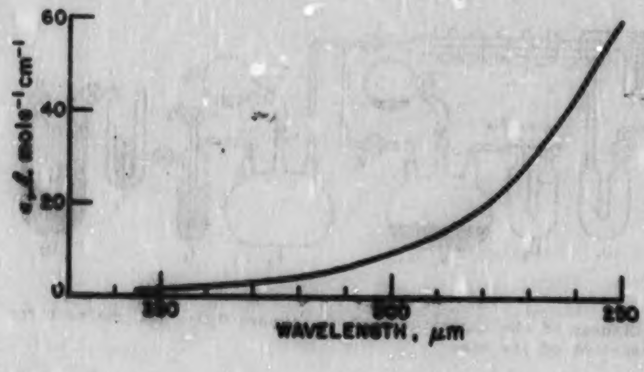

Fig. 31. The molar extinction coefficient ε for N_2O_5 vapor; $\varepsilon = [\log_{10}(I_0/I)]/[N_2O_5]\ell$, l. $mole^{-1}cm^{-1}$.

decrease in SO_2 absorption could be detected in run 1 after a period of several hours. Also no SO_3 was detected in run 2. After 20 min of contact of the reactants in run 3, the cell pressure had increased by 10.0 Torr (N_2O_5 catalyzed O_3 decomposition), and no SO_3 formation could be detected. Obviously the rates of the reactions 1 and 2 are very slow. We may use these data to estimate the upper limits for the k_1 and k_2 values.

From the detection limits of the methods employed we know that the maximum amount of SO_3 present in any of the experiments was less than 0.2 Torr (a generous upper limit). We may make the reasonable assumption that reactions 1 and 2 are second order elementary steps. Furthermore since SO_3 formation was undetectably low, it may be assumed that SO_2 does not significantly perturb the steady state concentration of NO_3, $[NO_3]_{ss}$. N_2O_5 is a catalyst for the O_3 decomposition in the N_2O_5-O_3 system, so that $[N_2O_5]$ is a constant as long as there is a significant concentration of O_3 in the system. The kinetic equations which may be derived readily from the reaction sequence 1-6 outlined for these conditions and which apply to the k_1 evaluation in the N_2O_5-O_3-SO_2 systems are the following:

$$d[SO_3]/dt = k_1[SO_2][NO_3] \qquad (7)$$

$$[SO_2]_t = [SO_2]_o - [SO_3]_t \qquad (8)$$

$$[NO_3]_{ss} = K_{ss}[N_2O_5]^{1/3}[O_3]^{1/3} \qquad (9)$$

$$[O_3]_t^{1/3} = [O_3]_o^{1/3} - \frac{2}{3}k'[N_2O_5]^{2/3}t \qquad (10)$$

where $K_{ss} = (k_3k_5/2k_4k_6)^{1/3}$ and $k' = (1/2)(k_3k_5/k_4)^{2/3}(2k_6)^{1/3}$. Relations 8-10 may be substituted in 7 to obtain the differential equation which relates $[SO_3]$ and the reactant concentrations as a function of time:

$$\int_0^{[SO_3]_t} \frac{d[SO_3]}{[SO_2]_o - [SO_3]} = \int_0^t (k_1K_{ss}[N_2O_5]^{1/3}[O_3]_o^{1/3} - \frac{2}{3}k'k_1K_{ss}[N_2O_5]t)dt \qquad (11)$$

Integration of function 11 gives the desired function from which k_1 can be estimated:

$$k_1 = \frac{\ln([SO_2]_o/([SO_2]_o - [SO_3]_t))}{K_{ss}([N_2O_5])^{1/3}[O_3]_o^{1/3}t - \frac{1}{3}k'[N_2O_5]t^2)} \qquad (12)$$

For the temperature of 30° at which these experiments were performed, $k' = 7.3 \times 10^{-3}$ $(\ell./\text{mole})^{1/3}$ sec^{-1} and $K_{ss} = 3 \times 10^{-4}$ $(\text{mole}/\ell.)^{1/3}$. For the conditions of experiment 3 outlined above the appropriate concentrations (mole/ℓ.) are: $[N_2O_5] = 4.03 \times 10^{-4}$; $[O_3]_o = 1.88 \times 10^{-3}$; $[O_3]_{t = 1200\ \text{sec}} = 8.26 \times 10^{-4}$; $[SO_2]_o = 8.84 \times 10^{-4}$; $[SO_3]_{t = 1200\ \text{sec}} \leq 1.06 \times 10^{-5}$. Substituting these values in relation 12 we derive a lower limit for k_1:

$$k_1 = 4.2\ \text{l. mole}^{-1}\text{sec}^{-1}$$

In a similar fashion we may estimate a maximum limit for k_2:

$$d[SO_3]/dt = k_2[SO_2][N_2O_5] \qquad (13)$$

Substituting relation 8 in 13 and integrating between the limits of t = 0 and t relation 14 is obtained:

$$k_2 = \frac{\ln([SO_2]_o/([SO_2]_o - [SO_3]_t))}{[N_2O_5]t} \qquad (14)$$

Using the values applicable to run 3 in relation 14 we find:

$$k_2 = 2.5 \times 10^{-2}\ \text{l. mole}^{-1}\text{sec}^{-1}$$

It should be noted that the pressure change observed in the experiment 3 is entirely consistent with that expected simply on the basis of the N_2O_5-catalyzed decomposition of O_3, reactions 3-6, and the known rate constants. The integrated rate law for $[O_3]$ as a function of time in this system is had by cubing both sides of relation 10:

$$[O_3]_t = ([O_3]_o^{1/3} - \frac{2}{3}k'[N_2O_5]^{2/3}t)^3 \qquad (15)$$

Substituting the values applicable for run 3 for t = 1200 sec, we expect $[O_3] = 7.67 \times 10^{-4}$ M or $P_{O_3} = 14.5$ Torr. Within the uncertainty in the value of the rate constant function k' and the reactant concentrations, this is in reasonable accord with that estimated for the observed pressure change of 10.0 Torr: $P_{O_3} = 35.6 - 2(10.0) = 15.6$ Torr at 1200 sec. It can be seen that this result provides further evidence of the unimportance of reactions 1 and 2 for these conditions. If 1 and/or 2 occurred to a measurable extent then the observed increase in pressure would be significantly less than that calculated from the N_2O_5 catalysis of the O_3 decomposition in run 3. This is the expected result as well if these reactions occurred measurably and a non-volatile solid adduct formed by reaction between SO_3 product and NO_2 (See the last section of the discussion.) or the nonvolatile product H_2SO_4 resulted from the interaction of the initial product SO_3 with impurity HNO_3 or H_2O. There was no evidence of the formation of a solid in these experiments although an amount less than that formed from 0.5 Torr of SO_3 would have been observed. Also there were none of the changes in the ir transmission of the CaF_2 windows of the cell which appear characteristically if H_2SO_4 formation occurs; changes from H_2SO_4 action corresponding to as little as 0.2 Torr of SO_3 would have been seen. Thus all of the evidence at hand points to the unimportance of the reactions 1 and 2 at 30° C.

If we employ the maximum values for the rate constants k_1 and k_2 derived here, it can be shown in computer simulation of the complex chemical changes which occur in the atmosphere that reactions 1 and 2 cannot make a significant contribution to the rate of SO_2 removal which occurs in sunlight-irradiated NO_x-hydrocarbon-SO_2 polluted atmospheres[93]. Other alternatives must be considered to rationalize the smog chamber data in which these reactions have been invoked previously[131].

The Predicted Influence of N_2O_5 Photodecomposition on the Levels of N_2O_5 and NO_3 in the Sunlight-Irradiated Polluted Urban Atmosphere.

The extinction data for the near ultraviolet absorption by gaseous N_2O_5, presented in Figure 31 and the estimated solar irradiance data of Leighton[139] for typical atmospheric conditions, may be combined to estimate the rate of sunlight absorption by N_2O_5. These data for the solar zenith angle of 40°, give $k_a \cong 4.3 \times 10^{-3}\ \text{min}^{-1}$, where the rate of sunlight absorption = $k_a[N_2O_5]$. This rate is the maximum possible rate of the photodecomposition of N_2O_5 in the sunlight-irradiated lower atmosphere ($z = 40°$) which presumably would occur by reactions 16 and/or 17:

$$N_2O_5 + h\nu \rightarrow NO_3 + NO_2 \qquad (16)$$

$$N_2O_5 + h\nu \rightarrow N_2O_4 + O \qquad (17)$$

Compare the magnitude of the photochemical rate with that for the first order thermal decomposition of N_2O_5 at 298° C in reaction 3; $d[N_2O_5]/dt = k_3[N_2O_5]$; $k_3 = 1.5 \times 10^{1}\ \text{min}^{-1}$. It is clear that the maximum rate of photodecomposition of N_2O_5 in the solar irradiated polluted atmosphere is only 1/3500 of the rate of its thermal dissociation. Thus in the detailed theoretical modeling of the rates of chemical changes in urban atmospheres,[127] the occurrence of reactions 16 and 17 may be neglected; they have a negligible effect on the levels of NO_3 and N_2O_5 which will develop in these atmospheres.

The Reaction Between Gaseous SO_3 and NO_2.

Preliminary results which we have obtained show that a very dry mixture of SO_3 and NO_2 gases reacts rapidly to form a relatively nonvolatile white solid. Thus when 7.8 Torr of SO_3 and 9.15 Torr of NO_2[140] were allowed to come together in the gas phase, a white solid coated the walls of the vessel immediately (in less than about 2 sec), and a residual pressure of 1.82 Torr was observed. If it is assumed that SO_3 reacts with NO_2 in a 1:1 ratio to form a nonvolatile adduct and that the $N_2O_4 \rightleftarrows 2NO_2$ equilibrium is maintained, then we calculate that the residual pressure in the experiment described would be 1.80 Torr, equal within the experimental error to that measured experimentally. The material so formed was removed by raising the temperature to 100° C and evacuating the vessel. No detectable solid remained after 1 hour. The stoichiometry, vapor pressure, and other properties of this interesting compound are now under detailed study in this laboratory. However the preliminary data reported here suggest that the white solid is a 1:1 adduct with a relatively low vapor pressure at 30° C.

We could find no reference in the literature to the gas phase SO_3-NO_2 reaction observed here. However the white solid may be the same as that observed by Urone, Schroeder, and Miller[141] and Paul, Arora, and Malhotra[142] in more complicated systems. Urone, et al., irradiated dilute gaseous mixtures of SO_2 and NO_2 in dry air. Chemical analysis of the white solid which formed under their reasonably anhydrous conditions had the simplest formula, NSO_5, the composition corresponding to a 1:1 adduct of SO_3 and NO_2 suggested for the compound formed in the present work. It is reasonable to expect that this compound could arise in the Urone system through the same SO_3-NO_2 reaction we observed in this work, following the generation of SO_3 in the sequence, $NO_2 + h\nu \rightarrow O + NO$; $O + SO_2 + M \rightarrow SO_3 + M$. Paul, et al.,[142] isolated a white solid of composition and molecular weight in nitrobenzene corresponding to $N_2O_4 \cdot 2SO_3$, from the reaction between N_2O_4 and SO_3 in liquid SO_2. Some suggestions concerning the chemical structure of the white solid can be had from that proposed for solids of this and similar compositions which have been reported. Thus nitrosyl pyrosulfate[143], $N_2S_2O_9$, and nitryl pyrosulfate[144], $N_2S_2O_{11}$, have been prepared by a number of workers using a variety of reactants. From the limited data at hand it is a reasonable hypothesis to suggest that the white solid formed here may be nitrosyl nitryl pyrosulfate, $(NO)S_2O_7(NO_2)$.

Since there is such a paucity of data concerning SO_3 reaction rates, including the rate of the often invoked homogeneous reaction, $SO_3 + H_2O \rightarrow H_2SO_4$, it is not possible to say at this time how important the SO_3-NO_2 reactions observed here might be relative to other SO_3 reactions in the polluted atmosphere. The significance of the SO_3-NO_2 adduct as a participant in urban aerosol formation is an intriguing possibility which cannot be evaluated without further quantitative work.

II-B. The Reaction of O_3 with Perfluorinated Polyolefins[158]

The use of Teflons in chemical reaction systems is widespread today. For example, the Teflon valves and stopcocks have become increasingly popular for use in the control of reactive gases. Environmental scientists commonly employ Teflon tubing in the transport of ambient air samples to the detection equipment for specific pollutants. The Teflons are often used as protective coatings for metals in chemical reactors and environmental reaction chambers. In fact large bags constructed of sheets of the perfluorinated polymers are sometimes employed directly as environmental chambers for simulated smog studies. The Teflon, fluorocarbon polymers offer the important advantage of unreactivity toward a great variety of reagents[145]. It was therefore somewhat surprising to find in the experiments described here that exposure of Teflon substrates to ozone led to gaseous, infrared absorbing species. The results reported in this paper serve to identify the resulting products and to provide some insight into the reaction mechanism involved in their formation. Workers who utilize Teflon fixtures in ozone containing atmospheres should be cognizant of the occurrence of this reaction and the possible contamination which will result from this practice.

II-B-1. Experimental

Apparatus

The Pyrex vacuum line was designed to permit thorough elimination of water to facilitate the study of gaseous mixtures containing SO_3, SO_2, O_3, and O_2[132]. Briefly, it was grease and mercury free and was enclosed in an oven to permit extensive baking (100° C), while pumping, of all components up to the $N_2(\ell)$ trap preceding the diffusion pump. Rotaflo Teflon stopcocks, whose design eliminates O-rings of any kind, were used throughout. Pressures during line outgassing were monitored with a CVC ionization gauge. Typically a minimum pressure of less than 5×10^{-8} Torr was attainable. Reactant and product pressures were measured with a spiral manometer. A flow discharge system was used to generate O_3 from O_2. Traps filled with silica gel were located immediately prior to and immediately after the discharge. The first one was used to dry incoming O_2; the second trap removed O_3 from the O_3-O_2 mixture[146]. A U-tube completed the synthesis loop; as a cold zone, its function was to prevent atmospheric water from diffusing back through the outgoing O_2 stream. During O_3 synthesis both traps and the final U-tube were kept at -78° C except while desorbing O_3.

Reactant and product concentrations were monitored with infrared spectroscopy. The ir cell (designed for crossbeam photolysis) was constructed from 48 mm Pyrex tubing. Infrared windows were of CaF_2 (49.5 mm diameter, 6 mm thickness); windows for photolysis light were Pyrex and were fused to the cell body. The path length of the ir beam through the cell was 9.5 cm. Teflon rings (gaskets), machined from a 2 in. diameter cylindrical bar of polytetrafluoroethylene (TFE), were placed between the Pyrex body and CaF_2 windows. The CaF_2 windows were tightly held to the cell by means of brass end rings connected together with threaded rods. Several coats of Glyptal were applied over ends of the Pyrex cell. Teflon gaskets, and edges of CaF_2 windows. The cell was baked for eight hours at 100° C between successive coats. This cell was fixed in the analysis beam of a Perkin-Elmer Model 21 Infrared Spectrophotometer equipped with an ordinate scale expander.

In many experiments the ir cell was also the reaction vessel. For experiments with powdered Teflon and FEP film, the reaction cell was a round-bottom cylinder (volume 33.3 cm^3) formed from 20 mm Pyrex tubing.

High resolution mass spectra were taken with an Associated Electric Industries, Ltd., MS-9 instrument.

Materials

Three different Teflon samples were used. The first and most extensively used was chosen unintentionally as an ozone reactant in that it was the gasket material in an ir cell used in following gas phase reactions in O_3-containing mixtures. Assuming a smooth, nonporous surface for the gasket, we estimate that its area was 1.7×10^{-3} m^2. The second sample was powdered Johns-Manville Chromosorb T, 40/60 mesh, screened from Teflon 6. As specified by the supplier, the surface area was 7.8 m^2/g; the quantity used gave an area of 30.3 m^2. Finally a sample of FEP film of 0.005 in thickness was employed as reactant; this material was supplied by the Plastics Department of the E. I. duPont de Nemours Co. Assuming the sheet to be perfectly smooth, we estimate the area of this sample to be 0.18 m^2. To facilitate packing into the reaction cell, this film was cut in strips 6 cm x 21.5 cm. All Teflon samples were thoroughly outgassed at pressures less than 5×10^{-8} Torr at 100° C before experimental use.

Oxygen was Burdette extra dry. Ozone was synthesized from it using the apparatus described previously. O_3 collected in the silica gel trap was separated from O_2 impurity by gradually warming the trap to room temperature while transferring O_3 to a storage trap held at -196° C (while pumping). A one-liter expansion bulb joined the storage trap, and care was taken to avoid buildup of O_3 which would give a pressure above 100 Torr on complete vaporization in order to lower the danger of explosion[147].

Procedures.

The observation of an infrared absorbing product from O_3 was made first in routine blank experiments carried out in connection with a study of O_3 photolysis in the presence and absence of O_2. Such blanks were usually performed as follows: after the photolysis of O_3 or O_3-O_2 mixtures (λ = 590 nm), reaction components were allowed to stand in the ir cell (which was also the photolysis cell) for an extended dark period. In other experiments also involving the Teflon gaskets, the cell was simply filled with O_3 at a particular pressure and allowed to stand in the dark. The ir absorbances were of course recorded at appropriate times.

When powdered Teflon or FEP film was used, O_3 was taken at a desired pressure in a known volume and then transferred to a coldfinger, cooled with $N_2(\ell)$, on the reaction bulb. Cell pressures obtained on vaporization were calculated from known volume relationships assuming ideal gas behavior. After a suitable reaction time, the cell contents were expanded successively into a series of cold zones (-196° C), first from the cell into a single trap, then from the cell and trap into a second trap, and finally from the cell and two traps into a multiple U-tube with three cold zones, each separated by a zone kept at room temperature. Total volume of this trap train was 160 cm^3. After a holding time of one minute, the noncondensable gas (presumably O_2) was slowly removed by pumping through these cold zones. Finally, the outgassed O_3 and condensable products were transferred to the ir cell, the total pressure was measured, and appropriate absorbances were recorded. From an absorbance-pressure curve for O_3, the pressure of O_3 was determined; subtraction from the total cell pressure gave an estimate of the partial pressure of the products.

Products of the reaction were separated from O_3 following condensation of the entire O_3-product mixture in a trap at -196° C. The liquid nitrogen bath was replaced with an $O_2(\ell)$ bath, and O_3 was pumped away leaving a white solid. In order to accumulate a sufficient amount of products for mass spectral analysis, several such separations were carried out and the products were collected and stored, at room temperature, in a two liter bulb.

Ozone concentrations were monitored using the characteristic weak absorption at 4.69 and 4.75 μ; CaF_2 window absorption precluded use of the more intense 9.5 μ band. Instrument response as a function of O_3 pressure was calibrated over the range 0.3 to 120 Torr. For small concentrations the ordinate scale expansion was used. Since neither the optical nor electronic system was adjusted on expansion, absorbances calculated from responses on individual scales were identical, within the experimental error. Absorbances were often small (0.001-0.030 was the usual range) so that multiple readings were made (x1, x5, x10, up to x20) and the results were averaged with each measurable signal receiving equal weight.

II-B—2. Results and Discussion

When O_3 was introduced into the infrared cell in the dark at room temperature its absorption at 4.69 and 4.75 μ decreased slowly with time as absorption at several new bands appeared; see Figure 32. Bands at 5.10 and 5.17 μ were used to monitor continuously the product concentrations in every run, while the other bands were checked occasionally to see alterations which had occurred. This absorption was not due to an impurity released from the cell components since no absorption was detected over the entire accessible wavelength range when the evacuated cell was closed off from the rest of the vacuum line for a

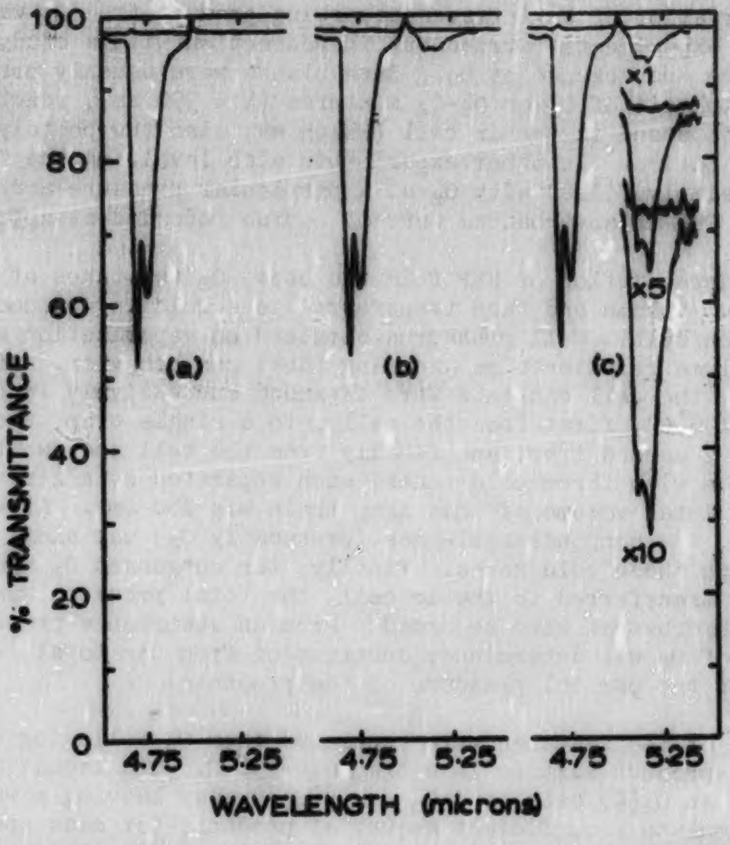

Fig. 32. Infrared spectral changes used to monitor the reaction of ozone and Teflon; (a) zero time, P_{O_3} = 96 Torr; (b) same mixture after 23,280 sec; (c) same mixture after 63,200 sec; Teflon sample employed in this case was the gaskets of the infrared cell; note the growth of the product bands at 5.10 and 5.17µ as the O_3-Teflon contact time lengthens.

time comparable to that used in runs. O_3 attack on the CaF_2 windows was further excluded as a source of the products; when O_3 was added to a cell containing CaF_2 powder an acceleration in the O_3 decomposition reaction resulted, but no absorption bands other than those due to O_3 were detected. A more complete spectrum of the product mixture that was retained after O_3 removal is presented in Figure 33. In addition to the bands at 5.10 and 5.17 µ, absorption appeared at 4.25, 8.0 and 9.75 µ. This mixture was the accumulated product from eight experiments in the ir cell. After each run the absorbances at 5.10 and 5.17 µ were determined. When account was taken of the small deviations of the pressure dependence of the absorbances from Beer's law, it was found that none of the product which absorbs at 5.10 and 5.17 µ was lost during a storage time of 27 days.

When O_3 was allowed to act on powdered Teflon or FEP film, ir spectra of products were obtained which were very similar to those given in Figure 33. These results show that a reaction between Teflon and O_3 gives rise to the gaseous products having the observed absorptions. Teflon gasket material used in the cell construction was the origin of the gaseous products in the first experiments

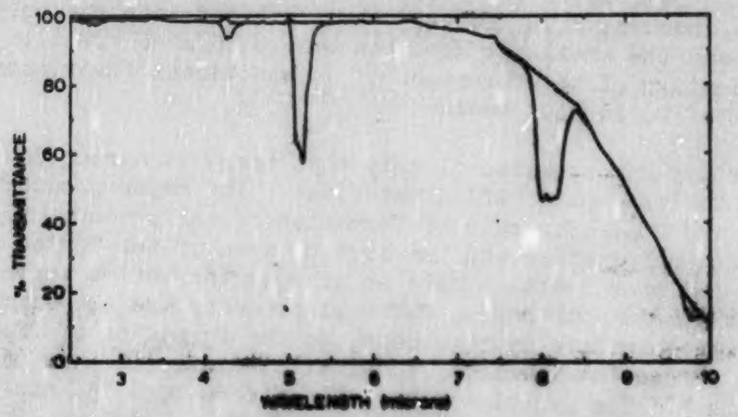

Fig.33. Infrared spectrum of products resulting from the reaction of ozone with Teflon; total pressure of the gaseous mixture, 7.75 Torr.

described above. The ratios of the total pressure (P_t) in Torr of products to the absorbance (A) at 5.10 and 5.17 μ were the same, within the experimental error, whether Teflon gaskets for the ir cell or powdered Teflon were used as the reactant: $P_t/A_{5.10\mu} = 32.6$ and $P_t/A_{5.17\mu} = 28.0$ for the Teflon gaskets, compared to $P_t/A_{5.10\mu} = 31.1$ and $P_t/A_{5.17\mu} = 28.6$ for powdered Teflon.

The ratio of absorbances $A_{4.25\mu}/A_{5.17\mu} = 0.115$ was obtained from the accumulated product mixture shown in Figure 33; this is typical of experiments employing Teflon gaskets with reaction times averaging about 27 hours. At longer times this ratio increased; thus after 60 hours, $A_{4.25\mu}/A_{5.17\mu}$ values of 0.271 and 0.269 were found.

The ratio $A_{8.0\mu}/A_{5.17\mu}$ was equal to 1.23 ± 0.05 for products derived from either the Teflon gaskets or powdered Teflon. For FEP film, the ratio was somewhat lower (1.05) and a very weak additional absorbance at about 8.85 ± was noted. The analytical data suggest strongly that the product distributions are nearly identical for the reaction of O_3 with Teflon gaskets or with powdered Teflon even though the Teflon samples had very different surface areas, reaction times, and reaction vessels in the two cases.

Mass spectral analysis of the sample whose ir spectrum is given in Figure 33, gave peaks at m/e = 104, 85, 66, 47, 46, 45, and 44. The high resolution masses of the 85 and 66 peaks were found to be: 84.9727 and 65.9915, respectively; these data show conclusively the peaks to be SiF_3^+ (84.9721) and CF_2O^+ (65.9918), respectively. Infrared peaks in the 2.60-2.80, 5.10-5.17, and 7.95-8.75 μ regions are attributed to CF_2O;[148,149] absorption at 4.20-4.35 μ is due to CO_2[150], and that at 9.70-9.80 μ is associated with SiF_4[151]. The high resolution mass spectra confirm the SiF_4, CF_2O, and CO_2 assignments. Both the infrared and mass spectral data indicate strongly that the product mixture is a three component system consisting of CF_2O, 54.6%; SiF_4, 5.7%; and CO_2, 39.7%. The extinction coefficient (base 10) for CF_2O at 5.10μ may be estimated from our work to be 0.0049 Torr^{-1} cm^{-1}; this is somewhat different than that reported previously, 0.013 Torr^{-1}cm^{-1} by Saunders and Heicklen[152].

The amounts of CF_2O and CO_2 formed in the O_3-Teflon reactions studied for several different experimental conditions are summarized in Tables XXX and XXXI in which the Teflon sample was the cell gasket material, Teflon powder, or FEP film. Note that in the case of the products of the FEP film, there is a somewhat lower ratio of absorbances, $A_{8.0\mu}/A_{5.17\mu}$, than obtained with the polytetrafluorethylene samples, and the small new absorbance at 8.85 μ observed in these experiments, may be indicative of the formation of an additional fluorinated carbonyl product, perhaps CF_3CFO, in this case.

The present study demonstrates clearly that there is a reaction between gaseous ozone and various solid Teflon materials. The major products of this reaction are CF_2O and CO_2. The rate of formation of the products ($CF_2O + CO_2$) is related to the ozone pressure and the surface area of the Teflon sample. See Figure 34. Ozone and some reactive site on or near the Teflon surface seem to be the most probably reactants here. Carbonyl products are the normal result of the ozonolysis of the olefinic hydrocarbons, so the formation of CF_2O very likely results from such a reaction involving terminal olefinic sites in the Teflon, reactions 1, 2, and 3. The symbol ~ used in reactions 1, 2, 3, and elsewhere in this work indicates attachment to the Teflon surface.

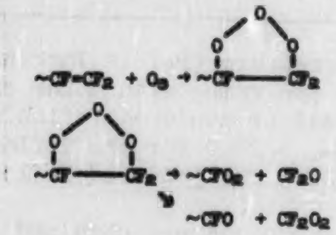

(1)

(2)

(3)

The source of the CO_2 product is less evident. It has been pointed out that CO_2 is sometimes formed from CF_2O by a slow, overall reaction 4 involving a glass wall surface[153].

$$2CF_2O + SiO_2(\text{glass wall}) \rightarrow 2CO_2 + SiF_4 \qquad (4)$$

However reaction 4 does not seem to be important here for several reasons. (1) The stoichiometry expected for reaction 4, $[CO_2]/[SiF_4]$ ratio of 2, is not observed here; at the shortest reaction times $[CO_2]/[SiF_4] \cong 7$. (2) Since no detectable loss of CF_2O was observed over a period of 27 days, it is clear that reaction 4 did not occur to any appreciable extent in the glass storage bulb which was used. The exceptional stability of CF_2O observed in this case is undoubtedly the result of thorough elimination of water. (3) The fraction of CF_2O in the gaseous products was the same whether the reaction was carried out using either a small Teflon surface area (gaskets only) and a relatively large Pyrex surface area and necessarily long reaction times, or a large Teflon surface area and a relatively small Pyrex surface area with comparatively short reaction time. It is unrealistic to assume that the glass walls of the two vessels would provide equal fractions of destruction of CF_2O and formation of CO_2 through reaction 4 under these very different conditions. It is more likely that CO_2 is formed by some other reactions in our present experiments with the very dry cells. The appearance of SiF_4 does imply, however, that a glass wall reaction of some kind is involved. It seems reasonable to associate SiF_4 and CO_2 formation with some other fragment than the CF_2O which results from the O_3 attack

TABLE XXX

Rate Data for the Reaction of Gaseous Ozone with Teflon Gasket Material at Room Temperature; Rates Given in the Last Column Have Been Normalized to 1.00 x 10^{20} Active Sites for Each Run.

Run No.	Reactant Pressure, Torr		Run Time, hr	O_3 loss, molec x 10^{-18}	$CF_2O + CO_2$ formed, molec. x 10^{-18}	$-R_{O_3}/(R_{CF_2O} + R_{CO_2})$	Reactive Sites at Start Run, x 10^{-18}	$R_{CF_2O} + R_{CO_2}$, molec /sec, x 10^{-13}
	O_3	O_2						
1	5.31	202	48.4	2.03	1.78	1.14	11.6	0.89
2	7.46	60.8	12.25	0.53	0.80	0.66	11.6	1.56
3	7.60	201	15.5	0.45	0.92	0.49	11.6	1.42
4	6.82	0	16.8	0.60	0.85	0.71	11.6	1.22
5	8.11	150	15.0	0.68	0.89	0.76	11.6	1.42
6	8.26	250	46.7	4.35	2.29	1.90	11.5	1.18
7	2.66	150	36.4	1.13	0.55	2.05	11.5	0.37
8	2.50	0	15.0	(0.08)	0.32	(0.25)	11.5	0.51
9	2.40	100	16.7	(0.08)	0.34	(0.23)	11.5	0.54
10	2.54	125	45.5	1.13	0.73	1.54	11.5	0.43
11	10.31	0	14.3	2.63	0.99	2.06	11.5	1.66
12	9.48	50	14.1	0.98	0.95	1.03	11.4	1.64
13	10.12	149	19.1	3.75	1.42	2.64	11.4	1.80
14	11.17	249	14.7	1.81	1.11	1.63	11.4	2.00
15	11.07	399	22.5	2.70	1.69	1.60	11.4	1.83
16	45.6	0	25.5	28.9	5.68	5.09	11.2	5.53
			40.0	57.8	7.99	7.23		
17	19.75	0	21.0	(0.1)	2.38	(0.03)	10.3	3.05
18	80.6	0	6.7	27.3	1.82	15.0	10.1	7.45
			26.8	66.0	6.38	10.3		
			43.3	77.3	8.33	9.3		
19	127.5	0	5.9	126.9	1.81	70.1	8.93	10.5
			15.8	177.0	4.75	37.3		
20	94.6	0	7.0	25.6	1.36	18.8	8.46	6.27
			16.3	42.6	3.13	13.6		
21	111.1	0	14.5	58.4	4.26	13.7	8.14	10.2
22	115.3	0	22.0	52.6	5.50	9.6	7.72	9.03
			51.5	101.6	8.45	12.0		
			62.0	116.8	8.65	13.5		
23	93.0	0	14.5	20.6	2.05	10.0	6.20	6.43

TABLE XXXI

Rate Data for the Reaction of Gaseous Ozone with Different Samples of Perfluorinated Polyolefins at Room Temperature

Run No.	Pressure O_3, Torr	Run Time, sec.	O_3 Loss, molec. x 10^{-18}	$CF_2O + CO_2$ formed, molec. x 10^{-18}	$\frac{-R_{O_3}}{R_{CF_2O} + R_{CO_2}}$	$R_{CF_2O} + R_{CO_2}$, molec./sec., 10^{-14}
a) Powdered Teflon Reactant:						
24	53.2	1080	7.13	2.95	2.42	27.3
25	14.7	2000	2.11	1.71	1.23	8.56
26	69.5	1000	7.68	2.81	2.73	28.1
27	99.2	1000	6.33	4.21	1.50	42.1
28	35.0	1800	3.07	3.16	0.97	17.5
29	7.74	2000	(0.34)	1.23	(0.28)	6.15
b) FEP Film Reactant:						
30	96.2	6300	(50.5)[a]	7.78	(6.49)	12.3
31	45.2	10140	9.78	8.12	1.20	8.0
32	10.0	11700	(0.38)	2.52	(0.15)	2.16
33	15.1	7080	2.02	2.50	0.81	3.54

[a] The high O_3 consumption in Run 30 probably resulted from sample contamination during handling and cutting of the film into strips. After this first exposure, O_3 loss was much decreased; see Run 31.

on Teflon. In line with the accepted mechanism of ozonolysis in solution[154], the initial ozonide product of reaction 1 will decompose by the two routes, 2 and 3, which generate the so-called zwitterionic species, $\sim CFO_2$ and CF_2O_2, in addition to a carbonyl compound. In theory there are a number of possible exothermic reactions in which the zwitterionic species may decay. For example they could decompose ozone by reactions 5 and 6.

$$CF_2O_2 + O_3 \rightarrow CF_2O + 2O_2 \qquad (5)$$

$$\sim CFO_2 + O_3 \rightarrow \sim CFO + 2O_2 \qquad (6)$$

However, other information to be considered later suggests that these reactions may not be important here. The alternative reactions with O_2 to form ozone are energetically possible in our experiments with added O_2.

$$CF_2O_2 + O_2 \rightarrow CF_2O + O_3 \qquad (7)$$

$$\sim CFO_2 + O_2 \rightarrow \sim CFO + O_3 \qquad (8)$$

However, reactions 7 and 8 are probably unimportant here since the rates of CF_2O formation and ozone loss are insensitive to the concentration of O_2 present in the reaction mixture; compare runs 4 and 5, 8 and 9, and 11 and 12 of Table XXX.

Some evidence concerning possible CO_2-forming reactions and the fate of the zwitterions can be had by a consideration of the reaction stoichiometry. Consider the data of the Tables XXX and XXXI. Teflon is the only source of carbon in the gaseous products. For ozone pressures varying from 2.4 to 11.2 Torr (runs 1-15, Table XXX) in experiments with Teflon gaskets, the average ratio of

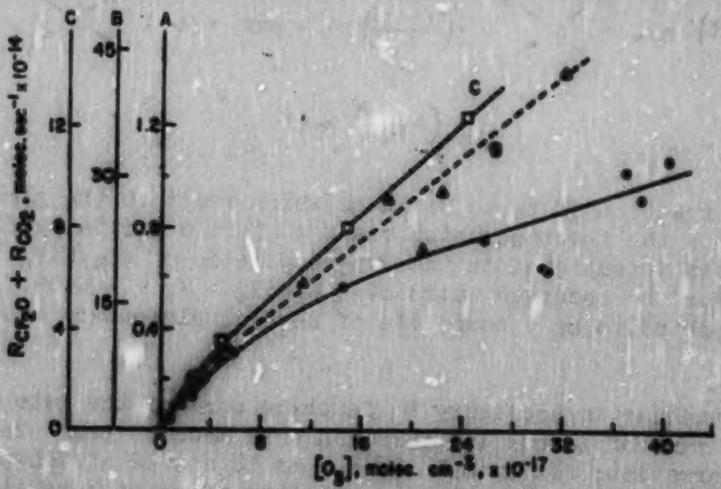

Fig. 24. Rate of Formation of CF_2O plus CO_2 products of the O_3-Teflon reaction versus the O_3 concentration: curve A, Teflon gaskets of the ir cell was the reactant in this case; curve B, Teflon powder reactant; curve C, FEP film reactant.

molecules of ozone lost to those of CO_2 plus CF_2O formed = 1.45 ± 0.70. For experiments at higher ozone pressures (runs 16-23, Table XXX) this ratio is much higher, in the range 5-70, and parallel paths for ozone decomposition and reaction to form gaseous products are obviously important here. In these experiments with the Teflon gaskets the ozone decomposition is most evident because of the relative slowness of the reaction which is a direct consequence of the very small Teflon surface area. For the experiments with powdered Teflon the average ratio of the molecules of ozone lost to those of CF_2O plus CO_2 formed = 1.77 ± 0.77. The average ratio from the two most reliable runs involving the O_3-FEP film is 1.0 ± 0.2. The observed variation between determinations of this ratio is believed to be a consequence of the inherent inaccuracy in measurement of the very small absorbance changes in the reactant ozone during the reaction. Although the scatter in the estimates of the ratio is large, there appears to be a somewhat larger number of ozone molecules destroyed than molecules of CF_2O and CO_2 produced. Of course the difference between the observed ratio and unity may simply be a measure of a parallel heterogeneous O_3 decomposition reaction. The observed stoichiometric ratios are not inconsistent with the consumption of a fraction of the surface and gaseous zwitterions by the reactions with ozone, reaction 5 and 6. If these occurred exclusively, then two ozone molecules would be decomposed for each CF_2O molecule formed as a product. However, other evidence which will be discussed subsequently favors the relative unimportance of reactions 5 and 6.

Since the mechanism forming the products CO_2 and SiF_4 must couple with the CF_2O formation in order to maintain the same product distribution observed experimentally for a variety of reaction conditions, it seems logical to utilize the gaseous zwitterion as a reactant for these products. One such possible overall reaction is 9:

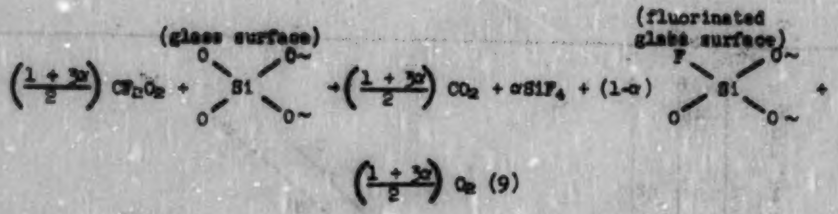

α represents the fraction of those Si atoms which react at the glass surface and form SiF_4; $1 - \alpha$ is the fraction which react to form a partially fluorinated glass surface. With this interpretation the expected ratio of CO_2/SiF_4 in the products $= (1 + 3\alpha)/2\alpha$. For the observed ratio of $CO_2/SiF_4 = 7$, $\alpha = 0.09$. Obviously reaction 9 is expected to be a composite of several elementary steps which remain undefined.

One other reaction is necessary to describe some of the rate data. In two cases successive runs of increasing duration were made to test the time dependence of the product formation; for example, see runs 18 and 22 of Table XXX. In these cases $[CF_2O]$ in the mixture approached a constant value at long times. We estimate by the technique described later that the number of reactive sites present in the Teflon was depleted by only about 16% during run 18 and about 20% in runn 22, so that the constant $[CF_2O]$ reached cannot be the result of olefinic site removal at these times. It appears more appropriate to assume that some reactive surface species, possibly the zwitterions, consumes CF_2O to form a secondary ozonide, reaction 10, in a process completely analogous to that observed in solution ozonolysis[154]. It is impossible to say definitely at this point whether or not the surface zwitterion is sufficiently stable (half-life of days at room temperature) to function in the fashion we require here. However, our results from another study[132] tend to support this possibility. Thus treatment of the infrared-photolysis cell with high ozone pressures gives rise to a reactive species (as evidenced by its complex but rapid reaction with added SO_2) which can not be pumped away at 25° C. It is removed by washing the cell with distilled water and subsequently outgassing at 100° C. It is not unreasonable to attribute this behavior to a surface zwitterion or surface ozonide.

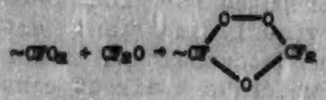

(10)

It is instructive to estimate the rate constant for the ozone reaction with the $CF_2{=}CF\sim$ reactive site in the Teflon from the present data. Note that the number of molecules of CF_2O and CO_2 product formed per unit time in Run 23 of Table XXX is 26.6% less than that of Run 20 although the initial pressure of O_3 is nearly the same. It is a reasonable hypothesis that this lowering in rate comes from the partial elimination of olefinic sites, and that a direct proportionality exists between the rate the number of sites. From the amount of products formed we can estimate that about 2.3×10^{19} sites were consumed in Runs 20, 21, and 22. Thus about 8.5×10^{19} sites would have been available at the start of Run 20. Similar less precise estimates can be made from other combinations of runs assuming the linear dependence of rate on the $[O_3]$. Thus, we estimate 5.5×10^{19} (Runs 18 and 20), 2.4×10^{19} (Runs 21 and 22), 16×10^{18} (Runs 19 and 22) active sites. It appears that the estimate of 8.5×10^{19} sites at the start of Run 20 is accurate to at least an order of magnitude. This number and observed initial rates have been used to estimate the number of reactive sites at the start of each experiment shown in Table XXX. The rates shown in the last column of this Table have been normalized to 1.0 x 10^{20} sites. These are plotted as a function of $[O_3]$ in Figure 34, curve A. The rate of the O_3-Teflon gasket reaction is seen to be roughly proportional to the $[O_3]$. Of course this is also the observed result from the much higher surface area samples of Teflon powder (curve B) and FEP film (curve C) where depletion of surface series during the series of runs was negligible. Departure of the Teflon gasket data from linearity at high $[O_3]$ may be an artifact which results in part from errors inherent in the estimation of the number of olefinic sites with a subsequent inaccurate normalization procedure. It is also probable that the reaction 10 may have occurred to a significant extent in the runs at the highest $[O_3]$ and caused some of the nonlinear behavior seen at high $[O_3]$'s. Deviations from the assumed linear Beer's law dependence of the absorptivity of CF_2O could also contribute to this curvature. In any case the initial rate data can be used to derive a reasonable estimate for the rate constant k_1; we find $k_1 = 5 \times 10^{-25}$ $cm^3 sec^{-1} site^{-1}$. The specific reactivity of the Teflon with ozone is considerably lower than that observed for the gaseous perfluoro-olefins studied by Heicklen[155]; he reported rate constants for O_3 plus C_2F_4, C_3F_6, and 2-C_4F_8 molecules as equal to: 1.3 x 10^{-19}, 2.2 x 10^{-20}, and 1.8 x 10^{-21} cc/mole-sec, respectively. The 72-fold decrease in rate constant for the reaction of ozone with olefin in the sequence C_2F_4 to 2-C_4F_8 observed by Heicklen, is opposite to the trend in reactivity observed for the hydrocarbon analogues. Thus Wei and Cvetanovic[156] found that the rate constant for the ozone reaction with C_2H_4 is over 10-times slower than that for cis-2-C_4H_8 and over 13-times slower than that for the trans-2-C_4H_8. However, the mechanism of O_3-perfluoro-olefin gas phase reaction is very complex and apparently in the case of 2-C_4F_8 involves a reaction of ozonide with a second molecule of the olefin. Of course this feature of the reaction is physically impossible for the relatively rigid Teflon structures studied here, and this difference may in part account for the apparent slowness of the reaction 1 in our system.

If we use our estimate of k_1 derived here together with the observed rates of the reaction for the different Teflon samples, we estimate that the number of olefinic groups available on the powdered Teflon and FEP samples are 2.2 x 10^{21} and 9 x 10^{20}, respectively. By comparison with other samples, the number of reactive sites per unit of apparent physical surface area is high for Teflon gaskets. Possible reasons for the apparent wide differences in the population of active surface sites in different samples include the following: (1) The actual surface area available for the gaskets is much greater than that calculated from its physical size due to roughness caused by machining; (2) The internal structure, which may contain more unsaturation than the surface, is uncovered by machining; (3) Machining may lead to unsaturation in the polymer.

The surface area for Teflon powder, determined by the supplier, presumably by the BET method, would appear most appropriate in determining the area occupied by each reactive surface site. The result is 1.4 x 10^{-16} cm^2/site. This would seem to indicate complete surface coverage by olefinic groups. Alternative explanations are probably more realistic: (1) Surface area determinations using the BET method for Teflons are possibly unreliable; this might be the case if, for example, N_2 adsorption occurs only at olefinic sites; (2) O_3 attack may be at saturated carbon rather than, or in addition to, that at olefinic sites; (3) Perhaps new olefinic sites are generated in large part in the ozonolysis process, so that the present method of estimating the number of sites is not appropriate; (4) O_3 may diffuse into the Teflon matrix and react with terminal olefinic groups situated somewhat below the surface.

Information on the magnitude of the rate constant for the reaction 10 can be gained from the data of Table XXX and the related data from these runs for the P_{CF_2O} attained as an asymptotic value at long times. If one equates the rate of CF_2O loss to that for its formation for this condition relation 11 should hold:

$$k_{10} = k_1 \left[\frac{R_{CF_2O}}{R_{CF_2O} + R_{CO_2}} \; \frac{[O_3]\, S_o}{[CF_2O]\, S_z} \right] \qquad (11)$$

Here S_o and S_z are the number of olefinic surface sites and number of zwitterionic surface sites, respectively, in the sample. All quantities required in the calculation have been estimated with the exception of S_z. A maximum for S_z can be derived assuming that the surface zwitterion is destroyed only in reaction 10 with CF_2O, and that the number of surface zwitterions generated is equal to the number of CF_2O molecules formed. From these assumptions and using the data for Runs 18 and 22, we calculate the following approximate upper limits for k_{10}: 2.3×10^{-22} and 2.2×10^{-22}, respectively.

The present study has provided some new insight into the reactions present in the ozone-Teflon system; although many fundamental questions remain open, the experimental approaches which can be used to press the study further are evident. It is clear that Teflon is not inert to ozone. Those scientists who study the photolysis or the thermal reactions of ozone at moderate to high pressures must be aware of the previously unexpected contamination which will result in the ozone mixture from the use of Teflon stopcocks, gaskets, etc., in these systems. Particular attention should be given to the complications possibly resulting therefrom in smog chamber studies employing Teflon bags or FEP coated chamber walls. Although reaction with O_3 is relatively slow for the low $[O_3]$'s commonly encountered in environmental systems, the carbonyl fluoride product is of major concern since it should be photochemically active to form highly reactive F-atoms and FCO radicals, and it is known to hydrolyze rapidly in the presence of water to form HF and CO_2 so the result would not appear benign[157]. On a more positive note, similar studies of ozone with related polymers have great potential for use in the determination of the properties of intermediates and products of ozonolysis.

PART III.

THE COMPUTER SIMULATION OF THE RATES OF CHEMICAL REACTIONS IN SUNLIGHT-IRRADIATED POLLUTED ATMOSPHERES.

A significant part of the study supported under this grant involved the computer simulation of the chemical changes expected to occur in various polluted atmospheres. Some new and seemingly significant findings were made which bear on the further development of control strategy. These studies are described in this section.

III-A. The Relative Importance of Various Active Intermediates in the Attack on Alkenes in the Polluted Atmosphere[159].

We have recently developed a detailed kinetic model for the simulation of smog chamber results from several laboratories[160] and applied it, (i) to determine the predicted effect of carbon monoxide on the ozone levels in photochemical smog systems[161] and (ii) to determine the relative importance of the various intermediate species in the olefin removal reactions in simulated photochemical smog chamber studies[162]. The success of the model in matching the product-time curves from the smog chamber experiments gives confidence in the general correctness of the kinetic mechanism and prompts us to apply this model to the computer simulation of the chemistry of a simple analogue to the sunlight-irradiated auto-exhaust polluted atmosphere.

III-A—1. Discussion

There is considerable sophistication of kinetic detail which we can employ with the mechanism in attempting to simulate the chemical events which occur in an auto-exhaust polluted atmosphere. Our present knowledge of photochemical smog systems does not justify any such elaborate attempt. Instead we have chosen a relatively simple mixture of the important classes of reactants to attempt to picture the chemistry of these systems. The mixture consists of 0.075 ppm NO, 0.025 ppm NO_2; 1.5 ppm CH_4, 10 ppm CO, 0.10 ppm trans-2-butene (typical level of total olefin), 0.10 ppm CH_2O and 0.06 ppm CH_3CHO (representative of all the higher aldehydes) in air with a relative humidity of 50% (25° C). These concentrations are typical for the major classes of primary and secondary pollutants in photochemical smog.

Figures 35A, B,36 show the skeleton reaction scheme for the photooxidation of trans-2-butene in a mixture with NO-NO_2-air. Full mechanistic details with the selected rate constants are given in reference[127]. The theoretical time-dependences of the products expected when the above synthetic mixture is irradiated in sunlight ($z = 40^\circ$) were calculated by computer simulation. These data are shown in Figs. 37a and 37b which have been calculated using two different assumptions concerning the rates of the reactions 1, 2, and 3.

$$N_2O_5 + H_2O \rightarrow 2HONO_2 \qquad (1)$$

$$NO + NO_2 + H_2O \rightarrow 2HONO \qquad (2)$$

$$2HONO \rightarrow NO + NO_2 + H_2O \qquad (3)$$

There is at present an uncertainty as to the degree of involvement of these reactions in the real atmosphere. Certainly the magnitude of the homogeneous component of these rates remains unclear today. Thus we have carried out the simulations using the two possible extreme views concerning the rates of reactions 1, 2, and 3. In both of the simulations shown in Fig. 37a and 37b we have assumed that there is no prior establishment of the equilibrium level of HONO before the sunlight-irradiation begins. In calculating the data of Fig. 37a we have taken "high" values for k_2 and k_3 estimated by Wayne and Yost[163] using conditions of high surface-to-volume ratio, and the value $k_1 = 1.0 \times 10^{-4}$ ppm^{-1} min^{-1}, which we derived from "best fits" in the simulation of several smog chamber studies; this value is about 25 times lower than the only published estimate[163] of k_1. On the other hand, in calculating the product concentrations in Fig. 37b, we have assumed that reactions 1, 2, and 3 do not occur at all; that is, k_1, k_2 and k_3 are all assumed to be zero.

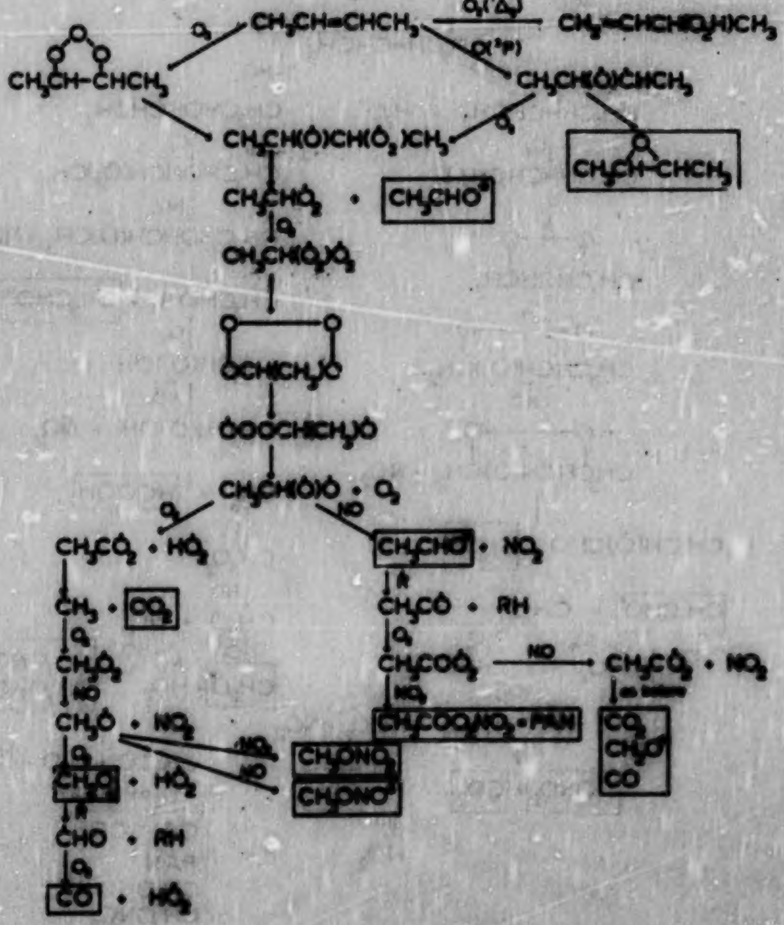
CH3CH=CHCH3
O3
O2(1Δg)
CH2=CHCH(O2H)CH3
O(3P)
CH3CH-CHCH3
CH3CH(O)CHCH3
CH3CH(O)CH(O2)CH3
CH3CHO2 + CH3CHO*
CH3CH(O2)O2
OCH(CH3)O
OOOCH(CH3)O
CH3CH(O)O + O2
NO
CH3CO2 + HO2
CH3CHO* + NO2
CH3 + CO2
R
CH3CO + RH
CH3O2
CH3CO3
CH3CO2 + NO2
CH3O + NO2
NO2
CH3COO2NO2 = PAN
CO2
CH3O*
CO
CH3ONO2
CH3ONO*
CH2O + HO2
CHO + RH
CO + HO2

Fig.[illegible]. The major reaction paths for degradation of trans-2-butene in a sunlight-irradiated, NO_x-polluted atmosphere; Fig.[illegible]: O_3, $O(^3P)$, and $O_2(^1\Delta_g)$ reactions with trans-2-butene. Products marked with an asterisk undergo significant photodecomposition in sunlight.

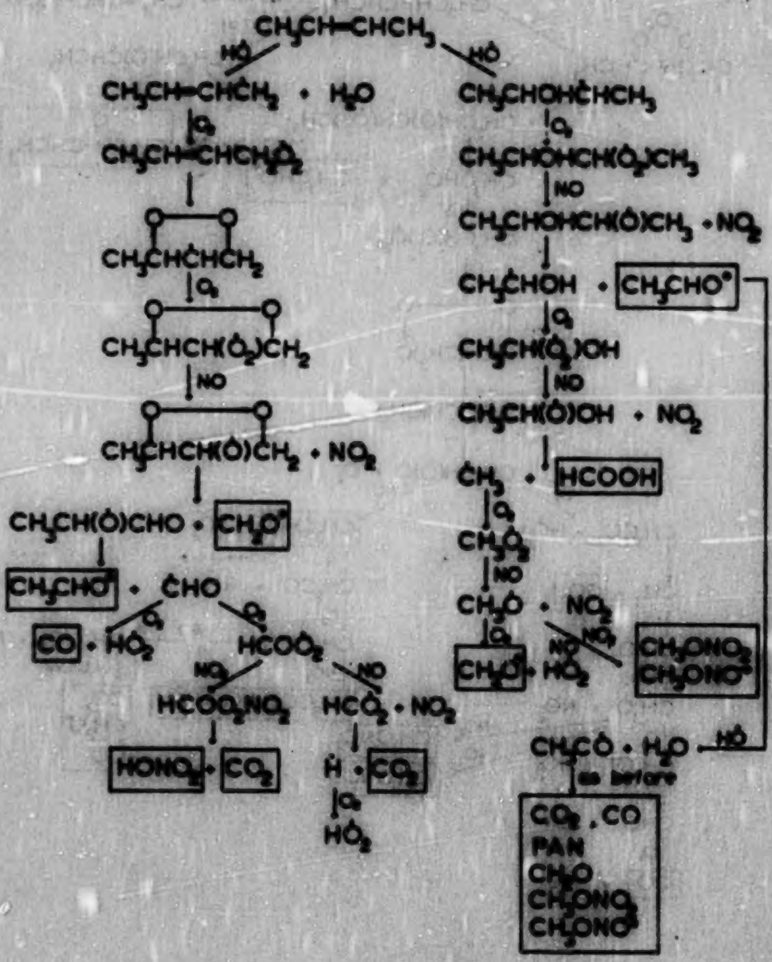
CH3CH=CHCH3
HO
HO
CH3CH=CHCH2 + H2O
CH3CHOHCHCH3
O2
CH3CH=CHCH2O2
CH3CHOHCH(O2)CH3
NO
CH3CHOHCH(O)CH3 + NO2
CH3CHCHCH2
CH3CHOH + CH3CHO*
O2
CH3CHCH(O2)CH2
CH3CH(O2)OH
NO
NO
CH3CH(O)OH + NO2
CH3CHCH(O)CH2 + NO2
CH3 + HCOOH
O2
CH3CH(O)CHO + CH2O*
CH3O2
NO
CH3CHO* + CHO
CH3O + NO2
O2
O2
CO + HO2
HCOO2
O2
NO
NO2
CH2O* + HO2
CH3ONO2
CH3ONO*
NO2
NO
HCOO2NO2
HCO2 + NO2
CH3CO + H2O
HO
as before
HONO2 + CO2
H + CO2
O2
HO2
CO2, CO
PAN
CH2O
CH3ONO2
CH3ONO*

Fig. [illegible] b: The HO radical reaction paths with trans-2-butene.

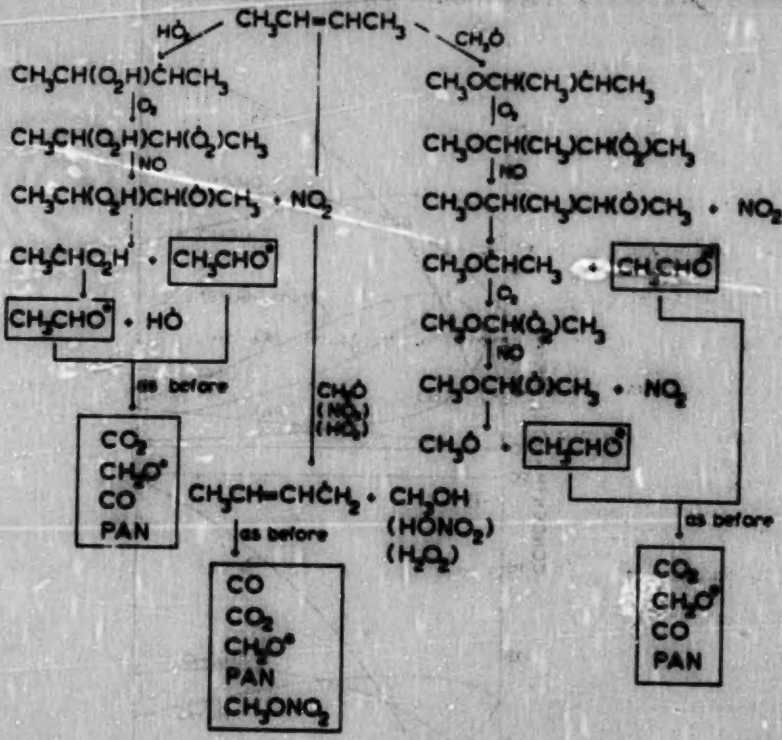
HO₂
CH₃CH=CHCH₃
CH₃O
CH₃CH(O₂H)CHCH₃
O₂
CH₃CH(O₂H)CH(O₂)CH₃
NO
CH₃CH(O₂H)CH(O)CH₃ + NO₂
CH₃CHO₂H + CH₃CHO*
CH₃CHO* + HO
as before
CO₂
CH₂O*
CO
PAN
CH₃O
(NO₂)
(HO₂)
CH₃CH=CHCH₂ + CH₃OH
(HONO₂)
(H₂O₂)
as before
CO
CO₂
CH₂O*
PAN
CH₃ONO₂
CH₃OCH(CH₃)CHCH₃
O₂
CH₃OCH(CH₃)CH(O₂)CH₃
NO
CH₃OCH(CH₃)CH(O)CH₃ + NO₂
CH₃OCHCH₃ + CH₃CHO*
O₂
CH₃OCH(O₂)CH₃
NO
CH₃OCH(O)CH₃ + NO₂
CH₃O + CH₃CHO*
as before
CO₂
CH₂O*
CO
PAN

Fig. 36. The HO_2, CH_3O, and NO_3 reaction paths with trans-2-butene.

In comparison of Figs 37A and 37B, one sees the surprising result that the choice of rate constants for reactions 1, 2, and 3 has very little influence on the results. Only minor differences are noted. In Fig. 37B a somewhat higher concentration of NO_2 and O_3 is seen at longer times. This is a direct consequence of our complete neglect of the rate of removal of N_2O_5 by water in this calculation. It is evident that the rapid occurrence of reactions 2 and 3 is not a critical feature in photooxidation of hydrocarbons at the levels encountered in real auto-exhaust polluted atmospheres.

We may use the simulations summarized in Figs. 37A and 37B to consider again the important question of what relative significance the various intermediates[162] may have in the attack on the hydrocarbons and aldehydes present in this simulated auto-exhaust polluted atmosphere. The reactant concentrations here are much more in line with those found in real atmospheres, and the results are of direct interest to the atmospheric scientist. These results are summarized in Table XXXII, and the various butene consuming reactions are shown in Fig. 35,36. The data predict the great importance of the HO radical species in the reaction with the olefin. Only at relatively long times do the O_3 and HO_2 species contribute rates which are comparable to those for HO. The attack of $O(^3P)$ atoms is only significant at short times, but even here its rate is much less than that for HO. The forced conversion of CH_3O to CH_2O occurs for these conditions of high $[O_2]/[\text{olefin}]$ ratio, and this lowers the contribution of the CH_3O-attack from the relative important position observed in our previous studies[162] for the

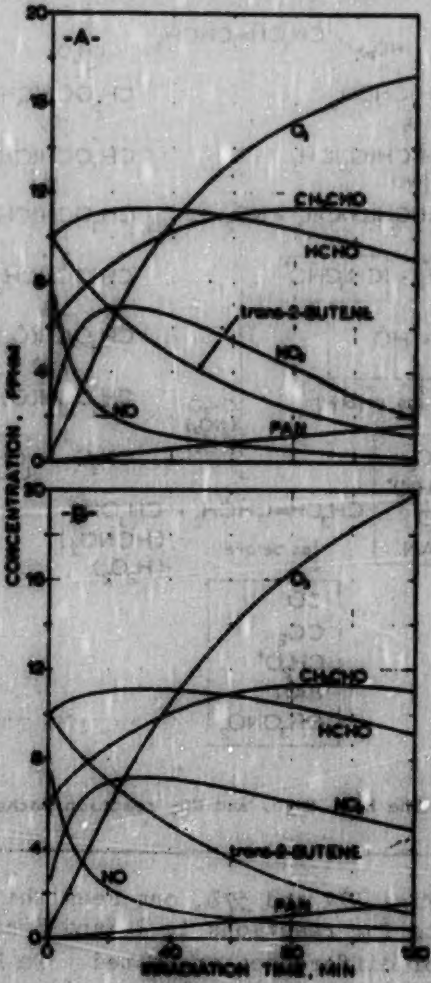

Fig.37A. Theoretical rates of product formation in a sunlight-irradiated ($z = 40°$), simulated auto-exhaust polluted atmosphere; initial concentrations (ppm): $[NO]° = 0.075$, $[NO_2]° = 0.025$, $[CO]° = 10.0$, $[CH_4]° = 1.5$, $[trans\text{-}2\text{-}C_4H_8]° = 0.10$, $[CH_2O]° = 0.10$, $[CH_3CHO]° = 0.06$, relative humidity, 50% (25°C); in these calculations we have chosen the rate constants of reactions 1, 2, and 3 to be finite values indicated in the literature.

Fig.37B. Analogous data to Fig.37A but in this case the rate constants of reactions 1, 2, and 3 have been assumed to be zero.

TABLE XXXII.

The Rate of Attack (ppm min^{-1} x 10^{4}) of Various Reactive Intermediate Species on Trans-2-Butene in a Sunlight-Irradiated (z = 40°), Simulated Auto-Exhaust Polluted Atmosphere; Initial Concentrations (ppm): $[NO]^{\circ} = 0.075$; $[NO_2]^{\circ} = 0.025$; $[trans\text{-}2\text{-}C_4H_8] = 0.10$; $[CO]^{\circ} = 10$; $[CH_2O]^{\circ} = 0.10$; $[CH_3CHO]^{\circ} = 0.060$; $[CH_4]^{\circ} = 1.5$; relative humidity = 50% (25°C)[a]

	- - - - - - - - - - - -	- - - - - -	- - - - - -	Reactive Species	- - - - - -	- - - - - -	- - - - - -
Time, min	$O(^3P)$	O_3	HO_2	HO	CH_3O	NO_3	$O_2(^1\Delta_g)$
2	0.13 (0.13)	0.26 (0.26)	1.69 (1.62)	18.1 (17.2)	0.026 (0.025)	0.00005 (0.00005)	0.000029 (0.000029)
10	0.20 (0.20)	0.83 (0.79)	1.84 (1.69)	12.5 (11.2)	0.018 (0.016)	0.00051 (0.00050)	0.000027 (0.000027)
30	0.17 (0.18)	1.58 (1.60)	1.49 (1.48)	5.9 (5.5)	0.008 (0.009)	0.0022 (0.0028)	0.000020 (0.000021)
60	0.08 (0.11)	1.43 (1.39)	0.88 (0.93)	2.6 (2.7)	0.004 (0.004)	0.0035 (0.0045)	0.000012 (0.000013)
90	0.03 (0.05)	1.00 (1.15)	0.49 (0.52)	1.2 (1.5)	0.002 (0.002)	0.0030 (0.0042)	0.000007 (0.000008)
120	0.01 (0.02)	0.65 (0.74)	0.28 (0.23)	0.7 (0.6)	0.001 (0.001)	0.0018 (0.0028)	0.000004 (0.000004)

[a] Results from two simulations are shown; one was made assuming finite literature values for the k_1, k_2 and k_3 rate constants; the other (results shown in parentheses) was made assuming k_1, k_2 and k_3 equal zero.

much higher olefin concentration. The theoretical fraction of olefin attack which results from NO_3 and $O_2(^1\Delta_g)$ is seen to be negligible for these conditions. Note in Table XXXII that the numbers in parentheses were calculated assuming k_1, k_2, and k_3 equal to zero as in the simulation shown in Fig. 57B. The other numbers were calculated using the finite values for these rate constants as designated previously for the simulation shown in Fig. 57A. Obviously there is no significant change in the rates of the several species obtained using these alternative assumptions.

Much concern has been focussed on the question of what reactions actually trigger the process of NO to NO_2 conversion in the sunlight-irradiated polluted atmospheres[139]. From the present simulation we can see that the HO radical is the most important transient species from the standpoint of initiating the olefin oxidation. However, any reactant which creates either HO or HO_2 will effectively generate HO radicals for us, since the reaction, $HO_2 + NO \rightarrow HO + NO_2$, is the major fate of HO_2 for these conditions. Then to understand this system it is important to investigate the relative importance of the several possible sources of both these radicals for the present system.

Again we should concern ourselves with the cases which represent the two possible extremes for the real atmosphere. First let us examine the happenings for the case of no initial HONO formation; that is, k_1 and k_2 equal zero. For our assumed impurity levels we will have only the following initial sources of stimulus to chemical change:

$$NO_2 + h\nu \rightarrow O(^3P) + NO \quad (4); \text{ Initial rate} = 120 \times 10^{-4} \text{ ppm min}^{-1}$$

$$H_2CO + h\nu \rightarrow HCO + H \quad (5); \text{ Initial rate} = 2.2 \times 10^{-4} \text{ ppm min}^{-1}$$

$$CH_3CHO + h\nu \rightarrow CH_3 + HCO \quad (6); \text{ Initial rate} = 1.5 \times 10^{-4} \text{ ppm min}^{-1}$$

Although the rate of O-atom formation is by far the largest of the intermediates formed here, very little impetus to the rate of photooxidation of the olefin or the conversion of NO to NO_2 is given by reaction 4. The occurrence of this reaction establishes an appreciable initial rate of O_3 formation, but this is never seen experimentally since O_3 destruction and the very fast regeneration of NO_2 occur through the reaction 7.

$$O_3 + NO \rightarrow O_2 + NO_2 \qquad (7)$$

The extent of chemical change in NO_2 and O_3 is limited very quickly. If only NO and NO_2 were present as impurities in this system, we would expect that the $[NO_2]$ would fall somewhat as 4 occurs, and O_3 would rise to a relatively small steady state value of about 5.1×10^{-3} ppm in about 2 min time. However, the reaction 4 provides only a relatively minute rate of O-atom attack on the olefin, 0.13×10^{-4} ppm min^{-1} at 2 min, unimportant in explaining the rates of chemical change observed in Fig. 37A.

Thus the major part of the initial push to oxidize NO and olefin in this system must come from the aldehyde photolyses in this case. Since most HCO radicals react to form HO_2 for these conditions, the total initial rate of HO_2 generation from the aldehyde photolyses is expected to be about 5.5×10^{-4} ppm min^{-1}. For the initial reactant concentrations employed, about 94.8% of the HO_2 radicals oxidize NO and about 5% react with olefin:

$$HO_2 + NO \rightarrow NO_2 + HO \qquad (8)$$

$$HO_2 + CH_3CH{=}CHCH_3 \rightarrow CH_3CH(HO_2)\dot{C}HCH_3 \qquad (9)$$

An additional reactant is formed in 6, the methyl radical, which will form CH_3O_2 in large part. Thus $R_{CH_3O_2} = 1.5 \times 10^{-4}$ ppm min^{-1}. For these conditions nearly all of the CH_3O_2 radicals will react to oxidize NO:

$$CH_3O_2 + NO \rightarrow CH_3O + NO_2 \qquad (10)$$

Thus the initial rate of NO_2 formation by way of 8 and 10 will be about 7×10^{-4} ppm min^{-1}. Of course this rate of formation is very much smaller than the initial rate of destruction of NO_2 by photolysis (120×10^{-4} ppm min^{-1}). The major key to the rise in NO_2 in the smog system is the participation of the HO-olefin reactions which generate the chain processes that allow indirectly each HO radical to oxidize several NO molecules. It is instructive to look into the details of these processes using the data for our present simulations.

Let us first note the rates of generation of HO and HO_2 free radicals from the several major sources in our system for several times throughout the photooxidation as pictured in Fig. 37. The major share of the HO radicals formed can be accounted for throughout the entire run by the following reactions:

(A) $HONO + h\nu \rightarrow HO + NO$ (11)

(B) $O(^1D) + H_2O \rightarrow 2HO$ (12)

(C) $\dot{H}O_2 + NO \rightarrow HO + NO_2$ (13)

(D) $H_2O_2 + h\nu \rightarrow 2HO$ (14)

(E) $CH_3\dot{C}HO_2H \rightarrow CH_3CHO + HO$ (15)

We have calculated the rates of HO-generation from each of these steps as function of the irradiation time, as shown in Table XXXIII.

TABLE XXXIII

Comparison of the Theoretical Rates of the HO-Radical Forming Reactions in a Simulated, Sunlight-Irradiated, Auto-Exhaust Polluted Atmosphere[a]

	Rate of HO-Formation (ppm min^{-1} x 10^4) from the Reaction Indicated				
Time, min	A (reaction 11)	B (reaction 12)	C (reaction 13)	D (reaction 14)	E (reaction 15)
0.05	0.0088	0.0015	28.3	0.0003	1.5
0.50	0.0907	0.0108	29.3	0.0029	1.6
2.0	0.32	0.023	27.8	0.013	1.6
10.0	0.64	0.082	18.5	0.080	1.7
30.0	0.29	0.23	10.0	0.33	1.3
60.0	0.12	0.38	5.9	0.79	0.9
90.0	0.07	0.40	4.0	1.2	0.5
120.0	0.03	0.35	1.2	1.6	0.2

[a] The simulated auto-exhaust polluted atmosphere has the same composition as in Table XXXII. The rate constants for the reactions 1, 2 and 3 are assumed to be equal to zero here as in Fig. 37B for this same system.

Obviously the photolysis of HONO is not important at very short times since we have excluded its presence for this consideration by setting $k_2 = 0$. However, even in this case it is formed in other reactions as the run progresses, and its photolysis contributes a maximum of about 3% to the total rate of HO generation at 10 min. Ozone of course is absent at the start of the run, and hence $O(^1D)$, its photolysis product, is also absent at this time, and reaction 12 is not important. However, late in the photooxidation, as O_3 builds up, the $O(^1D)$ generation of HO does become a significant contributor to the HO formation rate. The photolysis of H_2O_2, also unimportant initially, provides a steadily increasing source of HO as H_2O_2 builds up with time; in fact, after most of the butene has been oxidized at 120 min, reaction 14 is the major source of HO-radicals in the mixture. The reaction 15 provides a steady but rather minor source of HO radicals as well. The radical $CH_3\dot{C}HO_2H$ is one of the products of the reaction sequence which follows HO_2 addition to the butene.

Note in Table XXXIII that by far the largest rate of HO radical generation is through the HO_2-NO reaction 13. In fact the magnitude of this rate (e.g., 29.3×10^{-4} ppm min^{-1} at 0.5 min) is much greater than the rate at which we make HO_2 radicals in the sunlight initiated steps described previously; this rate totals to 7.0×10^{-4} ppm min^{-1}, 5.5×10^{-4} from H and HCO formed by aldehyde photolyses and about 1.5×10^{-4} ppm min^{-1} by way of CH_3 formation from acetaldehyde photolysis: ($CH_3 \xrightarrow{(O_2)} CH_3O_2 \xrightarrow{(NO)} CH_3O \xrightarrow{(O_2)} HO_2 + CH_2O$). Obviously the HO_2-radicals must be regenerated in a chain reaction to provide the observed rate of reaction 13. The details of this chain process can be understood by comparing the rates of HO_2 formation from the various major sources of this radical:

(F) $CH_2O + h\nu \rightarrow HCO + H;\ H + O_2 + M \rightarrow HO_2 + M$ (16)

$HCO + O_2 \rightarrow HO_2 + CO$

$\rightarrow HCO\dot{O}_2 \xrightarrow{(NO)} NO_2 + HCO_2 \xrightarrow{(O_2)} HO_2 + CO_2$

$\xrightarrow{(NO_2)} (HCOO_2NO_2) \rightarrow HONO + CO_2$

(G) $CH_3CHO + h\nu \rightarrow CH_3 + HCO$ (17)

$HCO + O_2$ [as in (A)] $\rightarrow \alpha HO_2$ + products

(H) $HO + CO \rightarrow CO_2 + H;\ H + O_2 + M \rightarrow HO_2 + M$ (18)

(I) $CH_3CH(\dot{O})CHO \rightarrow CH_3CHO + HCO$

$HCO + O_2$ [as in (A)] $\rightarrow \alpha HO_2$ + products

(J) $CH_3O + O_2 \rightarrow HO_2 + CH_2O$ (20)

(K) $CH_3CH(\dot{O})\dot{O} + O_2 \rightarrow CH_3CO_2 + HO_2$ (21)

The rates of HO_2 formation which arise from each of these sources are compared in Table XXXIV. Obviously the photolyses of both formaldehyde and acetaldehyde continue as significant sources of HO_2 through H and HCO formation; see column F and G in Table XXXIV. Acetaldehyde photolysis also forms HO_2 with rather high efficiency through the CH_3 radical reactions: $CH_3 \xrightarrow{(O_2)} CH_3O_2 \xrightarrow{(NO)} CH_3O$, as we have seen. The CH_3O radical generates HO_2 in reaction 20. However, only a small part, about 1.5×10^{-4} ppm min^{-1}, of the total rate shown in Column J at short times comes from this source; see the following discussion.

A third source of HO_2 is the HO-CO reaction 18. This reaction has been suggested to be the major HO_2 regeneration step in the chain oxidation of NO to NO_2;[8,9]

TABLE XXXIV.

Comparison of the Theoretical Rates of the HO_2-Forming Reactions in a Simulated, Sunlight-Irradiated, Auto-Exhaust Polluted Atmosphere[a]

	Rate of HO_2-Formation (ppm min^{-1} x 10^4) from the Reaction Indicated					
Time, min	F (reaction 16)	G (reaction 17)	H (reaction 18)	I (reaction 19)	J (reaction 20)	K (reaction 21)
0.05	4.0	1.5	4.2	5.1	15.8	0.05
0.5	4.0	1.5	4.4	5.2	16.5	0.1
2.0	4.1	1.6	4.3	4.9	15.9	0.2
10.0	4.3	1.8	3.2	3.0	11.8	0.6
30.0	4.3	2.2	2.2	1.5	8.8	1.1
60.0	4.2	2.5	1.8	0.7	6.9	1.1
90.0	3.8	2.5	1.7	0.4	5.4	0.8
120.0	3.4	2.4	1.3	0.2	3.9	0.5

---

[a] The simulated auto-exhaust polluted atmosphere has the same composition as in Table XXXII. Rate constants for the reactions 1, 2 and 3 are assumed to be equal to zero here as in Fig. 33b for this same system.

Although it is important in this regard here, it is by no means the main source of the HO to HO_2 conversion in this simulated polluted atmosphere.

The sequence I provides another source of the HO_2 radical from the decomposition of the intermediate radical, $CH_3CH(\dot{O})CHO$. Theoretically this radical is formed in the reaction sequence which follows the H-atom abstraction from the butene by the HO-radical (or other radicals, to the much smaller extent that H-abstraction by them occurs).

The rates in column J of Table XXXIV show that the largest source of HO_2 in this system is the methoxy radical reaction 20. Shortly after the photooxidation of the butene containing mixture is initiated, the CH_3O is formed from CH_3 radicals derived from several reaction paths. We have considered the relatively minor source from acetaldehyde photolysis previously. In addition it is formed in the reaction sequence which follows the HO-radical addition to the butene. Specifically we picture its formation in the following step:

$$CH_3CH(OH)\dot{O} \rightarrow CH_3 + HCO_2H \qquad (22)$$

Also HO-attack on acetaldehyde can lead to CH_3 radical formation through the sequence: $CH_3CHO \xrightarrow{(HO)} CH_3CO \xrightarrow{(O_2)} CH_3COO_2 \xrightarrow{(NO)} CH_3CO_2 \rightarrow CH_3 + CO_2$. When the $[NO]/[NO_2]$ ratio is relatively high, the CH_3COO_2 radicals oxidize NO in large part to lead to the CH_3CO_2 radical. PAN formation is the favored product only at low $[NO]/[NO_2]$ ratios (at long run times).

In theory the reaction sequence which follows ozone attack on the olefin leads to the radical $CH_3CH(\dot{O})\dot{O}$. Its reaction with O_2 is the fifth source of HO_2, reaction 21; this contribution to the rate, shown in column K of Table XXXIV, is negligible at short times, but as O_3 builds up at long exposure times, it has a finite contribution.

From these theoretical considerations we see that there is a complex interplay between the various reactants in this simulated smog forming atmosphere which stimulates the generation of the important HO and HO_2 radicals. For the reactant conditions which we have chosen here, the olefin acts as the major source of conversion of HO to HO_2 radicals. Both the abstraction of H-atoms from the olefin by HO and the addition of HO to olefin generates an HO_2 radical eventually with fair efficiency. In the sequence of reactions in which this occurs, at least one molecule of NO is oxidized to NO_2 by various RO_2 radicals as well. Thus for short exposure times in Fig. 37A, when each HO radical abstracts H-atoms from butene, about one molecule of NO is converted to NO_2 and one HO_2 radical is formed. For each HO radical which adds to butene about three molecules of NO form NO_2 and again one HO_2 molecule is formed as well. The HO_2 radicals are largely reconverted to HO at short times through the reaction, $HO_2 + NO \rightarrow HO + NO_2$, and hence the chain cycle of attack of HO on C_4H_8 continues to degrade the olefin until the chain is terminated. The rate of HO_2 formation in the primary photolytic processes (7.0×10^{-4} ppm min^{-1} at 2 min) and the total rate of HO and HO_2 attack on the olefin (19.8×10^{-4} at 2 min), suggests that there is a short chain reaction, about 2.8 cycles in length at 2 min, which involves the HO and HO_2 radical oxidation of olefin. Of course the chains are stopped whenever an HO_2 or an HO radical is removed by reactions with another radical or an odd electron molecule such as NO or NO_2. The dominant chain ending steps for our chosen concentration conditions in this system are the following:

$$2HO_2 \rightarrow H_2O_2 + O_2 \qquad (23)$$

$$HO + NO + M \rightarrow HONO + M \qquad (24)$$

$$HO + NO_2 + M \rightarrow HONO_2 + M \qquad (25)$$

$$CH_3O_2 + HO_2 \rightarrow CH_3O_2H + O_2 \qquad (26)$$

The rates of radical removal in these reactions for our simulation in Fig. 36A at 2 min, are as follows: $R_{23} = 4.6 \times 10^{-4}$; $R_{24} = 1.2 \times 10^{-4}$; $R_{25} = 0.8 \times 10^{-4}$; $R_{26} = 0.07 \times 10^{-4}$ ppm min^{-1}. The total of these rates accounts for a rate of HO_2 and HO radical removal = 6.6×10^{-4} ppm min^{-1}. This would match our rate of primary radical production (7.0×10^{-4} ppm min^{-1}) if all radical sources and termination reactions were included in our considerations.

Now let us return to consider the alternate hypotheses of HONO pre-equilibration in our simulated polluted atmosphere. We will allow HONO to have been formed at its equilibrium value, $[HONO] = 6.1 \times 10^{-3}$ ppm, before sunlight irradiation of the mixture. All other compounds are at the concentrations employed as before, and the HONO generating and destruction reactions, 2 and 3, are assumed to have their finite literature values. The initial rate of radical generation in this system will include the same rates of HO_2 and CH_3O_2 formation from CH_2O and CH_3CHO photolyses as before, but there will be an additional source of HO radical formation from the HONO photolysis:

$$HONO + h\nu \rightarrow HO + NO \qquad (11)$$

This rate will be about 7.3 x 10^{-4} ppm min^{-1} for $z = 40^\circ$. Compare this with the rate of NO_2 formation from all of the aldehyde photolysis processes; $R_{NO_2} = 7.0 \times 10^{-4}$. Obviously the HONO presence in the atmosphere can give a significant boost to the initial rate of olefin photooxidation and NO to NO_2 conversion; it would approximately double these initial rates for our simulations if we allowed HONO preequilibration before irradiation. Assuming preequilibration of HONO and allowing the finite values for the rate constants k_1, k_2, and k_3 as before, we predict from simulations not shown here that the maximum in the $[NO_2]$ would occur at 22 min. This compares with 24 min for the time of $[NO_2]_{max}$ for the same mixture but with HONO absent originally; see Fig. 37A. A period of 31 min is required to reach $[NO_2]_{max}$ when there is no HONO initially and we assume $k_2 = k_3 = 0$ as in Fig. 37B.

We have clearly seen that HONO is not a necessary component of the polluted atmosphere to account for the general features of smog formation, but its presence can enhance the initial rate of the smog forming reactions. Of course, its presence must be invoked to rationalize the photooxidation of NO in moist atmospheres containing carbon monoxide as the only other oxidizable component. It remains to be determined experimentally what levels of HONO are present in the real atmospheres, and which, if either of the two extremes considered above, best represents the real situation. It is our educated guess that the real auto-exhaust polluted atmospheres have levels of HONO which lie between the two extremes considered here.

We have also considered the expected effects of the presence of one additional constituent not originally included in our simulated atmosphere, namely n-butane, as representative of the saturated hydrocarbons. If n-butane is present in our simulated atmosphere at the same level as the olefin, 0.10 ppm, the rate of NO_2 formation is only increased by 2%. Thus with paraffin hydrocarbon additions at the levels near those of the olefins, the situation which exists in the real auto-exhaust polluted atmosphere in the early morning hours[167], we can expect only a relatively small perturbation of the above general reaction scheme.

III-B. The Effect of CO on the Chemistry of Photochemical Smog Systems.

A detailed kinetic model for the simulation of smog chamber results has recently been developed[160] and applied (i) to determine the predicted effect of carbon monoxide on the ozone levels in photochemical smog systems[161] and (ii) to determine the relative importance of the various intermediate species in the olefin removal reactions in photochemical smog[162]. The main features of the effect of CO on the rate of O_3 formation in NO-polluted atmospheres were interpreted in terms of the following simplified reaction sequence:[169]

$$2NO + O_2 \rightarrow 2NO_2 \qquad (1)$$

$$H_2O + NO + NO_2 \rightleftharpoons 2HONO \qquad (2)$$

$$HONO + h\nu \rightarrow HO + NO \qquad (3)$$

$$HO + CO \rightarrow H + CO_2 \qquad (4)$$

$$HO + NO\ (+N_2,O_2) \rightarrow HONO\ (+N_2,O_2) \qquad (5)$$

$$HO + NO_2\ (+N_2,O_2) \rightarrow HONO_2\ (+N_2,O_2) \qquad (6)$$

$$H + O_2\ (+N_2,O_2) \rightarrow HO_2\ (+N_2,O_2) \qquad (7)$$

$$HO_2 + NO \rightarrow HO + NO_2 \qquad (8)$$

$$2HO_2 \rightarrow H_2O_2 + O_2 \qquad (9)$$

$$NO_2 + h\nu \rightarrow O + NO \qquad (10)$$

$$O + O_2\ (+N_2,O_2) \rightarrow O_3\ (+N_2,O_2) \qquad (11)$$

$$O_3 + NO \rightarrow O_2 + NO_2 \qquad (12)$$

$$O_3 + NO_2 \rightarrow O_2 + NO_3 \qquad (13)$$

$$O_3 + h\nu \rightarrow O + O_2 \qquad (14)$$

$$NO_3 + NO \rightarrow 2NO_2 \qquad (15)$$

$$NO_3 + NO_2 \rightleftharpoons N_2O_5 \qquad (16)$$

$$N_2O_5 + H_2O \rightarrow 2HONO_2 \qquad (17)$$

Two recent developments prompt us to repeat and extend our computer simulations of this system. Firstly, reliable experimental data on reactions 5 and 6 indicate that the rate constants are significantly faster than formerly believed[170], and secondly, experimental data on the photooxidation of NO in the presence of CO have become available from smog chamber studies[171,172].

III-B—1. Results and Discussion

In view of the high rate constant[173] for reaction 4 and the relatively high CO levels present in polluted atmospheres, two groups of scientists, Heicklen et al.,[165] and Stedman et al.,[166] came to the conclusion that the rapid oxidation of NO to NO_2 which occurs in the polluted atmosphere may be linked to the occurrence of reaction 4 coupled with the reactions 7 and 8:

$$HO + CO \rightarrow CO_2 + H \qquad (4)$$

$$H + O_2 + \underline{M} \rightarrow HO_2 + \underline{M} \qquad (7)$$

$$HO_2 + NO \rightarrow HO + NO_2 \qquad (8)$$

This sequence provides a chain mechanism in which the formation of a single HO radical could conceivably initiate the oxidation of many NO molecules. Although absolute magnitude of k_8 remains somewhat open to question, using our "best" estimates of all of the rate constants for the reaction 1 - 17, we can simulate the chemical changes which we might expect for the NO-NO_2-CO-containing atmospheres and test our predictions with smog chamber data[169].

The striking effect of CO on the rate of NO oxidation in the NO-NO_2-H_2O system irradiated in air can be seen in Figs. 38A and 39A, obtained from the smog chamber experiments of Wilson and Miller[171], in which 100 and 400 ppm of CO respectively were added to the systems. The results of our computer simulation of this system based on the above mechanism are shown in Figs. 38B and 39B. It can be seen that the simulations match the experimentally observed time dependence of the measured reactants and products reasonably well. In addition the concentration and time dependence of the minor products, CO_2, HONO, $HONO_2$, and H_2O_2, which we predict from our simulations, are shown in Figs. 38C and 39C, but there are no experimental data with which to compare in these cases.

In view of the reasonably good match between experiment and simulation we have attempted to extrapolate these observed effects of CO to the concentration range of reactants commonly encountered in the polluted atmosphere. One such extrapolation is shown in Fig. 40C. The theoretical time dependence of the concentration of the reactants and products is shown for the sunlight-irradiated mixtures with the initial concentrations of impurities: $[NO]^\circ = 0.10$, $[NO_2]^\circ = 0.00$, and $[CO]^\circ = 10$ ppm, at a relative humidity, 50% (25° C). Although we have chosen conditions which minimize the chance for chemical change in the system, there is a remarkable change expected in the rates of product formation on addition of CO; compare the plots of Figs 40A, 40B, and 40C in which dry and moist atmospheres contaminated with identical levels of NO and NO_2 are present with and without carbon monoxide impurity. This effect is illustrated also in Figs. 41A and 41B; in this case the initial concentrations of the contaminants are: $[NO]^\circ = 0.075$, $[NO_2]^\circ = 0.025$ ppm, and the relative humidity = 50%. In Fig 41B the identical initial levels of NO, NO_2 and humidity are employed, but 10 ppm of CO is added as well. The predicted role of carbon monoxide in enhancing the NO oxidation to NO_2 through the reaction sequence 4, 7 and 8 is apparent in both comparisons. The decrease in the initial level of NO_2 observed in irradiated dry and moist atmospheres contaminated with only NO and NO_2 is in striking contrast to the rapid increase in NO_2 which occurs after a small delay in the CO-containing systems.

For given fixed NO and NO_2 impurity levels, the rate of NO oxidation increases most noticeably with increasing CO level when the CO impurity is in the 0-25 ppm range. Within this range the higher the initial [CO] the shorter is the sunlight irradiation time necessary to reach the maximum $[NO_2]$ and the higher is that maximum. (See the data presented in columns 2 and 3 of Table XXXV.). Thus at the initial reactant levels, $[NO_2]^\circ = 0.025$, $[NO]^\circ = 0.075$ ppm at the relative humidity = 50%, the $[NO_2]$ maximizes at 3.5 pphm in 232 min for [CO] = 5 ppm, and at about 5.7 pphm at 140 min for [CO] = 25 pphm. It can be seen that the $[NO_2]_{max}$ and the time to reach this level are both rather insensitive to increases in the concentration of CO when it is in the range 25-100 ppm. Obviously a major predicted effect of increasing the NO_2 level by the CO-sensitized photooxidation is to increase the rate of $O(^3P)$-atom generation and the ozone concentration in the system. The data of Table XXXV shows that the addition of 5 ppm of CO to the moist atmosphere contaminated with NO and NO_2 is predicted to cause more than a 10-fold increase in the ozone level reached after exposure to sunlight for 152 min.

The level of CO at which one expects significant effects on the rate of NO photooxidation is somewhat higher than that which we suggested in our earlier studies[161]. The present estimates are based on more accurate recent rate constant

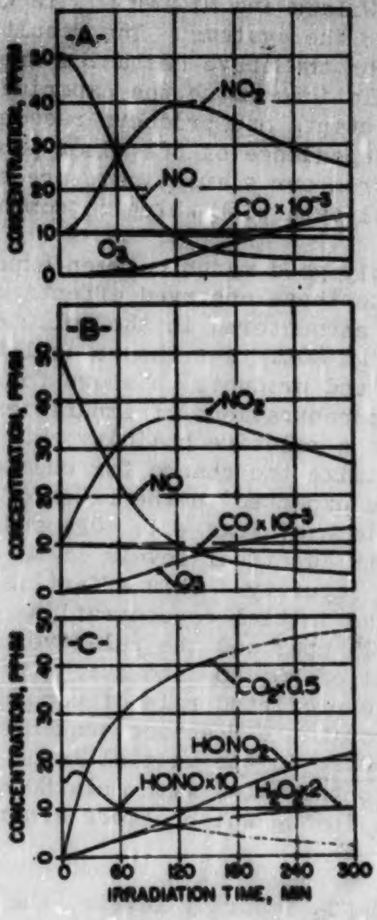

Fig.38. Comparison of experimental and computer simulated chemical changes in NO-NO_2-CO mixtures irradiated in moist air; Fig.38a experimental data of Wilson and Miller (ref.171) initial concentrations, $[NO]^\circ = 51$ pphm; $[NO_2]^\circ = 10$ pphm; $[CO]^\circ = 100$ ppm; relative humidity about 13% at 90°F; Fig. 38b computer simulation for the experimental conditions employed in Fig. 38a Fig. 38c computer simulation of the expected time dependence of the minor products for the conditions employed in Fig. 38a experimental analysis for these products was not made.

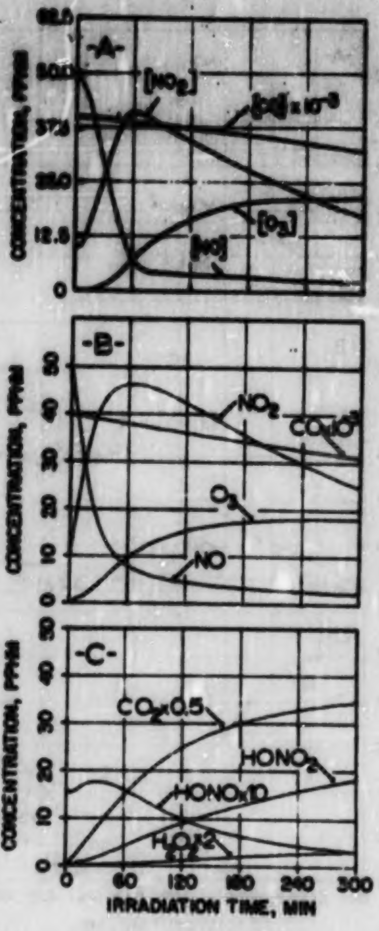

Fig. 39. Comparison of experimental and computer simulated chemical changes in NO-NO_2-CO mixtures irradiated in moist air; Fig. 39a experimental data of Wilson and Miller (ref 171 initial concentrations, [NO]° = 50 pphm; [NO_2]° = 10.5 pphm; [CO]° = 400 ppm; relative humidity about 13% at 90°F; Fig. 39b computer simulation for the conditions used in Fig. 39a; Fig. 39c simulation of the expected time dependence of the minor products for the conditions employed in Fig. 39a experimental analysis for these products was not made.

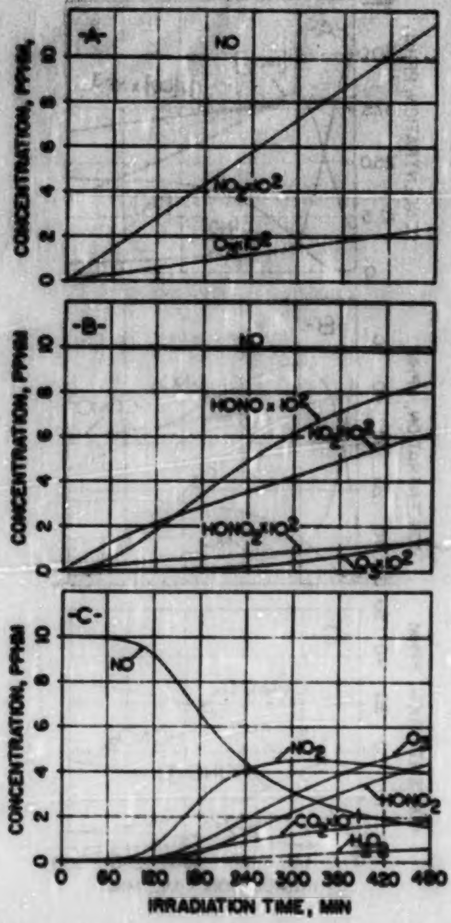

Fig. 40. The expected effects of water vapor and carbon monoxide addition on the products of the NO photooxidation in air; comparison of the computer simulated chemical changes in three sunlight irradiated (z = 40°), NO-polluted atmospheres; Fig.40a dry atmosphere; Fig.40b moist atmosphere (50% relative humidity, 25°C); Fig.40c moist atmosphere containing carbon monoxide, $[\mathrm{CO}]^\circ$ = 10 ppm; in each case the initial concentrations are $[\mathrm{NO}]^\circ$ = 10 pphm, $[\mathrm{NO_2}]^\circ$ = 0.0 pphm.

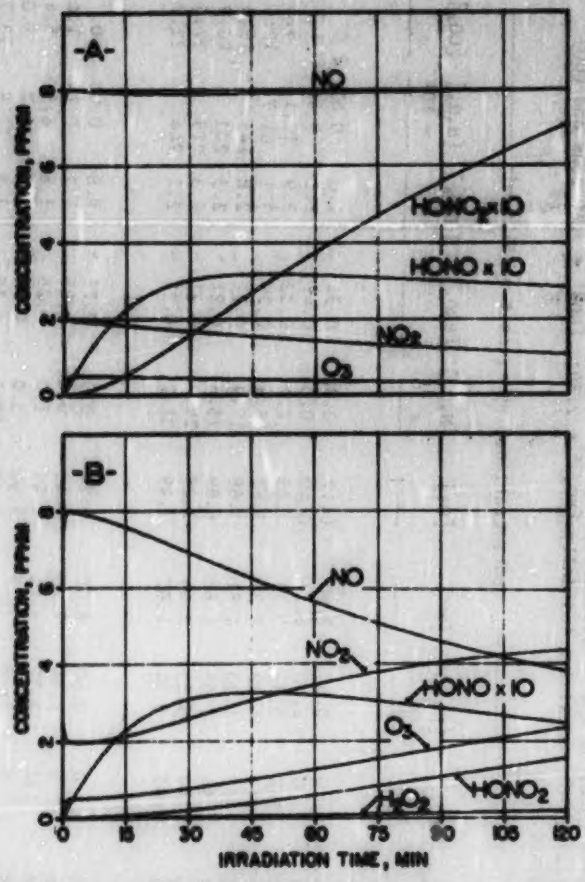

Fig.41. The NO-NO$_2$-CO-polluted atmosphere; simulation of the effects of added carbon monoxide on the time dependence of the major products formed in sunlight-irradiated (z = 40°), NO$_x$-polluted atmospheres; the initial concentrations in each case are: [NO]° = 7.5 pphm; [NO$_2$]° = 2.5 pphm; relative humidity, 50% (25°C); Fig.41a [CO]° = 0.0 ppm; Fig.41b [CO]° = 10 ppm.

TABLE XXXV.

The Effect of Carbon Monoxide Level on the Concentrations (pphm) of Products Formed in the Sunlight-Irradiated Moist Atmospheres (25°C) Containing Initially $[NO_2]^\circ$ = 2.50; $[NO]^\circ$ = 7.50 pphm and $[CO]^\circ$ as Indicated: z = 40° Assumed.

				Concentrations, pphm, at t = 151.6 min							
Relative Humidity, % (25°C)	$[CO]^\circ$ ppm	$[NO_2]_{max}$ ppm	t_{max} min	$[NO_2]$	$[NO]$	$[O_3]$	$[N_2O_5] \times 10^4$	$[HNO_2]$	$[HNO_3]$	$[H_2O_2] \times 10^3$	$[CO_2]$
100	0	2.50	0	0.64	7.98	0.17	0.00	0.34	1.0	0.03	0
	1	2.50	0	1.30	6.77	0.40	0.04	0.41	1.5	0.46	1.7
	5	3.37	148	3.37	3.39	2.05	1.7	0.33	2.9	19.1	8.2
	10	4.41	117	4.32	2.32	3.82	6.9	0.25	3.1	61.7	12.6
	25	5.50	102	5.20	1.81	5.88	17.9	0.22	2.8	145	18.0
	50	6.07	94	5.65	1.68	6.89	25.6	0.21	2.5	203	20.9
	75	6.30	92	5.83	1.64	7.28	29.2	0.21	2.3	229	22.3
	100	6.42	91	5.94	1.62	7.49	31.2	0.21	2.2	244	22.9
50	0	2.50	0	0.90	8.00	0.24	0.01	0.26	0.84	0.01	0
	1	2.50	0	1.44	7.20	0.42	0.04	0.29	1.1	0.19	1.1
	5	3.46	232	3.32	4.61	1.49	1.0	0.26	1.8	6.5	5.4
	10	4.56	176	4.53	3.22	2.90	5.0	0.21	2.0	24.7	9.0
	25	5.70	140	5.69	2.32	5.03	18.0	0.16	1.8	72.6	13.7
	50	6.28	128	6.24	2.07	6.17	28.8	0.15	1.5	110	16.3
	75	6.52	125	6.46	2.00	6.62	33.9	0.15	1.4	128	17.4
	100	6.65	123	6.58	1.96	6.88	36.9	0.14	1.3	138	18.0

determinations including that for the reaction, $HO + NO_2 + \underline{M} \rightarrow HONO_2 + \underline{M}$ (6).

It is important to note from the data of Table XXXV that the major effects of added CO impurity in an NO-NO_2-contaminated system are expected to be seen at relatively low concentrations of CO; the most dramatic increase in $[O_3]$ occurs in the range of $[CO] = 0$ to 5 ppm. A significant but smaller effect is seen also with [CO] increased from 5 to 25 ppm, while further increase in [CO] to 100 ppm has little further effect on the ozone level. Of course at very high CO levels the duration of the CO enhancement of NO photooxidation would be prolonged to much greater times for a given rate of dilution in the atmosphere.

Recent rate data have been obtained by Dodge and Bufalini[172] from a similar smog chamber study of the NO-NO_2-CO-H_2O-containing system. These results are shown in Figs. 42A and 43A. Although the effects of CO addition are similar to those observed by Wilson and Miller[171], there are some significant differences. In fact the same set of rate constants which we have employed with some success in the previous work fails to fit well these CO-containing runs. The reaction volumes are similar for the reaction vessels employed by the Wilson and Bufalini groups, and hence the surface-to-volume ratio is probably not very different. There are two major differences which one should recognize. First the black lamps employed by the Dodge and Bufalini group probably have a significantly different wavelength distribution from the selection of sun-lamps employed in the Wilson and Miller study. Although the rate of NO_2 photo-decomposition has been measured in both studies (k_{10}) and is a parameter which is not variable in the simulations, the rate of nitrous acid photolysis may be significantly larger in the study of Wilson and Miller, since there is probably a larger contribution from the shorter wavelength region of light (~ 3100 Å) with the lamps which they employed. There is an obvious second difference between the two studies: the gaseous mixture was circulated mechanically only in the study of Wilson and Miller. Presumably this circulation would allow a faster replenishment of the HONO if there were a significant heterogeneous component to the rate of reaction in the system of Wilson and Miller. Either one or both of these effects may be important. Since it is really impossible to judge correctly from the limited data at hand, we have arbitrarily chosen the first effect alone in an attempt to fit better the Dodge and Bufalini results. Using the value of $k_{26a} = 8.8 \times 10^{-3}$ instead of our adjusted sunlight value of 8.8×10^{-2} min^{-1}, we find the simulations shown in Figs. 42B and 43B. The fit is considerably better for this choice of rate data, but some real problems remain. Particularly, the ozone levels observed by Dodge and Bufalini are much lower than those predicted in the simulations. The explanation of this difference is not clear. Our mechanism may be incomplete in some as yet undetermined way, or conceivably there may be analytical problems in the data of Dodge and Bufalini. For example, the thermal reaction, $O_3 + NO \rightarrow O_2 + NO_2$, may occur significantly in the sampling line leading to the analytical instruments for O_3 and NO_2. This would result in higher NO_2 and lower O_3 levels than those actually present in the chamber. The error would be present until such times that the NO is largely converted to NO_2 or other products. This problem has been observed recently in smog chamber experiments[174]. As an example of the magnitude of this possible effect for the present case, consider the products in Fig. 43B at 100 minutes irradiation time. Note that a delay of only 1.6 min in transporting the NO, NO_2, O_3 mixture in the dark to the analysis systems results in lowering the ozone to one-half of its value when it was present in the chamber. Further speculation on this interesting NO-NO_2-CO-H_2O system must await more complete experimental data over a more complete range of experimental parameters.

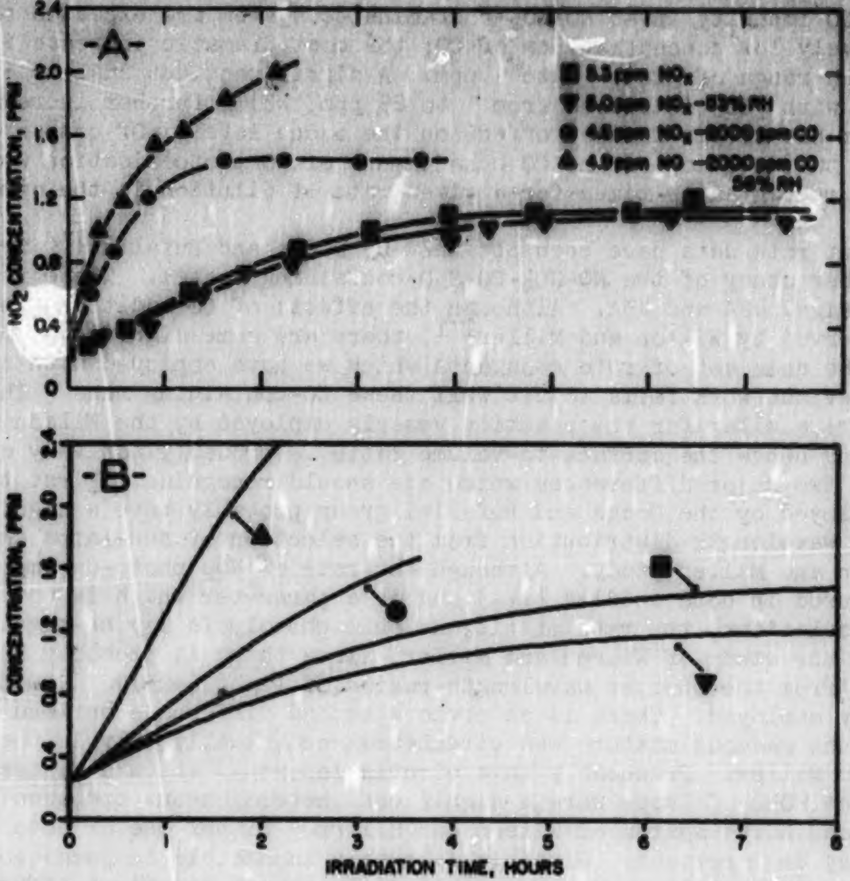

Fig.42. The photooxidation of NO in CO-containing mixtures; comparison of experimental and computer simulated chemical changes in NO-NO_2-CO mixtures irradiated in relatively dry and moist air; Fig.42a experimental data of Dodge and Bufalini (ref. 172 initial conditions as shown; Fig. 42b computer simulation of the product concentration data for the conditions employed in Fig. 42a.

From the available information on the CO-containing system and our simulation studies, we conclude that the atmospheric scientists should give careful consideration to the predicted enhancement of ozone levels by relatively small amounts of CO in an NO_x-polluted, but hydrocarbon free, atmosphere. In fact these unexpected effects should be considered in the future development of more detailed air quality standards. In view of the technological difficulties in removing NO_x and CO from auto exhaust and NO_x from stack gases, there is a reasonable possibility that significant ozone levels may continue to plague many urban areas even though a near total removal of the reactive hydrocarbons might be effected.

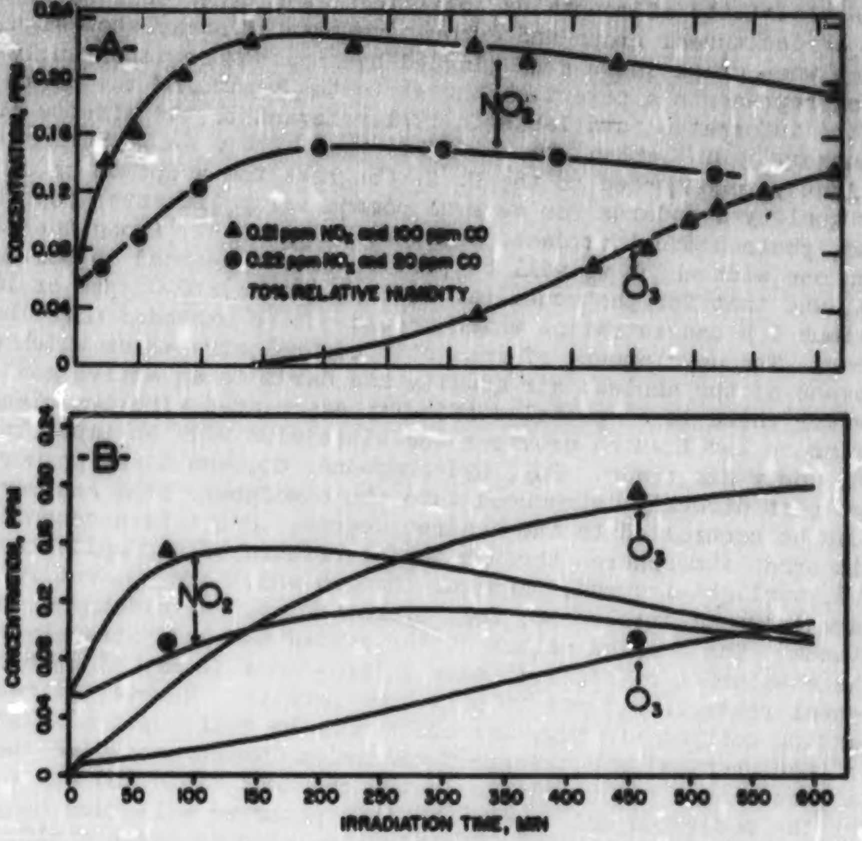

Fig. 43. The photooxidation of NO in CO-containing mixtures; comparison of the experimental and computer simulated chemical changes in $NO-NO_2-CO$ mixtures irradiated in moist air; Fig.43a experimental data of Dodge and Bufalini (ref 172 initial conditions as shown; Fig.43b computer simulation of the experiment shown in Fig. 43a.

III-C. Computer Simulation of the Rates and Mechanisms of Photochemical Smog Formation[175].

Today the phenomenon of photochemical smog formation, once considered peculiar to the Los Angeles area, occurs to some extent in most large cities throughout the world. In our rapidly growing urban areas, a high density of automobile traffic, nearby power generation, and high commercial and industrial activity are becoming more commonplace. When the relatively high ambient concentrations of NO, NO_2, and hydrocarbon emissions from these geographically concentrated sources are coupled with bright sunshine and poor atmospheric ventilation, photochemical smog formation is inevitable.

The unpleasant phenomenon of photochemical smog is characterized by the build up in the urban atmosphere of significant levels of ozone, peroxyacyl nitrates, and many other compounds such as the aldehydes, acids, etc., which arise from the partial oxidation of the hydrocarbons[139,176]. The resident of a smog-bound community may experience eye irritation from compounds not yet clearly defined. As the usual smoggy day develops, haze formation in the atmosphere may greatly restrict his visibility of mountains, buildings, and other objects of some distance away. Many agricultureal crops and decorative plantings may show significant deterioration when grown in an area plagued by smog. More importantly photochemical smog represents a potential threat to the health of the urban dweller. In view of the information available in 1971 relevant to the effects of the common air pollutants on human health, the Administrator of the U. S. Environmental Protection Agency recommended to the U. S. Congress the adoption of national ambient air quality standards for several common air pollutants: NO_2, CO, SO_2, hydrocarbons, photochemical oxidant, and particulates[177]. Among the standards adopted, and one with which we will be particularly concerned in our considerations here, was that for photochemical oxidant (ozone): 0.08 ppm or 160 $\mu g\text{-}m^{-3}$ for the maximum 1 h concentration which should not be exceeded more than one hour per year. The development of realistic control strategies which will ensure the achievement of the ambient air quality standards is an active goal of the E.P.A. However there is a special difficulty associated with the plans to control the ozone level which provides the kineticist with an important opportunity to apply his trade. SO_2, hydrocarbons, CO, and other primary pollutants are in large part directly introduced into the atmosphere from sources which in principle can be controlled to the desired degree. Ozone is a secondary pollutant, generated in urban atmospheres through the occurrence of a complicated series of interrelated, sunlight-induced, chemical changes which are not entirely understood, but which are known to involve NO, NO_2, hydrocarbons, CO, aldehydes, and perhaps other reactants. The complex nature of the system and the extremely short time base for the attainment of controls have stimulated a flurry of both Edisonian and fundamental research efforts to solve the problem. However it seems probable that any lasting control strategy for ozone must be built upon a solid scientific knowledge of the chemical and transport mechanisms which determine the ozone level. Such a data base is not now available in the chemical field and the same is likely the case for the meterological input. In this paper we will face only some of the chemical kinetic and mechanistic problems related to these goals.

Since the early 1950s the kineticists have had an active role in elucidating the elementary reactions in smog formation. Leighton was the first to make a comprehensive quantitative attempt to evaluate the alternative reaction paths which may be operative in photochemical smog[139]. Sophistication of the kinetics treatment of these systems has increased in recent years as our knowledge related to the various elementary reactions has grown, and computer techniques have become available for the practical solution of complex series of interrelated differential rate equations. However the research which bears on the mechanism of photochemical smog formation has left unanswered many critical questions. When one appreciates the full complexity of these systems the relatively slow progress is understandable. Kineticists soon realized that a full consideration of the many thousands of reactions between the many hundreds of reactants in the real urban polluted atmosheres was an overly ambitious plan. We and many others feel that the definition and characterization of the reactions which are important in the real atmosphere lies in the consideration of the simpler, well controlled, simulated polluted atmospheres of the "smog chamber". Even these systems are very complex[127] and difficult to treat quantitatively since many reactions which appear to be important in theory have not been studied in detail, and theoretical estimates of rate constants must be made in desperation; the thermochemical-kinetic techniques developed by Benson[178] have given us some reasonable guidance in this phase of our work.

In this article we will analyze the mechanism and kinetics of photochemical smog formation using an updated and expanded version of the chemical reaction mechanism developed some years ago by Demerjian, Kerr, and Calvert[160,161,162,127][*]. Our attempts at computer modeling of photochemical smog mixtures represent one of many efforts in this area[179-187]. Our chemical system is somewhat more complete than others in order to satisfy several unique demands of the kineticists. It should serve as a useful predictive tool which will allow a resonable selection of key chemical reactions needed for the highly abbreviated mechanisms used in the comprehensive urban air shed models. It should provide some insight into the nature and extent of some potentially important compounds as yet unidentified in the real atmosphere but expected in theory. However the major role which we hope our study can play is in the alerting of the kineticists to those reactions which are seemingly important but for which little or no reliable kinetic data now exist.

Before we consider the results of our simulations, let us understand the limitations of such considerations. In the simulations of the polluted atmosphere-like systems described in this work, we have assumed that there is no atmospheric dilution of products and reactants and that the sunlight is of fixed intensity. All photochemical rates have been estimated for a solar zenith angle of 40°, a value near the average encountered during a typical day in the United States. Estimates of the actinic irradiance were taken from Leighton[139]; these are theoretical estimates which should apply approximately for representative atmospheric conditions near sea level on a clear day. Suitable modifications which incorporate diffusion and regular change in solar zenith angle can be made readily, but they offer a degree of sophistication at this point in time which our current chemical knowledge does not warrant, and they actually mask some of the chemical features we are trying to identify. Obviously this choice of model will not allow us to describe well the product rates expected for positions near point or line sources such as smoke stacks or freeways where large fluctuations in the input pollutants levels occur[180]. The "box" models such as we employ here should give reasonably good answers to chemical questions related to urban atmosphere somewhat removed from major pollutant sources and for conditions of strong atmospheric temperature inversion. Obviously the coupling of such a reaction scheme, suitably pruned to acceptable complexity, to atmospheric diffusion models and local emission patterns must be made to achieve the full predictive potential of the comprehensive air pollution models which are necessary for local air pollution control strategies[180-182,183b,185,187].

---

[*] All of the results reported here have been calculated assuming that the rate constants for the reactions, $N_2O_5 + H_2O \rightarrow 2HONO_2$ (8), $NO + NO_2 + H_2O \rightarrow 2HONO$ (16a) and $2HONO \rightarrow NO + NO_2 + H_2O$ (16b) are zero. There remains some uncertainty as to the degree of involvement of these reactions in the real atmosphere[127]. Recent studies of Cox and Atkins[188] show clearly that k_{16a} and k_{16b} are very small. Morris and Niki[189] have reported that $k_8 \leq 1.9 \times 10^{-5}$ ppm^{-1} min^{-1} [liter/(mol-s) x 2.45×10^{-6} = ppm^{-1} min^{-1}]. In any case the alternative choices of these rate constants have only a very minor influence on most kinetic properties of the systems[127]. The rate constants and reaction mechanisms outlined by Demerjian et al.[127] have been used in most cases. The only significant rate constant change is that for the reaction (17) $HO_2 + NO_2 \rightarrow HONO + O_2$; here we used $k_{17} = 2.9 \times 10^1$ ppm^{-1} min^{-1}, based on work of Simonaitis and Heicklen[190], except where specific notation is given. Reference to the extensive review of Demerjian et al.[127] should be made for reaction details not outlined here. The new rate constants which we have employed in the SO_2-containing systems are outlined in Table XLIV.

III-C-1. Results and Discussion

Computer Analysis of the Chemistry of Smog formation in a Simulated NO_x-Hydrocarbon Polluted Atmosphere

For our first considerations we have chosen a relatively simple mixture of several important classes of reactants; to the mixture of NO at 0.075 ppm and NO_2 at 0.025 ppm, we have added the background level of CH_4, 1.5 ppm; a typical level of CO, 10 ppm; typical levels of the total olefinic hydrocarbon, represented by trans-2-butene at 0.10 ppm; and aldehydes, CH_2O at 0.10 ppm; and CH_3CHO, repsentative of all of the higher aldehydes, at 0.06 ppm. The effects of n-butane addition at 0.10 ppm, representing the saturated paraffinic hydrocarbons, and 0.10 ppm of SO_2, a molecule which is often present today in urban atmospheres, will be considered later. We will not consider the effects of the addition of the aromatic hydrocarbons since the authors are not aware of meaningful experimental evidence relating to their decay paths. We have assumed that the relative hunidity is at 50% and the temperature of the atmosphere is 25° C. Through the computer simulation of this system we have calculated the theoretical time dependence of the products expected when this mixture is irradiated in sunlight ($z = 40°$). The concentration-time profiles for a few of the major reactants and products are shown in Figure 44 for two different starting conditions: aldehydes are initially present for the solid curves, and aldehydes are absent initially for the dashed curves. Without the aldehydes present initially a small induction period appears in the rates of alkene removal, and NO_2, O_3, and peroxyacetyl nitrate (PAN) formation. Also recognize from a comparison of the final levels of the dashed and solid curves for the various products that the concentrations of such problem compounds as O_3 and PAN are raised when aldehydes are present initially. We will consider the effects of aldehydes in more detail in the next section. Note in Figure 44 the general features which characterize the chemistry of a smoggy atmosphere: NO is converted to NO_2 as the alkene is removed, and ozone and PAN build up with time. Present knowledge of these systems points to only three reactions as the major ones which control the ozone concentration[139,185,186,191,165,192]:

$$(1) \qquad NO_2 + h\nu(\lambda < 4300\ \text{Å}) \rightarrow O(^3P) + NO$$

$$(2) \qquad O(^3P) + O_2\ (+\ M) \rightarrow O_3\ (+\ M)$$

$$(3) \qquad O_3 + NO \rightarrow O_2 + NO_2$$

To a first approximation the concentration of the ozone which builds is related to the $[NO_2]/[NO]$ ratio and the intensity of solar radiation absorbed by NO_2 at the effective wavelength region ($\lambda < 4300$ Å).

$$(I) \qquad [O_3] \cong \frac{[NO_2]\ k_1}{[NO]\ k_3}$$

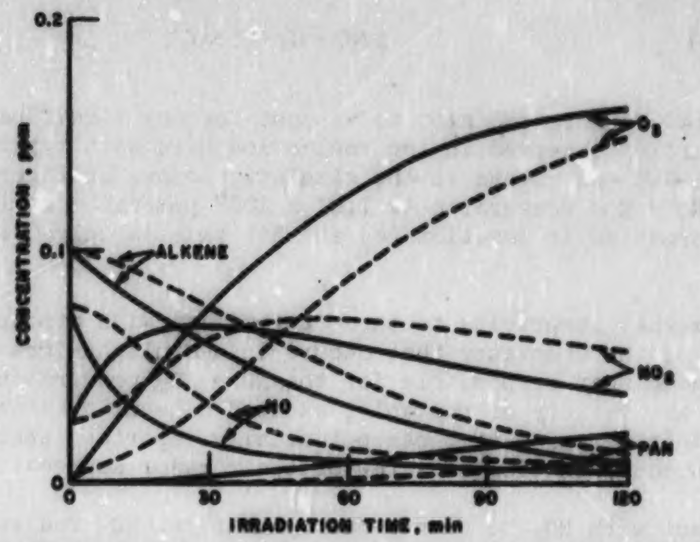

Figure 44. Theoretical rates of product formation in a computer simulated, sunlight-irradiated ($z = 40°$) NO_x-hydrocarbon-aldehyde-polluted atmosphere; initial concentrations (ppm) for the solid curves: $[NO_2]^\circ = 0.025$; $[NO]^\circ = 0.075$; $[C_4H_8]^\circ = 0.10$; $[CH_2O]^\circ = 0.10$; $[CH_3CHO]^\circ = 0.06$; $[CO] = 10$; $[CH_4] = 1.5$; relative humidity, 50% (25°C); dashed curves same but aldehyde concentrations are zero initially.

k_1 represents the apparent first-order rate constant for $O(^3P)$ atom formation in reaction (I) in the urban atmosphere. It is related to the integral over the wavelength range $2900 < \lambda < 4300$ Å to the product of the solar irradiance in the lower atmosphere at a given wavelength times the absorption coefficient of NO_2 at that λ, times the quantum yield of $O(^3P)$ formation from NO_2 at λ. We have estimated for a solar zenith angle $z = 40°$ and typical atmospheric conditions near sea level, $k_1/k_3 = 0.021$ ppm[127]. Thus from relation (I) we expect only very low levels of O_3 (< 0.01 ppm) to build up in an atmosphere which is loaded with a mixture of the oxides of nitrogen which is typical of the early morning hours: $[NO_2]/[NO] = 0.3$. For reasons which we will explore in detail later, the $[NO_2]/[NO]$ ratio increases dramatically as the sunlight irradiation of the pollutant mixture continues, and the $[O_3]$ is expected in theory to follow this change approximately in accord with relation (I). Thus for the simulation shown in Figure 44 (solid curves) the values of the ratio $[O_3][NO]/[NO_2]$ are 0.0188, 0.0191, 0.0194, 0.0197, 0.0193 ppm at 10, 30, 60, 90, and 120 min, respectively, very near the theoretical magnitude of k_1/k_3 for the conditions chosen. Since the NO, NO_2, and O_3 comprise a chemical system which is continually undergoing change, the $[O_3]$ at any time lags about a minute or two behind the value expected for a true photostationary state. Although subsequent improvements in the theoretical and experimental estimates of the ratio k_1/k_3 are necessary and expected, it appears from all available data that O_3 development occurs largely through the simple sequence of reactions (1-3) as Leighton suggested years ago[139].

The real problem in the kinetic treatment of the ozone build up lies in the realistic description of the processes which control the NO to NO_2 conversion rate. The reaction (4) can be important in generating a small level of NO_2 (up to 25% of the NO_x) during the early stages of the dilution of the exhaust of the automobile, the power plant, or other sources which often contain 500 ppm of NO initially.

$$(4) \qquad 2\,NO + O_2 \rightarrow 2\,NO_2$$

However reaction (4) is much too slow to account for any significant fraction of the NO → NO_2 conversion observed in the real atmosphere with typical ambient levels of NO, 0.05-0.5 ppm. Thus in the simulation shown in Figure 44, the observed rate of NO → NO_2 conversion is 1.87×10^{-3} ppm-min^{-1} at 10 min while the rate of NO_2 formation in reaction (4) at this time is only 0.0046×10^{-3} ppm-min^{-1}.

It may be somewhat surprising to those unfamiliar with atmospheric reactions to find that most of the chemistry that occurs in a sunlight-irradiated urban atmosphere, including that responsible for the NO → NO_2 conversion, involves the interaction of a vast variety of unstable, excited molecules, atoms, and free radicals. The origin of a few of these potentially important species can be appreciated from a consideration of a few of their major sources.

Ozone may react with NO_2 to create the symmetrical NO_3 radical in (5):

$$(5) \qquad O_3 + NO_2 \rightarrow NO_3 + O_2$$

The NO_3 species forms N_2O_5 by reaction with NO_2 or oxidizes NO to NO_2:

$$(6) \qquad (+\,M)\; NO_3 + NO_2 \rightarrow N_2O_5\; (+\,M)$$

$$(7) \qquad NO_3 + NO \rightarrow 2\,NO_2$$

N_2O_5 may dissociate to reform NO_3 and NO_2 or possibly react with water to generate nitric acid:

$$(8) \qquad (+\,M)\; N_2O_5 \rightarrow NO_3 + NO_2\; (+\,M)$$

$$(9) \qquad N_2O_5 + H_2O \rightarrow 2\,HONO_2$$

The two electronically excited and chemically reactive singlet molecular oxygen species, $O_2(^1\Delta_g)$ and $O_2(^1\Sigma_g{}^+)$, are produced in the atmosphere by direct absorption of sunlight in reactions (10a) and (10b), by electronic energy transfer from electronically excited $NO_2{}^*$ molecules formed by sunlight absorption by NO_2 at wavelengths greater than 4000 Å which provide insufficient energy to dissociate NO_2 in reaction (1), or by ozone photolysis in sunlight, reaction (12):

$$\begin{array}{ll} (10a) & \\ & O_2 + \text{sunlight} \begin{cases} 12{,}700\ \text{Å} \rightarrow O_2(^1\Delta_g) \\ 7{,}600\ \text{Å} \rightarrow O_2(^1\Sigma_g{}^+) \end{cases} \\ (10b) & \end{array}$$

$$(11) \qquad NO_2{}^* + O_2 \rightarrow NO_2 + O_2(^1\Delta_g)$$

$$\begin{array}{ll} (12a) & \\ (12b) & O_3 + \text{sunlight} \begin{cases} 2900\text{-}3060\ \text{Å} \rightarrow O_2(^1\Delta_g) + O(^1D) \\ 2900\text{-}3500\ \text{Å} \rightarrow O_2 + O(^1D)\text{: or } O(^3P) + O_2(^1\Delta_g, {}^3\Sigma_g{}^-) \\ 4500\text{-}7000\ \text{Å} \rightarrow O_2 + O(^3P) \end{cases} \\ (12c) & \end{array}$$

The $O(^1D)$ species formed in (12a) and (12b) is much more reactive than the $O(^3P)$ ground state atom; it reacts efficiently when it collides with a water molecule to form an important transient in smog, the hydroxyl radical:

$$(13) \qquad O(^1D) + H_2O \rightarrow 2\,HO$$

HO may react with NO to give nitrous acid in (14) or with NO_2 to give nitric acid in (15):

$$(14) \qquad HO + NO\ (+\,M) \rightarrow HONO\ (+\,M)$$

$$(15) \qquad HO + NO_2\ (+\,M) \rightarrow HONO_2\ (+\,M)$$

A small concentration of HONO is expected to appear in the polluted atmosphere as result of reactions (16)-(17) as well as (14), and it continues to supply another source of the HO radical in (18):

$$(16a) \qquad H_2O + NO + NO_2 \rightarrow 2\,HONO$$

$$(16b) \qquad 2\,HONO \rightarrow H_2O + NO + NO_2$$

$$(17) \qquad HO_2 + NO_2 \rightarrow HONO + O_2$$

$$(18) \qquad HONO + h\nu(2900\text{–}4100\ \text{Å}) \rightarrow HO + NO$$

However the homogeneous components of the rates of the reactions (16a) and (16b) are uncertain (see footnote in the introduction to this section).

A careful review of the net results of the occurrence of reactions (1)-(18) which we have outlined here will reveal that these reactions alone cannot explain the rapid conversion of NO to NO_2 observed in the atmosphere. In fact if these reactions alone occurred, we would expect that the original supply of NO_2 in our atmosphere to be depleted somewhat as irradiation with sunlight occurred, and a small and nearly constant $[O_3]$ would be created in a very few minutes. The key to the observed NO to NO_2 conversion lies in a sequence of reactions between the transient species which have been generated and the other reactive molecules such as carbon monoxide, the hydrocarbons, and the aldehydes present in the polluted atmosphere. One such rational sequence of reactions was first delineated independently by two groups of scientists, Heicklen and coworkers[193] and Weinstock and coworkers[166]. They noted that a chain reaction involved the HO and HO_2 radicals and CO may be important in driving NO to NO_2 in the atmosphere:

$$(19) \qquad HO + CO \rightarrow H + CO_2$$

$$(20) \qquad H + O_2\ (+\,M) \rightarrow HO_2\ (+\,M)$$

$$(21) \qquad HO_2 + NO \rightarrow NO_2 + HO$$

Many cycles of the sequence of ((19), (20), (21), (19)...) may occur and many molecules of NO may be oxidized to NO_2 for each HO radical that is formed originally.

Several other molecules present in the polluted atmosphere can assume the potentially important role suggested for CO. Thus the aldehydes and hydrocarbons may carry the chain and reform HO_2 radicals from HO radicals. With formaldehyde the path is fairly simple:

(22) $HO + CH_2O \rightarrow H_2O + HCO$

(23) $HCO + O_2 \rightarrow HO_2 + CO$

(21) $HO_2 + NO \rightarrow HO + NO_2$

The aldehydes in the polluted atmosphere can function in another fashion to generate the seemingly important HO_2 radical[194]. Thus formaldehyde is decomposed by sunlight according to the reactions (24a) and (24b):

(24a) $CH_2O + \text{sunlight } (3700\text{-}2900\ \text{Å}) \rightarrow H + HCO$

(24b) $\rightarrow H_2 + CO$

Both the formyl radical and the H atom formed in (24a) will react in air largely to form HO_2 through (20) and (23).

A direct clue to additional steps in the mechanism of smog formation is had from smog chamber studies of hydrocarbon-NO-NO_2 mixtures and the atmospheric studies of the changes in the relative composition of the hydrocarbon pollutants as the day progresses. For example, Stephens and Burleson[195] found that the complex mixture of hydrocarbon pollutants sampled in the atmosphere of the early morning, contained a much greater fraction of olefinic hydrocarbons than a similar sample taken in the late afternoon. Similar direct observations were made on the composition of products of trapped auto exhaust-polluted air before and after irradiation with ultraviolet lamps in the laboratory[195-196]. The clear implication of these results is that the chemical reactions initiated in the complex NO-NO_2-hydrocarbon mixtures by the action of sunlight remove the olefinic hydrocarbons at a much higher rate than the paraffinic hydrocarbons. A great variety of excellent work in both industrial and government laboratories has helped establish various reactivity scales for hydrocarbons based on the relative ability of the hydrocarbons to generate NO_2 from NO in chamber experiments[197]. From these experiments and many others, scientists have concluded that one or more intermediate species present in smog must react with the olefins and ultimately creat HO_2 radical and organic peroxy radicals which stimulate the observed NO to NO_2 conversion. Of course the olefins are transparent to the sunlight within the lower atmosphere so they themselves are not acted upon by the sunlight. However, when an olefin is added to an irradiated mix of the oxides of nitrogen in air, we expect its removal to be relatively rapid through the attack on it by the various reactive intermediates which we have discussed. Thus in the case of the alkene, propylene, the following primary reactions may occur with these species:

(25a) $$O + CH_3CH{=}CH_2 \rightarrow \dot{C}_3H_6\dot{O}$$

(25b) $$\rightarrow HO + CH_2{=}CH\dot{C}H_2$$

(26) $$O_3 + CH_3CH{=}CH_2 \rightarrow [CH_3\overline{\dot{C}HCH_2OO\dot{O}}]$$

(27a) $$HO + CH_3CH{=}CH_2 \rightarrow H_2O + CH_2{=}CH\dot{C}H_2$$

(27b) $$\rightarrow CH_3\dot{C}HCH_2OH$$

(27c) $$\rightarrow CH_3CHOH\dot{C}H_2$$

(28a) $$HO_2 + CH_3CH{=}CH_2 \rightarrow CH_3\dot{C}HCH_2O_2H$$

(28c) $$\rightarrow H_2O_2 + CH_2{=}CH\dot{C}H_2$$

(29) $$NO_3 + CH_2CH{=}CH_2 \rightarrow HONO_2 + CH_2{=}CH\dot{C}H_2$$

(30) $$O_2(^1\Delta_g) + CH_3CH{=}CH_2 \rightarrow CH_2{=}CHCH_2O_2H$$

A great variety of chemical reactions, many of which remain unclear, follow the formation of the initial products of reactions (25)-(30); even the extent of the partitioning of (27) between the several modes which are alternate in theory, is not well established today[127]. We will analyze the nature and the extent of all of these reactions following the somewhat arbitrary but reasonable scheme of Demerjian et al. Regardless of the details of these schemes, one important result of all those proposed to date is the ultimate generation of some number (α) of HO_2 radicals, some number (β) of alkylperoxy (RO_2) or acylperoxy ($RCOO_2$) radicals, and a variety of different molecules which are largely aldehydes, ketones, and acids:

(31) HO (or other intermediate in the mixture) + RH (alkene, alkane, aromatic hydrocarbon, aldehyde, etc.) →

$$\alpha\, HO_2 + \beta\, RO_2 \text{ (or } RCOO_2\text{) + other products}$$

The HO_2 radicals formed as a result of HO-alkene interactions in (31) may react as before to cause the NO to NO_2 conversion in (21). Presumably the alkylperoxy and acylperoxy radicals formed in (31) may oxidize NO as well in reactions (32) and (33), the analogues to (21) involving HO_2 radicals:

(32) $$RO_2 + NO \rightarrow RO + NO_2$$

(33) $$RCOO_2 + NO \rightarrow RCO_2 + NO_2$$

The notorious peroxyacyl nitrates, of which peroxyacetyl nitrate is the most common ($R = CH_3$), will form in the atmosphere on the association of acylperoxy radicals with NO_2[198]:

(34) $$RCOO_2 + NO_2 \rightarrow RCOO_2NO_2$$

There has been much speculation and a large uncertainty as to the relative importance of the various atmospheric intermediates in the attack on the olefin hydrocarbons in smog. Leighton[139] pointed to the probable importance in photochemical smog of O-atom and O_3-molecule reactions with the olefinic hydrocarbons. From the data available to him in 1961 he was unable to evaluate the relative importance of these reactions compared to those for the transients such as HO, HO_2, NO_3, alkoxy, and alkylperoxy radicals, and singlet oxygen, $O_2(^1\Delta_g)$ and $O_2(^1\Sigma_g^+)$. Since that time several investigators have given further insight into the probable importance of some of these possible reactions. Thus it appears to be generally accepted now that the theoretically calculated combined rate of attack of $O(^3P)$ atoms and O_3 molecules on olefinic hydrocarbon molecules in the photooxidation of NO-olefin systems in air may be significantly less than the experimentally observed rate of olefin loss in such systems[199]. Recently Heicklen[193] and Weinstock[166] and their coworkers have presented evidence that the HO radical plays a major role in both the NO-CO and the NO-olefin photooxidation chains in photochemical smog simulation studies. Also Bayes[200-202], Pitts[203], Kummler[204], and Berry[205] and their research groups have stimulated interest in reactions of singlet oxygen, $O_2(^1\Delta_g)$, in the atmosphere. Among the many other possible reactions, the participation of this species in the olefinic hydrocarbon removal reactions in photochemical smog has been suggested. The extent of this involvement has remained untested. Recently Stephens and Price[131b], Wilson et al.[131a], and Louw et al.[206] have speculated on the possible significant participation of NO_3 and N_2O_5 in the chemistry of polluted air. Demerjian, Kerr, and Calvert[127] considered this problem in their study completed in 1972. Using an updated kinetic data base we will consider this system here.

The data of Figure 45 provide our best estimates of the rates of attack of the various reactant species on the alkene for conditions used in Figure 44 (dashed curves). The height of the ordinant between the two curves defining the rate for a given species should be compared. Obviously the kinetic data suggest that the HO radical is the dominant olefin reactant for irradiation times up to 120 min; ozone becomes increasingly important as its concentration climbs. The rates of HO_2 radical attack appear to be somewhat less significant at all times. Note that although $O(^3P)$ atom formation in reaction (1) is by far the fastest photochemical reaction in the simulated smog mixture ($d[O(^3P)]/dt = 2.98 \times 10^{-2}$ ppm-min^{-1} at 30 min, aldehyde-free system), the reaction of $O(^3P)$ with O_2 is so much faster than those with the alkene and the aldehydes that $O(^3P)$ is only a minor source of reactions which drive NO to NO_2, The rates of attack on alkene for the CH_3O, NO_3, and $O_2(^1\Delta_g)$, presumed to be present in the simulated smog mixture, are also unimportant in this regard, 9.7×10^{-7}, 6.4×10^{-8}, and 3×10^{-9} ppm min^{-1}, respectively, at 30 min. When one compares the rate of the attack on the aldehydes by the transient species, a much greater discrimination which favors the HO reactions is seen than in the case of the alkene reactions. For the simulations shown in Figure 44, about 99% of the total rate of the H-abstraction reactions from the aldehydes occurs by the HO radical in reaction (22) and its analogues.

Now examine in greater detail the rates of the various reactions which are responsible for the net NO → NO_2 conversion at the shorter times. These data are given in Table XXXVI as derived from the computer simulation corresponding to Figure 44 (solid curves). Note that at 10 min into the simulation NO_2 is being destroyed by photodissociation at a rate which is 268.3×10^{-4} ppm-min^{-1}. Several other loss reactions shown contribute another 9.3×10^{-4} ppm-min^{-1} to the total loss rate of 277.6×10^{-4} ppm-min^{-1}. You will note that NO_2 is being formed at 10 min largely by reactions (3), (21), and (32),

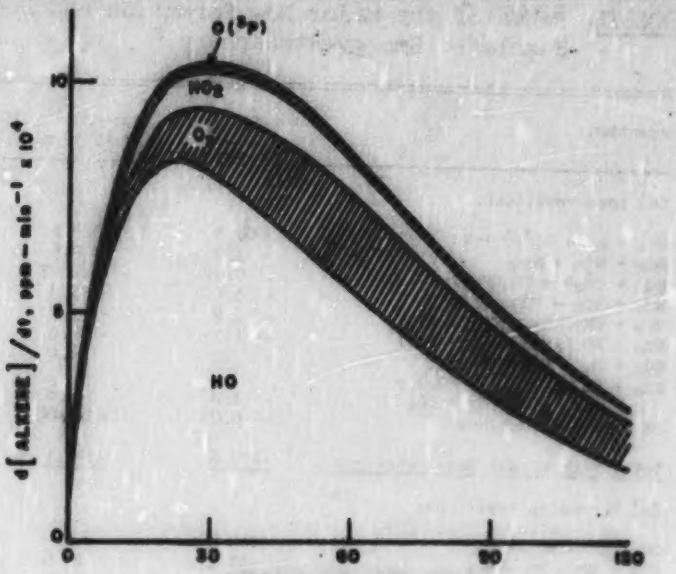

Figure [illegible] Theoretical rates of reaction of various free radical species with alkene in the simulated sunlight-irradiated, polluted atmosphere of Figure 4-4 (no initial aldehydes).

(3) $O_3 + NO \rightarrow NO_2 + O_2$

(21) $HO_2 + NO \rightarrow NO_2 + HO$

(32) $RO_2 + NO \rightarrow NO_2 + RO$

for which the rates are 240.7×10^{-4}, 17.0×10^{-4}, and 35.1×10^{-4} ppm-min^{-1}, respectively. The other reactions shown contribute 3.5×10^{-4} ppm-min^{-1} to the total rate of formation at 10 min, 296.3×10^{-4} ppm-min^{-1}. Thus the net rate of NO_2 formation given either by the tangent to the $[NO_2]$-time plot at 10 min or by the summation of the individual reaction rates, is $(296.3-277.6) \times 10^{-4} = 18.7 \times 10^{-4}$ ppm-min^{-1}. The situation changes at longer times as the supply of many of the reactants is exhausted; the rates of formation and destruction become equal as $[NO_2]$ maximizes near 30 min, and there is a net rate of loss of NO_2 at 60 min. Thus the detailed mechanism predicts that the oxidation of NO to NO_2 is really promoted by HO_2 and RO_2 radicals; it is suggested that the alkyl peroxyl radicals are about twice as important as the HO_2 species in the early stages of the reaction.

From the rate data summarized in Tables XXXVII to XLIII we can trace the origin of the HO_2 and RO_2 radicals to derive the theoretical relative importance of the various reactants and reactions as the sources of these important species. In Table XXXVII it can be seen that HONO photolysis is the major primary source of the HO radical, while the formaldehyde and acetaldehyde photolyses are the major primary sources of the HO_2 and RO_2 radicals. Note that these sunlight induced rates of generation of the radicals HO_2 (6.11×10^{-4}) and RO_2 (4.33×10^{-4}

TABLE XXXVI. Rates of the Major NO_2 Formation and Decay Reaction in a Simulated Smoggy Atmosphere.[a]

Reaction	$d[NO_2]/dt$, $ppm\text{-}min^{-1} \times 10^4$ At 10 min	At 30 min	At 60 min
(a) Loss reactions:			
$NO_2 + h\nu \rightarrow O(^3P) + NO$	-268.3	-323.2	-285.1
$NO_2 + NO_3 \rightarrow N_2O_5$	- 1.0	- 9.6	- 22.7
$NO_2 + CH_3O \rightarrow CH_3ONO_2$	- 0.07	- 0.07	- 0.05
$HO_2 + NO_2 \rightarrow HONO + O_2$	- 3.5	- 5.3	- 5.0
$NO_2 + CH_3COO_2 \rightarrow CH_3COO_2NO_2$	- 1.2	- 1.9	- 2.3
$NO_2 + HO\ (+M) \rightarrow HONO_2\ (+M)$	- 1.1	- 1.1	- 1.0
$NO_2 + O_3 \rightarrow NO_3 + O_2$	- 1.2	4.0	- 5.8
$NO_2 + HCOO_2 \rightarrow (HCOO_2NO_2) \rightarrow HONO_2 + CO_2$	- 1.2	- 1.8	- 1.9
Other loss reactions	- 0.04	- 0.08	- 0.08
Total rate of all loss reactions	-277.6	-347.1	-323.9
(b) Formation reactions:			
$O_3 + NO \rightarrow NO_2 + O_2$	240.7	295.0	265.0
$RO_2 + NO \rightarrow RO + NO_2$	35.1	24.6	15.6
$HO_2 + NO \rightarrow HO + NO_2$	17.0	9.3	5.4
$N_2O_5 \rightarrow NO_2 + NO_3$	1.0	9.6	22.7
$NO_3 + NO \rightarrow 2NO_2$	2.3	7.8	11.4
$CH_3COO_2NO_2 + NO \rightarrow 2NO_2 + CH_3CO_2$	0.1	0.2	0.3
Other formation reactions	0.1	0.1	0.3
Total rate of all formation reactions	296.3	346.6	320.4
Net rate of formation of NO_2	+18.7	-0.5	-3.5

[a] Initial concentrations (ppm) of reactants: $[NO_2]^\circ$, 0.025; $[NO]^\circ$, 0.075; [*trans*-2-$C_4H_8]^\circ$, 0.10; $[CH_2O]^\circ$, 0.10; $[CH_3CHO]^\circ$, 0.06; $[CO]^\circ$, 10; $[CH_4]^\circ$, 1.5; relative humidity, 50% (298°K); solar zenith angle, 40°.

$ppm\text{-}min^{-1}$ at 10 min) are not sufficient to account for the rate of the reactions $HO_2 + NO \rightarrow RO + NO_2$ (35.1×10^{-4} $ppm\text{-}min^{-4}$). Obviously there is a chain reaction involving these species and CO, CH_2O, CH_3CHO, and C_4H_8 molecules which develops the "extra" radicals which help drive NO to NO_2. For the reactant conditions which we have chosen in the simulation here, the chain length for the various species can be estimated. In Table XXXVIII we see the accounting of the rates of the major photochemical and thermal reactions leading to HO formation and destruction. Similar bookkeeping is shown for the HO_2 and the RO_2 radicals in Tables XXXIX and XL, respectively. The chain lengths for the various species calculated from these data are summarized in Table XLI. Thus at 10 min into the simulated sunlight irradiation, chain lengths are of the order of 8 for the HO and RO_2 species and about 4 for the HO_2 radical. These lengths decrease at longer times as the olefin is consumed. Termination of the chains occurs by a variety of reactions involving all the radical species; the major processes are shown in Table XLII. It is seen that the termination of chains by HO_2-HO_2 interaction and HO_2-NO_2 disproportionation are highly favored over reactions involving HO, RO and RO_2 radicals. This accounts for the shorter chain lengths involving the HO_2 radical. We see as expected that the rate of radical removal in the termination reactions is equal within the

Table XXXVII. The Theoretical Primary Rates of the Major Radical Generation Reactions in the Simulated Polluted Atmosphere.[a]

Reaction	------ Rate, $ppm\text{-}min^{-1} \times 10^4$ ------ At 10 min	At 30 min	At 60 min
a) HO formation:			
$HONO + h\nu \rightarrow HO + NO$	2.45	4.99	5.27
$O_3 + h\nu \rightarrow O(^1D) \ldots (+H_2O) \rightarrow 2HO$	0.07	0.19	0.31
$H_2O_2 + h\nu \rightarrow 2HO$	0.06	0.25	0.62
$NO_2, O_3 + h\nu \rightarrow O(^3P) \ldots (+RH) \rightarrow HO$	0.005	0.007	0.007
Total primary rate of HO formation	2.58	5.44	6.21
b) HO_2 formation:			
$CH_2O + h\nu \rightarrow H + HCO$	(2.13)	(2.23)	(2.20)
$H + O_2 \rightarrow HO_2$	2.13	2.23	2.20
$HCO + O_2 \rightarrow HO_2 + CO$	1.52	1.59	1.57
$CH_3CHO + h\nu \rightarrow CH_3 + HCO$	(1.85)	(2.37)	(2.70)
$HCO + O_2 \rightarrow HO_2 + CO$	1.32	1.69	1.93
$O_3 + C_4H_8 \rightarrow HO_2 \ldots$	1.14	2.12	1.89
Total primary rate of HO_2 formation	6.11	7.63	7.59
c) RO_2 formation:			
$CH_2O + h\nu \rightarrow H + HCO$	(2.13)	(2.23)	(2.20)
$HCO + O_2 \rightarrow HCOO_2$	0.61	0.64	0.63
$CH_3CHO + h\nu \rightarrow CH_3 + HCO$	(1.85)	(2.37)	(2.70)
$HCO + O_2 \rightarrow HCOO_2$	0.53	0.68	0.77
$CH_3 + O_2 \rightarrow CH_3O_2$	1.85	2.37	2.70
$NO_2, O_3 + h\nu \rightarrow O(^3P) \ldots (+RH) \rightarrow RO_2$	0.20	0.18	0.09
$O_3 + C_4H_8 \rightarrow RO_2 \ldots$	1.14	2.12	1.89
Total primary rate of RO_2 formation	4.33	5.99	6.08
Total primary rate of formation of all free radicals	13.0	19.1	19.9

[a] Initial concentrations of reactants as specified in Table XXXVI.

precision of our bookkeeping to the primary rate of radical generation.

Now we are in a position to investigate the net effect of each type of reactant on the rate of the NO conversion to NO_2 according to the chemical scheme adopted here. During the important early period of the irradiation in which the oxidation of NO is most rapid, we have estimated the percentage of the total rate of NO oxidation (by HO_2 and RO_2) which results directly from the participation of each of the major reactants. This breakdown is shown in Table XLIII. Clearly the results of this theoretical model confirm the common belief that the olefin is the major source of the HO_2 and RO_2 reactants (about 70% at 10 min) which convert to NO to NO_2 and hence establish the O_3 level through relation (I). The two aldehydes considered in our synthetic smog mixture contribute only about 12% each, while an even smaller amount, about 5%, of the NO → NO_2 conversion is a direct result of the CO reactions for the typical impurity concentrations chosen.

Table XXXVIII. Theoretical rates of the Major HO Formation and Loss Reactions in the Simulated Polluted Atmosphere.[a]

Reaction	------ Rate,	ppm-min^{-1} x 10^4	-----------
	At 10 min	At 30 min	At 60 min
a) Formation reactions:			
All photochemical sources (Table II)	2.58	5.44	6.21
$HO_2 + NO \rightarrow HO + NO_2$	17.00	9.32	5.36
$CH_3CHO_3H \rightarrow CH_3CHO + HO$	1.47	1.32	0.77
$HO_2 + O_3 \rightarrow HO + 2O_2$	0.09	0.31	0.54
Total rate of HO formation from all sources shown	21.1	16.4	12.9
b) Loss reactions:			
$HO + C_4H_8 \rightarrow HOC_4H_8$	11.28	7.10	3.80
$HO + C_4H_8 \rightarrow H_2O + CH_2CH{=}CHCH_3$			
$HO + CH_2O \rightarrow H_2O + HCO$	2.88	2.68	2.54
$HO + CH_3CHO \rightarrow H_2O + CH_3CO$	2.08	2.33	2.61
$HO + CO \rightarrow H + CO_2$	3.20	2.85	2.75
$HO + NO\ (+M) \rightarrow HONO\ (+M)$	0.60	0.25	0.12
$HO + NO_2\ (+M) \rightarrow HONO_2\ (+M)$	1.07	1.15	0.98
Total rate of HO destruction from all sources shown	21.1	16.3	12.8

[a] Initial concentrations of reactants as specified in Table XXXVI.

Table XXXIX. Theoretical Rates of the Major HO_2 Formation and Loss Reactions in the Simulated Polluted Atmosphere.[a]

Reaction	------ Rate,	ppm-min^{-1} x 10^4	-----------
	At 10 min	At 30 min	At 60 min
a) Formation reactions:			
$H + O_2\ (+M) \rightarrow HO_2\ (+M)$	5.33	5.08	4.95
(H from $HO + CO \rightarrow H + CO_2$	(3.20)	(2.85)	(2.75)
$CH_2O + h\nu \rightarrow H + HCO$)	(2.13)	(2.25)	(2.20)
$HCO + O_2 \rightarrow HO_2 + CO$	7.18	6.60	6.09
(HCO from $HO + CH_2O \rightarrow H_2O + HCO$	(2.17)	(1.88)	(1.64)
$CH_3CH(\dot{O})CHO \rightarrow CH_3CHO + HCO$	(2.41)	(2.00)	(1.77)
$CH_2O + h\nu \rightarrow H + HCO$	(1.61)	(1.56)	(1.42)
$CH_3CHO + h\nu \rightarrow HCO + CH_3$)	(0.99)	(1.16)	(1.24)
$CH_3O + O_2 \rightarrow HO_2 + CH_2O$	11.81	9.79	7.44
$CH_3CH(\dot{O})(\dot{O}) + O_2 \rightarrow HO_2 + CH_3CO_2$ (radical from O_3-C_4H_8 reaction)	1.14	2.12	1.89
$HCO_2 + O_2 \rightarrow HO_2 + CO_2$	1.63	0.84	0.55
Total rate of formation of HO_2	27.1	24.4	20.9
b) Destruction reactions:			
$HO_2 + NO \rightarrow HO + NO_2$	17.00	9.32	5.36
$HO_2 + O_3 \rightarrow HO + 2O_2$	0.09	0.31	0.54
$HO_2 + NO_2 \rightarrow HONO + O_2$	3.50	5.34	4.99
$HO_2 + C_4H_8 \rightarrow HO_2C_4H_8$	1.47	1.32	0.78
$2HO_2 \rightarrow H_2O_2 + O_2$	4.94	7.94	8.90
$CH_3O_2 + HO_2 \rightarrow CH_3O_2H + O_2$	0.09	0.22	0.33
Total rate of loss of HO_2	27.1	24.4	20.9

[a] Initial concentrations of reactants as specified in Table XXXVI.

Table XL. Theoretical Rates of RO_2 Formation and NO Oxidation to NO_2 by the Major RO_2 Radicals Formed in the Simulated Polluted Atmosphere.[a]

Radical	Primary sources of the radical	---- Rate, ppm-min^{-1}x10^4 --------- At 10 min	At 30 min	At 60 min
CH_3O_2	$CH_3 + O_2$;			
	a) CH_3 from CH_3CHO photolysis	1.85	2.33	2.70
	b) $CH_3CH(OH)\dot{O} \rightarrow CH_3 + HCO_2H$ (radical from HO addn C_4H_8)	8.05	5.05	2.71
	c) $CH_3CO_2 \rightarrow CH_3 + CO_2$	2.00	2.59	2.24
	[$CH_3CH(\dot{O})(\dot{O}) + O_2 \rightarrow CH_3CO_2 + HO_2$; radical from O_3 + C_4H_8]	(1.13)	(2.12)	(1.88)
	[$CH_3COO_2 + NO \rightarrow CH_3CO_2 + NO_2$; radical from HO attack on CH_3CHO]	(0.86)	(0.47)	(0.36)
$HCOO_2$	$HCO + O_2$; HCO from CH_2O and CH_3CHO photolysis and HO attack on CH_2O	1.63	0.84	0.54
CH_3COO_2	$CH_3CO + O_2$; CH_3CO from HO attack on CH_3CHO	0.87	0.47	0.36
$CH_3CH(OH)O_2$	Formed in reaction sequence following HO addn. to C_4H_8	8.03	5.05	2.70
$CH_3CH(OH)CH(\dot{O}_2)CH_3$		8.03	5.04	2.70
—O-O— $CH_3CH(\dot{O}_2)CHCH_3$	Formed in reaction sequence following H-abstraction from C_4H_8 by HO and other radicals	3.21	2.02	1.08
$CH_3CH(HO_2)CH(\dot{O}_2)CH_3$	Formed in sequence following HO_2 addn. to C_4H_8	1.47	1.31	0.76
$CH_3CH(CH_3O)CH(\dot{O}_2)CH_3$	Formed in sequence following CH_3O addn. to C_4H_8	0.02	0.01	0.00
Total rate of NO oxidation by all RO_2's shown (approximately equal to rate of RO_2 formation)		35.1	24.6	15.6

[a] Initial concentrations of reactants as specified in Table XXXVI.

The Theoretical Concentrations of HO and HO_2 in the Simulated Smoggy Atmospheres and Related Data from Real Atmospheres.

It is of some interest to the kineticists and spectroscopists to observe the concentrations of the HO and HO_2 species which are predicted to exist in the simulated atmosphere. These values are shown in Figure 46 for the conditions employed in the experiments used to construct Figure 44. The dashed curves and the solid curves, respectively, correspond to the simulations with and without aldehydes present initially. Values for [HO_2] climb to about 7 x 10^9 molec-cm^{-3} in the run with aldehyde present initially and to about 5.4 x 10^9 molec-cm^{-3} in the runs without initial aldehyde. The theoretical HO levels are much lower than those of HO_2, in the range of (2.7 ± 0.3) x 10^6 molec-cm^{-3} for these conditions. The concentration range of these transients is neither sensitive to alternative choices of most of the kinetic parameters employed nor to the initial concentrations of the impurities in our synthetic polluted atmosphere. The first of these points can be illustrated using the data of Figure 47. The rate constant

Table XLI. The Theoretical Chain Lengths for the HO, HO_2, and RO_2 Radical Reactions in the Simulated Polluted Atmosphere.[a]

Radical	Primary rate of generation, ppm-min^{-1} x 10^4	At 10 min	At 30 min	At 60 min
HO	Primary rate of generation, ppm-min^{-1} x 10^4	2.58	5.44	6.21
	Total rate all reactions, ppm-min^{-1} x 10^4	21.1	16.3	12.8
	Chain length	8.2	3.0	2.1
HO_2	Primary rate of generation, ppm-min^{-1} x 10^4	6.11	7.63	7.59
	Total rate all reactions, ppm-min^{-1} x 10^4	27.1	24.4	20.9
	Chain length	4.4	3.2	2.8
RO_2	Primary rate of generation, ppm-min^{-1} x 10^4	4.33	5.99	6.08
	Total rate all reactions, ppm-min^{-1} x 10^4	35.1	24.6	15.6
	Chain length	8.1	4.1	2.6

[a]Initial concentrations of reactants as specified in Table XXXVI.

Table XLII. The Theoretical Rates of the Major Chain Termination Reactions in the Simulated Polluted Atmosphere.[a]

Reaction	Rate of radical At 10 min	removal, At 30 min	ppm-min^{-1} x 10^4 At 60 min
$2HO_2 \rightarrow H_2O_2 + O_2$	4.94	7.94	8.90
$HO + NO\ (+M) \rightarrow HONO\ (+M)$	0.60	0.23	0.12
$HO + NO_2\ (+M) \rightarrow HONO_2\ (+M)$	1.07	1.15	0.98
$HO_2 + NO_2 \rightarrow HONO + O_2$	3.50	5.34	4.99
$CH_3O_2 + HO_2 \rightarrow CH_3O_2H + O_2$	0.09	0.22	0.33
$CH_3O + NO \rightarrow CH_3ONO$	0.02	0.01	0.00
$CH_3O + NO_2 \rightarrow CH_3ONO_2$	0.07	0.07	0.05
$CH_3O + NO_2 \rightarrow CH_2O + HONO$	0.01	0.01	0.01
$CH_3COO_2 + NO_2 \rightarrow CH_3COO_2NO_2$	1.21	1.85	2.26
$HCOO_2 + NO_2 \rightarrow (HCOO_2NO_2) \rightarrow HONO_2 + CO_2$	1.25	1.80	1.88
$NO_3 + HO_2 \rightarrow HONO_2 + O_2$	0.00	0.01	0.04
Total rate of HO, HO_2, RO, and RO_2 removal from above reactions	12.8	18.6	19.6
Total primary rate of HO, HO_2, RO, and RO_2 generation (Table II)	13.0	19.1	19.9

[a]Initial concentrations of reactants as specified in Table XXXVI.

Table XLIII. The Fractional NO → NO_2 Conversion Rate Due to the Various Reactants in the Simulated Polluted Atmosphere at 10 min into the Reaction.[a]

Radical		-- Rate of NO → NO_2 conversion, ppm-min^{-1} x 10^4 ----			
		CO	CH_2O	CH_3CHO	C_4H_8
HO_2		3.20	4.67(hν) 2.10(HO)	3.06(hν) 0.86(HO)	2.96(HO abst.) 8.03(HO addn.) 2.27[O_3, $O(^3P)$]
	Total	3.20	6.77	3.92	13.26
RO_2		0.00	0.36(hν) 0.49(HO)	2.07(hν) 1.73(HO)	24.09(HO addn.) 3.75(HO abst.) 1.13[O_3, $O(^3P)$] 1.47(HO_2 addn.) 0.02(CH_3O addn.)
	Total	0.00	0.85	3.80	30.46
%NO → NO_2 conversion directly attributable to reactant		5.1	12.2	12.4	70.3

[a] Initial concentrations of reactants as specified in Table XXXVI.

---

for the important HO_2 termination reaction (17), $HO_2 + NO_2 \rightarrow HONO + O_2$, was used as 5.0×10^{-2} ppm^{-1} min^{-1} here[127] rather than the value we now accept as much more reliable, $k_{17} = 2.9 \times 10^1$ ppm^{-1} min^{-1}[190]. Compare the curve representing the $[alkene]^o = 0.1$ ppm in Figure 47 with the solid curve for [HO] in Figure 46. Although the shape of the profile has changed significantly, the predicted levels of HO are of the same general magnitude, $(2.0 \pm 0.4) \times 10^3$ molec-cm^{-3}, as those observed in Figure 46 for the same initial concentrations of reactants, $(2.7 \times 0.4) \times 10^6$ molec-cm^{-3}. The relative insensitivity of [HO] to alkene level is seen in Figure 47. In these runs the $[alkene]^o$ was varied from 0.01 to 0.40 ppm while keeping all other reactants fixed as in the Figure 44 simulations. The highest levels for the HO radical are achieved at some intermediates value of the added alkene near 0.05 ppm. Increase or decrease of the alkene from this value lowers the [HO]-time profile somewhat. Of course the decrease at high [alkene] reflects in part the greater rate of its removal reaction involving the olefin. However the magnitude of the [HO] stays within the range $(2 \pm 0.7) \times 10^6$ molec-cm^{-3} over a wide range of olefin levels.

In Figure 48 compare the [HO]-time profiles expected in theory for the simulated smog-like atmospheres with varied $[NO]^o$ from 0.003 to 1.20 ppm. The rate of HO generation is very low for the mixtures at low $[NO_x]$; the HO removal rates are high, largely a result of HO attack on the alkene; this results in a rather low steady state concentrations of HO; e.g., $[HO] = 5 \times 10^5$ molec-cm^{-3} for the $[NO]^o = 0.01$ case. At somewhat higher NO levels the chain reaction involving $HO_2 + NO \rightarrow HO + NO_2$ becomes more important and HO levels rise. At very high NO concentrations the suppression of [HO] occurs in part through the reaction, $HO + NO_2\ (+ M) \rightarrow HONO_2\ (+ M)$ and the other chain termination reactions

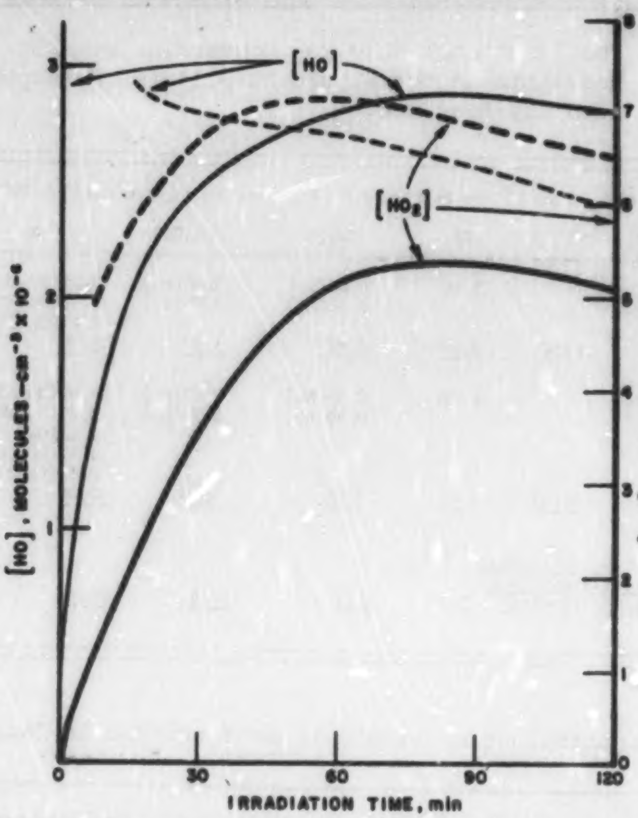

Figure 48. Theoretical HO and HO_2 concentrations as a function of irradiation time in the simulated sunlight-irradiated, polluted atmospheres of Figure 44dashed curves, aldehydes present initially; solid curves, aldehydes absent initially.

which involve NO_x; see Table XLII. Note again however that with variation of the $[NO]^o$ from 0.04 to 1.2 ppm the [HO] remains in the range $(2 \pm 1) \times 10^6$ molec-cm^{-3} over much of the time period shown.

The theoretical time profiles for the concentrations of HO and HO_2 in the simulated smog runs with varied CO are shown in Figure 49. Observe that the more significant effect of CO addition is on the [HO]. At [CO] = 50 ppm the reaction with CO becomes a dominant loss mechanism for HO. Nevertheless the range of [HO], $(2 \pm 1) \times 10^6$ molec-cm^{-3} is still not large. The changes in the $[HO_2]$ are much less pronounced as [CO] is increased from 1 to 50 ppm. A partial explanation of this effect which is expected in theory is that the HO_2 does not react significantly with CO, and its rates of generation and destruction (largely $2\ HO_2 \rightarrow H_2O_2 + O_2$ and $HO_2 + NO \rightarrow HO + NO_2$) remain about the same.

There is no direct measurement of the $[HO_2]$ in the real atmosphere of our smoggy communities, but we can make some qualitative estimates using the analytical data for H_2O_2 determined by Gay and Bufalini[207]. They estimated the concentrations of H_2O_2 in the smoggy atmospheres of several urban communities. The chemical kinetic and mechanistic data available to us today suggest that the major source of H_2O_2 in these atmospheres is the reaction, $2\ HO_2 \rightarrow H_2O_2 + O_2$.

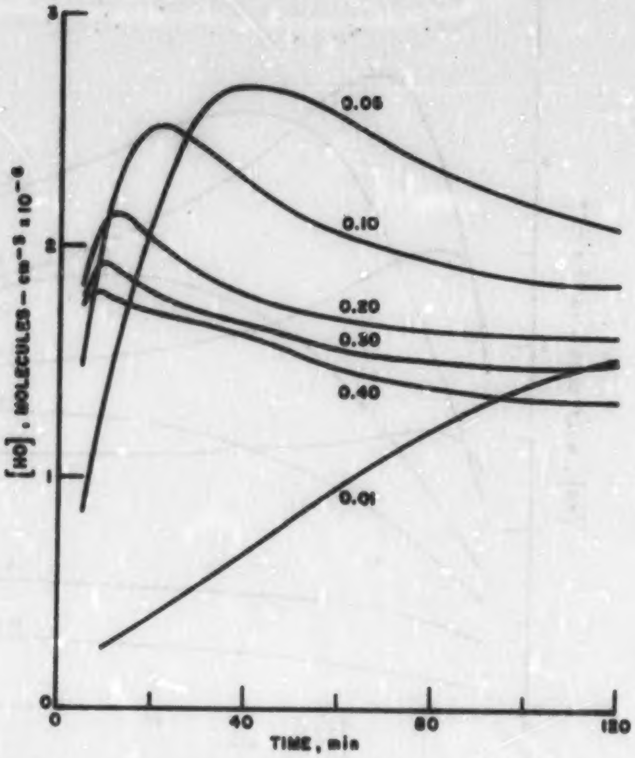

Figure 47. The theoretical effects of varied alkene concentration on the HO concentration in the simulated sunlight-irradiated, polluted atmospheres; concentrations of impurities as in Figure 44 except [alkene] is as shown (ppm); $k_{17} = 5.0 \times 10^{-3}$ ppm^{-1} min^{-1} is assumed in this case.

Our simulations show that the reactions such as $HO_2 + RCHO \rightarrow H_2O_2 + RCO$ are negligible in rate for the normal pollutant concentrations encountered. The rates of radical attack on H_2O_2 and H_2O_2 photolysis in sunlight are very slow and can be beglected here. H_2O_2 may be destroyed in the real atmospheres by a heterogeneous reaction with NO_2[208], but this is probably not fast. In Gay and Bufalini's experiments the $[H_2O_2]$ built up to values as high as 18 pphm in about 4.5 h period during a day of very severe smog in Riverside, California. More typical levels of H_2O_2 were those of 4 pphm found in the early afternoon hours during moderate photochemical smog episodes in Hoboken, N. J., and Riverside, California. If we assume a uniform rate of formation of H_2O_2 during the 4 or 5 h period of buildup to the 4 and 18 pphm levels attained then from the known rate constant for the $2\ HO_2 \rightarrow H_2O_2 + H_2O$ reaction (5.3×10^3 ppm^{-1} min^{-1}) we estimate that the average $[HO_2]$ during these measurements was in the range from 4×10^8 to 9×10^8 molec-cm^{-3}. These estimates correspond well to the range of levels estimated from our simulated polluted atmospheres in Figures 46 and 49; these varied from about 3×10^8 to about 7×10^8 molec-cm^{-3} for irradiation times longer than about 30 min, and they were relatively insensitive to the reactant concentrations over a rather wide range. Thus the limited available data on HO_2 seem to be in good accord with the expectations of our simulation. We may hope that the sensitivity of the new unambiguous spectroscopic

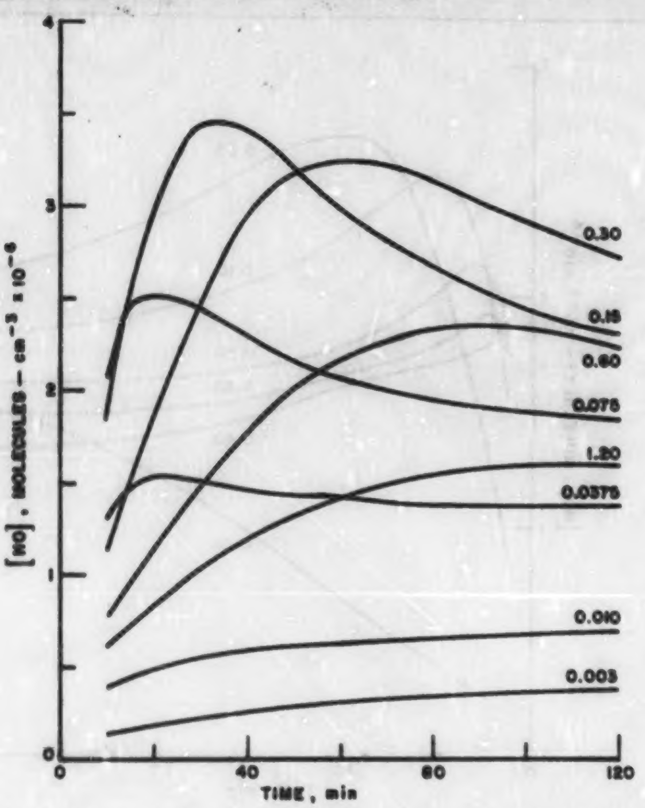

Figure 48. The theoretical effects of varied $[NO]^\circ$ on the HO concentration in the simulated sunlight-irradiated polluted atmospheres; concentrations of impurities as is shown in Figure 44 except $[NO]^\circ$ is as shown (ppm); $[NO]^\circ/[NO_2]^\circ = 3.0$; $k_{17} = 5.0 \times 10^{-5}$ ppm^{-1} min^{-1} is assumed in this case.

techniques for HO_2 detection will be extended to allow direct observations of the HO_2 concentrations in sunlight-irradiated, polluted urban atmospheres in the years ahead[209,210], and a much more critical test of reaction mechanisms can be had.

Direct measurements of the [HO] in air have been reported recently by Wang and Davis[211]. They detected the 3090 Å fluorescence of the HO radical excited with a tunable laser of output near 2825.8 Å. The monitored sample of air was brought into the apparatus from outside the Ford Motor Company research laboratories near Dearborn, Michigan with a transport time of about 6 s. The estimated concentrations of HO varied from 1.5×10^8 molec-cm^{-3} in the early afternoon (~ 2:00 P.M.) to 1.6×10^7 molec-cm^{-3} in the early evening (~ 6:00 P.M.). These experimental [HO] estimates are about a factor of 50 times higher than the concentrations predicted from all of our simulations; see Figures 46 47, 48, and 49. There seems to be little question that HO was the species seen in the experiments of Wang and Davis in view of its unique excitation spectrum, its rapid destruction when the incoming air was mixed with butane, and the careful detail given to the elimination of HO production by the laser beam itself. However in view of our simulations and other experimental results which we will consider, we question the accuracy of the absolute magnitude of the Wang and Davis estimate. We cannot visualize any other major sources

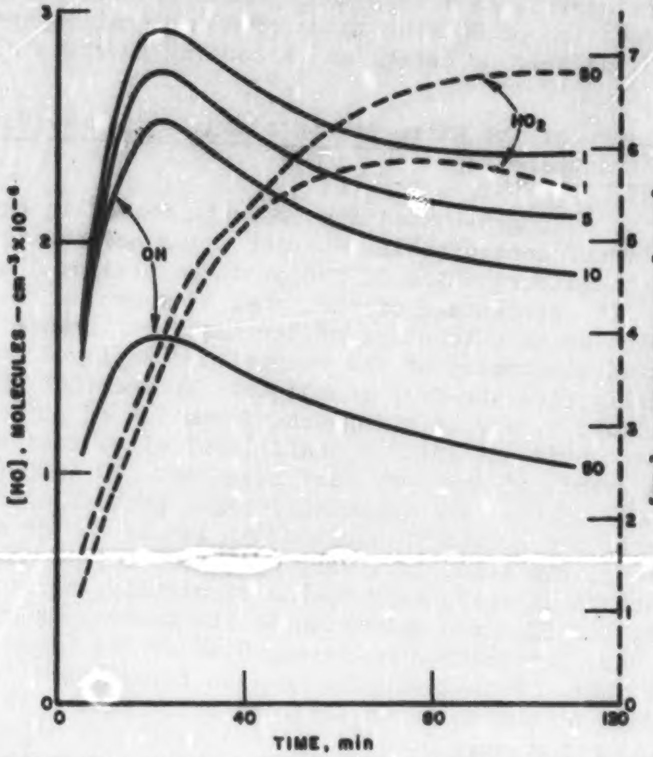

Figure 49. The theoretical effects of varied $[CO]^{\circ}$ on the HO and HO_2 concentrations in simulated sunlight-irradiated, polluted atmospheres; initial concentrations as in Figure 44 (aldehydes present); $[CO]^{\circ}$ (ppm) is as shown on curves; $k_{17} = 5.0 \times 10^{-2}$ ppm^{-1} min^{-1} is assumed in this case.

of HO than those included in our simulation, although this may indicate a weakness in the present authors rather than a problem in the results of Wang and Davis. Large variations in the proportions of the various impurity reactants was seen to have little effect on the [HO] in our simulations, so the difference cannot have its origin in some special blend of impurities in the Ford laboratories. It is important to realize that if the concentration of HO which was piped into the laboratory was at the 1.5×10^{8} molec-cm^{-3} level after a 6 s transport time, it would have to be even larger in the sunlight irradiated atmosphere itself; the decay of HO in the dark is reasonably rapid for typical impurity levels encountered. For HO at the concentrations reported by Wang and Davis the rates of impurity reactant removal in the polluted atmosphere would be unrealistically large: NO_2 would be removed at a rate greater than ~ 4 to 9% per min, depending on our choice of rate constant for reaction (15)[127,212]; the alkenes in this hypothetical atmosphere would be removed remarkably fast as well, greater than 15% per min for C_3H_6, 38% per min for iso-C_4H_8, and 64% per min for trans-2-C_4H_8. No such rates of removal of the impurity components of smog has ever been observed in irradiated atmospheric samples[195,196] and in the host of smog chamber experiments which have been reported through the years[197]. New direct measurements of the concentration of HO in the real urban atmospheres should be made to resolve this problem. When this is done again, the concentrations and the nature of the major impurities present in the air studied should be established within the same time period, and the dark decay time of the HO species determined. Such measurements would provide a much less ambiguous proof of the identification of HO, the modes of HO generation and destruction in the real atmosphere, and help to establish reasonably accurate simulation models.

Theoretical Mass Balance of the Nitrogen-Containing Compounds Formed in the Simulated Polluted Atmosphere

The nature of the nitrogen-containing products formed in photochemical smog has been a matter of considerable interest among scientists. It may be instructive to note the distribution of the products predicted by the present model. In Figure 50 the percentage of the total nitrogen which is present in a given compound is plotted as a function of the sunlight irradiation time for the synthetic polluted atmosphere of the composition employed in the mixture of Figure 44 for initially aldehyde-free reactants. We see that the conversion of NO to NO_2 is followed by a continuing transformation of NO and NO_2 into two major products, nitric acid and PAN. A small level of nitrous acid builds up rather quickly as a result of the very fast reactions, $HO + NO (+ M) \rightarrow HONO (+ M)$ and $HO_2 + NO_2 \rightarrow HONO + O_2$, but its reasonably rapid photochemical decay, $HONO + h\nu \rightarrow HO + NO_2$ prevents its growth to substantial levels in the atmosphere. Methyl nitrate, like nitric acid, is a very weak absorber of sunlight in the lower atmosphere, and it is reasonably stable chemically, so it is expected to accumulate; however, the CH_3O radical which is its source, is at very low concentrations. Thus very little CH_3ONO_2 forms; 0.4% of the total nitrogen is in this compound at 120 min. Methyl nitrite is also formed, but its rate of photochemical decomposition at the solar wavelengths below 4100 Å in the lower atmosphere restricts its growth; only 0.002% of the nitrogen is expected to be in the CH_3ONO. N_2O_5, not shown in Figure 50, also grows somewhat to account for another 0.24% of the nitrogen at 120 min. However it is highly speculative whether this compound will accumulate to this extent or be removed as nitric acid by reaction at moist aerosol surfaces. The transients NO_3 and HNO remain very low, amounting to only 7.4×10^{-3} and 5.7×10^{-8}%, respectively, of the total nitrogen at 120 min.

There are some data with which we can check the predictions of the model. Both PAN and nitric acid and its salts have been observed in the atmosphere of some cities, but generally PAN is in excess of the acid and its salts. In the real urban atmosphere nitric acid does not seem to build up to the extent that we predict from the present reactions scheme. Thus Miller and Spicer[213a] reported 24 h average $HONO_2$ concentrations in the Los Angeles area of about 3 ppb and 1-h average maximum values of 10 ppb. For the simulation shown in Figure 44, $HONO_2$ levels reach about 18ppb after 2 h of irradiation. Presumably the nitric acid created in the real atmosphere reacts with certain basic impurities which are present also, e.g., NH_3, the oxides of the metals, etc. The quantitative treatment of such heterogeneous reactions is not possible at this time, and no attempt has been made to include them in our mechanism. However, they must occur in the real atmosphere, and nitric acid may be converted efficiently to ammonium nitrate if the concentration of ammonia impurity is sufficiently high. Ammonium nitrate comprises approximately 10-15% of the total airborne particles in composite samples collected in the Los Angeles area over the year 1971-1972[213b]. One other factor may have contributed to an overestimation of the $HONO_2$ formed in our experiments. We used the Demerjian, Kerr, and Calvert[127] estimate of the rate constant for reaction (15). An equally reliable estimate of Tsang[212] is a factor of 3 lower for this constant. Thus if the Tsang estimate of k_{15} is used

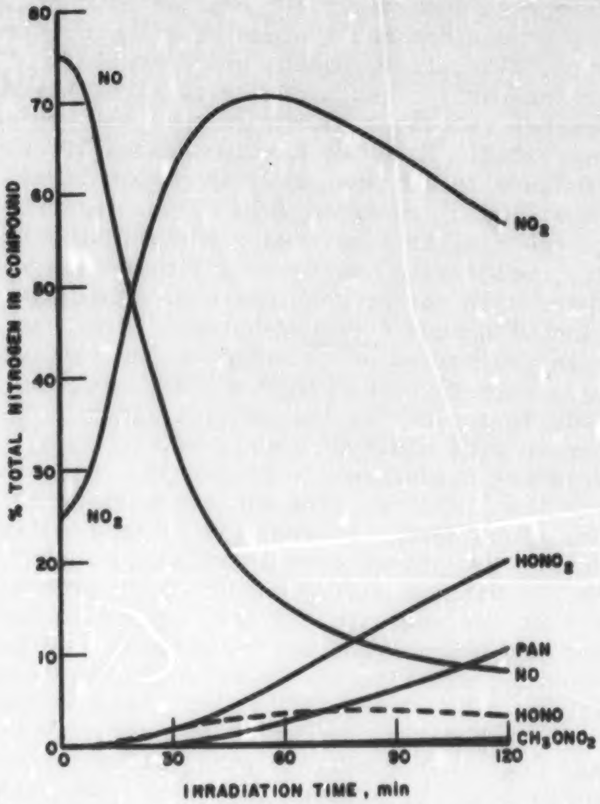

Figure 50. The time dependence of the theoretical composition of the nitrogen-containing compounds formed in the simulated, sunlight-irradiated polluted atmosphere of Figure 44 (no initial aldehydes).

in simulations like those in Figure 44, only 13 ppb of $HONO_2$ forms after 120 min. It follows that the amount of PAN and $HONO_2$ observed in our simulation could be more nearly equal with other reasonable choices of rate data.

The Effects of the Variation of the Concentrations of the Impurities on Product Formation in the Simulated Sunlight-Irradiated Polluted Atmosphere

The saturated "reactive" hydrocarbons. When n-butane is added to the components of the smog mixture at the 0.10 ppm level, there is little effect on the NO_2 oxidation rate, maximum O_3 reached etc. HO radicals do attack the alkanes at a moderate rate to abstract H atoms and generate alkyl peroxy and HO_2 radicals. However total rates of radical production are altered by only a few percent[127]. Thus with paraffin hydrocarbon additions at the levels near those of the olefins, the situation which exists in the real auto-exhaust-polluted atmosphere in the early morning hours[196], we can expect only a relatively small perturbation of the general reaction scheme outlined here for the simpler compositions.

The effects of variation of the olefinic hydrocarbon concentrations. Several observations have been made on the relationship of certain smog manifestations on the concentrations of hydrocarbons and the oxides of nitrogen. Thus Faith, Renzetti, and Rogers[215] derived the relation of eye irritation to NO_x and hydrocarbon levels in smog chamber studies shown in Figure 51. In Figure 52 the relationship between the maximum daily 1-h average oxidant levels and the 6-9 AM average concentration of non-methane hydrocarbons is shown for several cities as presented by Schuck, Altshuller, Barth, and Morton[216]. This is the relationship which was the basis of much of the original planning for the extent of control of hydrocarbon emissions to ensure that the ambient air standard for ozone would not be exceeded. Note the maximum values of oxidant observed define a curve which falls with decrease in hydrocarbon level, but the shape of the curve is obscure at low hydrocarbon values, the region of greatest interest. It is instructive to see similar predicted correlations with our model of the simulated atmosphere, recognizing the serious limitations which any such theoretical treatment must have with our present state of knowledge. The time dependence of ozone as a function of alkene (trans-2-butene) level was determined in computer simulations. In two series of experiments the initial concentrations of the oxides of nitrogen were fixed at $[NO]^{\circ} = 0.075$, and $[NO_2]^{\circ} = 0.025$ ppm, and the alkene was varied; in one series the initial aldehyde levels were taken at zero and in the other initial aldehyde levels were: $[CH_2O]^{\circ} = 0.10$, $[CH_3CHO]^{\circ} = 0.06$ ppm. The effects are summarized in Figure 53. Here the 8-h integrals of the $[O_3]$ vs. time and the [PAN] vs. time plots are shown as a function of the olefin concentration. Such dosage sources are of particular interest in health related considerations. The dashed curves and solid curves, respectively, correspond to runs with and without aldehydes initially present. The important point to observe is that the variation of the integrated oxidant and PAN levels with the initial olefinic hydrocarbon concentration, so important in our determinations of standards, are altered dramatically by the initial presence of aldehydes. A reference value of the $\int_0^{480}[O_3]dt$ data is had by the horizontal dashed line drawn at 38.6 ppm-min, the value of this integral if the maximum allowable 1-h average $[O_3]$ in the ambient air quality standards of the EPA were maintained for the 8 h. It appears from these data that the O_3 standard could not be met if the aldehydes remained high, $[CH_2O] = 0.10$, $[CH_3CHO] = 0.06$ ppm, even if nearly all of the olefinic hydrocarbon were removed. Also observe the theoretically expected large enhancement of the integrated [PAN]-time levels which results when the aldehydes are present; acetaldehyde is the main cause of this effect. We should learn from these data that the "true" relationship between nonmethane hydrocarbons and maximum 1-h oxidant at low hydrocarbon levels could be a critical function of a variable which is not routinely measured now, namely the concentration of the impurity aldehydes.

The effects of variation of the concentrations of the nitrogen oxides. It has been recognized for years from the results of smog chamber experiments that there is an inhibiting effect on product rates and certain smog manifestations seen at very high nitric oxide concentrations. Note for example in Figure 51 that if one considered the variation in eye irritation with runs at a fixed total hydrocarbon concentration of about 4.5 ppm, then the expected eye irritation passes through a maximum level and decreases again as runs at increasing $[NO_x]$ are considered. The inhibiting effect of high [NO] has been observed in product rate data determined by Tuesday and coworkers in smog chamber experiments using alkene-NO_x mixtures[197a]. We have applied our smog simulation model to this case as well. We calculated the time dependence of the theoretically expected ozone and PAN concentrations for runs at fixed hydrocarbon levels: $[C_4H_8]^{\circ} = 0.10$ ppm, $[\text{aldehydes}]^{\circ} = 0$; $[CO]^{\circ} = 10$ ppm; $[CH_4]^{\circ} = 1.5$ ppm; 50% relative humidity; the initial ratio $[NO]^{\circ}/[NO_2]^{\circ}$ was held constant at 3.0. The significance of these calculations is seen in the data of Figure 54. The 8-h

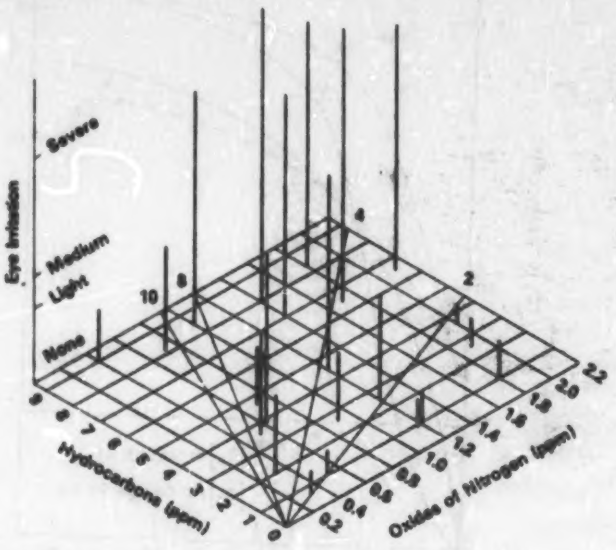

Figure 51. Relation of eye irritation to hydrocarbon and oxides of nitrogen levels in smog chamber experiments from Faith, Renzetti, and Rogers[215].

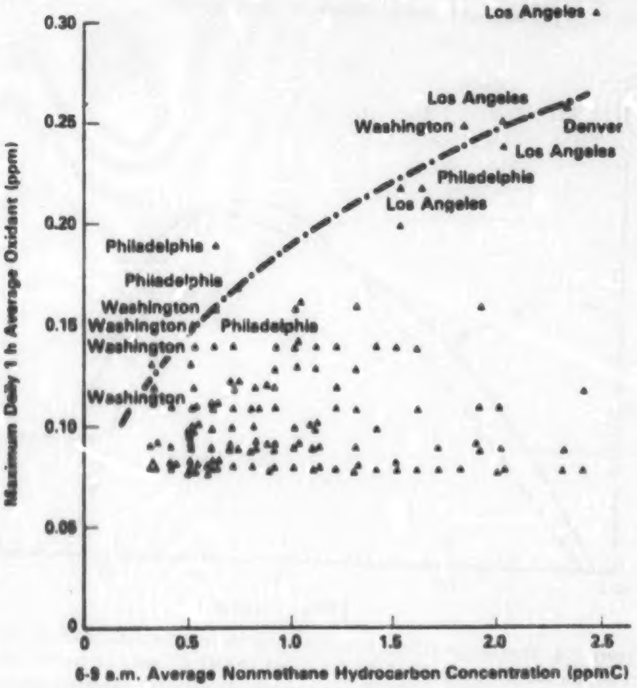

Figure 52. Relationship between the maximum daily 1-h average oxidant levels and the 6-9 AM average concentration of nonmethane hydrocarbons derived from the data from several cities, from Schuck, Altshuller, Barth, and Morgan[216].

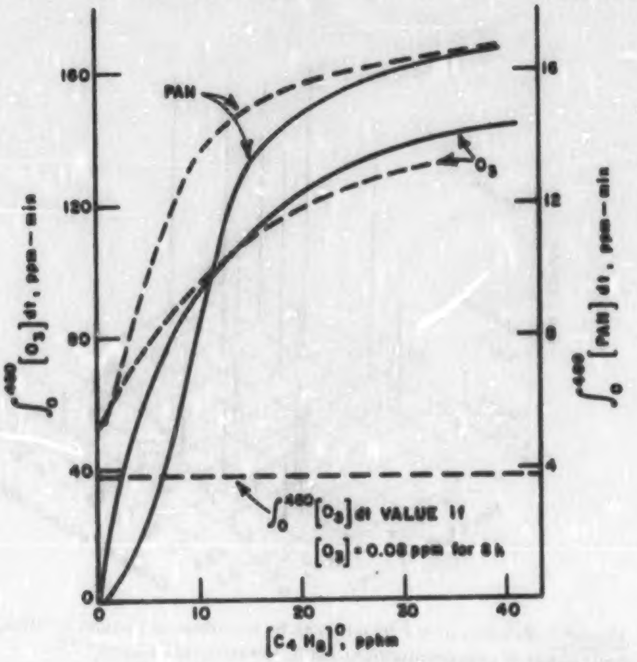

Figure 53. The theoretical effect of the reactive hydrocarbon concentration on the 8-h integral of the $[O_3]$ and [PAN] vs. time data derived from the simulated sunlight-irradiated, polluted atmospheres; reactant conditions as in Figure 44 dashed curves, aldehyde present; solid curves, aldehydes absent initially.

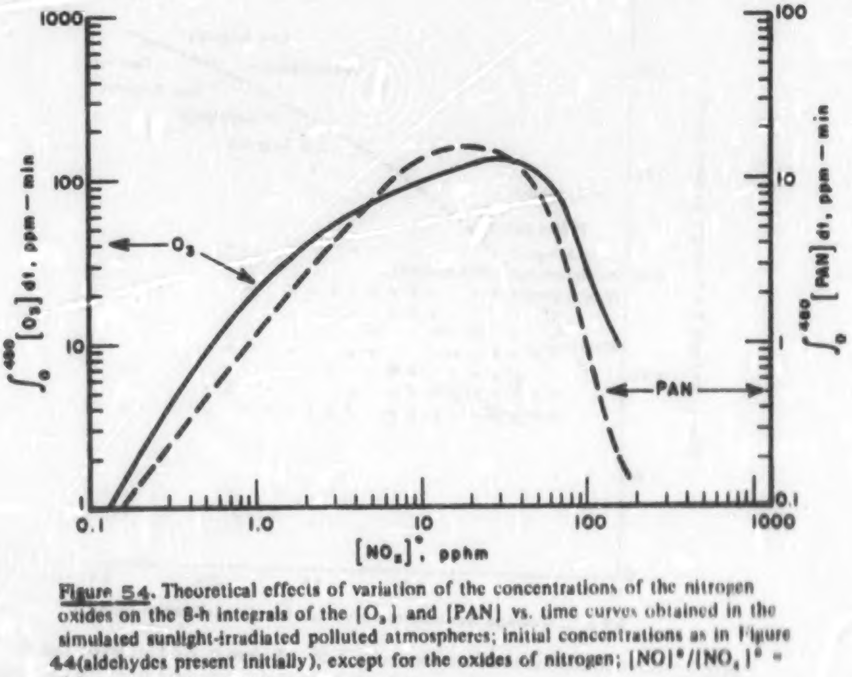

Figure 54. Theoretical effects of variation of the concentrations of the nitrogen oxides on the 8-h integrals of the $[O_3]$ and [PAN] vs. time curves obtained in the simulated sunlight-irradiated polluted atmospheres; initial concentrations as in Figure 44 (aldehydes present initially), except for the oxides of nitrogen; $[NO]^0/[NO_2]^0 = 3.0$.

integral of $[O_3]$- and [PAN]-time data are given as a function of the initial [NO]. As one progresses from the very low level of $[NO]^\circ = 0.15$ to 15 pphm there is a gradual increase in the magnitude of the integrals, but further increases of $[NO]^\circ$ to 30, 60, and 120 pphm cause a suppression in the dosage curves. The maximum in the integrals occurs near the stoichiometric mixture of the alkene and NO_x. These data should not be interpreted to imply that if unrestricted emissions of NO_x were allowed, our smog problem would be solved. Of course one must be concerned about the health effects of elevated NO_x levels themselves. However it seems the problems of large O_3 and PAN concentrations would be delayed in time to some extent.

In this regard compare the $[O_3]$ vs. time data given in Figure 55. The initial concentrations (ppm) of the reactants in the simulation were: [alkene] = 0.10; [CO] = 10; $[CH_2O]^\circ = 0.10$; $[CH_3CHO] = 0.06$; $[CH_4]^\circ = 1.5$; the relative humidity was chosen to be 50% (25°C); $[NO]^\circ/[NO_2]^\circ = 3.0$. The initial level of NO was taken as 0.15 ppm in one case and 0.375 ppm in the other. Note that at the lower NO level the ozone climbs above 0.1 ppm after about 45 min of irradiation. However about two hours are required for the mixture at the higher initial [NO] to climb above 0.1 ppm level of O_3, although the final level reached after 6 h is not much lower than that of the mixture with $[NO]^\circ = 0.15$ ppm. The delay in ozone growth in the run at $[NO]^\circ = 0.375$ ppm results from the additional time necessary for the $NO \rightarrow NO_2$ conversion reactions to transform the larger quantity of NO with basically the same radical supply, and to establish a suitable high ratio of $[NO_2]/[NO]$ necessary to produce a significant concentration of ozone.

One other factor which bears on the problem of smog suppression through regulation of the NO pollutant levels can be illustrated in Figure 56. This was constructed from simulations in which the ratio of impurities was held constant; $[CO]^\circ : [C_4H_8]^\circ : [NO]^\circ : [NO_2] : [CH_2O]^\circ :: 100 : 1 : 0.75 : 0.25 : 1 : 0.6$, but the concentration was changed over a 100-fold range: [alkene] = 0.01 to 1 ppm. The solid curves are for mixtures in which aldehydes are not present initially and the dashed curves are for runs with aldehydes. Note from these data that the dosages of ozone and PAN are not simple linear functions of the impurity concentrations. Thus if a 10-fold dilution of the highly polluted atmosphere occurs as an air mass moves across an air basin, the simulation suggests that as little as a 3.8-fold reduction in the potential O_3 8-h dosage may result. With a 100-fold dilution as little as a 23-fold reduction in the ozone dosage could result. Recent experience in the Los Angeles area probably relates to the two phenomena described here. The ozone levels appear to be down somewhat in downtown Los Angeles compared to previous years, probably as a result of the [NO] increase which has occured in recent years; yet very high levels of O_3 and other smog products are seen in the Riverside area after some modification of the Los Angeles mixture has occurred in route and the air mass has been transported to Riverside by the prevailing atmospheric motion.

Effects of variation in the initial carbon monoxide concentrations. At relatively low levels of CO in NO_x-hydrocarbon polluted atmospheres there is no dramatic effect seen in the rates of products formed in simulation runs; see Figure 57. An increase in the initial concentration of CO from 10 to 50 ppm decreases somewhat the O_3 and PAN concentrations for a given sunlight exposure time. As we have discussed previously, most of the attack on the hydrocarbons and aldehydes occurs by HO radicals which are generated in the smog system. The reaction of HO with CO becomes competitive with that of the

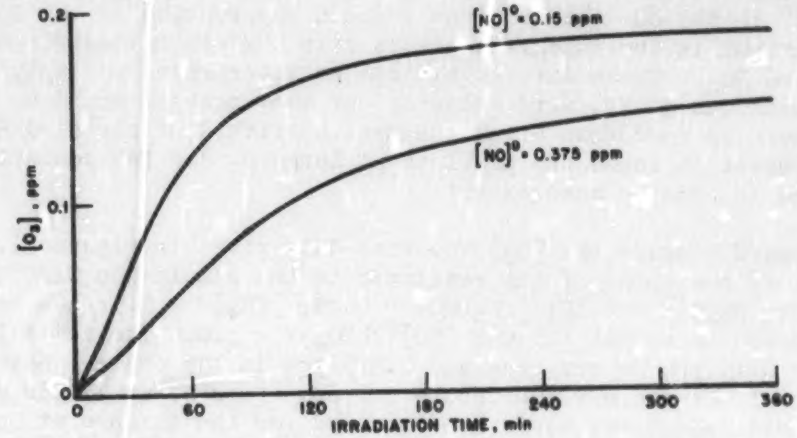

Figure 55. Theoretical effect of increased $[\mathrm{NO}]^\circ$ on the $[\mathrm{O}_3]$-time profile in simulated sunlight-irradiated, polluted atmospheres; impurity concentrations as in Figure 44 (aldehydes present initially), except for the oxides of nitrogen; $[\mathrm{NO}]^\circ/[\mathrm{NO}_2]^\circ = 3.0$; $[\mathrm{NO}]^\circ$ as shown on the curves.

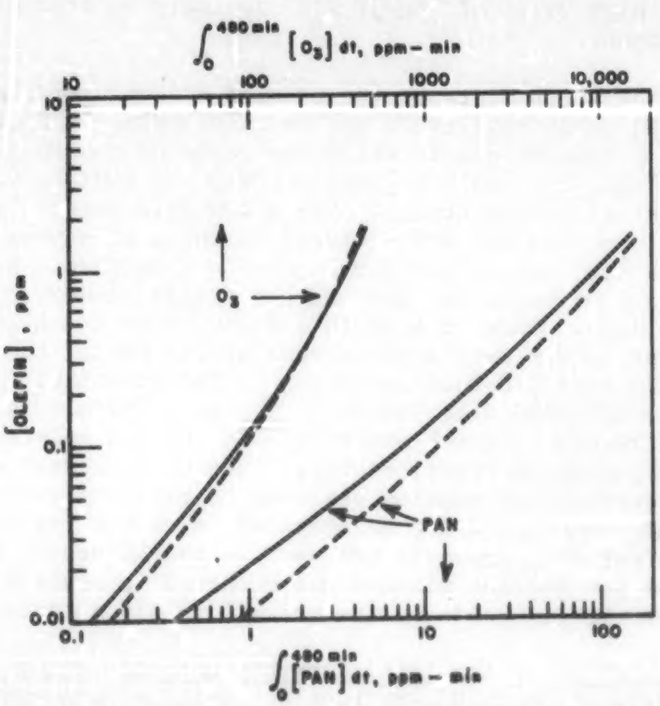

Figure 56. The theoretical effect of the dilution of a highly polluted atmosphere on the 8-h integrals of the $[\mathrm{O}_3]$ and $[\mathrm{PAN}]$ vs. time curves obtained in simulated sunlight-irradiated, polluted atmospheres; initial pollutant concentration ratios held constant: $\mathrm{CO:C_4H_8:NO:NO_2:CH_2O:CH_3CHO}$: 100:1:0.75:0.25:1:0.6 for dashed curves; aldehydes were absent initially in the solid curves.

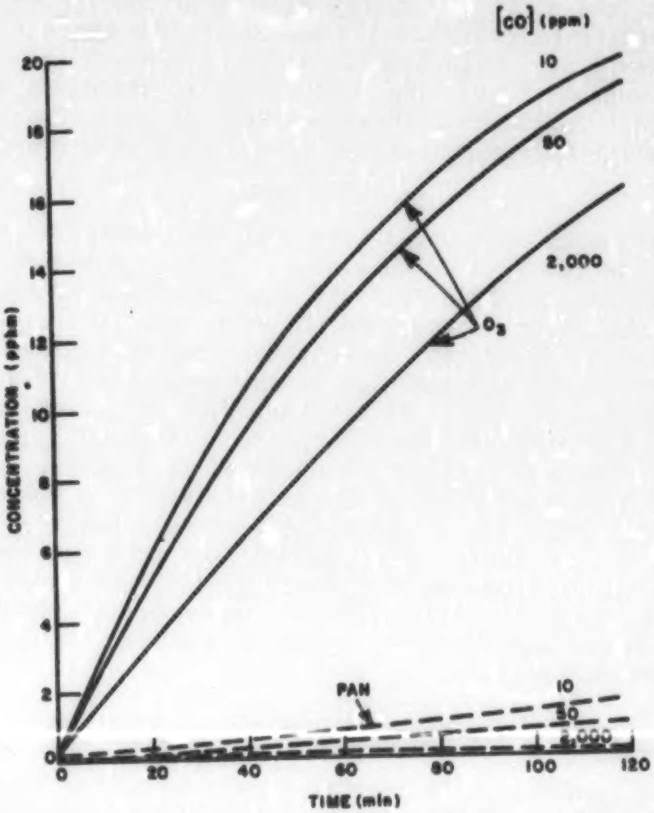

Figure 57. The theoretical effect of variation of the initial concentration of the carbon monoxide on the O_3 and PAN formation in a simulated sunlight-irradiated, polluted atmosphere; concentrations as in Figure 44 (aldehydes present initially) and $[CO]^0$ as shown with the curves; $k_{19} = 5 \times 10^{-2}$ assumed in this case.

alkenes and aldehydes at the higher CO concentrations, and an increasing share of the chain regeneration of the HO_2 radicals from HO is then born by the sequence (19)-(21). Lowered attack of HO on aldehyde and alkene occurs with resulting lowered rates of alkylperoxy and acetylperoxy radical formation. Thus at higher [CO] we tend to lose some of the boost in the NO to NO_2 conversion associated with the alternative chain processes involving the hydrocarbons and aldehydes. As a result of O_3 concentrations are lowered somewhat. The lowered rate of CH_3COO_2 radical generation results in large part from the less important attack of HO on acetaldehyde and alkene, and this is reflected in a lowered PAN concentration since PAN comes largely for the following sequence:

(35) $CH_3CHO + HO \rightarrow CH_3CO + H_2O$

(36) $CH_3CO + O_2 \rightarrow CH_3COO_2$

(37) $CH_3COO_2 + NO_2 \rightarrow CH_3COO_2NO_2$

We see in Figure 57 that at extremely high levels of CO (2000 ppm), PAN formation is practically eliminated since attack of HO on acetaldehyde and alkene is no longer competitive with the CO reaction (19). Obviously we would not suggest that PAN formation be reduced in our polluted atmospheres by removing controls on CO emissions; the toxic properties of this compound alone then outweigh the useful influence gained in theory by PAN reduction. Some free radical scavengers have been considered by Heicklen and coworkers as possible inhibitors of smog formation[217]. However the chain lengths in these systems are not very great and relatively large amounts of even the most effective additives would be necessary to have a significant influence. There are few, if any, compounds which would not introduce a health hazard as serious as the smog when present at useful smog inhibiting levels.

One other previously unexpected aspect of the chemistry of CO-containing atmospheres should be reviewed briefly here. If the hydrocarbon and aldehyde impurities were entirely removed from the atmosphere and CO allowed to rise along with the oxides of nitrogen, then CO may be a relatively effective reactant to pump NO to NO_2, and significant ozone levels may be achieved[168]. In this case the only driving force for the reaction is the generation of HO radicals from nitrous acid photolysis in (18). If the reactions of nitrous acid formation and destruction (16a, 16b) occur in the atmosphere, either homogeneously or heterogeneously, at rates comparable to those observed in chambers, then the CO-effect can be significant for relatively small ambient levels of NO_x and CO. In theory sunlight-irradiated, moist air contaminated with only NO, NO_2, and CO at 0.075, 0.025, and 50 ppm, respectively, could generate ozone concentrations approaching the 1-h maximum level of 0.08 ppm of the air quality standards after about two and one-half hours of sunlight irradiation. One expects in theory that the same kind of influence noted here for CO, in mixtures of the reactive alkanes with NO_x, but free from alkenes.

Effects of SO_2 Addition on the Reactions in the Simulated Polluted Atmospheres

The available quantitative information related to the chemistry of SO_2 in the urban atmosphere leaves many unanswered questions. However interest in the sulfur dioxide removal mechanisms in the urban atmosphere remains high among atmospheric scientists. The potentially harmful health effects associated with urban atmospheres containing moderately low levels of SO_2 and the apparent enhancement of these effects when there is a significant concentration of suspended particulates and a relatively high humidity, have stimulated this interest. The special problem of aerosols containing high sulfate levels has focused new concern on atmospheric SO_2 levels since the recent CHESS report[1]. However there is now little evidence as to the chemical nature of the active species responsible for these observed effects. The detailed mechanism of sulfur dioxide oxidation in the urban atmosphere remains unclear. The majority of existing evidence suggests that a major fraction of the sulfur dioxide is ultimately converted to sulfuric acid and sulfate salts, but the intermediate species involved and the reaction paths which lead to these products are open to question.

The relatively slow rates of photooxidation of sulfur dioxide in air exposed to sunlight[6-8], and the demonstrated catalytic influence of certain solids and moisture on the rate of SO_2 oxidation[9-15] have led to the common belief that heterogeneous paths for SO_2 oxidation probably far outweigh the homogeneous modes. Although this conclusion is probably true for the overcast, high humidity conditions which prevailed during the Donora and London episodes in 1948 and 1952, respectively, it is by no means established that the conclusion is true for the sunny, NO-NO_2-hydrocarbon-polluted atmospheres often encountered today. There is a real question as to the availability of sufficient reactive metallic oxide, catalyst particles, and acid-neutralizing compounds in many atmospheres to promote

SO_2 removal by heterogeneous reactions at the observed rates. The most compelling argument which has favored the importance of the heterogeneous removal processes has been the apparent lack of alternative homogeneous reaction paths of sufficient rate which might be involved. This situation has changed some in recent years. Many research groups, including our own, have suggested some possible paths, and these are summarized in Table XLIV. Shown are the approximate enthalpy changes

---

Table XLIV. Estimated Enthalpy Changes, Rate Constants of Possible Homogeneous Elementary Reaction Paths for SO_2 in a Polluted Urban Atmosphere.

Reaction	$-\Delta H_{298}$, kcal/mol	k[a]	Reference
(38) $SO_2 + h\nu\ (O_2) \rightarrow SO_3$	24	$\Phi_{SO_3} \cong 3 \times 10^{-4}$	218
(39) $O(^3P) + SO_2\ (+M) \rightarrow SO_3\ (+M)$	83	2.7×10^9	240
(40) $O_3 + SO_2 \rightarrow SO_3 + O_2$	58	$<5 \times 10^{-3}$	128
(41) $NO_2 + SO_2 \rightarrow SO_3 + NO$	10	5.3×10^{-9}	222
(42) $NO_3 + SO_2 \rightarrow SO_3 + NO_2$	33	<4.2	128
(43) $N_2O_5 + SO_2 \rightarrow SO_3 + N_2O_4$	24	$<2.5 \times 10^{-2}$	128
(44) 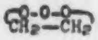 $\overset{O-O-O}{CH_2—CH_2} + SO_2 \rightarrow SO_3 + 2CH_2O$	81	?	221,223
(45) $\cdot CH_2OC\cdot + SO_2 \rightarrow SO_3 + CH_2O$	117	?	221,223
$CH_2=O{\bullet}O + SO_2 \rightarrow SO_3 + CH_2O$	85	?	
(46) $HO_2 + SO_2 \rightarrow HO + SO_3$	19	1.8×10^5	230
(47) $HO_2 + SO_2 \rightarrow HO_2SO_2$	>25	?	
(48) $CH_3O_2 + SO_2 \rightarrow CH_3O + SO_3$	30	$\sim 1.8 \times 10^5$	(estd.)
(49) $CH_3O_2 + SO_2 \rightarrow CH_3O_2SO_2$	>25	?	
(50) $HO + SO_2\ (+M) \rightarrow HOSO_2\ (+M)$	~37	3.4×10^8 2.4×10^8	231 232
(51) $CH_3O + SO_2 \rightarrow CH_3OSO_2$	~30	$\sim 1.8 \times 10^6$	(estd.)

[a] Units on rate constants, $l\ mol^{-1}s^{-1}$ for all reactions but 38 (dimensionless) and 39 ($l^2 \cdot mol^{-2}s^{-1}$).

---

for the reactions and the rate constants where they are known or can be estimated approximately. All of the reactions shown are rather exothermic and are favored from the viewpoint of thermodynamics. However the reactions (38)-(43), including the photooxidation of SO_2, and oxidation by $O(^3P)$, O_3, NO_2, NO_3, and N_2O_5, appear to be severely rate limited. If one couples the quantum yield data of Cox[218] for the photooxidation of SO_2 in air with our estimated solar absorption rates of SO_2 at $z = 40°30$, the rates of SO_2 removal by the as yet unresolved detailed mechanism of photooxidation, are very small. The Cox estimate of Φ_{SO_3} is somewhat lower than that of Allen, McQuigg, and Cadle[48], and it is considerably greater than that of Friend, et al.[219]. However use of any of these rate data does not alter the conclusion that the overall reaction (38) is relatively slow in the lower atmosphere. The $O(^3P)$ reaction (39) is also slow but not negligible; we will include this in our simulation. The homogeneous rate constant for (40) is reported by several workers to be too low to measure; for example see Cadle[220]. Daubendiek and Calvert[128] recently derived the upper limit for k_{40} given in Table XLIV. Cox and Penkett[221] found a measurable rate of reaction (40) corresponding to as much as 0.07% conversion of SO_2 per hour, but it seems to us that this may result from heterogeneous reactions. On the basis of our estimate of k_{40} we conclude that (40) is unimportant as a homogeneous removal path of SO_2. The rate data for reaction (41) were obtained by extrapolation to 298° K of the data of Boreskov and Illarionov[222] obtained in experiments at 434-504° K; its significant participation in the SO_2 removal paths in the atmosphere is also excluded. The reactions (42) and (43) have been considered and envoked to explain quantitatively product trends observed in some previous smog chamber work[131,206], but our recent estimates[128] also rule out their significant contribution in the urban atmosphere.

The reactions (44) and (45) of Table XLIV have been suggested recently by Cox and Penkett[221,223] from kinetic studies of synthetic olefin-ozone-SO_2 mixtures at low concentration. They found that SO_2 is oxidized at an appreciable rate by some reactive species formed in the dark on reaction between ozone and alkene. The rate of 3% SO_2 removal per hour was observed when the alkene was cis-2-pentene, while with propylene a rate of 0.4% per hour was seen. They suggested that two likely candidates for the specific oxidizing agent in these experiments are the ozonide of the alkene shown for that of ethylene in reaction (44) of Table XLIV, and the so-called "zwitterion" intermediate formed in the O_3-alkene reaction. Ripperton et al.[224] also suggested this role for the zwitterion. Wilson et al.[225], favor this interpretation in their computer simulation of the Cox and Penkett reaction rate from cis-2-butene-ozone-SO_2 mixtures. The structure and reactivity of the zwitterionic species can be considered to be diradical in character (as shown for the intermediate resulting from ethylene in the first reaction (45) shown in Table XLIV) or it may be like an aldehyde oxide in structure (as shown for the second reaction (45)). In either case there seems to be little doubt that such transients would have very high reactivity. However that one or both of these species may be the agent which oxidizes SO_2 in these systems is open to question. For example if the $\cdot CH_2OO\cdot$ entity is generated in the O_2-rich atmosphere, it has several paths of reaction which appear to be rapid in theory. We have speculated that the following sequence will generate the $\cdot OCH_2O\cdot$ radical[127].

(52) $\cdot CH_2OO\cdot + O_2 \rightarrow \cdot OOCH_2OO\cdot$

(53)

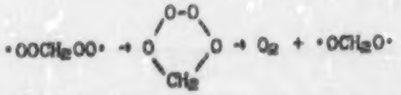

O'Neal and Blumstein[226] postulate that the same intermediate $\cdot OCH_2O\cdot$ will be generated quickly in the sequence (54), presumably in the absence of O_2.

(54)

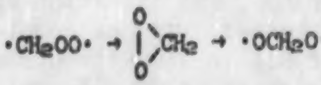

In any case the $\cdot OCH_2O\cdot$ species might be expected to form very quickly in air from the initial fragmentation product, $\cdot CH_2OO\cdot$. We have pictured it reacting further with O_2 to generate other radical species; e.g., $\cdot OCH_2O\cdot + O_2 \rightarrow HCO_2 + HO_2$; $HCO_2 + O_2 \rightarrow CO_2 + HO_2$, both very exothermic reactions. O'Neal and Blumstein suggested that the destruction of the $\cdot OCH_2O\cdot$ species (again presumably in an O_2-free system) occurs through H-atom transfer to form formic acid. If new

Reproduced from best available copy.

transients are sought to oxidize SO_2 in dilute O_3-alkene-air mixtures it seems to us that the $\cdot OCH_2O\cdot$ species (or its analogues in the higher alkenes) or other radical species derived from it, might be a better choice than the original diradical fragment $\cdot CH_2OO\cdot$ (the so-called zwitterionic species). There is abundant evidence that the fragmentation of the initial ozonide formed from the simple alkenes creates highly excited free radicals including HO and other molecular species[227]. The chemiluminescence from such excited species of the C_2H_4-O_3 reaction observed even at atmospheric pressure is sufficiently intense to allow its use as a detection system for ozone today. In the Demerjian Kerr, and Calvert mechanism of the O_3-alkene reactions which we employed in this study, the HO_2, HCO_2, CH_3CO_2, CH_3O_2, and other radicals are presumed to be formed in subsequent reaction of the initial diradical species with oxygen[127]. O'Neal and Blumstein[226] have suggested several other paths of ozonide decomposition which better explain some of the chemiluminescent products observed in O_3-alkene reactions[227]. The reactions of HO and HO_2 with SO_2 are fast and it is reasonable to expect that other free radicals not yet studied may react rapidly with SO_2 as well. One cannot at this point in time assess the rate constants for reactions such as (44) and (45) since the observed reactions may be due to the other reactive free radicals formed in these reactions. Thus we have not included reactions (44) and (45) as elementary reactions in our simulations.

The HO_2 and HO radical reactions (46) and (50) have been studied recently, and present kinetic data indicate their potential importance[230-232]. We have included these reactions in our simulations. The analogous reactions of CH_3O_2 (reaction (48)) and CH_3O (reaction (51)) would appear to be potentially significant as well, although there are no experimental estimates of these rate constants available; our rough "theoretical" estimates are shown in Table XLIV.*

There are no experimental kinetic data now available on the potentially significant HO_2 and CH_3O_2 addition reactions (47) and (49). Our estimates[127] for the analogous addition reactions of these radicals with alkenes, based largely on the considerations of Lloyd[229], suggest that these reactions have considerably smaller rate constants (1/10,000th) than those of the HO addition. If this relationship is maintained for the SO_2 system then the reactions (47) and (49) would remove SO_2 at a rate of less than 0.1% per h for a typical smog mixture. We will neglect these reactions in our simulation although their true importance remains uncertain.

Little is now known about the ultimate fate in the urban atmosphere for the initial free radical products of the radical addition reactions ((47), (49), (50), and (51)), although we have speculated about the nature of these reactions[233,93,234]. Presumably radical addition to SO_2 would be followed by subsequent steps which will lead to sulfuric acid, peroxysulfuric acid, alkyl sulfates, and various other theoretically possible precursors to sulfuric acid, nitric acid, and the salts of these acids. All of the compounds should ultimately give sulfuric acid, sulfate, peroxysulfate, nitrate, or nitrite salts as a further modification of the primary products would occur, probably in a dynamic liquid phase on an aerosol particle. One such reaction sequence which we felt may be important in urban atmospheres and which will illustrate the possible mechanism for HO attack on SO_2 in the following:

---

*In deriving our estimates given in Table XLIV we have made the assumption that $k_{48} = k_{46}$. One would expect in theory that the preexponential factor for these reactions would be nearly the same, and the activation energy for reaction (48) may be somewhat lower than that for (46), since the overall reaction (48) is somewhat more exothermic. The value for k_{51} was estimated assuming the reactivity of CH_3O may be approximated by that for CF_3. The rate constant for HO addition to C_2H_4 is the same order of magnitude as that for HO addition to SO_2. Thus the ratio of the measured rate constants for CF_3 and HO addition to the π-system of C_2H_4 (6.3×10^{-3})[228] was used to estimate $k_{51} = 6.3 \times 10^{-3}\ k_{50}$. These are obviously only rough approximations.

$$\mathrm{HO + SO_2\ (+\ M) \rightarrow HOSO_2\ (+\ M)} \tag{50}$$

$$\mathrm{HOSO_2 + O_2 \rightarrow HOSO_2O_2} \tag{55}$$

$$\mathrm{HOSO_2O_2 + NO \rightarrow HOSO_2O + NO_2} \tag{56}$$

$$\mathrm{HOSO_2O_2 + NO_2 \rightarrow HOSO_2O_2NO_2} \tag{57}$$

$$\mathrm{HOSO_2O_2 + HO_2 \rightarrow HOSO_2O_2H + O_2} \tag{58}$$

$$\mathrm{HOSO_2O + HO_2 \rightarrow HOSO_2OH + O_2} \tag{59}$$

$$\mathrm{HOSO_2O + NO \rightarrow HOSO_2ONO} \tag{60}$$

$$\mathrm{HOSO_2O + NO_2 \rightarrow HOSO_2ONO_2} \tag{61}$$

$$\mathrm{HOSO_2O + RH \rightarrow HOSO_2OH + R} \tag{62a}$$

$$\mathrm{HOSO_2O + RH(alkene) \rightarrow HOSO_2O\dot{R}H} \tag{62b}$$

$$\mathrm{H_2SO_4 + H_2O(NH_3,\ CH_2O,\ C_nH_{2n},\ etc.) \rightarrow growing\ aerosol} \tag{63}$$

$$\mathrm{HOSO_2ONO_2 + H_2O \rightarrow H_2SO_4 + HONO_2 \overset{(H_2O)}{\rightarrow} growing\ aerosol} \tag{64}$$

$$\mathrm{HOSO_2ONO + sunlight \rightarrow HOSO_2O + NO} \tag{65}$$

$$\mathrm{HOSO_2ONO + H_2O \rightarrow H_2SO_4 + HONO \overset{(H_2O)}{\rightarrow} growing\ aerosol} \tag{66}$$

Some of the species expected as products of the HO radical addition to SO_2 should be highly reactive. Especially interesting is the presumed formation of an inorganic analogue to the acylperoxy nitrates, $HOSO_2O_2NO_2$, in reaction (57). Note that free radical addition to SO_2 in a smog mixture need not result directly in chain termination reactions. By analogy with the HO_2 radical reaction (21), presumably the $HOSO_2O_2$ radical would normally oxidize NO to NO_2 in reaction (56). The reactivity of the $HOSO_2O$ free radical may be similar to those of HO and RO radicals. It should abstract H-atoms from alkene, alkane, or aldehyde (reaction 62a) and add to alkenes (reaction 62b) as well as terminate chains through reactions (60) and (61). The chain oxidation of the SO_2 molecules through the regeneration of the HO radical in (67) is not likely since this reaction is very endothermic ($\Delta H = 43$ kcal-mole^{-1}), and it could not compete with the alternative reactions of this species.

$$\mathrm{HOSO_2O \rightarrow SO_3 + HO} \tag{67}$$

Any mechanism which we consider seriously should satisfy the few requirements which seem to evolve from the limited chamber data for NO_x-hydrocarbon-SO_2 mixtures in air[131a,235-239]. These results show: (1) the presence of SO_2 does not alter significantly the ultimate ozone level reached or the rate of olefin removal in the system. (2) The removal rate for SO_2 shows an induction period characteristic of the time delay expected for the buildup of the reactive radical species (HO, HO_2, etc.) which are generated in the chain reactions involving the alkenes. With the proper choice of rate constants for the sequence of reactions (50), (55)-(67), one can easily satisfy these limited requirements. At this point in time it will be sufficient to assume that the primary radical reactions with SO_2 are rate determining in the removal of SO_2, and that none of the primary products regenerate SO_2.

The primary reaction scheme outlined for the SO_2 reactions in Table XLIV was added to the general smog reaction scheme and simulations made. The results of one such experiment are shown in Figure 58. The initial concentrations of the impurities have been picked as follows: $[SO_2]^\circ = 0.10$; $[NO]^\circ = 0.15$; $[NO_2]^\circ = 0.05$; $[C_4H_8]^\circ = 0.10$; $[CO]^\circ = 10$; $[CH_4]^\circ = 1.5$; relative humidity, 50% (25° C). The length of the ordinate between curves defining each species represents the theoretical rate of SO_2 removal by this species. We observe a near equal importance of the HO_2 and HO reactions with SO_2 (46) and (50). Much smaller, but much less certain, estimated contributions come from the CH_3O_2 reaction (48), the CH_3O addition in (51), and $O(^3P)$ addition in (39). SO_2 removal in these reactions corresponds to a maximum rate of conversion of about 1.1% per h. In similar situations with aldehydes present initially ($[CH_2O]^\circ = 0.10$, $[CH_3CHO]^\circ = 0.06$), rates of SO_2 removal are a maximum of about 1.5% per h. Obviously the rates of homogeneous removal of SO_2 in a smoggy atmosphere may be significant. When one recognizes that there are probably other processes analogous to (48) and (50) which may occur involving other RO_2 and RO species, and the likelihood of the occurrence of other homogeneous reactions not yet identified, the gas phase kineticist is assured of an important task in the ultimate characterization and control of the SO_2-containing smog mixtures.

Summary

The apparent success today of computer modeling of photochemical smog formation in both the smog chambers and the real urban atmospheres must be at least in part related to the few demands which the present incomplete product analysis data place on the modeler and his reaction schemes. Any computer simulation of a complex system can only be good as the input parameters will allow. One must not take too seriously the results from complex simulations at this stage of our knowledge. In particular the development of sound reaction schemes and realistic smog models require much more quantitative kinetic information as to the detailed reaction paths which appear to be important in photochemical smog. Specifically we feel that the most important needs today are kinetic and mechanism studies related to the reactions of O_3, HO, and HO_2 with the alkenes and aromatic hydrocarbons at low concentration in air at 1 atm pressure. With the increasing use of high sulfur fuels it is imperative that we delineate the SO_2 removal modes which are operative in the NO_x-hydrocarbon polluted urban atmosphere. There is no question that as such information becomes available, present models will require substantial changes. In this light it should be apparent to those who use chemical models to simulate the photochemical smog formation that there are potentially serious deficiencies in present systems which must be adequately tested for and removed. One should not

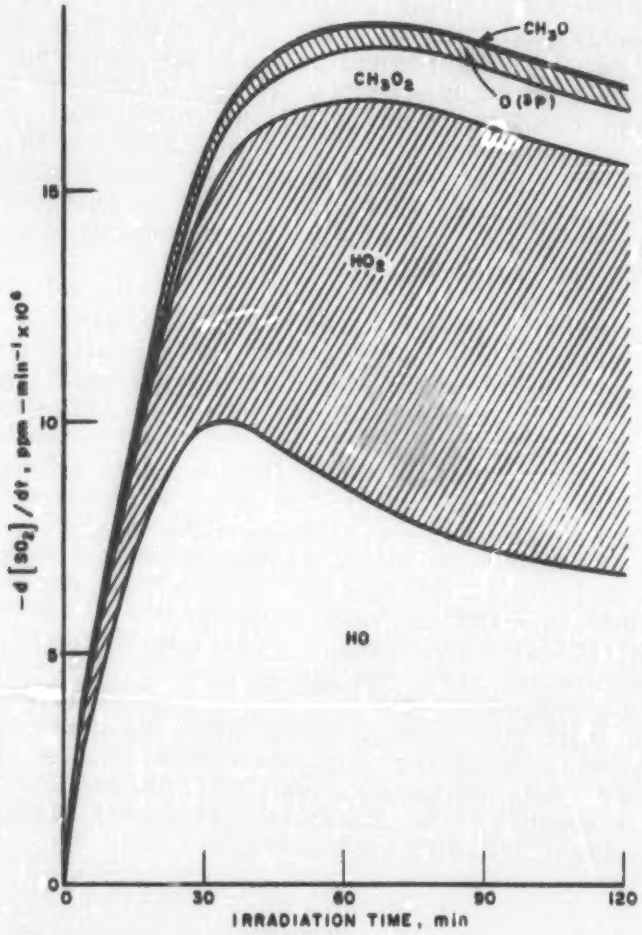

Figure 58. The theoretical rate of attack of various free radical species on SO_2 for a simulated sunlight-irradiated ($z = 40°$), polluted atmosphere, initial concentrations (ppm): $[SO_2]° = 0.10$; $[NO]° = 0.15$; $[NO_2]° = 0.05$; $[C_4H_8]° = 0.10$; $[CO]° = 10$; $[CH_4]° = 1.5$; relative humidity, 50% (25°C); the total maximum rate of SO_2 removal from the reactants shown is about 1.1% per h.

at this stage of our knowledge of smog systems bet our lives on the development of air pollution control programs based on these necessarily speculative schemes. However it is our belief that computer modeling of photochemical smog will continue to be a very useful guide to the experimentalist, and it will ultimately serve us well in comprehensive air shed models which are based on sound kinetic schemes.

References

(1) Community Health and Environmental Surveillance System Committee of the Environmental Protection Agency Report, "Health Consequences of Sulfur Oxides," EPA-650/1-74-004, May, 1974.

(2) a) A. P. Altshuller and J. J. Bulfalini, Photochem. Photobiol, 4, 97, (1965); b) Ibid., Environ. Sci. Technol., 5, 39 (1971).

(3) R. D. Cadle and E. R. Allen, Sci., 167, 243 (1970).

(4) M. Katz, Can. J. Chem. Eng., 48, 3 (1970).

(5) P. Urone and W. H. Schroeder, Environ. Sci. Technol., 3, 436 (1969).

(6) T. C. Hall, Jr., "Photochemical Studies of Nitrogen Dioxide and Sulfur Dioxide," Ph.D. Thesis, Univ. Calif., Los Angeles, 1953.

(7) E. R. Gerhard and H. F. Johnstone, Ind. Eng. Chem., 47, 972 (1958).

(8) R. A. Cox and S. A. Penkett, Atmos. Environ., 4, 425 (1970).

(9) P. M. Foster, Atmos. Environ., 3, 157 (1969).

(10) H. F. Johnstone and D. R. Coughanowr, Ind. Eng. Chem., 50, 1169 (1958).

(11) H. F. Johnstone and A. J. Moll, Ibid., 52, 861 (1960).

(12) C. E. Junge and T. G. Ryan, Quart. J. Roy. Meteor. Soc., 84, 46 (1958).

(13) M. J. Matteson, W. Stöber, and H. Luther, Ind. Eng. Chem. Fundam., 8, 677 (1969).

(14) A. P. van den Heuval, B. J. Mason, Quart. J. Roy. Meteorol. Soc., 89, 271 (1963).

(15) M. Corn and R. T. Cheng, J. Air Polln. Control Assocn., 22, 871 (1972).

(16) This portion of the work under this grant was published during the first year of our present study: F. B. Wampler, J. G. Calvert, and E. K. Damon, Int. J. Chem. Kinet., 5, 107-117 (1973).

(17) S. Okuda, T. N. Rao, D. H. Slater, and J. G. Calvert, J. Phys. Chem., 73, 4412 (1969).

(18) T. N. Rao, S. S. Collier, and J. G. Calvert, J. Amer. Chem. Soc., 91, 1609 (1969).

References (continued

(19) C. C. Badcock, H. W. Sidebottom, J. G. Calvert, G. W. Reinhardt, and E. K. Damon, *J. Amer. Chem. Soc.*, 93, 3115 (1971).

(20) H. W. Sidebottom, C. C. Badcock, J. G. Calvert, B. R. Rabe, and E. K. Damon, *J. Amer. Chem. Soc.*, 93, 3121 (1971).

(21) E. Cehelnik, C. W. Spicer, and J. Heicklen, *J. Amer. Chem. Soc.*, 93, 5371 (1971).

(22) F. B. Wampler, A. Horowitz, and J. G. Calvert, *J. Amer. Chem. Soc.*, 94, 5523 (1972).

(23) T. N. Rao and J. G. Calvert, *J. Phys. Chem.*, 74, 681 (1970).

(24) A. Horowitz and J. G. Calvert, *Int. J. Chem. Kinet.*, 4, 175 (1972).

(25) A. Horowitz and J. G. Calvert, *Int. J. Chem. Kinet.*, 4, 191 (1972).

(26) H. W. Sidebottom, C. C. Badcock, J. G. Calvert, G. W. Reinhardt, B. R. Rabe, and E. K. Damon, *J. Amer. Chem. Soc.*, 93, 2587 (1971).

(27) H. W. Sidebottom, J. G. Calvert, B. R. Rabe, and E. K. Damon, to be published.

(28) H. D. Mettee, *J. Phys. Chem.*, 73, 1071 (1969).

(29) T. N. Rao, S. S. Collier, and J. G. Calvert, *J. Amer. Chem. Soc.*, 91, 1616 (1969).

(30) H. W. Sidebottom, C. C. Badcock, G. E. Jackson, J. G. Calvert, G. W. Reinhardt, and E. K. Damon, *Enivon. Sci. Technol.*, 6, 72 (1972).

(31) This portion of the work under this grant was published during the first year of our present study: A. Horowitz and J. G. Calvert, *Int. J. Chem. Kinet.*, 5, 243 (1973).

(32) G. E. Jackson and J. G. Calvert, *J. Amer. Chem. Soc.*, 93, 2593 (1971).

(33) A. Horowitz and J. G. Calvert, *Int. J. Chem. Kinet.*, 4, 207 (1972).

(34) H. D. Mettee, *J. Chem. Phys.*, 49, 1784 (1968).

(35) H. D. Mettee, *J. Phys. Chem.*, 73, 1071 (1969).

(36) S. J. Strickler and D. B. Howell, *J. Chem. Phys.* 49, 1947 (1968).

(37) T. N. Rao, S. S. Collier, and J. G. Calvert, *J. Amer. Chem. Soc.*, 91, 1609 (1969).

(38) T. N. Rao and J. G. Calvert, *J. Phys. Chem.*, 74, 681 (1970).

(39) A. Horowitz and J. G. Calvert, *Int. J. Chem. Kinet.*, 4, 175 (1972).

References (continued)

(40) A. Horowitz and J. G. Calvert, Int. J. Chem. Kinet., 4, 191 (1972).

(41) H. W. Sidebottom, C. C. Badcock, G. E. Jackson, J. G. Calvert, G. W. Reinhardt, and E. K. Damon, Environ. Sci. Technol., 6, 72 (1972).

(42) H. W. Sidebottom, C. C. Badcock, J. G. Calvert, B. R. Rabe, and E. K. Damon, J. Amer. Chem. Soc., 93, 3121 (1971).

(43) A. Horowitz and J. G. Calvert, unpublished results.

(44) a) G. M. Almy and P. R. Gillette, J. Chem. Phys., 11, 188 (1943); b) S. S. Collier, D. H. Slater, and J. G. Calvert, Photochem. Photobiol., 7, 737 (1968).

(45) A. Fatta and J. Heicklen, communication to the authors.

(46) F. B. Wampler, A. Horowitz, and J. G. Calvert, J. Amer. Chem. Soc., 94, 5523 (1972).

(47) This portion of the work under this grant was published during the first year of our present study: F. B. Wampler, K. Otsuka, J. G. Calvert, and E. K. Damon, Int. J. Chem. Kinet., 5, 669 (1973).

(48) E. R. Allen, R. D. McQuigg, and R. D. Cadle, Chemosphere, 1, 25 (1972).

(49) J. A. Davidson and E. W. Abrahamson, Photochem. Photobiol., 15, 403 (1972).

(50) S. S. Collier, A. Morikawa, D. H. Slater, J. G. Calvert, G. W. Reinhardt, and E. K. Damon, J. Amer. Chem. Soc., 92, 217 (1970).

(51) K. Otsuka and J. G. Calvert, J. Amer. Chem. Soc., 93, 2581 (1971).

(52) J. C. D. Brand, V. T. Jones, and C. di Lauro, J. Molec. Spectrosc., 40, 616 (1971).

(53) I. H. Hillier and V. R. Saunders, Molec. Phys. 22, 193 (1971).

(54) K. J. Chung and C. R. Clayton, Department of Chemistry, The Ohio State University and the Battelle Memorial Institute, Columbus, Ohio 43210, unpublished calculations.

(55) a) G. Herzberg, "Molecular Spectra and Molecular Structure. III. Electronic Spectra and Electronic Structure of Polyatomic Molecules," Van Nostrand, Princeton, N.J., 1966, p. 605; b) J. C. D. Brand and K. Srikameswaran, Chem. Phys. Lett., 15, 130 (1972); c) J. C. D. Brand and R. Nanes, J. Mol. Spectrosc., in press.

(56) E. Cehelnik, C. W. Spicer, and J. Heicklen, J. Amer. Chem. Soc., 93, 5371 (1971).

(57) S. E. Braslavsky, and J. Heicklen, J. Amer. Chem. Soc., 94, 4864 (1972).

References (continued)

(58) F. S. Dainton and K. J. Ivin, *Trans. Faraday Soc.*, 46, 374 (1950).

(59) R. B. Timmons, *Photochem. Photobiol.*, 12, 219 (1970).

(60) K. L. Demerjian, Ph.D. Dissertation, The Ohio State University, Chemistry Department, Columbus, Ohio, Winter 1973, to be published.

(61) C. C. Badcock and J. G. Calvert, to be published.

(62) R. B. Cundall and T. F. Palmer, *Trans. Faraday Soc.*, 56, 1211 (1960).

(63) a) R. J. Cvetanovic, *Can. J. Chem.*, 38, 1678 (1960); b) R. J. Cvetanovic and R. S. Irwin, *J. Chem. Phys.*, 46, 1702 (1967).

(64) This portion of the work under this grant was published during the second year of our present study: K. L. Demerjian, J. G. Calvert, and D. L. Thorsell, *Int. J. Chem. Kinet.*, 6, 829 (1974).

(65) G. M. Bristow and F. S. Dainton, *Proc. Roy. Soc. A*, 229, 525 (1955).

(66) R. D. Penzhorn and H. Güsten, *Z. Naturforsch.*, 27a, 1401 (1972).

(67) R. A. Cox, *J. Photochem.*, 2, 1 (1973-74).

(68) P. W. Jones and A. H. Adelman, *Environ. Sci. Technol.*, 6, 933 (1972).

(69) J. G. Calvert and J. N. Pitts, Jr., "Photochemistry," New York, 1967, p. 734.

(70) G. E. Jackson and J. G. Calvert, *J. Amer. Chem. Soc.*, 93, 2593 (1971).

(71) C. G. Hatchard and C. A. Parker, *Proc. Roy. Soc. A*, 235, 518 (1956).

(72) D. J. Brookman and D. T. Sawyer, *Anal. Chem.*, 40, 106 (1968).

(73) D. M. Golden, K. W. Egger, and S. W. Benson, *J. Amer. Chem. Soc.*, 86, 5416 (1964).

(74) S. Sato, K. Kikuchi, and M. Tanaka, *J. Chem. Phys.*, 39, 239 (1963).

(75) M. Tanaka, T. Terumi, and S. Sato, *Bull. Chem. Soc. Japan*, 38, 1645 (1965).

(76) G. A. Haninger, Jr., and E. K. C. Lee, *J. Phys. Chem.*, 71, 3104 (1967).

(77) E. K. C. Lee, H. O. Denschlag, and G. A. Haninger, *J. Chem. Phys.*, 48, 4547 (1968).

(78) K. Fukano and S. Sato, *Kogyu Kogaku Zasshi*, 72, 213 (1969).

(79) Y. G. Shekk and M. V. Alfimov, *Opt. Spect.*, 32, 335 (1972).

References (continued)

(80) P. J. Wagner and G. S. Hammond, Adv. Photochem., 5, 21 (1968).

(81) R. E. Rebbert and P. Ausloos, J. Amer. Chem. Soc., 87, 5569 (1965).

(82) W. A. Noyes, Jr., G. B. Porter, and J. E. Jolley, Chem. Rev., 56, 49 (1956).

(83) J. W. Gall, D. H. Slater, and J. G. Calvert, in "Chemical Reactions in the Urban Atmospheres," American Elsevier, New York, 1971, p. 133.

(84) J. H. Moore, Jr., J. Phys. Chem., 76, 1130 (1972).

(85) W. Flicker, O. Mosher, and A. Kupperman, to be published.

(86) R. A. Caldwell and S. P. James, J. Amer. Chem. Soc., 91, 5184 (1969).

(87) I. E. Kochevar and P. J. Wagner, J. Amer. Chem. Soc., 94, 3859 (1972).

(88) L. Stockburger, III, S. Braslavsky, and J. Heicklen, "Photolysis of SO_2 in the Presence of Foreign Gases. III.--Quenching of Emission by Foreign Gases," preprint of work provided by Heicklen to the authors.

(89) E. Cehelnik, J. Heicklen, S. Braslavsky, L. Stockburger, III, and E. Mathias, "Photolysis of SO_2 in the Presence of Foreign Gases. IV.--Wavelength and Temperature Effects with CO," Center for Air Environment Studies Publ. 241-72, Pennsylvania State University (Oct. 1972).

(90) A. M. Fatta, E. Mathias, J. Heicklen, L. Stockburger, III, and S. Braslavsky, "Photolysis of SO_2 in the Presence of Foreign Gases. V.--Sensitized Phosphorescence of Biacetyl," Center for Air Environment Studies, Publ. 217-71, Pennsylvania State University, (Oct. 1972).

(91) See section I-F; also Ph.D. dissertation of K. J. Chung, Ohio State University, Columbus, (1974).

(92) J. D. Brand, V. T. Jones, and C. di Lauro, J. Molec. Spectro., 40, 616 (1971).

(93) J. G. Calvert, "Interactions of Air Pollutants," in Proc. Conf. on Health Effects of Air Pollutants, pp. 19-101, National Academy of Sciences, October 3-5, 1973, Stock 5270-02105, U.S. Government Printing Office, Washington, D.C., 20402.

(94) The work reported in this section was completed during the present study and was published during the present year of the study: K. L. Demerjian and J. G. Calvert, Int. J. Chem. Kinet., 7, 45 (1975).

(95) a) Y. Hamada and A. J. Merer, presented at the 29th Symp. on Molecular Structure and Spectroscopy, Ohio State University, Columbus, June 14, 1974, paper FB3; b) D. R. Humphrey, J. L. Hardwick, J. C. D. Brand, Y. Hamada, and A. J. Merer, presented at the 29th Symp. on Molecular Structure and Spectroscopy, Ohio State University, Columbus, June 14, 1974, paper FB1.

References (continued)

(96) J. R. McDonald and L. E. Brus, presented at the 29th Symp. on Molecular Structure and Spectroscopy, Ohio State University, Columbus, June 14, 1974, paper FB2.

(97) H. W. Sidebottom, J. G. Calvert, K. Chung, and E. K. Damon, in preparation.

(98) H. W. Sidebottom, K. Otsuka, A. Horowitz, J. G. Calvert, B. R. Rabe, and E. K. Damon, *Chem. Phys. Lett.*, 13, 337 (1972).

(99) J. G. Calvert, *Chem. Phys. Lett.*, 20, 484 (1973).

(100) H. D. Mettee, *J. Phys. Chem.*, 73, 1071 (1969).

(101) The work reported in this section was completed during the present study and was published during the present year: K. Chung, J. G. Calvert, and J. W. Bottenheim, *Int. J. Chem. Kinet.*, 7, 161 (1975).

(102) R. A. Cox, *J. Phys. Chem.*, 76, 814 (1972).

(103) E. R. Allen and J. E. Bonelli, Abstracts, 6th Informal Photochemistry Conference, Oklahoma State Univ., June, 1972; we thank Dr. Allen for providing us with the quantum yield data obtained in these experiments before publication of this work.

(104) H. N. S. Schafer, *Anal. Chem.*, 39, 1719 (1967).

(105) J. W. Laxton and P. J. Jackson, *J. Inst. Fuel*, 12 (1964).

(106) P. W. Schenk and H. Platz, *Z. Anorg. u. Allg. Chem.*, 222, 177 (1935).

(107) A. Kurtenacker and E. Furstenan, *Z. Anorg. u. Allg. Chem.*, 215, 257 (1933).

(108) G. Nickless, "Inorganic Sulfur Chemistry," Elsevier, New York, 1968, ch. 14.

(109) R. G. W. Norrish and G. A. Oldershaw, *Proc. Roy. Soc. A*, 249, 498 (1959).

(110) N. Basco and R. D. Morse, *Chem. Phys. Lett.*, 20, 557 (1973).

(111) F. C. James, J. A. Kerr, and J. P. Simons, *Chem. Phys. Lett.*, 25, 431 (1974); the authors are grateful to Dr. Kerr for a preprint of this work given to them before publication.

(112) D. S. Sethi, *J. Air. Polln. Control Assocn.*, 21, 418 (1971).

(113) P. J. Warneck, G. C. A., Technology Div., Belford, Mass., personal communication to one of the authors (J.G.C.).

(114) E. R. Allen, private communication to one of the authors (J.G.C.).

(115) R. L. Daubendiek and J. G. Calvert, paper in preparation.

References (continued)

(116) K. Schofield, *J. Phys. Chem., Ref. Data*, 2, 25 (1973).

(117) C. J. Halstead and B. A. Thrush, *Photochem. Photobiol.*, 4, 1007 (1965).

(118) K. H. Hoyermann, G. Wagner, and J. Wolfrum, *Ber. Bunsenges. Physik. Chem.*, 71, 603 (1967).

(119) R. J. Donovan, D. Husain, and P. T. Jackson, *Trans. Faraday Soc.*, 65, 2930 (1969).

(120) W. H. Breckenridge and T. A. Miller, *J. Chem. Phys.*, 56, 465 (1972).

(121) J. G. Calvert, *Chem. Phys. Lett.*, 20, 484 (1973).

(122) L. E. Brus and J. R. McDonald, *Chem. Phys. Lett.*, 21, 283 (1973).

(123) H. W. Sidebottom, J. G. Calvert, K. J. Chung, and E. K. Damon, to be published.

(124) This portion of the work under this grant was published during the study period; see reference 121.

(125) K. F. Greenough and A. B. F. Duncan, *J. Am. Chem. Soc.*, 83, 555 (1961).

(126) H. D. Mettee and T. Fisher, private communication to the author.

(127) K. L. Demerjian, J. A. Kerr, and J. G. Calvert, *Environ. Sci. Technol.*, 4, 1 (1974).

(128) This portion of the work under this grant was completed during the project period and published during the final year of the grant: R. L. Daubendiek and J. G. Calvert, *Environ. Letters*, 8, 103 (1975).

(129) C. F. H. Tipper and R. K. Williams, *Trans. Faraday Soc.*, 57, 79 (1961).

(130) C. F. Cullis, R. M. Henson, and D. L. Trimm, *Proc. Roy. Soc. (London)*, A295, 72 (1966).

(131) For recent examples see: a) W. E. Wilson, Jr., A. Levy, and D. B. Wimmer, *J. Air Polln. Control Assocn.*, 22, 27 (1970); b) E. R. Stephens and M. A. Price, *J. Coll. and Interface Science*, 39, 272 (1972).

(132) R. L. Daubendiek and J. G. Calvert, "A Photochemical Study Involving SO_2, O_2, SO_3, and O_3" presented at the 165th National Meeting of the American Chemical Society, Dallas, Texas, April, 1973, paper in preparation for publication.

(133) See for example, H. S. Johnston, "Gas Phase Reaction Rate Theory," Ronald Press, New York, 1966, p. 14-32.

(134) N. S. Grunhut, M. Goldfrank, M. L. Cushing, and G. V. Caesar, in *Inorg. Syn.* Vol. 3, Editor, L. F. Audrieth, McGraw-Hill, 1950, p. 78.

References (continued)

(135) G. Schott and N. Davidson, *J. Amer. Chem. Soc.*, 80, 1841 (1958).

(136) Environmental Protection Agency, National Primary and Secondary Ambient Air Quality Standards, Part II, *Federal Register*, Vol. 36, No. 84, 8196, 1971.

(137) R. H. Pierson, A. N. Fletcher, and E. St.Clair Gantz, *Anal. Chem.*, 28, 1218 (1956).

(138) E. J. Jones and O. R. Wulf, *J. Chem. Phys.*, 5, 873 (1937).

(139) P. A. Leighton, "Photochemistry of Air Pollution," Academic Press, New York, 1961, p. 29.

(140) This is the total pressure of NO_2 and N_2O_4. At the temperature of 30° the calculated partial pressures of NO_2 and N_2O_4 are 8.68 and 0.47 Torr, respectively.

(141) P. Urone, W. H. Schroeder, and S. R. Miller, "Reactions of Sulfur Dioxide in Air," in "Proceedings of the Clean Air Conference," Washington, D.C., 1970.

(142) R. C. Paul, C. L. Arora, and K. C. Malhotra, *Indian J. Chem.*, 10, 94 (1972).

(143) For some recent examples of $(NO)_2S_2O_7$ preparation see: a) K. Stopperka and F. Kilz, Z. Chem., 8, 435 (1968); prepared from N_2O_3 and fuming sulfuric acid; b) K. Stopperka, F. Wolf, and G. Suess, *Z. Anorg. Allg. Chem.*, 359, 14 (1968); prepared from gaseous SO_2 and NO_2 at 225-230°C; c) R. DeJaeger, B. Vandorpe, and J. Heubel, *Rev. Chim. Miner.*, 4, 195 (1967); prepared from $NOClSO_3$ on heating; d) R. DeJaeger, P. Legrand, and J. Heubel, *Compt. Rend. Acad. Sci. Paris*, Ser. C, 265, 1117 (1967); prepared from $NOSO_3Cl$ reaction with N_2O_3 or N_2O_4.

(144) For some recent examples of $(NO_2)_2S_2O_7$ preparation see: a) B. Vandorpe and J. Heubel, *Compt. Rend.*, 260, 6619 (1965); formed from N_2O_5 in liquid SO_3; b) K. Stopperka and V. Grove, *Z. Chem.*, 5, 111 (1965); formed from NO_2 and SO_2Cl_2 at 70-125°C.

(145) E. I. DuPont de Nemours and Co. (Inc.), product literature on Teflon FEP film available from the Plastics Department, Fluorocarbon Divison, Wilmington, Delaware, 19898, 1973.

(146) P. M. McClough and B. A. Thrush, *Chem. Ind. (London)*, 1966, Nov. 19, p. 1971.

(147) S. W. Benson and A. E. Axworthy, Jr., *J. Chem. Phys.*, 26, 1718 (1957).

(148) P. J. H. Woltz and E. A. Jones, *J. Chem. Phys.*, 17, 502 (1949).

(149) A. H. Nielsen, T. G. Burke, P. J. H. Woltz, and E. A. Jones, *J. Chem. Phys.*, 20, 596 (1952).

References (continued)

(150) R. H. Pierson, A. N. Fletcher, and E. St.Clair-Gantz, Anal. Chem., 28, 1218 (1956).

(151) E. A. Jones, J. S. Kirby-Smith, P. J. H. Woltz, and A. Nielsen, J. Chem. Phys., 19, 242 (1951).

(152) D. Saunders and J. Heicklen, J. Amer. Chem. Soc., 87, 2088 (1965). It appears to us that Saunders and Heicklen underestimated their CF_2O concentrations. They "measured" CF_2O by introducing it into a g.c. column, and then determined the amount of CO_2 produced from an assumed stoichiometry for the reaction between CF_2O and the silica gel column packing. Actually the conversion may have been incomplete. The effect of the presence of impurities in the sample would lead also to an overestimation of the extinction coefficient.

(153) J. Heicklen in "Advances in Photochemistry," Vol. 7, Wiley-Interscience, New York, N. Y., 1969, p. 79.

(154) R. W. Murray, Accounts Chem. Res., 1, 313 (1968).

(155) J. Heicklen, J. Phys. Chem., 70, 477 (1966).

(156) Y. K. Wei and R. J. Cvetanovic, Can. J. Chem., 41, 913 (1963).

(157) P. G. Stecher, Editor, "The Merck Index," 8th Edition, Merck and Company, Inc., Rahway, N. J., 1968, p. 209.

(158) This portion of the work under the present grant was carried out and published during the second year of the grant period: R. L. Daubendiek and J. G. Calvert, Environ. Letters, 6, 253 (1974).

(159) This portion of the work under the present grant was carried out and published during the first year of the grant period: J. G. Calvert, K. L. Demerjian, and J. A. Kerr, Environ. Letters, 4, 123 (1973).

(160) a) K. L. Demerjian, Masters Thesis, The Ohio State University, Columbus, Ohio, 1970; b) K. L. Demerjian, J. A. Kerr, and J. G. Calvert, ref. 127; c) J. A. Kerr, J. G. Calvert, and K. L. Demerjian, Chem. Brit., 8, 252 (1972).

(161) K. L. Demerjian, J. A. Kerr, and J. G. Calvert, Environ. Letters, 3, 73 (1972).

(162) K. L. Demerjian, J. A. Kerr, and J. G. Calvert, Environ. Letters, 3, 137 (1972).

(163) L. G. Wayne and D. M. Yost, J. Chem. Phys., 19, 41 (1951).

(164) S. Jaffe and H. W. Ford, J. Phys. Chem., 71, 1832 (1967).

(165) J. Heicklen, K. Westberg, and N. Cohen, Publications No. 115-69 (Center for Air Environmental Studies, University Park, Pa., 1969); K. Westberg, N. Cohen and K. W. Wilson, Science, 171, 1013 (1971).

References (continued)

(166) H. Stedman, E. D. Morris, Jr., E. E. Daby, H. Niki, and B. Weinstock, paper in the Division of Water, Air, and Waste Chemistry, 160th National American Chemical Society Meeting, Chicago, Ill., Sept. 1970.

(167) E. R. Stephens and F. R. Burleson, *J. Air Pollution Control Assoc.*, 17, 147 (1967).

(168) This portion of the work under this grant was carried out and published during the first year of the grant period: J. G. Calvert, K. L. Demerjian, and J. A. Kerr, *Environ. Letters*, 4, 281 (1973).

(169) The reaction scheme shown involves only 17 of the most important of the total of 58 chemical reactions considered in our more complete reaction scheme employed in the simulations of Figs. 38-43; the complete mechanism and the rate constant data selection is published elsewhere.[127]

(170) C. Morley and I. W. M. Smith, *J. Chem. Soc. Faraday Trans. II*, 68, 1016 (1972).

(171) W. E. Wilson, Jr. and D. Miller, unpublished results from studies made in the large smog chamber at Battelle Memorial Institute, Columbus, Ohio; we are grateful for the use of these data before publication.

(172) M. C. Dodge and J. J. Bufalini, private communication; the authors are grateful for the use of a preprint of this work before publication.

(173) G. Dixon-Lewis, W. E. Wilson and A. A. Westenberg, *J. Chem. Phys.*, 44, 2877 (1966).

(174) K. Westberg, N. Cohen and K. W. Wilson, *Science*, 171, 1013 (1971).

(175) This portion of the work under the grant was carried out and published during the final year of the grant period: J. G. Calvert and R. D. McQuigg, *Int. J. Chem. Kinet., Symp.* 1, 113 (1975).

(176) A. Stern, "Air Pollution," 2nd Ed., Academic Press, New York, 1968.

(177) *Fed. Reg.*, 36, 8186 (1971).

(178) S. W. Benson, "Thermochemical Kinetics," John Wiley and Sons, Inc., New York, 1968.

(179) K. Westberg and N. Cohen, "The Chemical Kinetics of Photochemical Smog as Analyzed by Computer," Report No. ATR-70(8107)-1, Aerospace Corporation, El Secundo, Calif., Dec., 1969.

(180) G. Hilst, "A Coupled Two Dimensional Diffusion and Chemistry Model for Turbulent and Inhomogeneously Mixed Reaction Systems," Report from Aeronautical Research Associates of Princeton, Inc., Princeton, N.J., 1973, Contract R4-73-016C to the Office of Research and Monitoring, U.S. Environmental Protection Agency.

References (continued)

(181) a) A. Q. Eschenroeder and J. R. Martinez, Final Report, Contract No. CPA-22-69-127, General Research Corporation, Santa Barbara, Calif., Nov. 1969; b) A. Q. Eschenroeder and J. R. Martinez, Advan. Chem. Ser., 113, 101 (1972).

(182) S. K. Friedlander and J. H. Seinfeld, Environ. Sci. Technol., 3, 1175 (1969).

(183) a) T. A. Hecht and J. H. Seinfeld, Environ. Sci. Technol., 6, 47 (1972); b) J. H. Seinfeld, S. D. Reynolds, and P. M. Roth, Advan. Chem. Ser., 113, 581 (1972).

(184) L. G. Wayne and J. E. Ernest, "Photochemical Smog, Simulated by Computer," presented at the 62nd Annual Meeting of the Air Pollution Control Association, New York, June 1969.

(185) L. G. Wayne, M. Weisburd, R. Danchick, and A. Kokin, "Final Report--Development of a Simulation Model for Estimating Ground Level Concentrations of Photochemical Pollutants," System Development Corp., Santa Monica, Calif., 1971.

(186) H. Niki, E. E. Daby, and B. Weinstock, Advan. Chem. Ser., 113, 16 (1972).

(187) T. A. Hecht, J. H. Seinfeld, and M. C. Dodge, Curr. Res., 8, 327 (1974).

(188) R. A. Cox and R. Atkins, Atomic Energy Research Establishment, Harwell, personal communication to J. G. C. from Dr. A. E. J. Eggleton.

(189) E. D. Morris, Jr., and H. Niki, J. Phys. Chem., 77, 1929 (1973).

(190) R. Simonaitis and J. Heicklen, J. Phys. Chem., 78, 653 (1974).

(191) D. H. Stedman and H. Niki, Environ. Sci. Technol., 7, 735 (1973).

(192) D. H. Stedman and J. O. Jackson, paper in "Symposium on Chemical Kinetics Data for the Lower and Upper Atmosphere," Airlie House, Va., Sept., 1974.

(193) J. Heicklen, K. Westberg, and N. Cohen, Publication No. 115-69, Center for Air Environmental Studies, University of Pennsylvania, University Park, Pa., 1969.

(194) J. G. Calvert, J. A. Kerr, K. L. Demerjian, and R. D. McQuigg, Science, 175, 751 (1972).

(195) E. R. Stephens and F. R. Burleson, J. Air Pollut. Contr. Assoc., 19, 929 (1969).

(196) E. R. Stephens and F. R. Burleson, J. Air Pollut. Contr. Assoc., 17, 147 (1967).

References (continued)

(197) a) C. S. Tuesday in "Chemical Reactions in the Urban Atmosphere," R. D. Cadle, Ed., Interscience Publishers, New York, 1961, p. 15; b) E. A. Schuck, G. J. Doyle and N. Endow, Report 31, Air Pollution Foundation, San Marino, Calif., Dec. 1960; c) A. P. Altshuller, S. L. Kopczynski, W. A. Lonneman, T. L. Becker, and R. Slater, *Environ. Sci. Technol.*, 1, 899 (1967); d) W. E. Wilson, Jr., and A. Levy, *J. Air Pollut. Contr. Assoc.*, 20, 385 (1970); e) J. J. Bufalini and K. L. Brubaker, in "Chemical Reactions in Urban Atmospheres," C. S. Tuesday, Ed., Elsevier Publishing Co., New York, 1971, p. 225; f) B. Dimitriades and T. C. Wesson, *J. Air Pollut. Contr. Assoc.*, 22, 33 (1972); g) A. P. Altshuller and J. J. Bufalini, *Environ. Sci. Technol.*, 5, 39 (1971).

(198) E. R. Stephens, *Advan. Environ. Sci.*, 1, 73 (1969).

(199) a) E. A. Schuck and G. J. Doyle, Report 29, Air Pollution Foundation, San Marino, Calif., 1959; b) A. P. Altshuller and J. J. Bufalini, *Photochem. Photobiol.*, 4, 97 (1965), and ref. 29g; c) E. R. Stephens in "Chemical Reactions in Urban Atmospheres," C. S. Tuesday, Ed., Elsevier Publishing Co., New York, 1971, p. 45; d) B. Dimitriades and M. L. Whisman, "Chemical Reactions in Urban Atmospheres," C. S. Tuesday, Ed., Elsevier Publishing Co., New York, 1971, p. 89; e) see also ref. 186.

(200) K. D. Bayes, presented at the 6th Informal Photochemistry Conference, University of California, Davis, June 1964.

(201) T. N. Jones and K. D. Bayes, *Chem. Phys. Lett.*, 11, 163 (1971).

(202) A. M. Winter and K. D. Bayes, *J. Phys. Chem.*, 70, 302 (1966).

(203) A. U. Khan, J. N. Pitts, Jr., and E. B. Smith, *Environ. Sci. Technol.*, 1, 656 (1967).

(204) R. H. Kummler, M. H. Bortner, and T. Baurer, *Environ. Sci. Technol.*, 3, 248 (1969).

(205) T. Frankiewicz and R. S. Berry, *Environ. Sci. Technol.*, 6, 365 (1972).

(206) R. Louw, J. van Ham, and H. Nieboer, *J. Air Pollut. Contr. Assoc.*, 23, 716 (1973).

(207) B. W. Gay, Jr., and J. J. Bufalini, *Advan. Chem. Ser.*, 113, 255 (1972).

(208) D. Gray, E. Lissi, and J. Heicklen, *J. Phys. Chem.*, 76, 1919 (1972).

(209) H. E. Hunziker and H. R. Wendt, *J. Chem. Phys.* 60, 4622 (1974).

(210) H. E. Radford, K. M. Evenson, and C. J. Howard, *J. Chem. Phys.*, 60, 3178 (1974).

(211) C. C. Wang and L. I. Davis, Jr., *Phys. Rev. Lett.*, 32, 349 (1974).

References (continued)

(212) W. Tsang, in "Chemical Kinetic Data Survey VI: Photochemical and Rate Data for Twelve Gas Phase Reactions of Interest for Atmospheric Chemistry," N.B.S.I.R., 73-207, R. F. Hampton, Ed., National Bureau of Standards, Aug., 1973.

(213) a) D. F. Miller and C. W. Spicer, "A Continuous Analyzer for Detecting Nitric Acid," paper 74-17 presented at the 67th Meeting of the Air Pollution Control Assoc., Denver, Colorado, June, 1974; b) R. J. Gordon and R. J. Bryan, *Environ. Sci. Technol.*, 7, 645 (1973).

(214) E. R. Stephens, Advan. *Environ. Sci.*, 1, 119 (1969).

(215) W. L. Faith, N.A. Renzetti, and L. H. Rogers, Report 22, Air Pollution Foundation, San Marino, Calif., March 1958.

(216) E. A. Schuck, A. P. Altshuller, D. S. Barth, and G. B. Morgan, *J. Air Pollut. Contr. Assoc.*, 20, 297 (1970).

(217) a) A. Gitchell, R. Simonaitis, and J. Heicklen, *J. Air Pollut. Contr. Assoc.*, 24, 357 (1974); b) *J. Air Pollut. Contr. Assoc.*, 24, 772 (1974).

(218) R. A. Cox, *J. Phys. Chem.*, 76, 814 (1972).

(219) J. P. Friend, R. Leifer, and M. Trichon, *J. Atmos. Sci.*, 30, 465 (1973).

(220) R. D. Cadle in "Air Pollution Handbook," P. L. Magill, F. R. Holden, and C. Ackley, Eds., McGraw-Hill, New York, 1956, p. 3.

(221) R. A. Cox and S. A. Penkett, *J. Chem. Soc. Faraday Trans. I*, 68, 1735 (1972).

(222) G. K. Boreskov and V. V. Illarionov, *J. Phys. Chem. Moscow*, 14, 1428 (1940).

(223) a) R. A. Cox and S. A. Penkett, *Nature*, 229, 486 (1971); b) *Nature*, 230, 321 (1971).

(224) L. A. Ripperton, H. E. Jefferies, and O. White, *Advan. Chem. Ser.*, 113, 219 (1972).

(225) W. E. Wilson, M. C. Dodge, D. N. McNelis, and J. Overton, paper presented before Division of Environmental Chemistry, American Chemical Society, Los Angeles, April 1974.

(226) H. E. O'Neal and C. Blumstein, *Int. J. Chem. Kinet.*, 5, 397 (1973).

(227) a) R. Atkinson, B. J. Finlayson, and J. N. Pitts, Jr., *J. Amer. Chem. Soc.*, 95, 7592 (1973); b) B. J. Finlayson, J. N. Pitts, Jr., and H. Akimoto, *Chem. Phys. Lett.*, 12, 495 (1972); c) W. A. Kummer, J. N. Pitts, Jr., and R. P. Steer, *Environ. Sci. Technol.*, 10, 1045 (1971); d) J. N. Pitts, Jr., R. P. Steer, and B. J. Finlayson, *Advan. Chem. Ser.*, 113, 246 (1972).

References (continued)

(228) J. A. Kerr and M. J. Parsonage, "Evaluated Kinetic Data on Gas Phase Addition Reactions," Butterworths, University of Birmingham, England, 1972.

(229) A. C. Lloyd, "Evaluated and Estimated Kinetic Data for the Gas Phase Reactions of the Hydroperoxyl Radical," National Bureau of Standards (U.S.), report 10447 (1970).

(230) D. D. Davis, W. A. Payne, and L. J. Stief, *Science*, 179, 280 (1973).

(231) R. A. Cox, *J. Photochem*, in press.

(232) A. W. Castleman, Jr., R. E. Davis, H. R. Munkelwitz, I. N. Tang, and W. P. Wood, paper in "Symposium on Chemical Kinetics Data for the Lower and Upper Atmosphere," Airlie House, Va., Sept. 1974.

(233) J. G. Calvert, D. H. Slater, and J. W. Gall, in "Chemical Reactions in Urban Atmospheres," C. S. Tuesday, Ed., Elsevier Publishing Co., New York, 1971, p. 133.

(234) J. G. Calvert, "Modes of Formation of the Salts of Sulfur and Nitrogen in an NO_x-SO_2-Hydrocarbon-Polluted Atmosphere," paper at Conference of Atmospheric Salts and Gases of Sulfur and Nitrogen in Association with Photochemical Oxidant, University of California, Irvine, Jan. 1974; State of California Air Resources Board Report, ARB Contract 3-197, T. T. Crocker, Ed.

(235) N. A. Renzetti and G. J. Doyle, *Int. J. Air Pollut.*, 2, 327 (1960).

(236) A. P. Altshuller, S. J. Kopczynski, W. A. Lonneman, T. L. Becker, and D. L. Wilson, *Environ. Sci. Technol.*, 2, 696 (1968).

(237) W. E. Wilson, Jr., and A. Levy, *J. Air Pollut. Contr. Assoc.*, 20, 385 (1970).

(238) W. E. Wilson, Jr., and A. Levy, *Curr. Res.*, 6, 423 (1972).

(239) J. P. Smith and P. Urone, *Environ. Sci. Technol.*, 8, 742 (1974).

(240) M. F. R. Mulcahy, J. R. Stephen, and J. C. Ward, *J. Phys. Chem.*, 71, 2124 (1967).

CONCLUSIONS

In this work several significant new observations have been made related to the chemical reactions which occur in sunlight-irradiated, NO_x-hydrocarbon-aldehyde-CO-SO_2-polluted atmospheres.

I. In the first part of this study we have investigated many of the primary reactions necessary for the quantitative evaluation of the mechanism of photo-oxidation of SO_2 in the atmosphere. The rate constants were determined for the reactions of the excited states of SO_2 with many of the compounds which occur in the polluted lower atmosphere. In view of these results several conclusions can be made which bear on the SO_2 atmospheric removal reactions.

1) The theoretical maximum rates of SO_2-photooxidation in sunlight-irradiated, SO_2-containing atmospheres is 1.9% per hour at a solar zenith angle of 20°; see Sections I-A-2, p. 11, and I-B-2, p. 24. In view of the high proportion of chemically unreactive quenching collisions between excited SO_2 and O_2, it is probable that the actual rate of SO_2 photooxidation is 0.2% per hour or less. This rate of SO_2 conversion is small compared to the rates of other removal reactions which occur in a highly polluted atmosphere. It may be significant in atmospheres in which SO_2 is the dominant pollutant present.

2) The reaction of excited sulfur dioxide molecules with the alkene hydrocarbons has been found to be extremely rapid. The rate constants are near equal to the collision number for these systems. However the major result of this interaction is the isomerization of the olefinic hydrocarbon; the extent of incorporation of SO_2 into the carbon-containing products is small. See Section I-D, p. 54. We conclude that aerosol formation in urban atmospheres probably does not involve excited SO_2-alkene reactions to any significant extent.

3) The mechanism and quantum efficiency of the SO_3 formation in irradiated SO_2-containing mixtures were determined in a flow system with various added reactants. See Section I-F, p. 69-86. The apparently divergent results from previous steady-state measurements of other workers and our results from flow systems are rationized well in terms of the significant occurrence of the reaction $SO + SO_3 \rightarrow 2SO_2$ in the steady-state systems. In this work the first unambiguous and interpretable kinetic study of the rates of SO_3 formation has been made. The results point to the significantly greater importance of the SO_3 product in the irradiated SO_2-containing systems. Previous steady state measurements of SO_3 rates in these systems probably do not apply to the atmospheric system in view of the neglect of SO_3 destruction steps in the interpretation of these experiments.

II. In the second phase of this study several rate constants were estimated which are of immediate value in estimation of SO_2 conversion rates in the polluted urban atmosphere.

1) We have established that the rate constant for the gas phase reaction, $O_3 + SO_2 \rightarrow SO_3 + O_2$, is: $k \leq 5 \times 10^{-3}$ liter mole^{-1} sec^{-1} at room temperature; see Section II-A, p. 93. This estimate is very much smaller than the previously published upper limits for this rate constant. There remains no doubt that the rate of the homogeneous oxidation of SO_2 by O_3 in urban atmospheres is insignificant.

2) We have estimated the rate constants for the homogeneous gas phase reactions, $NO_3 + SO_2 \rightarrow NO_2 + SO_3$, and $N_2O_5 + SO_2 \rightarrow N_2O_4 + SO_3$; these are $k \leq 4.2$ liter mole^{-1} sec^{-1} and $k \leq 2.5 \times 10^{-2}$ liter mole^{-1} sec^{-1}, respectively. See

Reproduced from best available copy.

Section II-A-2, p. 97. These results when coupled with computer simulation studies show that the rate of NO_3 and N_2O_5 oxidation of SO_2 cannot be important paths in the polluted atmospheres.

3) Preliminary observations in this work point to a previously unexpected result which deserves further study. The gaseous reaction of SO_3 with NO_2 appears to be extremely fast, and a solid product forms which may be nitrosyl nitryl pyrosulfate: $(NO)S_2O_7(NO_2)$. See Section II-A-2, p. 98. It is not possible to say at this time how important the SO_3-NO_2 reaction observed here might be relative to other SO_3 reactions in the polluted atmosphere. The significance of the SO_3-NO_2 adduct as a participant in urban aerosol formation is an intriguing possibility which cannot be evaluated without further quantitative work.

4) Our work has shown that ozone reacts with Teflon to form CF_2O among other products. See Section II-B, p. 99. Workers who utilize Teflon fixtures and Teflon-coated chambers or bags in the study of atmospheric reactions should be alerted to this reaction and the possible contamination which will result from this practice.

III. In the third part of this work, an evaluation was made of the photochemical smog mechanisms using the computer to simulate the rates of change in various polluted atmospheres. Several important features of special interest in the development of control strategy were observed.

1) Our results show that the dominant reactive entity which chemically removes the olefinic and paraffinic hydrocarbons and aldehydes in smog is the HO-radical. HO_2, O_3, and $O(^3P)$ reactions with the olefinic hydrocarbons can be significant for certain conditions as well. See Sections III-A, p. 112 and III-C-1, p. 136.

2) The effect of carbon monoxide on the rate of O_3 development in NO_x-CO-polluted atmospheres has been investigated. From this work we conclude that atmospheric scientists should give careful consideration to the predicted enhancement of ozone levels by relatively small amounts of CO in an NO_x-polluted, but hydrocarbon-free, atmosphere. In view of the technological difficulties associated with the removal of NO_x and CO from exhaust gases, there is a reasonable possibility that significant ozone levels (0.08 ppm) may continue to plague many urban areas even though a near total removal of the reactive hydrocarbons might be effected.

3) Theoretical estimates based on computer simulation of reactions in a smog system show that the concentrations of the dominant chain carrier species, the HO and HO_2 radicals, are not strongly affected by variations in pollutant concentrations over a rather wide range. See Section III-C-1, p. 147. These data should prove very useful in guiding the development of direct experimentation for the direct detection of these reactive species in the urban atmospheres.

4) Theoretical estimates of the nitrogen mass balance during reactions in a simulated polluted atmospheres show that nitric acid and PAN are expected to be the dominant first nitrogen-containing products in smog mixtures, and these compounds may be formed in near equal amounts. See Section III-C-1, p. 154.

5) Calculations based on computer simulations of smog systems show that the initial presence of aldehydes in the reactant mixtures is expected to accelerate hydrocarbon and NO oxidations and ozone formation. It appears from

these data that the E.P.A. National photochemical oxidant standard could not be met if the aldehydes remained high, (CH_3CHO) ≥ 0.06, (CH_2O) ≥ 0.10 ppm, even if nearly all of the olefinic hydrocarbons were removed. We should learn from these studies that the "true" relationship between non-methane hydrocarbons and maximum 1-h oxidant at low hydrocarbon levels could be a critical function of a variable which is not now measured routinely, namely the concentration of impurity aldehydes.

6) The predicted effects of variation of the concentration of NO_x and hydrocarbons on the integrated (O_3)-time and (PAN)-time data for computer simulated atmospheres show that the control strategy for photochemical oxidant based on NO_x and RH regulation should be reasonable sound provided that impurity aldehydes and CO are controlled as well.

7) Finally we have studied through computer simulation the potentially important reactions which control SO_2 conversion in an NO_x-RH-SO_2 contaminated atmosphere. It is concluded that the rate of oxidation of SO_2 to SO_3, H_2SO_4, and the other sulfate-containing species will be promoted by homogeneous reactions at a rate ≥ 1.1-1.5% per hour. The dominant rate determining steps appear to be: $HO + SO_2 \rightarrow HOSO_2$ and $HO_2 + SO_2 \rightarrow HO + SO_3$; see Section III-C-1, p. 162. It is important to note that several previously unidentified yet potentially important secondary products of SO_2 oxidation may form as a precursor to sulfuric acid and sulfate salts; namely we would anticipate the formation of an inorganic analogue to the notorious peroxyacylnitrates, $HOSO_2O_2NO_2$, as well as peroxysulfuric acid (Caro's acid) and other seemingly important reactive intermediate species. These should be considered as potential members of the ill-defined "sulfate" fraction of the urban aerosol which correlates well with respiratory problems in humans.